EPFL

Thèse n° 10 180

Hydromorphological assessment of sediment augmentation measures in gravel-bed rivers

Présentée le 27 avril 2023

Faculté de l'environnement naturel, architectural et construit
Plateforme de constructions hydrauliques
Programme doctoral en génie civil et environnement

pour l'obtention du grade de Docteur ès Sciences

par

Christian MÖRTL

Acceptée sur proposition du jury

Prof. M. E. S. Violay, présidente du jury
Prof. C. Ancey, Dr G. De Cesare, directeurs de thèse
Dr R. Loire, rapporteur
Prof. S. Kantoush, rapporteur
Dr D. Vanzo, rapporteur

École polytechnique fédérale de Lausanne

2023

"A river cuts through rock,
not because of its power,
but because of its persistence."

– James N. Watkins

Für meinen Großvater Gernot Mörtl

Acknowledgements

The study is funded by the Swiss Federal Office for the Environment (FOEN-BAFU) in the framework of the research project *Riverscape – Sediment Dynamics and Connectivity*.

First, I would like to thank Professor Christophe Ancey for providing me with the opportunity to write my thesis at the Platform of Hydraulic Construction (PL-LCH) of the EPFL. My greatest gratitude goes to Dr Giovanni De Cesare, for guiding me through my thesis. Thank you, Giovanni, for your advice, trust, and encouragement. I would also like to thank Dr Paolo Perona for reviewing this thesis. Furthermore, I would like to thank Dr Davide Vanzo (ETH), Professor Sameh Kantoush (Kyoto University) and Dr Rémi Loire (EDF) for taking on the role of an examiner and Professor Marie Violay (EPFL) for her role as the president in my oral exam. The review comments provided by the examiners after the oral exam were much appreciated and helped to improve the quality of the thesis manuscript.

Thank you to the team of styx4D, Johan Berthet, Pierre-Allain Duvillard and Alexandre Baratier, for their collaboration on the drone-based image analysis. I also want to acknowledge Cédric Bron, Yohan Rouiller, Michel Teuscher, and the team from the workshop for the technical support, especially Julien Rotzetter, who built large parts of my flume. A special thanks goes to Robin Schroff for his fieldwork, shared experience, and reviews and also to Lionel Julien Pattaroni, for his help with the numerical model calibration.

I joined the PL-LCH during a period of uncertainty, marked by the recent departure of a large part of the team, the temporary closure of the campus and long periods of mandatory home office and other unprecedented restrictions. The more important it was to have a small number of cheerful colleagues who stuck together, managed to adapt, shared the workload, and consistently contributed to a pleasant atmosphere in the office or our virtual meetings. A big thanks goes to Romain Dubuis, for all the good moments inside and outside the office. Thank you also to Samuel, Mona, Najla, Jean-Noël, Romain Van Mol, Pedram, Séverine, Azin and Pedro, for their advice and kindness.

Ich möchte mich auch bei meiner Familie und Freunden für die große Unterstützung bedanken. Ein besonderer Dank geht an meine Mutter und meine Großeltern für ihr Verständnis und ihre Zuversicht. Zuletzt, danke Agi, für deine Liebe und deine Fröhlichkeit.

Abstract

In the riverine environment, the riverscape, sediment and flow regime are essential drivers for natural habitat dynamics. Today, most water courses in Europe are regulated, and their natural dynamics are impaired. Flood releases coupled with the artificial addition of sediment, called sediment augmentation, downstream of obstructing hydraulic structures can help to restore ecological functions and mitigate adverse morphological effects from sediment deficit and an invariable, low discharge.

Although many scientific studies have emerged on some design criteria and related physical processes of sediment augmentation measures, there is still a lack of knowledge regarding different restoration phases and site characteristics. This thesis investigates hydromorphological assessment strategies and design optimisation. It focuses on alternating in-channel deposits in low-gradient, sediment-starved, gravel-bed rivers.

The influence of hydrograph shape and sediment augmentation repetition frequency on sediment transport dynamics and morphology evolution were investigated in different experimental series in the laboratory. Hydrograph skewness was distinguished by left-skewed, right-skewed and symmetrical shapes. Symmetrical hydrographs increased overall bedload mobilisation and transport rates, and left-skewed hydrographs increased the mean transport distance compared to right-skewed hydrographs. Repetition frequency was separated in augmentation scenarios before every and every second mobilising flood and was performed with up to four consecutive augmentations. Increasing the repetition frequency led to increased persistence of sediment patches and deposition rates in the downstream section. Calculations based on numerical simulations showed a significant increase in hydromorphological diversity until the fourth repetition.

The influence of channel geomorphic units on river morphology and the validity of different indicator types for assessing physical habitat were investigated in the field. Tagged bedload particles (tracers) from a sediment augmentation measure were tracked in the river before and after a low-magnitude bed-forming flood. Channel geomorphic units were mapped according to qualitative definitions. The physical habitat assessment was performed in parallel at the restoration and an upstream control reach. Channel geomorphic units influenced tracer distribution and persistence during a flood. The persistence of tracers was highest in riffles and lowest in runs. The investigated flood did not significantly restructure the channel geomorphic units' organisational patterns. Not all assessment indicators proved to be valid for quantifying the impact of the sediment augmentation measure on habitat diversity. Riverbed structure, substrate mobilisability, water depth and velocity distributions were best suited for the impact assessment at the study site.

The thesis provides important design recommendations for adapting sediment augmentation measures to different site conditions and restoration phases.

Keywords: sediment augmentation, hydrograph shape, repetition frequency, channel geomorphic units, hydromorphological assessment

Résumé

Dans l'environnement fluvial, les sédiments et le régime d'écoulement sont des facteurs essentiels pour la dynamique naturelle des habitats. Aujourd'hui, la plupart des cours d'eau en Europe sont réglementés et leur dynamique naturelle est perturbée. Les lâchers de crues couplés à l'ajout artificiel de sédiments, appelé augmentation des sédiments, en aval des structures hydrauliques obturantes, peuvent aider à renaturer les fonctions écologiques et à atténuer les effets morphologiques néfastes du manque de sédiments et d'un débit faible et invariable.

Bien qu'un nombre croissant d'études scientifiques émerge sur certains critères de conception et les processus physiques associés des mesures d'augmentation des sédiments, il existe encore un manque de connaissances concernant différentes phases de renaturation et différentes caractéristiques de sites. Cette thèse étudie les stratégies d'évaluation hydromorphologique et l'optimisation de la conception. Elle se concentre sur les dépôts alternés dans des rivières à lit de gravier à faible gradient et pauvres en sédiments.

L'influence de la forme de l'hydrogramme et de la fréquence de répétition de l'augmentation des sédiments sur la dynamique du transport des sédiments et l'évolution de la morphologie a été étudiée dans différentes séries expérimentales en laboratoire. L'asymétrie des hydrogrammes a été distinguée selon les formes asymétriques à gauche, asymétriques à droite et symétriques. Les hydrogrammes symétriques ont provoqué une augmentation des taux de mobilisation et de transport du charriage et les hydrogrammes asymétriques à gauche ont augmenté la distance moyenne de transport par rapport aux hydrogrammes asymétriques à droite. La fréquence de répétition a été séparée dans les scénarios d'augmentation à chaque et à toutes les deux crues. Les expériences ont été effectuées jusqu'à quatre augmentations consécutives. L'augmentation de la fréquence de répétition a entraîné une augmentation de la persistance des assemblages des sédiments et le taux de déposition dans la section aval. Les calculs basés sur des simulations numériques ont montré une augmentation significative de la diversité hydromorphologique jusqu'à la quatrième répétition.

L'influence des unités géomorphologiques à l'échelle du chenal (UGCs) sur la morphologie de la rivière et la validité de différents types d'indicateurs pour l'évaluation des habitats ont été étudiées sur le terrain. Des particules de charriage marquées d'une mesure d'augmentation des sédiments (traceurs) ont été suivies dans la rivière avant et après une crue morphogène de faible magnitude. Les UGCs ont été cartographiées selon des définitions qualitatives. L'évaluation des habitats a été réalisée en parallèle dans la zone de renaturation et dans une zone de contrôle en amont. Les UGCs ont influencé la distribution et la persistance des traceurs pendant la crue. La persistance des traceurs était la plus élevée dans les unités « plat » et la plus faible dans les unités « radier ». La crue étudiée n'a pas restructuré de manière significative les configurations spatiales des UGCs. Pas tous les indicateurs d'évaluation se sont avérés valables pour quantifier

l'impact de la mesure d'augmentation des sédiments sur la diversité des habitats. La structure du lit de la rivière, la capacité à la mobilisation du substrat ainsi que les distributions de la profondeur d'eau et de la vitesse ont été les indicateurs les mieux adaptés sur le site étudié.

La thèse fournit d'importantes recommandations de conception pour adapter les mesures d'augmentation des sédiments aux différentes conditions du site et aux différentes phases de restauration.

Mots clés : augmentation des sédiments, forme de l'hydrogramme, fréquence de répétition, unités géomorphologiques, évaluation hydromorphologique

Zusammenfassung

In der Flusslandschaft üben das Sediment- und Abflussregime einen wesentlichen Einfluss auf die natürliche Dynamik der Lebensräume aus. Heutzutage sind die meisten Fliessgewässer in Europa reguliert und ihre natürliche Dynamik ist beeinträchtigt. Flussabwärts von Querbauwerken können Flutungen in Verbindung mit der künstlichen Zugabe von Sediment, sogenannten Sedimentanreicherungen, dazu beitragen ökologische Funktionen wiederherzustellen und negative morphologische Auswirkungen in Folge eines Sedimentmangels und eines kontrollierten, niedrigen Abflusses abzumildern.

Obwohl es eine wachsende Zahl wissenschaftlicher Studien zu einigen Planungskriterien und den zugrunde liegenden physikalischen Prozessen von Sedimentanreicherungen gibt, bestehen nach wie vor Wissenslücken hinsichtlich verschiedener Restaurierungsphasen und gewässerspezifischen Gegebenheiten. In dieser Doktorarbeit werden Strategien zur hydromorphologischen Wirkungskontrolle und die Optimierung von Planungskriterien untersucht. Die Arbeit konzentriert sich auf alternierende Schüttungen in kiesführenden Flüssen mit geringem Gefälle und starkem Sedimentmangel.

Der Einfluss der Form der Hochwasserganglinie und der Wiederholungsrate der Sedimentanreicherung auf die Dynamik des Sedimenttransports und die Entwicklung der Morphologie wurde in unterschiedlichen Versuchsreihen im Labor untersucht. Bei der Schiefe der Ganglinien wurde zwischen linksschiefer, rechtsschiefer und symmetrischer Form unterschieden. Symmetrische Ganglinien führten zu einer höheren Mobilisations- und Transportrate des Geschiebes und linksschiefe Ganglinien erhöhten die mittlere Transportdistanz im Vergleich zu rechtsschiefen Ganglinien. Die Wiederholungsrate der Sedimentanreicherung wurde in Szenarien mit jeder einzelnen oder jeder zweiten Flut unterschieden. Es wurden bis zu vier aufeinanderfolgende Sedimentanreicherungen durchgeführt. Eine Erhöhung der Wiederholungsrate führte zu einer erhöhten Beständigkeit von Sedimentansammlungen und der Depositionsrate im stromabwärts gelegenen Abschnitt. Berechnungen auf der Grundlage numerischer Simulationen zeigten zudem eine signifikante Zunahme der hydromorphologischen Vielfalt bis zur vierten Wiederholung.

Der Einfluss geomorphologischer Einheiten auf Gerinneebene (GEG) auf die Flussmorphologie und die Aussagekraft verschiedener Indikatortypen für die Bewertung der Lebensräume wurden im Feld untersucht. Markierte Geschiebepartikel (Marker) aus einer Sedimentanreicherung wurden im Fluss vor und nach einem geschiebebildenden Hochwasser geringen Ausmasses verfolgt. Die GEG wurden nach qualitativen Merkmalen kartiert. Die Wirkungskontrolle zur Bewertung der Lebensräume wurde parallel in der Renaturierungsstrecke und einer flussaufwärts gelegenen Kontrollstrecke durchgeführt. Die GEG beeinflussten die Verteilung und Beständigkeit der Marker während des Hochwassers. Die grösste Beständigkeit der Marker wurde in dem GEG-Typen «Furt» verzeichnet und die geringste Beständigkeit in «Schnellen». Das untersuchte

Hochwasser führte nicht zu einem signifikanten Umstrukturieren der Anordnungsmuster der GEG. Nicht alle Bewertungsindikatoren erwiesen sich als aussagekräftig für die Quantifizierung der Auswirkungen der Sedimentanreicherung auf die Habitatvielfalt. Die Sohlstrukturen, die Mobilisierbarkeit des Substrats sowie die Verteilungen der Wassertiefe und der Fließgeschwindigkeit eigneten sich am besten für die Wirkungskontrolle im Untersuchungsgebiet.

Die Doktorarbeit liefert wichtige Planungsempfehlungen zur Anpassung von Massnahmen zur Sedimentanreicherung an unterschiedliche Standortbedingungen und Sanierungsphasen.

Schlüsselwörter: Sedimentanreicherung, Ganglinienform, Wiederholungsrate, geomorphologische Einheiten, hydromorphologische Wirkungskontrolle

Content

Chapter 1 Introduction 1

1.1 Context 1

1.2 Motivation 2

1.3 Framework of the study 4

1.4 Structure of the report 4

Chapter 2 Background and state of the art 7

2.1 Fluvial forms and processes 7

2.1.1 Channel forms and geomorphic units 8

2.1.2 Channel processes 9

2.2 Interrupted sediment continuity due to hydropower 11

2.3 Sediment augmentation measures 13

2.3.1 Primary objectives 13

2.3.2 Design approaches 15

2.3.3 Case studies 20

2.3.4 Physical model studies 22

2.3.5 Numerical model studies 23

2.4 Eco-geomorphological assessment 24

2.5 River restoration in Switzerland 26

2.5.1 Legal framework 26

2.5.2 Eco-geomorphological state of Swiss rivers downstream of reservoirs 27

2.6 Rationale for research 31

2.6.1 Gaps 31

2.6.2 Research questions 32

2.6.3 Working hypotheses 32

Chapter 3 Methodology 33

3.1 Methodological approach 33

3.2 Field observations 34

3.2.1 Site description 34

3.2.2 Grain size distribution from drone imagery ... 36
3.2.3 Flood hydrographs and sediment transport capacity ... 42
3.2.4 Sediment supply ... 43
3.2.5 Mapping of channel geomorphic units ... 45
3.2.6 Tracking of bedload particles ... 45
3.2.7 Assessment of hydromorphological changes ... 47
3.2.8 Assessment of habitat diversity ... 48

3.3 Physical modelling ... 49
3.3.1 Experimental flume ... 49
3.3.2 Test procedure ... 52
3.3.3 Data analysis ... 55
3.3.4 Case study ... 57
3.3.5 Parametric study ... 60
3.3.6 Error assessment ... 66
3.3.7 Limitations ... 69

3.4 Numerical modelling ... 69
3.4.1 Initial conditions ... 69
3.4.2 Boundary conditions ... 70
3.4.3 Model calibration ... 70
3.4.4 Limitations ... 73

Chapter 4 Influence of hydrograph shape on sediment transport dynamics of alternating in-channel sediment deposits 74

4.1 Introduction ... 74
4.2 Test configuration ... 75
4.3 Bed morphology evolution ... 76
4.4 Bedload transport rates ... 80
4.5 Pulse evolution ... 82
4.6 Conclusion ... 84

Chapter 5 Influence of sediment augmentation repetition frequency on bed morphology evolution 85

5.1 Introduction ... 85
5.2 Test configuration ... 86
5.3 Bed morphology evolution ... 87

5.4 Deposition and percentage of cover ... 90
5.5 Persistence of mobile sediment ... 92
5.6 Hydromorphological diversity ... 93
5.7 Conclusion ... 96

Chapter 6 Influence of channel geomorphic units on river morphology evolution during artificial floods coupled with sediment augmentation 99

6.1 Introduction ... 99
6.2 Bedload particle transport ... 100
6.3 Hydromorphological changes ... 106
6.4 Influence of CGUs on bedload transport ... 108
6.5 Evolution of CGU organisational patterns and reach scale hydromorphological diversity ... 110
6.6 Transferability of results ... 111
6.7 Conclusion ... 111

Chapter 7 Impact assessment of sediment augmentation measures on habitat diversity 113

7.1 Introduction ... 113
7.2 Study framework ... 114
7.3 Indicators of habitat diversity ... 115
7.3.1 Riverbed structures ... 116
7.3.2 Riverbank structures ... 118
7.3.3 Hydromorphological diversity ... 120
7.3.4 Presence of cover ... 121
7.3.5 Substrate quality ... 122
7.4 Conclusion ... 124

Chapter 8 Recommendations for sediment augmentation measures 125

8.1 Introduction ... 125
8.2 Restrictions ... 126
8.3 Morphologic site conditions ... 126
8.4 Origin of sediment ... 127
8.5 Artificial floods ... 128

8.5.1 Hydrograph shape 128
8.5.1 Ecological design 130
8.6 Assessment strategies 130
8.7 Conceptual design framework 132
8.8 Long-term restoration strategies 133

Chapter 9 Conclusion and Outlook 136

9.1 Overview 136
9.2 Influence of hydrograph shape on sediment transport dynamics of alternating in channel sediment deposits 136
9.3 Influence of sediment augmentation repetition frequency on bed morphology evolution 137
9.4 Influence of channel geomorphic units on river morphology evolution during artificial floods coupled with sediment augmentation 137
9.5 Impact assessment of sediment augmentation measures on habitat diversity 138
9.6 Future work 139

Bibliography 141

Appendix i

Curriculum Vitae xxvi
i

List of Figures

Figure 1.1 Pictures of an artificial flood release and a sediment augmentation measure ... 3

Figure 2.1 Scheme of different elements of a fluvial system and their order of scale ... 8

Figure 2.2 Schematic drawing of sediment-related issues in regulated rivers ... 12

Figure 2.3 Diagram of the temporal and spatial impact scale of sediment augmentation measures (SAMs) with different primary restoration and management objectives ... 13

Figure 2.4 Photos of different types of sediment deposits ... 18

Figure 2.5 Scatter plots of design parameters of single sediment augmentation measures (SAMs) from representative scientific case studies from Japan, USA, and Europe since the year 2000 ... 22

Figure 2.6 Map of hydropower installations in Switzerland with the average Eco-Morphology Class (EMC) of their tailwater sections. ... 28

Figure 2.7 Shema of different reservoir shapes used in the *SEDCON* database ... 29

Figure 2.8 Box plot for the relation between the Eco-Morphology Class Ratio ($EMCR$) of the tailwater section of Swiss hydropower installations and different reservoir characteristics and management types ... 30

Figure 3.1 Schematic overview of the main methodological approaches to address the research questions (RQs). ... 34

Figure 3.2 Maps and orthophoto of the study site location with initial deposit positions from 2016 and measured cross-sections ... 35

Figure 3.3 Scatter plot of the b-axis of 40 cobbles at the Chéran River from analogue measurements ($danalog$) and from calculations by GALET ($dGALET$) ... 38

Figure 3.4 Graphic of the difference of relative occurrence (ΔRO) of 25 grain size distributions (GSDs) from the Sarine River and the Ain River between *GALET* and analogue reference measurements by size class and different orthoimage resolution ... 39

Figure 3.5 Orthophotos with the spatial distribution of different grain size parameters of the surface layer of a natural gravel bar at the Sarine River calculated by *GALET* 40

Figure 3.6 Hydrographs and average bedload transport capacity of *Flood 2016* (a) and *Flood 2020* (b) 43

Figure 3.7 Orthophoto with the evolution of the unwetted area of the artificial deposits during mean flow from before *Food 2016* (initial) to after *Flood 2020* 44

Figure 3.8 Photo of the upstream part of the experimental flume with four initial sediment deposits. View in the downstream direction. © Platform of hydraulic construction of the EPFL (PL-LCH). 50

Figure 3.9 Diagram of the grain size distributions (GSDs) of the mobile and the fixed sediment of the physical model 51

Figure 3.10 Pictures of experimental channel instrumentation, including the laser scanner and an ultrasonic sensor (USS) 52

Figure 3.11 Flow chart of the experimental test procedure 53

Figure 3.12 Schematic sketch with the control elements of the experimental flume 53

Figure 3.13 Schema of the experimental channel at *state 2* with the two initial deposit positions 54

Figure 3.14 Photo of the pool section in the downstream part of the experimental flume in channel *state 3* 57

Figure 3.15 Probability density functions (pdf) with the frequency (f) of the amount of augmented sediment along the central channel axis in the model and in the field after *Flood2016* and after *Flood2020* 59

Figure 3.16 Schema of the experimental channel of the parametric study 61

Figure 3.17 Schema of the experimental planning of the parametric study in model scale 62

Figure 3.18 Hydraulic conditions along the centre axis of the experimental channel in initial condition for a constant model discharge (Qm) of $80\ ls$ 63

Figure 3.19 Shields diagrams showing the condition of motion for the median particle diameter of the mobile material ($d50, mobile$) in all seven channel sections for four scenarios (a-d) of different constant model discharge (Qm) in model and field scale 65

Figure 3.20 Revised version of the *da Silva and Yalin's plan* (Ahmari & Da Silva, 2011), including the characteristic region of the represented river section by the parametric model study 66

Figure 3.21 Graphic display of the spatial distribution of the vertical change (Δz) between the channel after the first flood of *Run_D* to *Run_F* (a–c) and the initial empty channel 68

Figure 3.22 Graphic display of the geometry and attributes of the quality mesh 69

Figure 3.23 Location of the ten measurement points of the Ultrasonic Velocity Profiling (UVP) and water level measurements at the reference cross-section (CS) in the experimental channel 71

Figure 3.24 Photos of the physical model in flow direction during different calibration phases of the numerical model 72

Figure 4.1 Schema of the experimental planning and the experimental channel relevant to the experiments of Chapter 4 76

Figure 4.2 Graphic display of the vertical change (Δz) during the first flood of *Run_A* 77

Figure 4.3 Graphic display of the vertical change (Δz) during the first flood of *Run_B* 78

Figure 4.4 Graphic display of the vertical change (Δz) during the first flood of *Run_C* 79

Figure 4.5 Graphs of the average bedload transport rates (Qb) during periods of constant discharge (Q) for cross-section (CS) CS1 (a) and CS2 (b) 81

Figure 4.6 Graphs of the elevation difference (ED, a–c) and the cumulative elevation difference (CED, d–f) in the near downstream zone (ZOI2) between different channel states during the first floods of Run A to Run C and the empty channel state (S0) 83

Figure 5.1 Schema of the experimental planning and the experimental channel relevant to the experiments of Chapter 5 86

Figure 5.2 Graphic display of the vertical change (Δz) after every flood of *Run_D* 87

Figure 5.3 Graphic display of the vertical change (Δz) after every flood of *Run_E* 88

Figure 5.4 Graphic display of the vertical change (Δz) after every flood of *Run_F* 89

Figure 5.5 Graphs of the dimensionless deposition ($D*$, a–c) and the percentage of cover (POC, d–f) for the number of released floods ($nflood$) of *Run_D* to *Run_F* in the three zones of interest (ZOI) *ZOI1* to *ZOI3* 90

Figure 5.6 Bar plots of the persistence of sediment ($P*$) after two to four floods ($nflood$) of *Run_D* to *Run_F* (a-c) in the zone of interest (ZOI) *ZOI2* 92

Figure 5.7 Graphic display of the simulated water depth (h) and flow field of the initial channel state (a) and after four floods of *Run_E* to *Run_F* (b-d) 93

Figure 5.8 Graphs of the hydromorphological index of diversity ($HMID$) for the number of released floods ($nflood$) of *Run_D* to *Run_F* 94

Figure 6.1 Orthophotos with channel geomorphic units (CGUs) and tracer stone positions after *Flood 2016* and *Flood 2020* 102

Figure 6.2 Probability density function (pdf) of RFID PIT tags (tracer) positions along the channel centreline 103

Figure 6.3 Relative number of RFID PIT tags (tracers) and joint area of channel geomorphic units (CGUs) by CGU type for the two channel states after *Flood 2016* ($TF16$) and after *Flood 2020* ($TF20$) 105

Figure 6.4 Cross-section (CS) profiles for the three channel states before *Flood 2016* ($T0$), after *Flood 2016* ($TF16$) and after *Flood 2020* ($TF20$) 107

Figure 7.1 Map of the study sections used for the physical habitat assessment. 114

Figure 7.2 Assessment timeline (a) and hydrographs and transport capacity of *Flood 2016* (b) and *Flood 2020* (c) 115

Figure 7.3 Mapped riverbed structures (CGUs) at different study reaches and assessment times 117

Figure 7.4 Mapped riverbank structures at different study reaches and assessment times 119

Figure 7.5 Mapped presence of cover at different study reaches and assessment times 121

Figure 7.6 Mapped substrate mobilisability at different study reaches and assessment times 123

Figure 8.1 Schematic sketch of sample organisational pattern of channel geomorphic units (CGUs) in a restoration reach and predicted

deposition from indirect sediment augmentation at two different locations after a low-magnitude bed-forming flood 127

Figure 8.2 Schematic sketch of possible extraction sites for sediment augmentation in a residual-flow reach. 128

Figure 8.3 Schematic sketch of different hydrograph shapes with minimal and ecological flood volume 130

Figure 8.4 Indicator for eco-geomorphological assessment of sediment augmentation measures (SAMs) with different primary objectives 131

Figure 8.5 Schematic sketch of promoting the evolution of an impaired river reach towards a near-natural state by sediment augmentation measures (SAMs). 135

Figure A2.1 Graph of the rating curve at the measurement location, based on the eight calibration points ii

Figure A3.1 Pictures of the experimental flume at different test phases iii

Figure A4.1 Hydraulic conditions along the centre axis of the experimental channel in initial condition for a constant model discharge (Qm) of $2.2ls$ iv

Figure A4.2 Hydraulic conditions along the centre axis of the experimental channel in initial condition for a constant model discharge (Qm) of $20ls$ iv

Figure A4.3 Hydraulic conditions along the centre axis of the experimental channel in initial condition for a constant model discharge (Qm) of $35ls$ v

Figure 9.4 Hydraulic conditions along the centre axis of the experimental channel in initial condition for a constant model discharge (Qm) of $45ls$ v

Figure A6.1 Graphic display of the vertical change during the first flood of *Run_A* vii

Figure A6.2 Graphic display of the vertical change during the first flood of *Run_B* viii

Figure A6.3 Graphic display of the vertical change during the first flood of *Run_C* ix

Figure A7.1 Graphic display of the vertical change between every flood of *Run_D* x

Figure A7.2 Graphic display of the vertical change between every flood of *Run_E* xi

Figure A7.3 Graphic display of the vertical change between every flood of *Run_F* xi

Figure A8.1 Graphic display of the simulated water depth and flow field after the three first floods of *Run_D* xii

Figure A8.2 Graphic display of the simulated water depth and flow field after the three first floods of *Run_E* xii

Figure A8.3 Graphic display of the simulated water depth and flow field after the three first floods of *Run_F* xiii

Figure A10.1 Graphic display of channel geomorphic units (CGUs) after *Flood 2016* with the expected tracer distribution along the channel axis, following $H_{0,2}$ xvi

Figure A11.1 Cross-section (CS) profile of CS1 for the three channel states before *Flood 2016* ($T0$), after *Flood 2016* ($TF16$) and after *Flood 2020* ($TF20$) xviii

Figure A11.2 Cross-section (CS) profile of CS1b for the three channel states before *Flood 2016* ($T0$), after *Flood 2016* ($TF16$) and after *Flood 2020* ($TF20$) xviii

Figure A11.3 Cross-section (CS) profile of CS2 for the three channel states before *Flood 2016* ($T0$), after *Flood 2016* ($TF16$) and after *Flood 2020* ($TF20$) xix

Figure A11.4 Cross-section (CS) profile of CS3 for the three channel states before *Flood 2016* ($T0$), after *Flood 2016* ($TF16$) and after *Flood 2020* ($TF20$) xix

Figure A11.5 Cross-section (CS) profile of CS4 for the three channel states before *Flood 2016* ($T0$), after *Flood 2016* ($TF16$) and after *Flood 2020* ($TF20$) xx

Figure A11.6 Cross-section (CS) profile of CS5 for the three channel states before *Flood 2016* ($T0$), after *Flood 2016* ($TF16$) and after *Flood 2020* ($TF20$) xx

Figure A11.7 Cross-section (CS) profile of CS6 for the three channel states before *Flood 2016* ($T0$), after *Flood 2016* ($TF16$) and after *Flood 2020* ($TF20$) xxi

Figure A11.8 Cross-section (CS) profile of CS7 for the three channel states before *Flood 2016* ($T0$), after *Flood 2016* ($TF16$) and after *Flood 2020* ($TF20$) xxi

Figure A11.9 Cross-section (CS) profile of CS8 for the three channel states before *Flood 2016* ($T0$), after *Flood 2016* ($TF16$) and after *Flood 2020* ($TF20$) xxii

Figure A11.10 Cross-section (CS) profile of CS9 for the three channel states before *Flood 2016* ($T0$), after *Flood 2016* ($TF16$) and after *Flood 2020* ($TF20$) xxii

Figure A12.1 Mapped substrate composition at different study reaches and assessment times xxv

List of Tables

Table 2.1 Classification and description of different reservoir flushing scenarios. 29

Table 3.1 River characteristics and measurements at three study sites for the assessment of *GALET* 37

Table 3.2 Description of channel geomorphic unit (CGU) types 45

Table 3.3 Attributes of tracer stones. The variable dm is the mean diameter and $d90$ is the 90th percentile diameter 46

Table 3.4 Categories of the hydromorphological diversity index 48

Table 3.5 Indicator and attributes of *Indicator set 1* of the *Guideline for evaluating the outcome of restoration projects* (EOR) of the Swiss Federal Office of the Environment (2019) 49

Table 3.6 Attribute table of channel sections of the physical model 50

Table 3.7 Attribute table of channel states of the physical model 51

Table 3.8 Comparison of deposit volume change between model (M) and field conditions (F) for deposit 1 (D1) to D4 58

Table 3.9 Erosion rates (E) of deposits (Ds) D1 to D4 after the first flood of experimental run D to F 67

Table 3.10 Mean values (μ) of depth-averaged velocity (μv) and water level measurements (μh) over the reference cross-section (CS) in calibration phase 1. 72

Table 3.11 Mean values (μ) of depth-averaged velocity μv and water level measurements μh over the reference cross-section (CS) in calibration phase 2 73

Table 6.1 Descriptive statistics of RFID PIT tags (tracer) 100

Table 6.2 Absolute number of RFID PIT tags (tracer) by channel geomorphic unit (CGU) type for the two channel states after *Flood 2016* ($TF16$) and after *Flood 2020* ($TF20$) 106

Table 6.3 Hydromorphological diversity index ($HMID$) of different channel sections for the three channel states before *Flood 2016* ($T0$), after *Flood 2016* ($TF16$) and after *Flood 2020* ($TF20$) 108

Table 7.1 Results of the assessments of the first indicator set of the guideline for evaluating the outcome of restoration projects of the Swiss Federal Office of the Environment (EOR1) 116

Table 8.1 Conceptual framework for identifying relevant restrictions, design approaches and assessment methods for four primary restoration and management objectives of sediment augmentation measures. 133

Table A1.1 References for representative case studies of sediment augmentation measures (SAMs), displayed in **Figure 2.5** i

Table A2.1 Data table for **Figure A2.1**, listing all eight calibration points ii

Table A5.1 Data table for **Figure 3.19**, including a calculation of the ratio of Shields Number (θ) to critical Shields Number ($\theta c = 0.045$)..... vi

Table A9.1 Data table for **Figure 4.5**..... xiv

Table A9.2 Data table for **Figure 5.5**..... xv

Table A9.3 Data table for **Figure 5.8**..... xv

Table A10.1 Comparison of observed (O) and expected (E) number of tracers for the null hypotheses (H_0) $H_{0,1}$ and $H_{0,2}$ by channel geomorphic unit (CGU) type for the two channel states after Flood 2016 ($TF16$) and after Flood 2020 ($TF20$)..... xvii

Table A12.1 Evaluation criteria for Indicator 1.1 of the guideline for evaluating the outcome of restoration projects of the Swiss Federal Office of the Environment (Hunzinger et al., 2019)..... xxiii

Table A12.2 Evaluation criteria for Indicator 1.2 of the guideline for evaluating the outcome of restoration projects of the Swiss Federal Office of the Environment (Hunzinger et al., 2019)..... xxiii

Table A12.3 Evaluation criteria for Indicator 1.5 of the guideline for evaluating the outcome of restoration projects of the Swiss Federal Office of the Environment (Hunzinger et al., 2019) xxiii

Table A12.4 Evaluation criteria for Indicator 1.6 A2 of the guideline for evaluating the outcome of restoration projects of the Swiss Federal Office of the Environment (Hunzinger et al., 2019) xxiv

List of Acronyms

ADCP	acoustic doppler current profiler
ADV	acoustic doppler velocimeter
CGU	channel geomorphic unit
CR	control reach
CRediT	Contributor Roles Taxonomy
CS	cross-section
D	deposit
DGPS	Differential Global Positioning System
DS	downstream section
Eawag	Swiss Federal Institute of Aquatic Science and Technology
EFR	environmental flow release
EOR	Guideline for Evaluating the Outcome of Restoration projects of the Swiss Federal Office of the Environment
EOR1	Indicator set 1 of the EOR
ET	entrainment threshold
EPFL	École Polytechnique Fédérale de Lausanne
FOEN	Swiss Federal Office of the Environment
GNSS	Global Navigation Satellite System
GSD	grain size distribution
H	hypothesis
H_0	null hypothesis
H_A	alternative hypothesis
IS	intervention section
MIZ	morphological impact zone
MSP	Modular Stepwise Procedure
PIT	passive integrated transponder
PL-LCH	Platform of Hydraulic Constructions
Qx	flood event with a return period of x years
RFID	radio frequency identification
RTK	real-time kinematic positioning
Run	experimental run
RQ	research question
RR	restoration reach
S	scan
SAEFL	Swiss Agency for the Environment, Forests and Landscape
SAM	sediment augmentation measure
SHR	spawning habitat restoration
SWEs	Shallow Water Equations
SZ	scan zone
USS	ultrasonic sensor
UVP	ultrasonic velocity profiling
VAW	Laboratory of Hydraulics, Hydrology and Glaciology
WSL	Swiss Federal Institute for Forest, Snow and Landscape Research
WPA	Federal Act on the Protection of Waters
ZOI	zone of interest
χ^2-test	Chi-square goodness-of-fit test

List of Notations

$\hat{A}$	sum of all areas of a CGU type normalised by the total area of all CGUs
b	flow width
b_0	standard bed width
CED	Cumulative Elevation Difference
COV	coefficient of variation
d	characteristic particle diameter
D^*	dimensionless deposition
d_x	xth-percentile particle diameter
d_m	mean grain size diameter
DOA	degree of armouring
E	erosion rate
ED	Elevation Difference
EMC	Eco-Morphology Class
$EMCR$	Eco-Morphology Class Ratio
f	frequency
Fr	Froude Number
g	gravitational acceleration
h	flow depth
h_b	burial depth of RFID PIT tags in the artificial deposits
h_{max}	maximum flow depth
$HMID$	Hydromorphological Index of Diversity
IAM	Indicator for the Attractiveness of river Morphology
IRS	Indicator for Reproduction Suitability based on substrate degradation
IQR	Inter-Quartile Range
J	longitudinal slope
K_{st}	Strickler hydraulic roughness
kdf	Gaussian kernel density function
l	length
L_{crown}	length of the dam crown
MAE	Mean Absolute Error
ME	Mean Error
n	number of samples
$\hat{n}$	number of detected tracers of a CGU type normalised by the total number of detected tracers
p	p-Value for statistical significance
P^*	persistence of sediment
PCC	Pearson Correlation Coefficient
pdf	Probability Density Function
POC	Percentage of Cover
POF	Percentage of Fines
Q	discharge
$\overline{Q}_{s,cap}$	average bedload transport capacity
R	Pearson Coefficient
$\overline{R}$	statistical range
R^2	Coefficient of Determination
R_h	hydraulic radius
RAE	Relative Absolute Error
Re_p	Particle Reynolds Number
$RMSE$	Root Mean Square Error
$RRSE$	Root Relative Squared Error

t	time
u_*	friction velocity
v	velocity
V	volume
V_t	total volume of augmented material
W_{max}	maximum width of a reservoir's planform shape
x	longitudinal coordinate
y	lateral coordinate
z	vertical coordinate
ΔRO	Difference in Relative Occurrence
ΔV_t	volume imbalance
θ	Shields Number
λ	Froude scaling factor
λ_r	geometrical scaling
μ	arithmetic mean
υ	kinematic viscosity of the fluid
ρ_f	fluid density
ρ_s	sediment density
σ	standard deviation
τ_b	bed shear stress
τ_b^*	non-dimensional bed shear stress
τ_c^*	critical non-dimensional shear stress

Chapter 1
Introduction

Natural sediment transport dynamics are vital for many river ecosystem services. In regulated rivers, the sediment regime is often impaired. An impaired sediment regime can have numerous adverse effects on the eco-morphodynamics of the riverscape. The artificial supply of sediment, commonly referred to as sediment augmentation measures, can help to promote those dynamics in sediment-depleted river sections. In the framework of the "Hydraulic Engineering and Ecology" research program, several issues are raised for the design and hydromorphological assessment of sediment augmentation measures. In this thesis, the challenges from the practice were addressed by scientific research. The first two sections about context and motivation briefly introduce the topic. After the introduction, a literature review is followed by the research rationale and the methodology chapter. The research questions are addressed in four subsequent chapters. In the final chapters, practical design recommendations are derived, and the conclusions and outlook are presented.

Note: Section 1.1 and Section 1.2 are based on an article accepted for a technical journal[1], a translated article published in another technical journal[2], an article published in reviewed conference proceedings[3] and an article published in a peer-reviewed journal[4].

1.1 Context

From source to delta, rivers transport sediment along their course. In situations where natural sediment sources exist, and the discharge varies undisturbed with flood events and seasons, a continuous process of erosion and deposition shapes a river's planform and bed morphology. This natural dynamic is vital for a diverse riverine habitat space (BAFU (Hrsg.), 2017).

In regulated rivers, the natural sediment regime is often disturbed by (i) an impaired discharge regime, (ii) increased transport capacity resulting from channelisation or (iii) reduced bedload availability. An impaired discharge regime mainly comes from

[1] "Sediment continuity and augmentation measures" by C. Mörtl, R. Schroff and G. De Cesare, accepted in *FactSheet Collection of the project Riverscape – sediment dynamics and connectivity*. Contribution of the doctoral candidate according to the *CRediT* (Contributor Roles Taxonomy): conceptualisation; data curation; formal analysis; investigation; methodology; resources; software; validation; visualisation; writing – original draft; writing – reviewing and editing.

[2] "Sedimentzugaben in Fliessgewässern. Überblick über Methoden und Fallbeispiele [Sediment augmentation in flowing waters. Overview of methods and case studies]" by C. Mörtl and G. De Cesare, published in 2022 in *Ingenieurbiologie* (Mörtl & De Cesare, 2022a). Contribution of the doctoral candidate according to the *CRediT*: conceptualisation; data curation; investigation; resources; validation; visualisation; writing – original draft; writing – reviewing and editing.

[3] "The sediment challenge of Swiss river corridors interrupted by man-made reservoirs" by C. Mörtl, S.L. Vorlet, P. Manso and G. De Cesare, published in 2020 in *Riverflow 2020* (Mörtl et al., 2020). Contribution of the doctoral candidate according to the *CRediT*: conceptualisation; data curation; formal analysis; investigation; methodology; validation; visualisation; writing – original draft; writing – reviewing and editing.

[4] "Sediment augmentation for river rehabilitation and management - a review" by C. Mörtl and G. De Cesare, published in 2021 in *Land* (Mörtl & De Cesare, 2021). Contribution of the doctoral candidate according to the *CRediT*: conceptualisation; data curation; investigation; validation; visualisation; writing – original draft; writing – reviewing and editing.

regulating flow for energy production (residual flow and hydropeaking) or flood protection. It reduces peak discharges required for major bedload mobilisation events. As part of historical river modification, channelisation increases transport capacity and causes riverbed incision and a progressive flattening of the channel slope. Bedload availability can be reduced by riverbank protection or alluvial sediment extraction. The longitudinal continuity of sediment transport can be interrupted by sediment traps or hydraulic structures, such as river runoff plants and dams with large reservoirs. It can lead to a complete depletion of bedload in the downstream reach.

A near-natural, dynamic sediment regime is not only essential for aquatic communities (e.g. Hauer, Leitner, et al., 2018). It also guarantees the proper functioning of many other ecosystem services of a watercourse, which often appear less in the public discourse. These include, for example, the balancing of the water household (basic), the improvement of drinking and service water quality (supply), nutrient retention (regulation) or the shaping of the landscape (culture) (Podschun et al., 2018). A sediment deficit over several decades can primarily lead to a deepening of the riverbed, lowering the groundwater level, armouring of the bed and loss of dynamic habitat.

1.2 Motivation

Operators and authorities have increasingly addressed sediment management of regulated rivers in the Alpine region over the last decades. Several mitigation measures and strategies have been developed and put into practice. They can be classified into measures within the catchment area, inside the reservoir, at the dam or along its downstream reach.

Measures within the catchment area include soil conservation, slope and bank protection, bypass structures or off-stream storage reservoirs. Inside the reservoir, mitigation measures, besides mechanical dredging operations, are designed to avoid the settling of fine sediment, evacuate settled material or control turbidity currents. These are namely flushing and emptying operations, hydro-suction and airlifting. At the dam, sluicing, venting of turbidity currents, turbining of fine, suspended sediments and the heightening of water intake or bottom outlet are the most widespread mitigation measures. At the downstream river reach, settling basins and the dilution of evacuated sediment-loaded flows with clear water can reduce the effect of clogging.

Only some of these standard practices have yielded satisfactory effectiveness, efficiency, and sustainability results. Many of these follow-up effects still need to be described and quantified to be addressed accordingly. Additionally, innovative measures such as sediment augmentation in the downstream reach, advanced flushing operations or dam decommissioning should be further investigated concerning the longitudinal connectivity of the river. Optimising those operations is of great interest, as large-scale mitigation methods are typically highly cost-effective and can cause unwanted effects further downstream (Arnaud et al., 2017).

The artificial supply of sediment, commonly referred to as sediment augmentation or sediment replenishment, is increasingly used to address sediment-related issues in regulated rivers. The term sediment augmentation is used in this thesis as a general term because it is free of implications on design and objectives. Coupled with a near-natural flow regime, Sediment Augmentation Measures (SAMs) can promote natural eco-morphodynamics (Figure 1.1)

Figure 1.1 Pictures of an artificial flood release and a sediment augmentation measure. a: Two water jets coming out of the bottom outlets of the Rossens Dam in the Canton of Fribourg during the 2016 artificial flood. ©PL-LCH. Photo: Severin Stähly. b: View in the upstream direction of artificial sediment deposits in the residual-flow reach of the Sarine River downstream of the Rossens Dam shortly before the 2016 flood release. adapted from (Mörtl & De Cesare, 2021).

Sediment augmentation has been widely practised over the last decades, particularly in Japan, the USA and Europe (Kondolf et al., 2014). While SAMs are practised in river engineering for at least half a century, the number of related scientific papers has increased significantly since the beginning of the new millennium, with only a small percentage of the described measures being related to a restoration action (Staentzel et al., 2020). Scattered information can be found in company reports, newspapers, or other public media but requires careful crosschecking in each case.

The design of SAMs can vastly vary and depends on the defined objectives and the morphological, hydrological, and ecological conditions. Even though the number of scientific studies about SAM has increased, they often focus on particular revitalisation objectives and site conditions (Mörtl & De Cesare, 2021). For the design of a SAM, practitioners are often faced with the challenge of finding tailor-made solutions. This can result in the encounter of numerous remaining knowledge gaps. Another problem for the practice is that design recommendations derived from physical or numerical modelling studies are scarcely validated by field observations. Experience from case studies can show discrepancies between the observed and the modelled morphological evolution (e.g. Mörtl & De Cesare, n.d.). The ecological implications are even more complex to assess and difficult to compare between sites because the response of biological communities and, thus, the result of ecological indicators can change with environmental

conditions (Pander & Geist, 2013). These factors make investigating the hydromorphological assessment of sediment augmentation in the context of ecological restoration a particular scientific challenge and require further research.

1.3 Framework of the study

The research program *Hydraulic Engineering and Ecology* is a joint initiative by the *Swiss Federal Office of the Environment* (FOEN) and four research institutions from the ETH domain (ETH-Bereich):

- The *Platform of Hydraulic Constructions* (PL-LCH) of the *École Polytechnique Fédérale de Lausanne* (EPFL)
- The *Laboratory of Hydraulics, Hydrology and Glaciology* (VAW) of the ETH Zurich
- The *Federal Institute of Aquatic Science and Technology* (Eawag)
- The *Federal Institute for Forest, Snow and Landscape Research* (WSL)

The program aims to develop scientific foundations for answering recent practical questions in river management and to prepare outreach products for knowledge transfer.

The associated research project *Riverscapes - Sediment Dynamics and Connectivity* has a design project phase from 2017 to 2021 and consists of thirteen subprojects. Several partner initiatives and semi-annual plenary meetings promote close cooperation among research project members and their institutions. This thesis involves work on *subproject 5* with the topic of *Ecomorphological assessment of sediment replenishment downstream of dams*. The project guidelines raise the following issues regarding the design and the assessment of sediment augmentation measures (Vetsch et al., 2018):

- Influence of hydrographs and duration of artificial floods on alternating gravel bars (or similar morphological structures): distribution, structure, layer thickness
- Durability of the gravel bars regarding natural flood events
- Emerging river morphological structures from deposits in different river morphologies, especially in the case of slightly meandering rivers and rivers with variable channel width
- Influence of bedload additions on bed stability in channel widenings
- Characterisation of the ecological value of the resulting habitat structures (*meso* approach and hydraulic-morphological diversity index)

1.4 Structure of the report

The thesis is divided into nine chapters:

Chapter 1 introduces the context of the topic and the motivation for research. The framework of the associated research project and relevant research interests are explained. The practical issues raised in the project are described and the manuscript's structure is presented.

Chapter 2 contains the literature research and the rationale for the research. The focus of the literature research was determined by the practical issues raised in the associated research project. From the literature review, relevant research gaps were identified. Research questions were then defined based on the practical issues and the defined research gaps under consideration of the available resources. Several hypotheses were formulated regarding the research questions and stated at the end of the chapter.

Chapter 3 outlines the methodology used to test the hypotheses and answer the research questions. It is separated into the three main approaches used in this thesis: Field observations, physical modelling, and numerical modelling. These subchapters also contain preliminary studies which present a groundwork for the primary research approach.

Chapter 4 to Chapter 7 separately address the four main research questions. The first paragraph of each chapter discusses the terminology used in the original research question and the final study objectives derived from it. Each of these chapters contains a composition of relevant results from the main approaches. The results are analysed, and the key points are summarised. The results are discussed by quantitative analysis of specific scenarios regarding the defined study objectives and the corresponding hypotheses. The conclusion at the end of the chapters summarises the main trends discovered.

Chapter 8 provides a summary of practical design recommendations derived from analysing the results in the previous chapters. The discrepancy between practical issues raised at the beginning of the research project and the key findings is discussed.

Chapter 9 concludes the content of the thesis and provides a proposal for future work.

The candidate performed all work presented in this thesis if not cited or stated otherwise. The balance of results is not oriented on the methodological approaches but on the response to the four research questions (Chapters 4-7). Tables, figures, and equations are numbered according to the chapter and in ascending order, starting at 1 for each chapter. The appendix contains supplementary material.

Chapter 2
Background and state of the art

This chapter provides a classification of watercourses and a definition of geomorphological terms. A short overview is given about driving and influencing factors of channel processes at different scales and known fundamentals on the bank erosion and sediment transport process. Primary objectives of sediment augmentation measures are identified from the literature. Common design approaches are provided for the main design criteria sediment properties, volume, injection method, mobilisation event, injection period and repetition frequency. Experience and examples from scientific studies on sediment augmentation measures are summarised separately for case studies, and physical and numerical model studies. Eco-geomorphological assessment by biotic and abiotic indicators, topographic surveys and bedload measurements is discussed. A section on the legal framework of the restoration of watercourses in Switzerland explains how SAMs can be a part of so-called hydropower mitigation or rehabilitation measures. A pre-study on interrupted sediment continuity due to hydropower assesses the potential for SAMs in the context of hydropower mitigation measures on a national scale. Based on the literature research, the last section presents the identified research gaps, the research questions, and the formulated hypotheses.

Note: This chapter is based on an article published in a peer-reviewed journal[1], an article submitted to a peer-reviewed journal[2], an article accepted for a technical journal[3] and an article published in reviewed conference proceedings[4].

2.1 Fluvial forms and processes

This section focuses on geomorphic processes and terminology essential for a process-based understanding of the morphological impact of sediment augmentation measures and hydromorphological assessment. It provides the scientific background needed for the development of the research questions.

[1] "Sediment augmentation for river rehabilitation and management - a review" by C. Mörtl and G. De Cesare, published in 2021 in *Land* (Mörtl & De Cesare, 2021). Contribution of the doctoral candidate according to the *CRediT*: conceptualisation; data curation; investigation; validation; visualisation; writing – original draft; writing – reviewing and editing.

[2] "Influence of channel geomorphic units on the evolution of river morphology during low magnitude bed-forming floods coupled with sediment augmentation" by C. Mörtl, R. Schroff, S. Stähly and G. De Cesare, submitted to *Earth Surface Processes and Landforms*. Contribution of the doctoral candidate according to the *CRediT*: conceptualisation; data curation; formal analysis; investigation; methodology; resources; software; validation; visualisation; writing – original draft; writing – reviewing and editing.

[3] "Sediment continuity and augmentation measures" by C. Mörtl, R. Schroff and G. De Cesare, accepted in *FactSheet Collection of the project Riverscape – sediment dynamics and connectivity*. Contribution of the doctoral candidate according to the *CRediT*: conceptualisation; data curation; formal analysis; investigation; methodology; resources; software; validation; visualisation; writing – original draft; writing – reviewing and editing.

[4] "The sediment challenge of Swiss river corridors interrupted by man-made reservoirs" by C. Mörtl, S.L. Vorlet, P. Manso and G. De Cesare, published in 2020 in *Riverflow 2020* (Mörtl et al., 2020). Contribution of the doctoral candidate according to the *CRediT*: conceptualisation; data curation; formal analysis; investigation; methodology; validation; visualisation; writing – original draft; writing – reviewing and editing.

2.1.1 Channel forms and geomorphic units

A stream system consists of a network of watercourses. There are different ways of classifying elements of a stream system (Figure 2.1). Segments can be classified by stream order, for example, with the Strahler Number (Strahler, 1957). Another approach is to distinguish between different process domains, like sediment production, transfer, and deposition zones (Schumm, 1977).

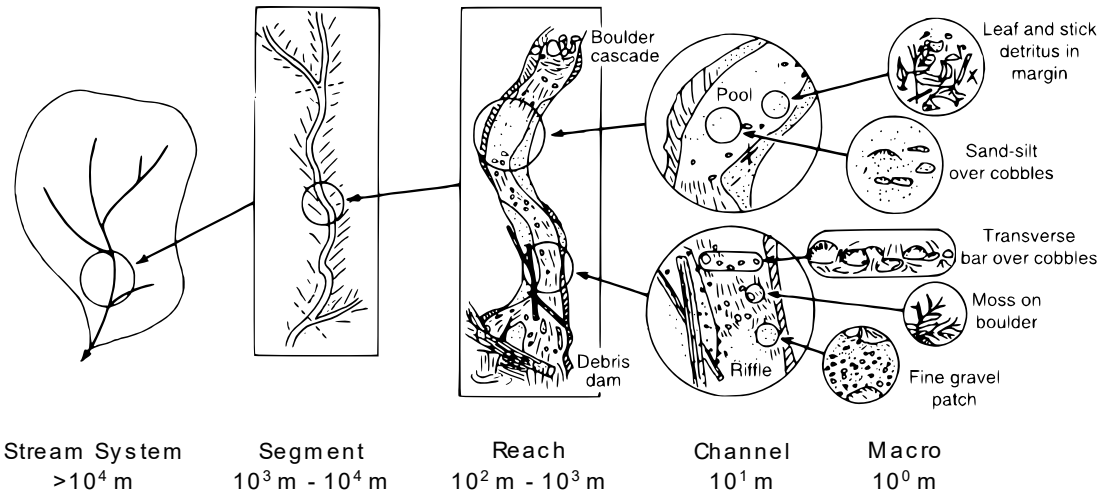

Figure 2.1 Scheme of different elements of a fluvial system and their order of scale. Reused with permission from *Springer Nature*: (Frissell et al., 1986).

Channel forms describe the pattern of single or multiple channels of a watercourse. This term refers to the planform geometry (e.g. straight, meandering or braided). Quantitative relations have been developed between the emergence of channel forms and fundamental hydromorphological parameters, for example, discharge and slope (Leopold & Wolman, 1957). In the da Silva and Yalin's plan (2011), regions of channel forms are separated based on the relation between the ratio of flow width and flow depth ($b \div h$) to the ratio of flow depth to characteristic particle size ($h \div d$).

Channel forms should not be confused with channel morphology. For example, each channel can have a different type of morphology in a braided channel form. The morphology of a channel is typically described by geomorphic units. Geomorphic units subdivide the morphology of a channel by hydraulic or morphologic characteristics at different scales. A channel geomorphic unit (CGU) describes a morphological feature at the channel scale, in the order of the width of the riverbed (e.g. riffle). Typical sequences of CGUs make up the reach morphology (e.g. glide-riffle-run). Most types of CGUs are confined to in-channel classification (Buffington & Montgomery, 2022). However, they can also include floodplain elements like bars and islands, as defined in the geomorphic unit survey and classification system (Rinaldi et al., 2015). CGUs can be described qualitatively (e.g. Hunzinger et al., 2021; Rinaldi et al., 2015) or quantitatively by hydraulic (e.g. Rosenfeld

et al., 2011), geomorphic (e.g. Halwas et al., 2005), or sedimentary characteristics (e.g. Moir & Pasternack, 2008).

2.1.2 Channel processes

Channel processes govern the evolution of channel forms (e.g. lateral migration) and channel morphology (e.g. bar evolution). Channel processes are based on sediment transport processes, which consist of a combination of erosion, transport, and deposition. Two driving factors for channel processes are sediment supply and transport capacity (Montgomery & Buffington, 1998). In gravel-bed rivers, prominent influencing factors are lateral confinement, riparian vegetation and large woody debris loading (Montgomery & Buffington, 1997).

Large-scale channel processes and forms at larger scales dominate and determine processes and forms at smaller scales (Belletti et al., 2017). An appropriate order of magnitude to link reach morphologies to channel processes, response potential, and habitat characteristics is a minimum of 10 to 20 channel widths (Montgomery & Buffington, 1997). Local influencing factors, such as CGUs, are expected to influence local sediment transport processes at the reach scale due to their characteristic hydraulic and geomorphic conditions.

Assessing the interaction of individual CGUs with channel processes on a reach scale is important to predict the evolution of channel conditions (e.g. Belletti et al., 2017; Wheaton et al., 2015), functional habitat for fish (e.g. Sato et al., 2016; Schwartz, 2016), or macrozoobenthos (e.g. Halwas et al., 2005), within and between sites. The interaction between CGUs and channel processes varies across different flow stages. The restructuring of CGUs is driven by channel-forming flow, with a return period greater than one decade (>Q10) (Pasternack et al., 2018). It can be assumed that in lower-magnitude, bed-forming flows (~Q2), existing CGUs are more persistent while strongly influencing local sediment transport processes.

Bank erosion

Deposits used in SAMs in gravel-bed rivers typically consist of primarily non-cohesive sediment with a medium particle size between $16mm$ to $64mm$. If newly created no significant influence on their stability from fluctuating pore water pressure or rooting is to be expected. Fluvial bank erosion and intermitted mass failure of coarse gravel banks are the most relevant erosion process for gravel deposit erosion (Friedl et al., 2017).

Most related bank failure models are based on the geometrical concept of a critical failure angle and an angle of repose. As scour of the foot of the bank occurs, the slope steepens until a certain angle is exceeded and finally collapses to a point where a static state is reached again. One primary example is Pizzuto's failure model (Pizzuto, 1990). Based on this concept, Volz et al. (2012) applied a more elaborate model with the software *BASEMENT.* They distinguished between three different critical angles for (i)

partially saturated material at the breach sidewalls above the water surface, (ii) compacted or parent bank material below the water surface, and (iii) deposited material resulting from slope collapses. Their approach is experimentally supported by (Spinewine et al., 2002) and (Soares-Frazão et al., 2007). Vonwiller et al. (2018) later identified (i) gravitational bank collapse, (ii) lateral bed slope effect on the bedload transport direction and (iii) local bed slope effect on the critical Shields stress as relevant model approaches to reproduce lateral streambank erosion successfully.

Sediment transport

There are different ways of categorising sediment transport in watercourses. One way is the categorisation by the mode of transport (e.g. Leopold et al., 1965). In their work, the authors define *bedload* as sediment transported by rolling, sliding, and bouncing along the riverbed. *Suspended load* refers to sediment, which is transported in suspension. *Mixed load* is sediment, which is transported by a combination of those two modes. Hemond and Fechner (2015) describe bedload as *"*[...] *particles that spend the majority of the time on the bottom but are periodically entrained into the turbulent water flow and carried a short distance downstream before settling again."*.

The boundary between bedload and suspended load is not sharp and depends on the flow strength, where grains coarser than about $8mm$ tend to always travel as bedload (P. Wilcock et al., 2009). A common concept of bedload motion is visualising an active layer (du Boys, 1879), which has recently been distinguished into an event-active and dynamical active layer (Church & Haschenburger, 2017). Here, it is correspondingly referred to as a *dynamically active* or *event-active* bedload. The latter is defined as the coarser fraction of bedload material, which is only mobilised during a channel-forming flood event with a return period greater than two years (>Q2).

A good approximation of bedload transport dynamics requires an estimation of the shear stress distribution of the riverbed. One commonly applied approach in river engineering is the estimation of bed shear stress under uniform conditions

$$\tau_b = \rho_f \times g \times R_h \times J \tag{2.1}$$

where ρ_f is the fluid density, g the gravitational acceleration, R_h the hydraulic radius and J the longitudinal slope. For a rectangular, open channel

$$R_h = \frac{b \times h}{b + 2h} \tag{2.2}$$

where b is the flow width and h is the flow depth. For wide channels, R_h is commonly approximated by h.

The mobilisation of bedload by fluvial force is commonly estimated by an excess shear stress model. It describes the threshold for motion, for example, as the excess of a

non-dimensional bed shear stress τ_b^* over a corresponding critical non-dimensional shear stress τ_c^*.

$$\tau_b^* > \tau_c^* \tag{2.3}$$

The normalisation of shear stress is typically represented by the *Shields Number* θ (Shields, 1936)

$$\theta = \frac{\tau_b}{(\rho_s - \rho_f) \times g \times d} \tag{2.4}$$

where ρ_s is the sediment density and d is the characteristic particle diameter. The *Shields diagram* (Shields, 1936) yields θ as a function of the *Particle Reynolds Number* Re_p

$$Re_p = \frac{u_* \times d}{\upsilon} \tag{2.5}$$

where u_* is the fiction velocity and υ the kinematic viscosity of the fluid and

$$u_* = \sqrt{\frac{\tau_b}{\rho_f}} \tag{2.6}$$

Meyer-Peter & Müller (1948) experimentally determined the value of τ_c^* for well-sorted fine gravel to be 0.047.

2.2 Interrupted sediment continuity due to hydropower

This section focuses on the relationship between transversal hydraulic structures and sediment transport. Together with Section 2.1, it provides the scientific background needed to develop the research questions.

Sediment-related issues present an ongoing challenge to integrated and sustainable management of regulated rivers. Independent of their type, reservoirs affect the longitudinal continuity of fluvial waters and their sediment dynamics. The alteration of the natural regime can cause unwanted effects inside and downstream of the reservoir (Figure 2.2).

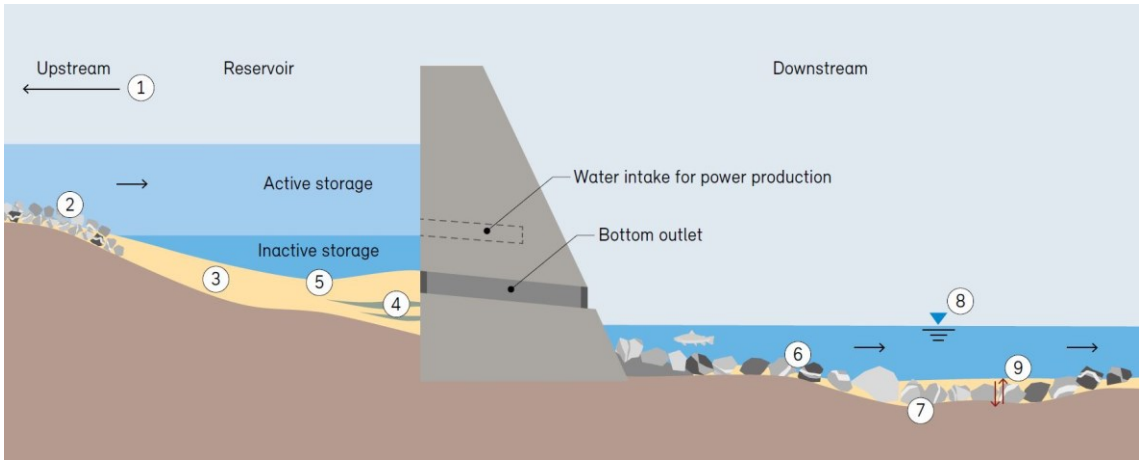

Figure 2.2 Schematic drawing of sediment-related issues in regulated rivers, regarding discontinuity and morphological changes. Sediment discontinuity: (1) accumulation of sediment, (2) trapping of coarse sediment, (3) trapping of fine sediment, (4) trapping of organic matter, (6) deficit of bedload, and (9) surplus of suspended fine sediment. Morphological changes: (1) riverbed aggradation, (5) reservoir sedimentation, (6) development of static bed armour, (7) riverbed incision, (8) loss of morphological dynamics, and (9) clogging of pore spaces.

At the upstream entrance of large reservoirs, bedload material accumulates as a result of reduced flow velocities. This can lead to riverbed aggradation and, in some cases, an increased risk of flooding. The impact of upstream changes in river morphology is generally limited to a relatively short river reach (Liro et al., 2020).

Inside the reservoir, coarse material can accumulate, and fine material can deposit, leading to a progressive filling of the reservoir with sediments. This process is called reservoir sedimentation. Deposits are sorted out across the reservoir by different physical processes according to reservoir morphology, the layout of the hydraulic works, and hydraulic operation (Manso et al., 2018). Reservoir sedimentation may cause a reduction of storage capacity and thereby reduce the capability of flow regulation. It can lead to several issues for hydropower production, such as reducing live storage, blockage of power intakes, turbine abrasion or dam safety in case of bottom outlet blockage (Manso et al., 2018; Schleiss et al., 2016). Another risk is the trapping of toxic substances in the sediments at the bottom of the reservoir, which constitute a hazard to the downstream valley (SedNet Organisation, 2004). The average sedimentation rate of reservoirs in Switzerland was estimated to be 0.2 % (Schleiss et al., 2010). The effects of climate change will further increase the sediment supply to the reservoirs in the future (Ehrbar et al., 2018; Schleiss et al., 2016).

Downstream of the reservoir, sediment deficit can lead to morphological, hydrological, and ecological consequences (S. A. Kantoush, Sumi, Kubota, et al., 2010). Sediment transfer and flow regime changes can result in substantial geomorphological adjustments (Petts & Gurnell, 2005). Those channel alterations (e.g. river incision/degradation, loss of morphological diversity) provoke potential hydrological, groundwater and ecological risks that can have far-reaching effects throughout the river. Reduced flow velocities promote the settling of suspended sediments and cause the clogging of open pore spaces in the bed material (Dubuis & De Cesare, 2023), the natural spawning ground of some fish

species. The accumulation of fine substratum elements also negatively affects benthic stream communities (Bo et al., 2007). The lack of coarse sediments provokes extended streambank erosion and river channelisation (Petts & Gurnell, 2005). This restricts channel evolution and the development of dynamic habitat space and thus decreases the potential for large biodiversity. In addition, the channel capacity is impacted by the narrowing and widening of riverbanks. A reduction in channel capacity may amplify flood hazards for a similar flood frequency (Slater, Singer, and Kirchner 2015).

2.3 Sediment augmentation measures

This section summarises the state-of-the-art knowledge about sediment augmentation measures. It outlines different objectives and design approaches and focuses on existing case studies, and physical-, and numerical model studies. It presents the basis for the identification of existing research gaps.

2.3.1 Primary objectives

Different types of SAM are commonly classified by their injection method (Ock, Sumi, et al., 2013). With largely varying conditions and objectives in river restoration (Hillman & Brierley, 2005), this classification does not provide the degree of comparability between different projects required for system-scale analysis.

Four primary restoration and management objectives for SAMs are defined:

- bedload budget (1)
- channel dynamics (2)
- riverbed structure (3)
- interstitial (spawning) habitat (4)

All these objectives target a morphological or ecological improvement on a different spatial and temporal scale (Figure 2.3).

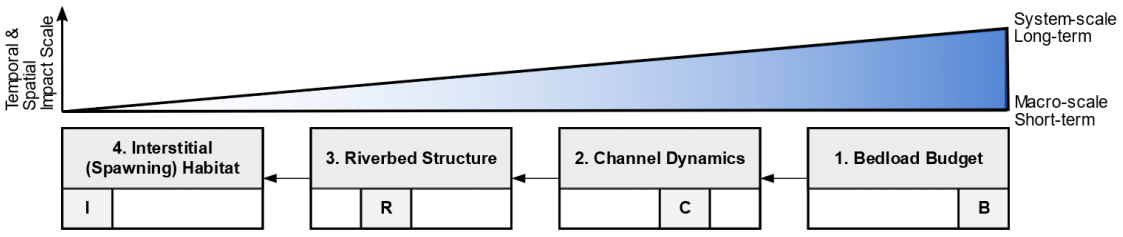

Figure 2.3 Diagram of the temporal and spatial impact scale of sediment augmentation measures (SAMs) with different primary restoration and management objectives. The definitions of the spatial scales (macro to system) are given in Figure 2.1. The *short-term* temporal scale refers to a period in the order of 10^0 years (a). The temporal scale *long-term* refers to a period equal to or greater than $10^2 a$.

For example, a SAM, which focuses on balancing the bedload budget, is designed for system-scale, long-term ecological or morphological improvement of a watercourse (e.g.

Frings, Döring, et al., 2014). Combined with other restoration measures, like ecological flood regimes (e.g. Benke, 2001; Scheurer & Molinari, 2003) and sufficient space for the river corridor (e.g. Rohde et al., 2005), it creates the prerequisite for a natural evolution towards a sustainable, eco-geomorphological reference state. On the other hand, a SAM, which focuses on spawning habitat restoration (SHR), can produce positive, macro-scale and channel scale effects in the short term (e.g. Pulg et al., 2013). It can be implemented in sections of watercourses with hydromorphological restrictions, like in residual flow sections. The expected positive impacts are usually less sustainable and can appear after several years (a) (e.g. Pulg et al., 2013).

Bedload budget

The most practised application of SAMs has the primary objective of balancing the bedload budget on a system scale (e.g. Frings et al., 2019). The intention is to control equilibrium channel geometry in gravel rivers (e.g. Pfeiffer et al., 2017) and to mitigate varying adverse morphological and ecological effects in sediment-starved watercourses. In this context, sediment augmentation can be referred to as "replenishment", as it is used to replenish the natural budget. The SAM is usually initiated at several spots along the watercourse, typically downstream of sediment barriers (lakes, reservoirs) and upstream of continuous watercourse sections with sufficiently strong hydromorphological processes to ensure a periodic downstream migration of the augmented sediment. System-scale response, especially in large stream systems like the Rhine, can be expected only after decades of continuous replenishment effort (e.g. Frings, Gehres, et al., 2014). The morphological goal of a SAM in this context is that the augmented sediment is mobilised, and that near-natural sediment dynamics re-emerge after constant repetition (Chardon et al., 2021).

Channel dynamics

The promotion of channel dynamics can be another objective of SAMs. With sufficient aggradation in the active channel, sediment supply rates can drive lateral mobility (Rachelly et al., 2018). If appropriately designed, the augmented sediment can provide the required sediment load during formative flow to promote lateral channel migration (Eaton & Church, 2004), for example, in dynamic river widenings (Rachelly et al., 2018) and the creation (Gaeuman, 2014) and maintenance (Venditti et al., 2012) of channel bars. Active channel dynamics promote the evolution of new dynamic habitat space (e.g. Ock et al., 2015), like riverbanks for riparian vegetation, and increased flow complexity in the river (Harrison et al., 2011). The target impact section is usually a large restoration site, or an unimpaired flow section and the objectives are defined for several years. The morphological goal of a SAM in this context is to provide enough sediments to trigger and amplify lateral erosion and regionally or locally reshape the channel form.

Riverbed structure

SAMs can promote several positive, eco-geomorphological processes to enhance riverbed structure at the reach scale, even under highly impaired hydromorphological conditions. One example is the creation of riffle structures in a residual-flow reach to free the benthic zone of nuisance algae from the reservoir (Ock, Kondolf, et al., 2013). The hydromorphological diversity can also be increased in this context (Stähly et al., 2019, 2020). Another theoretical benefit of SAMs for the riverbed structure is the deconsolidation and mobilisation of the top layer by fine bedload (Miwa & Parker, 2017). Deconsolidation of the armour layer reduces the clogging of the interstitial pore space and can lead to the release of bedload from below in case of a partial or complete breakup. The target impact section of an individual measure can stretch for several hundred meters downstream of the point of injection, with the potential for positive effects emerging already after the first mobilising flood. The morphological goal of a SAM in this context is to create new or restructure existing CGUs.

Interstitial (spawning) habitat

Where bed substrate quality is low and poorly suited for macroinvertebrates or spawning habitats, SAMs can improve interstitial habitat locally (e.g. Gaeuman et al., 2017; Wheaton et al., 2004b). Different species have different habitat requirements on substrate layer thickness, grain size diameter and the percentage of fines (POF), as well as on water depth flow velocities and bed morphology. The design of SAMs in this context needs to be adapted to the requirements of the target or dominant species. For brown trout, for example, spawning riffles were successfully constructed in the Moosach River in South Germany by introducing an adapted spawning substrate ($d = [16,\ 32]mm;\ POF < 1\%$) (Pulg et al., 2013). With this primary objective, SAMs typically target small areas of spawning grounds and can trigger an immediate (seasonal) response from the target species. The morphological goal for interstitial habitat restoration by SAM is to deposit suitable sediment in sufficient quantities at the location of potential habitat grounds.

2.3.2 Design approaches

Sediment properties

The properties of augmented sediment should reflect the properties of naturally occurring sediment. This means that the material should have a relatively low POF (washed) to reduce clogging (Schälchli, 1992) and the abraded surface texture of alluvial sediment (rolled) to promote mobilisation (Staudt et al., 2019). In regulated, gravel-bed rivers, gravel ($d = [2,\ 16]mm$) is usually more beneficial for improving the eco-geomorphological state than fine sediment ($d < 2mm$). Fine sediment can cause clogging of the substratum at low flow velocities and high turbidity in the event of extensive augmentation (Hartmann, 2009). (Schälchli, 1993) provides a rough estimation for the diameter of suspended grains, which can cause internal clogging ($d > 0.02mm$) and external clogging ($d > 1\ mm$),

depending on the filter medium. These properties can vary if sediment is added for other management purposes (e.g. bed scour) or sediment is supplied from a reservoir or the adjacent floodplain. Organic materials like earth or mud can lead to biological clogging (Newcomer et al., 2016) or eutrophication (Hilton et al., 2006). If the amount of organic input remains low, the adverse effect becomes negligible compared to the quantities of natural organic matter transported during a major flood event (Fuller et al., 2014).

If the primary objective of SAMs is the creation of new spawning habitat, the grain size distribution (GSD) of the augmented sediment should depend on the target fish species. Usually, the dominant fish species of the region are targeted. It can be roughly assessed from the mean slope and channel width (Huet, 1949). Diminishing numbers of specific fish stock can lead to the selection of different target species. Based on a review of 22 publications, the Atlantic Salmon (*Salmo salar*) and Brown Trout (*Salmo trutta*) generally prefer stones from $16mm$ to $64mm$ for spawning (Louhi et al., 2008). In European studies, smaller grain sizes of around $20mm$ to $30mm$ were observed at spawning grounds (e.g. Crisp & Carling, 1989). A smaller POF ($< 20\%$) sharply increased fish survival from embryos to emergence (Chapman, 1988). This can be linked to the fact that the oxygen concentration may be reduced by deposited fine sediment (Louhi et al., 2008).

For diversifying the riverbed structure or promoting channel dynamics, a broader GSD is possible, depending on the desired morphological impact in the target section. Laboratory experiments have shown that sediment pulses with material finer than the median diameter of the surface layer can promote mobilisation and surface fining (Venditti et al., 2010). On the other side, numerical investigation of the grain size effect on bed deformation in meandering channels has shown that a coarser GSD of the bed surface (i) increases bed form height, (ii) decreases the bed form length, and (iii) changes gradually the bed configurations from alternate bars shape to ripple shape (Eizel-Din et al., 2010). If the primary objective targets the balancing of the bedload budget, the GSD of the augmented sediment should represent the GSD of the dynamically active or event-active bedload of the watercourse.

Volume

The volume (V) of single SAMs varies in case studies from small ($< 10^3 m^3$); (e.g. Gaeuman et al., 2017; S. A. Kantoush & Sumi, 2011) to medium ($[10^3, 10^4] m^3$); (Heckmann et al., 2017; Stähly et al., 2020) and large ($[10^4, 10^5] m^3$); (Brousse et al., 2020; Chardon et al., 2021) volumes.

Assessing the missing spawning substrate in the target section can estimate the required volume for SHR. The criteria for potential spawning habitat area varies with species and is primarily determined by the hydraulic factors of *water depth* and *flow velocity* (Lamouroux et al., 1999) and the morphologic factors *spawning pit depth* and *bed surface structure* (Zimmer & Power, 2006). Salmon spawns mostly in a flow depth of $20cm$ to $50cm$ at an average flow velocity of $0.35ms^{-1}$ to $0.65ms^{-1}$. Trout spawning areas were found at

slightly shallower sites ($[15, 45]cm$) with lower flow velocities ($[0.2, 0.55]ms^{-1}$); (Louhi et al., 2008). The mean spawning pit depth of the Brown Trout by channel form and the geomorphic unit was assessed from 268 randomly sampled pits between $6.6cm$ and $9.4cm$ (Zimmer & Power, 2006). According to the species, this height determines the minimum height of spawning suitable substrate required at potential spawning ground locations. The typical bed surface structure of the Brown Trout spawning site is in the upward front slope of a riffle structure (Pulg et al., 2013). A similar preference for bed surface structure was reported for the Chinook Salmon, where most spawning occurred upstream of the riffles crest (73%); (Mesick, 2001).

If morphological changes are the primary objectives, the required volume for SAMs can be estimated by hydromorphological modelling (e.g. Juez et al., 2016; Vonwiller, 2017; Vonwiller et al., 2018). Single, small, or medium size SAMs have been shown to change riverbed structure (Gaeuman et al., 2017; Stähly et al., 2019). Significant channel shifting, on the other hand, was not reported even for single large SAM (e.g. Brousse et al., 2020). Laboratory experiments suggest sediment supply has an important control on CGUs (Venditti et al., 2012), if the channel form is not fixed by lateral restrictions and the discharge is unsteady (Nelson et al., 2015). Channel dynamics are likely to be altered significantly only by recurring volume supply. For example, for the morphological development of dynamic river widenings, a sufficiently large, constant sediment supply is required (Rachelly et al., 2018).

Some federal guidelines have lately addressed a uniform definition and calculation of bedload budget for sediment regime restoration by SAMs. The French guideline for measuring and modelling bedload transport (Camenen & Melun, 2021) defines *transport capacity* as the temporal mean of bedload transport. The numerical calculation is based on an equilibrium state, supposing a uniform flow and bedload regime, and sufficient material at disposal. The Swiss guideline for bedload regime restoration states that the evaluation of the sediment augmentation volume required to balance the bedload budget should be based on a defined reference state of the watercourse (Schälchli & Kirchhofer, 2012). Schälchli and Hunzinger (2018) define five primary goals (channel shape, sediment deposits, substratum, groundwater regime and flood protection) that must be met and provide empirical-based evaluation methods for the corresponding bedload volume.

Injection method

Direct installation means sediment is mechanically deposited at pre-designed target locations inside the channel area. It often includes reworking the channel to modify existing CGUs, for example, to create spawning riffles. This allows for the direct creation of spawning habitat (e.g. Schwindt et al., 2019). Such measures can be planned with the help of hydrodynamical (e.g. Cepello et al., 2009) or ecological modelling (e.g. Schwindt & Pasternack, 2020). In recent years, artificial riffles were also constructed to improve water flow and sediment transport and initiate the processes that lead to restoring natural riffle-pool sequences (Korpak et al., 2019).

If accessibility, budget, or other reasons limit the options for direct sediment supply, the indirect upstream supply of sediment is a common alternative. Sediment is placed in in-channel, point bar or high-flow deposits (Figure 2.4) and mobilised during an artificial or natural flood (Ock, Sumi, et al., 2013).

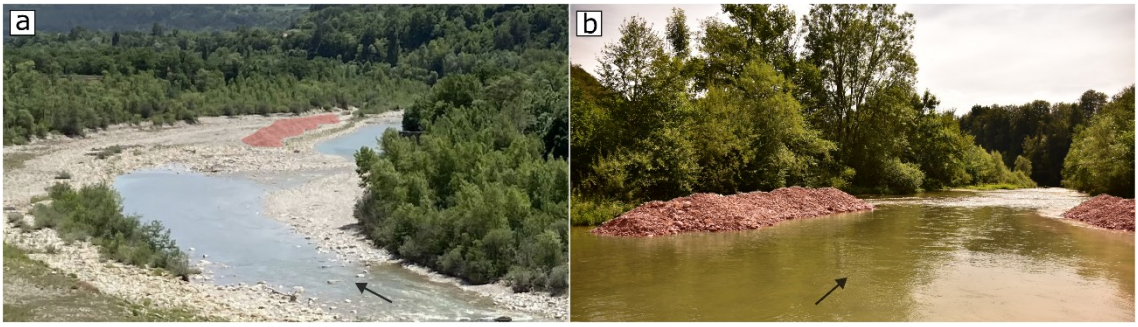

Figure 2.4 Photos of different types of sediment deposits. The augmented sediment is highlighted in red. The arrows indicate the direction of flow. a: High-flow sediment deposit downstream of the Saint-Sauveur Dam in France. © Platform for Hydraulic Engineering of the École Polytechnique Fédérale de Lausanne (PL-LCH). Photo: Christian Mörtl. b: In-channel sediment deposit downstream of the Rossens Dam in Switzerland. © PL-LCH. Photo: Christian Mörtl.

For SAMs with the primary objective of SHR, indirect sediment supply by upstream deposits requires supplementary conditions. A mobilisation event must occur before vegetation stabilises the deposits. It also needs to be ensured that the sediment is mobilised and deposited in sufficient quantity at the location of potential spawning sites (Wheaton et al., 2004b). To avoid the risk of deposit stabilisation by vegetation, high-flow constant injection, for example, by trucks or a conveyer belt (Gaeuman, 2014), presents another method for sediment injection. Laboratory experiments suggest high dispersion of sediment pulses from a high-flow injection, with only some translational transport behaviour occurring for bed-forming flow (Humphries et al., 2012). Depending on the objective of the SAM, the dispersal behaviour of the expected sediment pulse might require the adaption of other design criteria, for example, the volume.

A way of passively supplying sediments to a watercourse is by induced bank erosion. Rohde et al. (2005) describe three types of measures: Self-dynamic development, self-dynamic development with initial measures or mechanical widening. One example is the Töss River in Switzerland, where the flow was divided by an artificial island of large boulders (Friedl, 2017). At the Mur River in Austria, dredging a sidearm and removing bank protection structures enabled bank erosion. The rehabilitation works, coupled with in-channel sediment injection, led to short-term success in countering channel incision (Klösch et al., 2011). Since riverbank failure, basal residence time, and the supply of material to the in-channel sediment transfer system are coupled processes and difficult to simulate (Darby et al., 2007), the prediction of the morphological impact of a corresponding SAM entails large uncertainties. SAMs by reactivating old side channels can increase sediment transport (e.g. Marteau et al., 2020a), but it may take decades until a new (quasi-)equilibrium of the bedload budget is reached.

Mobilisation event

If sediment is not injected by direct installation, SAMs require flood events to mobilise indirectly supplied sediment. Natural flood events are often difficult to predict and might not fulfil the right timing and magnitude for SHR. For the remaining primary objectives of SAMs (1–3; Figure 2.3), single or multiple natural flood events were successfully used to mobilise parts of mostly large deposit volumes (e.g. Arnaud et al., 2017; Brousse et al., 2020). In Japan, natural floods are expected in the monsoon season and can be controlled to favour reservoir flushing operations coupled with downstream SAMs (e.g. S. A. Kantoush & Sumi, 2010).

Environmental Flow Releases (EFRs) from reservoirs target downstream ecological or management objectives (King et al., 2003). An EFR scheme ideally contains large channel-forming and smaller floods for habitat maintenance (Acreman & Ferguson, 2010). Therefore, it can be coupled with all forms of SAMs.

Other than EFRs, reservoir flushing operations focus on issues inside the reservoir, such as emptying the reservoir of sediment (Schleiss et al., 2016). Even though a coupling of reservoir flushing operations and downstream restoration measures, such as SAMs, has been called for (Mörtl et al., 2020), multiple objectives are often too far apart to allow for a single specification of required discharge and water volume (Kondolf & Wilcock, 1996). Therefore, reservoir flushing as part of a SAM is a relevant design approach for SAMs with less specific morphological goals.

Period and frequency

The period and frequency of SAMs depend on the primary objective. In any case, in-channel construction works should fall outside susceptible aquatic species' flooding and spawning season. SAMs with the primary objective of SHR should be implemented shortly before the spawning period of the target fish species to provide a clean and unclogged spawning substrate. In Switzerland, the FOEN recommends SAMs for SHR from late summer to autumn, between the reproduction period of cyprinid and salmonid (Breitenstein & Kirchhofer, 2010). Depending on the size of the watercourse, a repetition after one or two years has proven a reasonable repetition frequency to maintain positive effects on the fish fauna (Pulg et al., 2013).

Changing riverbed structure or channel form by upstream sediment supply requires major flood events (e.g. Brousse et al., 2020; Heckmann et al., 2017). The corresponding SAMs should be coordinated with flood season and be repeated based on repeated assessments. SAMs for bedload regime restoration should be repeated with a frequency that bedload is regularly available for transport. If this is not feasible, the repetition frequency and the individual volume can be adapted to correspond to the target annual bedload rate on average over for a few years.

2.3.3 Case studies

Japan

In Japan, SAMs are frequently performed downstream of nearly 25% of its dams (Sumi et al., 2017), aiming to reduce reservoir sedimentation and re-establish sediment continuity across reservoirs. Mainly coarse sediments are commonly dredged out at check dams at the head of the reservoirs and placed in high-flow stockpiles at the downstream reach to be mobilised during controlled natural or artificial floods (Sumi et al., 2017). The median grain size diameter (d_{50}) of this material ranges from about $0.25mm$ to $28mm$, depending on the dredging location (Sumi & Kantoush, 2011). Over the last decade, research focus has turned towards mitigating adverse morphological effects and riverine habitat revitalisation in downstream reaches of dams.

Downstream of the Nunome Dam at the Nunome River, sediment augmentation coupled with floodplain habitat restoration successfully restored bedload transport and the associated habitat (S. A. Kantoush, Sumi, & Kubota, 2010). In addition, riffle structures from previous SAMs showed retention capacity for removing reservoir-derived plankton, which subsequently contributed to macroinvertebrates species richness (Ock, Kondolf, et al., 2013). Downstream of the Murou Dam at the Uda River, improvement in riverbed formation, riverbed materials, benthic organisms and algae were tracked in a four-year survey of annual sediment augmentation (S. A. Kantoush & Sumi, 2011).

USA

In the USA, SAMs have primarily focused on SHR for salmonids and have been implemented episodically by various government agencies since the 1960s and 1970s (Bunte, 2004). The d_{50} of supplied material in prominent case studies lies between $32mm$ and $64mm$, in the upper region of the sizes for salmonid spawning gravels ($d_{50} = [5.4, 78]mm$) (Kondolf & Wolman, 1993).

The most famous study site is the Trinity River in California, where research efforts are dedicated towards a process-based understanding of the initiation of in-channel morphological features, like spawning riffles, by upstream sediment supply (Gaeuman, 2014; Gaeuman et al., 2017; Ock, Kondolf, et al., 2013). The increase of spawning substrate and bed enhancement has been investigated for different design objectives and validation methods for SHR (Wheaton et al., 2004a). Both efforts combined are suggested to be successful in spawning habitat enhancement (Sellheim et al., 2016; Wheaton et al., 2004b; Zeug et al., 2014) and beneficial to macroinvertebrate assemblages (Merz & Ochikubo Chan, 2005). Improvement in spawning habitat quality for salmon and steelhead was tracked after the direct placement of suitable spawning substrate in the side channel and spawning riffle construction in the main channel at the Feather River in California (Cepello et al., 2009).

Europe

In Europe, where most rivers are heavily regulated and modified around settlement and infrastructure, SAMs focus on morphological changes and ecological upgrading. A wide range of project objectives at varying scales has led to a growing diversity of design and assessment strategies.

The positive impact of a single SAM on the morphological conditions was achieved with the reduction of local riverbed incision at the Buëch River in France (Brousse et al., 2020). Studies on consecutive augmentation at reach scale were performed over four years at the Rhine River (Arnaud et al., 2017) and almost two decades at the Isar River in Germany (Heckmann et al., 2017). At the restoration section of the Rhine, the augmentation measure led to local habitat diversification, but sediment starvation conditions reappeared after more than five years (Chardon et al., 2021). The local impact on biological communities was positive, with the gravel augmentation found to tend to promote the taxonomic richness of macroinvertebrate communities (Staentzel et al., 2018).

Basin-scale observations at the Rhine River indicate that in large river systems, natural erosion and sedimentation phenomena still dominate present-day morphodynamics, even though, today, SAM is the largest source of gravel and cobbles (Frings et al., 2019). The total mass of introduced material amounts to approximately 8.4 million tons of allochthonous sediment (mainly gravel) (Frings, Döring, et al., 2014). In the lower reach of the Rhine, it was shown that present-day degradation rates would have been much higher without the upstream sediment augmentation (Frings, Döring, et al., 2014). Another successful example at the catchment scale is the restoration project of the River Ehen in Northwest England (Marteau et al., 2020b). Sediment augmentation was performed by reconnecting a previously diverted headwater sub-catchment to its mainstem. The reconnected tributary exerts an important control on coarse sediment supply and dynamics and has proven to be an important source of fine material (Marteau et al., 2020a).

Comparison of representative studies

Three representative scientific case studies of single SAMs from Japan, the USA, and Europe were compared regarding important design parameters (Figure 2.5).

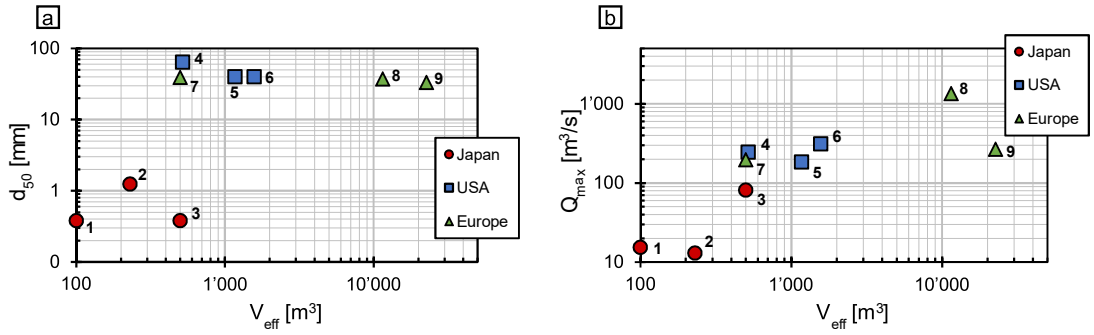

Figure 2.5 Scatter plots of design parameters of single sediment augmentation measures (SAMs) from representative scientific case studies from Japan, USA, and Europe since the year 2000. a: Median grain size diameter (d_{50}) against the effective volume (V_{eff}) of the SAM. b: Peak discharge of the first flood event after the SAM (Q_{max}) against V_{eff}. The numbers next to the points mark the number of the case study. The corresponding references can be found in **Table A1.1** in the appendix.

Japanese mountain rivers generally have low suspended sediment concentrations and low bedload yields, except during periods of heavy rainfall activity (Mizuyama et al., 2010). In addition, SAMs are frequently performed downstream of dams to transfer a volume equivalent to 0.1% to 10% of annual reservoir sedimentation (Sumi et al., 2017). Therefore, the selected SAMs' total and effective volumes are characteristically low ($[100, 500] m^3$). In comparison, effective volumes vary with each project in the selected case studies from Europe and are generally higher ($[500, 22'650] m^3$), as SAMs focus primarily on morphological changes. In the examples from the USA, where the primary focus of SAMs is set on SHR, the effective volumes are correspondingly lower ($[520, 1'570] m^3$) than in the examples from Europe.

In this data set, the characteristic grain size diameter of augmented sediments in the Japanese rivers is small ($[0.38, 1.25] mm$) compared to the other two regions ($[33, 64] mm$). The material size represents the mixture dredged out at the head of the reservoir. In the selected case studies from Europe and USA, the material is dredged out at the floodplain, usually accounting for larger bedload sizes during pre-dam conditions. The peak discharge of the mobilising flood event increases with augmented volume and characteristic diameter across all regions because, typically, it is designed to create sufficient erosion and transport capacity for the augmented sediments.

2.3.4 Physical model studies

To investigate the hydromorphological effects of different design criteria of SAMs, physical model studies have focused mainly on fluvial bank erosion, sediment transport dynamics, and bed morphology evolution.

The erosion process of artificial gravel deposits is a combination of fluvial erosion at the bank toe and intermittent mass failure, depending on the deposit submergence rate (Battisacco et al., 2016; Friedl et al., 2018). For short deposits ($length \div width < [5, 10]$), the mean erosion rate increases with a higher ratio of the initial deposit width to the bed

width without the deposit (blocking ratio) and decreases with increasing mean grain size diameter (d_m) (Friedl et al., 2018).

Sediment transport dynamics in the context of sediment augmentation are often described by pulse evolution behaviour or the temporal distribution of bedload transport rates. Pulse evolution behaviour is commonly described by a conceptual framework, which distinguishes between translational and dispersional pulse evolution (Sklar et al., 2009). Bed morphology impacts sediment pulse evolution locally (Humphries et al., 2012; Nelson et al., 2015). In a straight channel, GSD has a low influence on pulse evolution, and the most pronounced translational behaviour occurs in small-volume pulses, which represent the equivalent volume required to cover the entire flume bed to a height of $0.25d_{50}$ (Sklar et al., 2009). Single, large sediment pulses cause stronger, short-term ($< 10h$) bedload transport rates than a sequence of repeated smaller pulses with similar total volume (Elgueta-Astaburuaga & Hassan, 2017). In a straight channel with periodically varying width, sediment pulse evolution occurs mainly by dispersion during constant discharge of about two times the entrainment threshold (ET) (Nelson et al., 2015). The ET is defined here as the critical Shields Number for d_{50} ($\tau_c^* \approx 0.045$). In a meandering gravel-bed river, floods with a peak discharge 2.5 times the ET cause mostly dispersion of the sediment pulse, while floods with larger peak discharge (> 3 times the ET) and the same flood volume also cause some translation (Humphries et al., 2012).

For the evolution of bed morphology in a straight washed-out channel, the supply of sediments by multiple, alternated deposits promotes cyclic patterns of sediment deposition, while a parallel configuration of deposits increases the distance of the morphological impact section (Battisacco et al., 2016). Consecutive augmentation can be effective if an equilibrium state of the bed morphology was not reached after a single augmentation measure (Bösch et al., 2016). In a meandering gravel-bed river, different fine GSDs ($d_{50} = [0.5, 0.9]mm$) of constantly supplied sediment exert limited control over the morphological response, while higher discharge and sediment supply increase the spatial scale of sediment relocation (Rachelly, Friedl, et al., 2021). Higher sediment supply rates of fine bedload material can also lead to major channel aggradation and fining of bed surface texture (Madej et al., 2009). Where net aggradation occurs in response to sediment supply in the upper part of the study reach, a narrowing of the channel width promotes the evolution of an equilibrium state of the bed morphology across the channel (Eaton & Church, 2009).

2.3.5 Numerical model studies

Numerical models, which are designed to predict bed morphology evolution from sediment augmentation in the form of deposits, require the coupling of hydrodynamic simulations and morphological simulations. The morphological simulations must represent sediment transport and bed level changes. Numerical simulations of SAMs in gravel-bed rivers are typically restricted to bedload transport. In the case of partially submerged deposits, a bank collapse model is additionally required. Until today, only a

few published numerical studies have focused on predicting morphological changes from in-channel gravel deposits.

To reproduce a flume experiment on sediment augmentation by multiple, fully submerged in-channel deposits (Battisacco et al., 2016), Juez et al. (2016) used depth-averaged 2D Shallow Water Equations (SWEs) for the flow simulation and the Exner Equation to account for bedlevel changes. Bedload transport was modelled by an excess bed shear stress approach. The numerically modelled erosion pattern generally agreed with the observed erosion pattern. However, a difference still occurred from the deficient representation of particle-particle interactions and particle transport behaviour under high flow velocities. Vonwiller et al. (2018) compared their numerical model of gravel deposit erosion to a flume experiment with a single partially submerged in-channel deposit with different geometrical configurations (Friedl, 2018). They used a similar SWEs approach with a 2D Exner Equation and the Meyer-Peter Müller Formula for bedload transport (Meyer-Peter & Müller, 1948). Bank collapse was modelled by the geometrical concept of a critical failure angle (Wu, 2007). A comparison with the flume experiment showed that the numerical 2D model could reasonably well determine local erosion rates of artificial deposits.

Numerical models with finer sediment in the range between coarse sand and very fine gravel were developed to simulate low-flow channel evolution (Miwa & Parker, 2012) or to evaluate the effect of supplied sediment on spawning redds (S. Kantoush et al., 2018). Other than in gravel-bed rivers, numerical simulations are a standard tool for assessing the impact of sediment augmentation on a channel-, (e.g. Czapiga et al., 2022) or shoreline evolution (e.g. Coelho et al., 2020) in low-land rivers or coastal zones.

2.4 Eco-geomorphological assessment

This section summarises the state-of-the-art knowledge about eco-geomorphological assessment from a general perspective and in the context of sediment augmentation measures. It presents the basis for the identification of existing research gaps.

Eco-geomorphology is an interdisciplinary approach to studying river systems that integrates hydrology, fluvial geomorphology, and ecology (Thoms & Parsons, 2002). Eco-geomorphological assessment methods are typically based on biotic and/or abiotic indicators. Biotic indicators, like communities of fish (e.g. Grimardias et al., 2017; Reckendorfer et al., 2019), benthic macroinvertebrates (e.g. Espa et al., 2016) or riparian vegetation (Pasquale et al., 2011), as well as suspended particle organic matter (Ock et al., 2015), have been used to investigate effects of SAMs. The selection of biotic indicators varies with location and should be proven to show a measurable and quantifiable relationship to biodiversity (Feld et al., 2010).

Abiotic indicators are often based on field records of hydromorphological parameters. One example is the hydromorphological index of diversity (HMID; Gostner et al., 2013), which is calculated from records of flow velocity and water depth along predefined transects. It provides a quantification measure for the degree of flow complexity and

morphological variability. It was successfully used to assess the variability of channel form (Harrison et al., 2011) and the diversity of channel morphology after a SAM (Schroff et al., 2021a; Stähly et al., 2018). Abiotic indicators can also provide insights into spawning habitat suitability, for example, by assessing clogging (Schroff et al., 2021b).

Hydromorphological assessment can also focus on sediment transport processes. The assessment is then typically based on bedload measurements. Direct measurement of bedload is done with specially designed sediment traps (e.g. Yang et al., 2007). For indirect, continuous measurements, acoustic instruments like geophones, hydrophones, underwater microphones (e.g. Rickenmann, 2017) and acoustic Doppler current profilers (e.g. Rennie et al., 2002) can be used. Passive measurements were also performed in recent years by more sensitive seismic measurements (e.g. Bakker et al., 2020). An indirect measurement of bedload transport, successfully used to assess the impact of SAMs, is using radio frequency identification (RFID) passive integrated transponder (PIT; e.g. Arnaud et al., 2017; Stähly et al., 2019). To create a tracer stone, a hole is drilled into a stone, an RFID PIT is placed inside, and the hole is sealed by silicon. Several tracer stones are placed with the augmented sediment and located with the help of a mobile antenna after a mobilisation event.

Topographic surveys by satellite, aerial imagery or bathymetry can be used to assess morphodynamical development. Topographic surveys were performed to assess the eco-geomorphological impact of SAMs on both reach- (e.g. Heckmann et al., 2017) and basin scale (e.g. Frings et al., 2019). These methods are particularly suited for large-scale and long-term impact assessment at reduced costs due to the typically high degree of automatisation in the data acquisition and processing procedure.

In any case, the selection of assessment methods, the defined indicators, and the interpretation of their development after project implementation must be made carefully. Woolsey et al. (2007) suggest four guidelines for project-specific indicator selection of river restoration projects. They recommend (i) the limitation of indicator numbers, which together represent all project objectives, (ii) the use of direct indicators over indirect ones, (iii) the choice of indicators that require low effort, where financial and time constraints are critical and (iv) the selection of survey intervals, that represent both interannual patterns and years elapsed after restoration. In addition, for an ecologically more holistic approach, combining different assessment methods and indicators can lead to a better representation of the interaction of communities of species and habitat properties (Pander & Geist, 2013).

The recently published *guideline for evaluating the outcome of restoration projects* (EOR) of the FOEN (2019) describes a holistic approach to eco-geomorphological assessment. The EOR comprises twenty-two indicators, which are bundled into ten indicator sets. Indicator Set 1 *Habitat Diversity* (EOR1; Hunzinger et al., 2019) is the only mandatory indicator set for rehabilitation projects in Switzerland and forms the basis of any impact monitoring. It describes the mapping and indicator evaluation of riverbed structures, riverbank structures, water depth, flow velocity, presence of cover and substrate. The

EOR1 has not been applied in the context of SAMs and its validity for assessing the impact of SAMs on habitat diversity.

2.5 River restoration in Switzerland

This section focuses on a current state assessment of the legal framework in Switzerland regarding sediment augmentation measures and the eco-geomorphological state of rivers downstream of reservoirs. It provides another important part of the groundwork for the development of the research questions and the derivation of practical design recommendations based on the scientific results of this thesis.

2.5.1 Legal framework

In Swiss legislation, river restoration[1] is distinguished between river rehabilitation[2], remediation of the negative impacts due to hydropower (hydropower mitigation)[3], and the creation of sufficient space for waters[4] (*Bundesgesetz Über Den Schutz Der Gewässer [Federal Act on the Protection of Waters]*, 1991). Rehabilitation measures are intended to restore the natural functions of watercourses by counteracting former human interference with channel morphology by means of civil engineering. Hydropower mitigation involves re-establishing the longitudinal connectivity for fish migration, mitigating hydropeaking effects, and restoring the sediment regime downstream of an artificial barrier.

Sediment regime restoration as a measure of hydropower mitigation is today the most common case of application of SAMs in Switzerland. A SAM presents a possible operational mitigation measure if it is neither feasible nor proportionate to re-establish sediment continuity across an existing structure by constructional measures (Schälchli & Kirchhofer, 2012). Constructional measures can be the construction of a sediment bypass tunnel at a dam or a drainage channel at a bedload trap.

Even though rarely considered, a SAM can also be integrated into the context of river rehabilitation projects. It can be part of the rehabilitation measure by creating spawning habitat (e.g. Pulg et al., 2013) or the enrichment of structural diversity (e.g. Stähly et al., 2019). It can also promote the functioning of a rehabilitation measure, for example, in dynamic river widenings (Rachelly et al., 2022). A SAM can also mitigate the secondary effects of rehabilitation measures, for example, by compensating downstream bedload deficit because of river-widening works.

[1] DE: Renaturierung; FR: Renaturation

[2] DE: Revitalisierung, FR: Revitalisation

[3] DE: Sanierung der negativen Auswirkungen der Wasserkraftnutzung, FR: Assainissement des atteintes écologiques induites par l'utilisation de la force hydraulique

[4] DE: Sicherung des Gewässerraums, FR: Espace réservé aux eaux

2.5.2 Eco-geomorphological state of Swiss rivers downstream of reservoirs

This section summarises a study aimed to identify sections of high potential for SAMs in the context of hydropower mitigation on a national level (Mörtl et al., 2020). It investigates the impact of interrupted sediment continuity by Swiss hydropower installations on the eco-geomorphological state of their tailwater sections. The study also assesses the influence of reservoir shape, operation type and flushing scenario. This section presents a current state analysis for the main issue addressed by this thesis and provides support for the motivation of research.

The eco-geomorphological state of the tailwater section is classified according to the module *F-Ecomorphology* (Hütte & Niederhauser, 1998) of the *modular stepwise procedure* (MSP; Bundi et al., 1998) of the FOEN (former Swiss Agency for the Environment, Forests and Landscape SAEFL). The corresponding geodata set contains a nationwide evaluation of river segments from on-site inspections. There are four evaluation criteria which assess (i) the water level variability and the type of artificial control on (ii) the bed, (iii) the embankment toe and (iv) the riparian zone. The criteria are combined in a scoring system and classified by the *Eco-Morphology Class* (EMC) between 1 (*natural/near-natural*) and 4 (*unnatural/artificial*). A lower EMC represents a more natural eco-geomorphological state.

From this geodata set, 128 tailwater sections of hydropower installations with a length of $2km$ were identified and isolated by geospatial operations. The resulting sections were assigned the corresponding *Strahler Number* (Strahler, 1957) from a second geospatial data set. The average EMC of each tailwater section was rounded to the nearest integer and linked to the upstream hydropower installation. The results are displayed on a map of Switzerland (Figure 2.6).

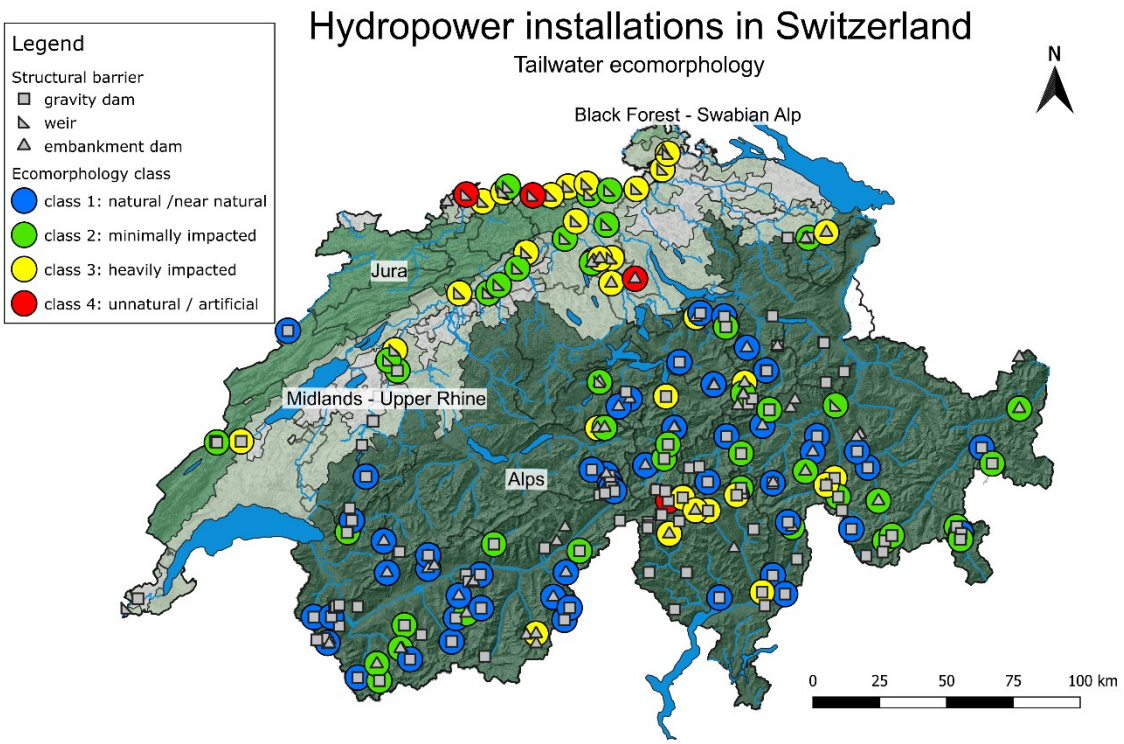

Figure 2.6 Map of hydropower installations in Switzerland with the average Eco-Morphology Class (EMC) of their tailwater sections. The tailwater sections are the sections of the watercourse up to $2km$ downstream from the structural barrier. No data for the EMC represents missing information in the original geodata set. From Mörtl et al. (2020). Copyright 2020 by Imprint. Reproduced by permission of Taylor & Francis Group.

The map shows the spatial dependence of the EMC. There is, for example, a tendency for higher EMC in the lower *Swiss Plateau* (*Midland*s – *Upper Rhein*) than in the higher Alpine region (*Alps*). This can be explained by increased human intervention with distance from the source. The *Strahler Number* reflects the trend. To eliminate biasing from stream order and regional effects, the Eco-Morphology Class Ratio ($EMCR$) is defined as

$$EMCR = \frac{EMC_{ref} - EMC_{tail}}{EMC_{ref}} \tag{2.7}$$

where EMC_{ref} is the EMC of the reference section, and EMC_{tail} is the EMC of the tailwater section. The reference section is the river downstream of the tailwater section until a maximum distance of $6km$ from the dam. A negative $EMCR$ is therefore an unbiased indication of the negative impact of the hydropower installation on the eco-geomorphological state of its tailwater section.

Data about reservoir shape, operation type and the flushing scenario was obtained from the *SEDCON* database (Mörtl et al., 2020) for several Swiss hydropower installations. The *SEDCON* database consists of a survey amongst Swiss dam operators and geospatial data on national rivers. The workgroup *Reservoir Flushing and Emptying* of the *Swiss Committee on Dams* conducted the survey. Sixty-nine hydropower operators replied to questions on reservoir and catchment characteristics, sedimentation issues and flushing

scenarios. The latter two categories demanded only a qualitative response. Results were processed and grouped to improve data consistency. Additional data on sediment-related issues of some Swiss reservoirs was collected by specific literature research to complete the missing survey data information. The parameter *operation type* distinguishes between *daily*, *weekly,* and *seasonal* operations. Classifications and descriptions of the parameters reservoir shape and flushing scenario are shown in Figure 2.7 and Table 2.1.

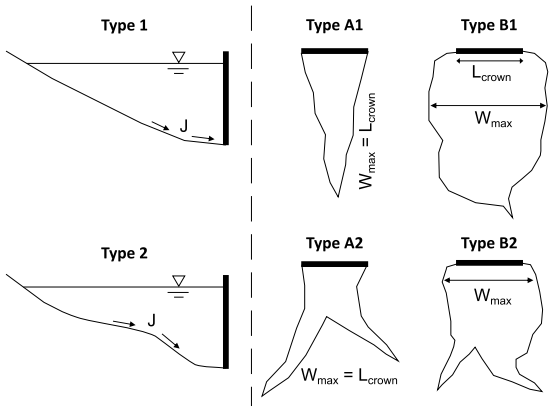

Figure 2.7 Shema of different reservoir shapes used in the *SEDCON* database (Mörtl et al., 2020). Type 1: The thalweg profile is strictly convex, where the longitudinal slope (J) of the thalweg decreases continuously with a smaller distance to the dam. Type 2: The thalweg profile has different variations of S. Type A: The maximal width of the planform shape (W_{max}) is equal to the length of the dam's crown (L_{crown}). Type B: W_{max} is equal to L_{crown}. Type A1/B1: The reservoir has one branch. Type A2/B2: The reservoir has several branches. From Mörtl et al. (2020). Copyright 2020 by Imprint. Reproduced by permission of Taylor & Francis Group.

Table 2.1 Classification and description of different reservoir flushing scenarios.

classification	description
short-term	regular flushing or emptying performed over the last ten years
long-term	regular flushing or emptying performed over the complete lifespan
occasional	single flushing or emptying performed over the complete lifespan
none	no flushing or emptying performed over the complete lifespan

The $EMCR$ was compared against *reservoir shape* (thalweg and planimetric), *operation type* and *flushing scenario* for all hydropower installations with available data (Figure 2.8).

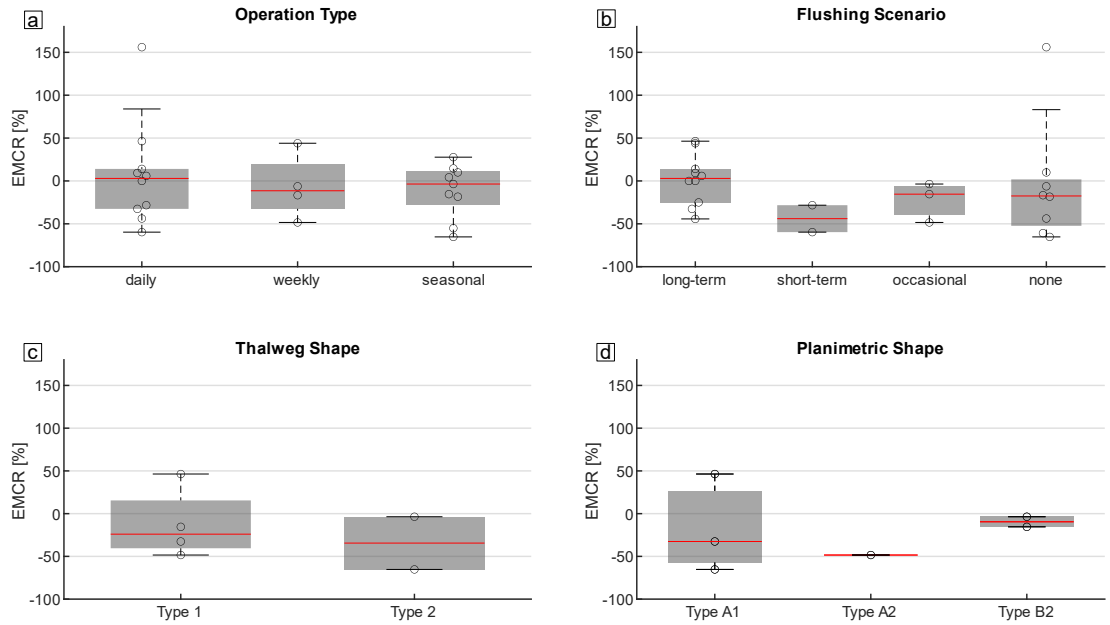

Figure 2.8 Box plot for the relation between the Eco-Morphology Class Ratio ($EMCR$) of the tailwater section of Swiss hydropower installations and different reservoir characteristics and management types. a: *operation type* b: *flushing scenario* (**Figure 2.7**). c and d: thalweg shape and planimetric shape (**Table 2.1**). From Mörtl et al. (2020). Copyright 2020 by Imprint. Reproduced by permission of Taylor & Francis Group.

Comparing the $median\ EMCR$ against the operation type suggests that *daily* and *seasonally* operated hydropower installations have a lower impact on tailwater eco-geomorphology ($[2.9; -3.6]\%$) than *weekly* operated hydropower installations (-11.5%). However, the Interquartile Range (IQR) of the operation types shows a very similar spread ($[-30.9, 14.7]\% \pm 4.2\%$), indicating that the distributions are not significantly different.

The flushing scenario seems to be a more significant factor for the eco-geomorphological state of the tailwater section than the operation type. For example, the p-value (p) of the Student's t-test quantifies a low relationship between the mean of *long-term* and *short-term* flushing scenarios (0.07). The $median\ EMCR$ indicates a lower impact on the tailwater eco-geomorphology for hydropower installations with *long-term* flushing (2.9%) than for other flushing scenarios ($[-44.0, -15.4]\%$). Furthermore, it suggests that *short-term* flushing is less effective for improving the eco-geomorphological state in the tailwater section compared to the one in the reference section (-44.0%) than *occasional* flushing (-15.4%). However, this interpretation is only based on a few samples ($n = [2; 3]$).

The $median\ EMCR$ for reservoirs with thalweg shape *Type 1* (convex profile; -24.0%) and planimetric shape *Type B* ($W_{max} > L_{crown}$; -9.5%) indicates a better eco-geomorphological quality of the tailwater section compared to the corresponding reference section than for reservoirs with different thalweg shape (-34.5%) and planform shape ($[-48.4,\ -32.6]\%$). The influence of the number of connected branches cannot be assessed due to a lack of data.

2.6 Rationale for research

This section outlines the rationales for the research, including the research gaps, research questions and working hypotheses.

2.6.1 Gaps

The literature review outlined important sediment transport processes and influencing factors of bed morphology evolution in response to sediment augmentation in gravel-bed rivers. It revealed that in this context, relatively few studies have focused on the influence of hydrograph shape on sediment transport dynamics. Humphries et al., (2012) studied the influence of floods with varying peak discharge on sediment pulse evolution in response to single sediment pulses in a sinusoidal channel. Plumb et al., (2019) studied the influence of repeated floods with varying duration and flashiness (Poff et al., 1997) on sediment transport dynamics in response to constant sediment supply in a straight channel. Battisacco (2016) studied the influence of transient flow releases with different skewness on bed morphology evolution by analysing parameters such as surface cover or bed roughness. No study has yet focused on the influence of hydrograph skewness on sediment transport dynamics in a straight channel with varying slopes and widths.

Another research gap was identified for the influence of sediment augmentation repetition frequency on bed morphology evolution. Bösch et al., (2016) studied the influence of two consecutive sediment augmentation of in-channel deposits on bed morphology evolution in a straight channel. Elgueta-Astaburuaga and Hassan (2017) studied the influence of multiple sediment pulses on bedload transport and pulse dynamics in a straight channel. No study has yet focused on the influence of augmentation frequency with several repetitions on bed morphology evolution.

In field conditions, the literature shows that existing geomorphic units influence channel processes on a reach scale. However, few studies exist on the interaction between local channel processes and CGUs other than pools or riffles. An exception is the assessment of geospatial patterns of various types of CGUs (Wyrick & Pasternack, 2014) and their evolution during floods six to nine times the bankfull discharge (Woodworth & Pasternack, 2022). Altogether, the governing processes of reach scale channel morphology evolution in response to different disturbances of the discharge and sediment regimes are not fully understood.

Different eco-geomorphological assessment methods exist to assess the impact of restoration measures. The literature review has highlighted what types of assessment approaches were used in the context of SAMs in previous case studies (Section 2.4). So far, the assessment has predominantly been based on a single or minimal number of indicators. In many case studies, the eco-geomorphological changes are quantitatively or qualitatively described without referral to pre-defined objectives and corresponding assessment criteria. It remains unclear whether existing elaborate assessment methods, which consider the full complexity of a diverse mosaic of aquatic and terrestrial habitats

(e.g. Hunzinger et al., 2019), are also valid for quantifying the impact of SAMs on habitat diversity.

2.6.2 Research questions

The motivation for the research was guided by the practical issues raised in the associated research program. The following main research questions (RQs) are based on the identified research gaps in the literature review. They aim to respond to some of the practical issues raised by the research program depending on their relevance and feasibility.

- RQ1: What is the influence of the mobilising flow hydrograph on emerging bed forms from alternating sediment deposits?
- RQ2: How can the persistence of the resulting bed forms be estimated on a morphologic timescale for a given hydrologic pattern?
- RQ3: What are typical emerging bed forms from alternating sediment deposits in different longitudinal riverbed structures (e.g. pools, channels, riffles)?
- RQ4: How can the eco-morphological effectiveness of sediment augmentation measures be quantified?

2.6.3 Working hypotheses

The following hypotheses (Hs) are made regarding the corresponding research questions.

- H1: The hydrograph skewness of the mobilising flood influences sediment transport dynamics from in-channel sediment deposits.
- H2: Sediment augmentation before every mobilising flood, instead of every second, is beneficial for creating morphological diversity.
- H3: Channel geomorphic units influence bedload transport during low-magnitude bed-forming floods coupled with sediment augmentation.
- H4: *Indicator set 1* of the *Swiss Guideline for Evaluating the Outcome of Restoration Projects* is valid for assessing the impact of sediment augmentation measures on habitat diversity.

Chapter 3
Methodology

This chapter presents the methods and data used to investigate the research questions. It is separated into field observations, physical modelling, and numerical modelling. The field study was performed at the Sarine River residual-flow reach downstream of the Rossens Dam in the Canton of Fribourg. Two field campaigns were conducted, in 2020 and 2021, to investigate bedload transport and physical habitat evolution after a sediment augmentation measure from 2016. The experimental flume was designed with dimensions from the field study. It was used for a parametric study addressing the first two research questions. A representative case study reproduces the sediment augmentation measure at the Sarine River to provide information about the model's validity. At the end of the chapter, the numerical model setup is presented. The numerical model was created with the software BASEMENT and represents the experimental flume. It was used to perform hydrodynamical simulations with constant low-flow discharge for different morphological states of the physical flume during the experiment.

Note: Section 3.2 is based on an article submitted to a peer-reviewed journal[1], a published article in a technical journal[2] and an article published in reviewed conference proceedings[3]. Sections 3.3 and 3.4 are based on an article accepted in reviewed conference proceedings[4].

3.1 Methodological approach

A combined methodological approach of physical and numerical modelling and a field study was pursued to address the research questions (**Figure 3.1**).

[1] "Influence of channel geomorphic units on the evolution of river morphology during low magnitude bed-forming floods coupled with sediment augmentation" by C. Mörtl, R. Schroff, S. Stähly and G. De Cesare, under review in *Earth Surface Processes and Landforms*. Contribution of the doctoral candidate according to the *CRediT*: conceptualisation; data curation; formal analysis; investigation; methodology; resources; software; validation; visualisation; writing – original draft; writing – reviewing and editing.

[2] Wirkungskontrolle einer Sedimentzugabe: Habitatvielfalt und Kolmation [Eco-morphological evaluation of a sediment augmentation measure] by R. Schroff, C. Mörtl and G. De Cesare, published in *Wasserwirtschaft*. Contribution of the doctoral candidate according to the *CRediT*: conceptualisation; investigation; project administration; resources; supervision; writing – reviewing and editing.

[3] "GALET: A deep learning image segmentation model for drone-based grain size analysis of gravel bars" by C. Mörtl, A. Baratier, J. Berhet, P. Duvillard and G. De Cesare, published in 2022 in *Proceedings of the 39th IAHR World Congress* (Mörtl et al., 2022). Contribution of the doctoral candidate according to the *CRediT*: conceptualisation; data curation; formal analysis; investigation; resources; validation; visualisation; writing – original draft; writing – reviewing and editing.

[4] "Continuous monitoring of morphological changes from sediment augmentation by field measurements and flume experiments" by C. Mörtl and G. De Cesare, accepted on 23.09.2022 in *Riverflow 2022*. Contribution of the doctoral candidate according to the *CRediT*: conceptualisation; data curation; formal analysis; investigation; methodology; resources; software; validation; visualisation; writing – original draft; writing – reviewing and editing.

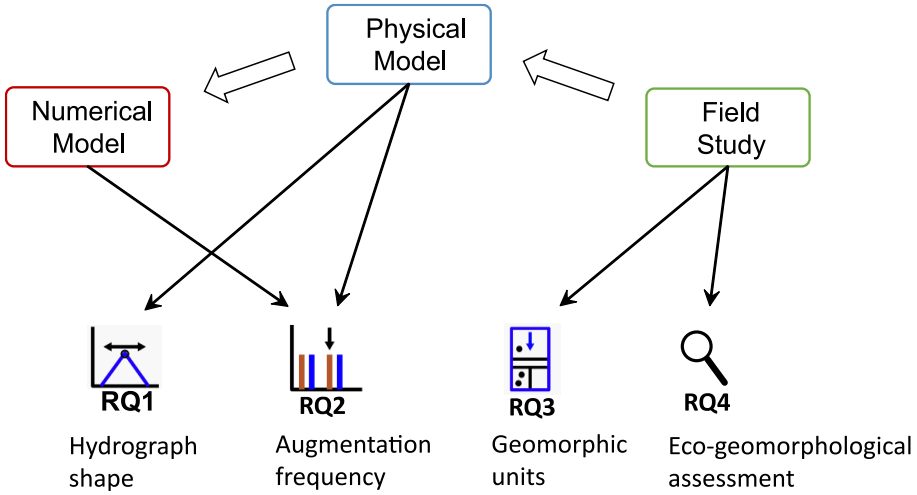

Figure 3.1 Schematic overview of the main methodological approaches to address the research questions (RQs). The large arrows indicate the reference study used for the conceptual design for each approach. The small arrows indicate which approach was used to reply to the RQs.

The physical model was designed with dimension criteria from the field study. Those criteria include channel geometry, bed level elevations, characteristic discharges, grain size distributions, and roughness parameters. The numerical model was designed as a representation of the experimental flume. Morphological processes were only reproduced in the experimental (physical) flume. Hydrodynamic, constant flow simulations were performed with the numerical model for some of the resulting bed morphologies.

3.2 Field observations

3.2.1 Site description

This section describes field measurements at a sediment augmentation site at the Sarine River in Switzerland. Data from reference studies about the study reach (Schroff et al., 2022; Stähly et al., 2019, 2020) was combined with data from new measurement campaigns in the framework of this thesis. The study site is located at the residual-flow reach of the Sarine River, downstream of the Rossens Dam in the canton of Fribourg (**Figure 3.2**: a, b).

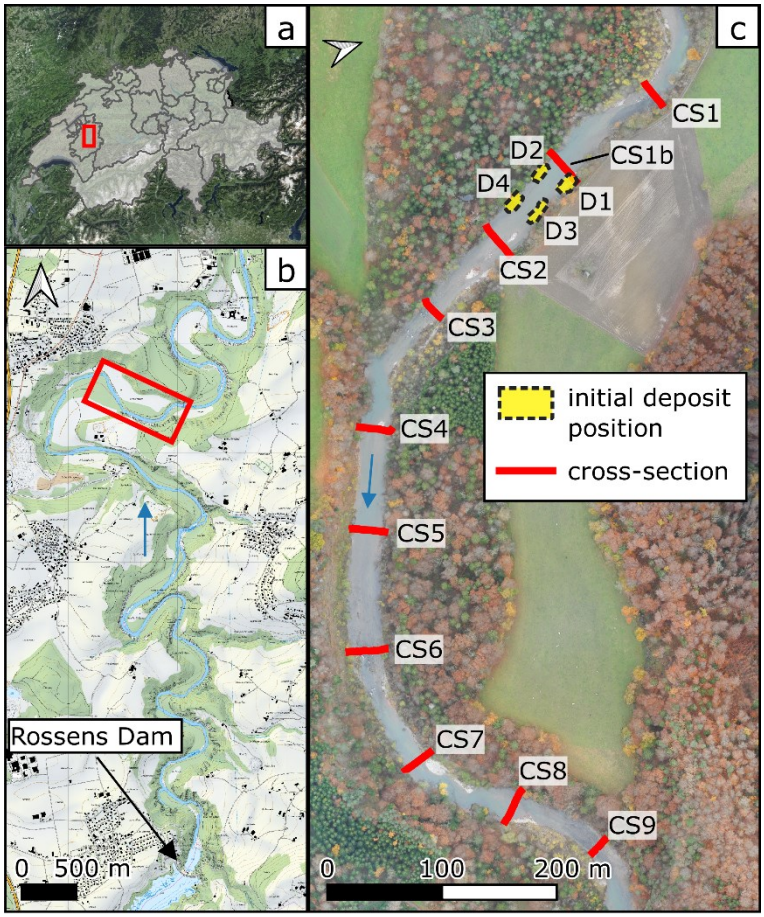

Figure 3.2 Maps and orthophoto of the study site location with initial deposit positions from 2016 and measured cross-sections. a: Map of Switzerland (background image: *swisstopo*); b: Map of Sarine River residual-flow reach downstream of the Rossens Dam (background image: *swisstopo*); c: Orthophoto of the *study reach* with numbered cross-sections (*CS1 – CS9*) and four initial deposit positions (D1–D4). Background image: November 2020, *Research unit Ecohydrology, Zurich University of Applied Sciences (ZHAW)*.

The Sarine is a bedrock alluvial river. The residual flow section has a length of $13km$ and an average slope of 0.3%. Over seven decades of drastically reduced flood activity and interrupted sediment supply have led to a vegetation-driven stabilisation process of the entire floodplain and substantially reduced active channel width (Tonolla et al., 2021). Today, the average channel width of the residual-flow reach is $25m$. The incision has progressed down to bedrock on a substantial section of the residual-flow reach.

In 2016, $1'000m^3$ of sediment from the adjacent floodplain was placed in the river (Stähly et al., 2019). The goal was to increase the hydromorphological diversity in the near downstream section and to study the efficiency of the injection method. The mean diameter (d_m) of the augmented sediment corresponded to 57mm. The volume was selected to supply a sufficiently high amount of sediment to expect measurable morphological changes at a low cost. The sediment was placed in four alternating deposits along both riverbanks, $9km$ downstream of the dam. The deposits were partly mobilised during an artificial flood in September 2016 (*Flood 2016*). No more bed-forming flows occurred until another artificial flood in October 2020 (*Flood 2020*).

The *study reach* has a length of $900m$ and started $100m$ upstream of the initial deposits (Figure 3.2: c). In the reference studies, nine cross-sections (*CS1–CS9*) were defined with an equal spacing of around $95m$. Along the left bank until *CS2*, the alluvial gravel has cemented and collapsed into enormous blocks that slide on the ancient glacial-lacustrine clays (Weidemann, 2005). The right bank, downstream of the river bend between *CS3* and *CS4,* consists of a cliff of molasse rock. Along the left bank around *CS3*, a small stripe of loosely vegetated sediment is present. Mature hardwood forests cover all remaining banks. Aquatic vegetation is limited to patches of loose thread algae, which become detached during bank-forming flow (Döring et al., 2018). Further site description and examination of the 2016 sediment augmentation measure and *Flood 2016* are documented in the reference studies.

The four deposits of the 2016 sediment augmentation measure were labelled in the downstream direction (*D1–D4*). The part of the active channel, where the flow varied greatly from the influence of the initial deposits, was defined as the *hydraulic impact zone* (in the reference studies called the "replenishment zone"). It extends from the upstream end of *D1* to 1 channel width (b_0) downstream of *D4*. This length was derived from experience in the field and laboratory experiments (Battisacco et al., 2016). The active channel from *D1* to $300m$ downstream was defined as the *target section (*in the reference studies called "impact zone"). The remaining part of the active channel inside the *study reach* was defined as the *reference section* (in the reference studies called "rest zone"). The unwetted areas of the deposits were not considered part of the active channel after 2017 because vegetation encroachment had stabilised the bars to a point where they were no longer considered mobilisable during low flood events (<Q2).

3.2.2 Grain size distribution from drone imagery

The GSD of a river plays a crucial role in its classification and the understanding of its morphological and hydraulic processes. Measuring a representative GSD at different river sections still poses a fundamental challenge today. Many analogue sampling techniques for GSD exist but require a trade-off between time-consuming measurement campaigns and inaccuracy due to insufficient or biased sampling. Simple semantic segmentation image processing solutions like *BASEGRAIN* (Detert & Weitbrecht, 2012, 2013) allow for the automatisation of the process but often present considerable shortcomings in object recognition and application in complex environments (e.g. vegetation, shade, or humidity). A few deep learning models are also starting to emerge, such as *Sedinet* (Buscombe, 2020), *GRAINet* (Lang et al., 2021) and *Clast Size Mapping* (Soloy et al. 2020). Common shortcomings are the lack of training data, as deep learning models require large amounts of data to be effective. A direct application on a user-friendly interface is not always the case, or the models are based on texture analysis, depriving the user of the possibility of visual checks.

This subsection presents the deep learning image segmentation model for drone-based grain size analysis of gravel bars called *GALET*. It was developed by the company *styx4D*.

In the framework of this thesis, the performance of *GALET* was assessed, and the model was applied to determine the GSD of bedload and the degree of armouring of a natural bar at the Sarine River study site. Drone photos from different drone types, varying flight heights and resolutions were used to test the performance of *GALET* against analogue reference measurements at three different study sites (Table 3.1).

Table 3.1 River characteristics and measurements at three study sites for the assessment of *GALET*.

	Sarine River	Ain River	Chéran River
River characteristics			
Planform morphology	meandering	alternating bars	alternating bars
Average slope [−]	0.003	0.02	0.01
Flow regime	residual flow	near natural reference reach & residual flow study reach	near natural
Sediment regime	sediment starved	near natural reference reach & sediment starved study reach	near natural
Geology	limestone	limestone	limestone
Measurements			
Investigated gravel bars [−]	1	15	4
Flight height drone $[m]$	$[5;\ 10;\ 20]$	5	10
Resolution drone photos $[mm/pixel]$	$[0.7, 1.5]$	$[0.6, 1.1]$	3
Environmental conditions	cloudy (shadows)	sunny; vegetation on some bars	sunny
Analogue field measurements	4 *Fehr line counts* (~500 grains)	21 *Fehr line counts* (~5000 grains)	40 individual cobble measurements
Laboratory analysis	1 sieve analysis	-	-

To test the accuracy of individual grain size measurements by *GALET*, reference cobbles in the range of $80mm$ to $290mm$ were measured and tagged in the field by a differential global positioning system (DGPS). The grain size was chosen for easier manual detection on the orthoimages. The intermediate grain axis (b-axis) was used for a characteristic representation of the grain diameter. The dimensions calculated by *GALET* were then compared to the analogue field measurements.

Analogue field measurements of GSD were performed with *Fehr line counts* (Fehr, 1987). This method relies on grain counts by size classes and yields a grid-by-number GSD. The measurement of the b-axis likewise represents the characteristic grain size. To ensure good representativity of the sample, a minimum of 150 stones with at least 30 stones in the middle fractions should be measured and counted along a transect (Fehr, 1987). Typically, at least two measurements were performed on a gravel bar, one parallel and one perpendicular to the flow direction. The performance of *GALET* was tested on rectangular extracts around the transects from the field. The conversion from the area-by-number GSD of *GALET* to the grid-by-number GSD of the *Fehr line count* was done with the *modified cube model*.

The degree of deviation from the analogue reference measurement is given as the difference in the relative occurrence of particles by size class

$$\Delta RO_i = RO_{i,GALET} - RO_{i,analog} \tag{3.1}$$

where $RO_{i,GALET}$ is the relative occurrence of grains of a size class i calculated by GALET, and $RO_{i,analog}$ is the relative occurrence of grains of a size class i from analogue reference measurements.

The degree of armouring is calculated as

$$DOA = \frac{d_{50,GALET}}{d_{50,sub}} \tag{3.2}$$

where $d_{50,GALET}$ is the d_{50} of the surface layer calculated by GALET, and $d_{50,sub}$ is the d_{50} of a subsurface volumetric sample from a depth of $20cm$, which was analysed in the laboratory by sieve analysis. To be comparable to the results of *GALET*, the grain fraction smaller than $8mm$ was excluded from the sieve analysis.

Analogue measurements of the b-axis of 40 randomly selected cobbles at the Chéran River in the range of $80mm$ to $290mm$ were compared to the results of *GALET*.

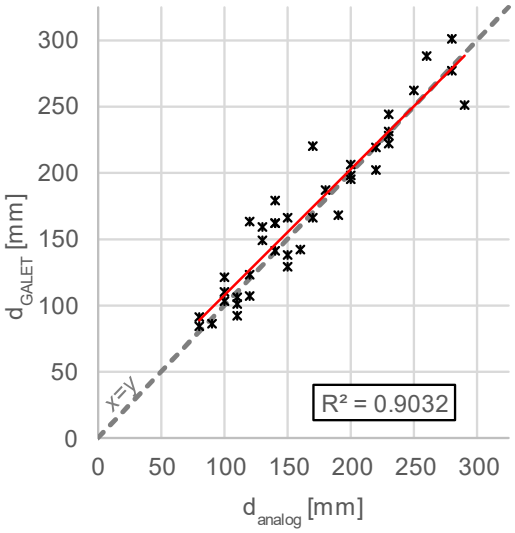

Figure 3.3 Scatter plot of the b-axis of 40 cobbles at the Chéran River from analogue measurements (d_{analog}) and from calculations by GALET (d_{GALET}). The red line represents the linear fit.

The mean error (ME) of the length of the b-axis calculated by *GALET* compared to the analogue measurements is $4.5mm$. It means that *GALET* tends to overestimate the grain sizes of individual cobbles. The difference is largest for cobbles from $120mm$ to $150mm$. The R^2 of the linear regression is 0.9, and the root mean square error ($RMSE$) is $19.1mm$. The relative absolute error (RAE) is 0.29, and the root relative squared error ($RRSE$) is 0.32.

For the validation of the model, the GSD of 25 sample areas at the Sarine River and the Ain River were calculated by GALET and compared against analogue reference measurements.

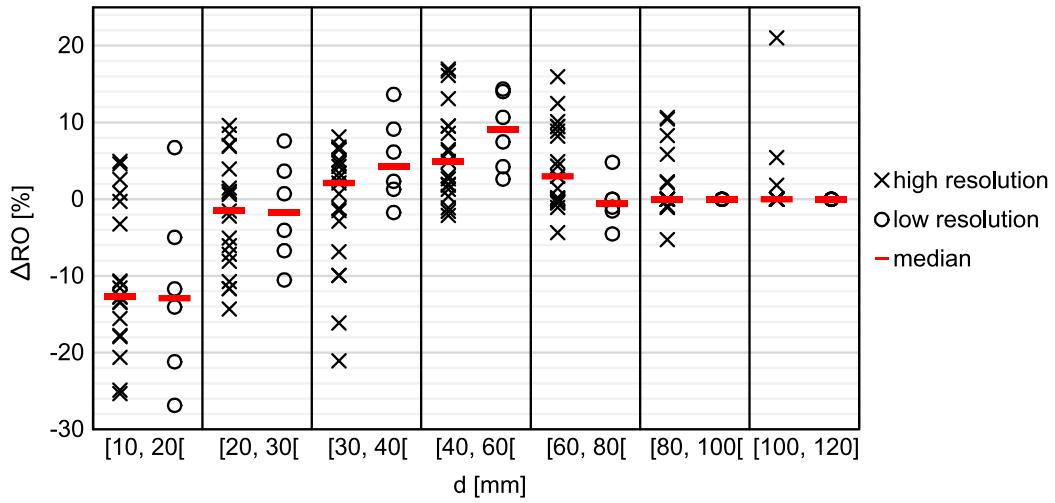

Figure 3.4 Graphic of the difference of relative occurrence (ΔRO) of 25 grain size distributions (GSDs) from the Sarine River and the Ain River between *GALET* and analogue reference measurements by size class and different orthoimage resolution. The variable d is the characteristic particle diameter (b-axis). High resolution signifies $[0.5, 1[mm$ per pixel. Low resolution signifies $[1, 1.5]mm$ per pixel.

The finest size class ($[10, 20]mm$) has the lowest ΔRO of all size classes for both resolutions ($[-25.3, -26.9]\%$). The $median\ \Delta RO$ is -12.7% and -12.9% for high and low resolution. For size classes from $20mm$ to $80mm$, the $median\ \Delta RO$ ranges from -1.6% to 4.9% for high resolutions and -1.7% to -9.1% for low resolutions. For size classes from $80mm$ to $120mm$, the $median\ \Delta RO$ is 0 for both resolutions. The d_m of all 25 GSDs from both *GALET* and analogue reference measurements were compared for both resolutions together. The mean absolute error (MAE) is $6.1mm$, and the $RMSE$ is $8.9mm$.

The spatial distribution of the d_{50} and the DOA from *GALET* were visualised for a gravel bar at the Sarine River (**Figure 3.5**).

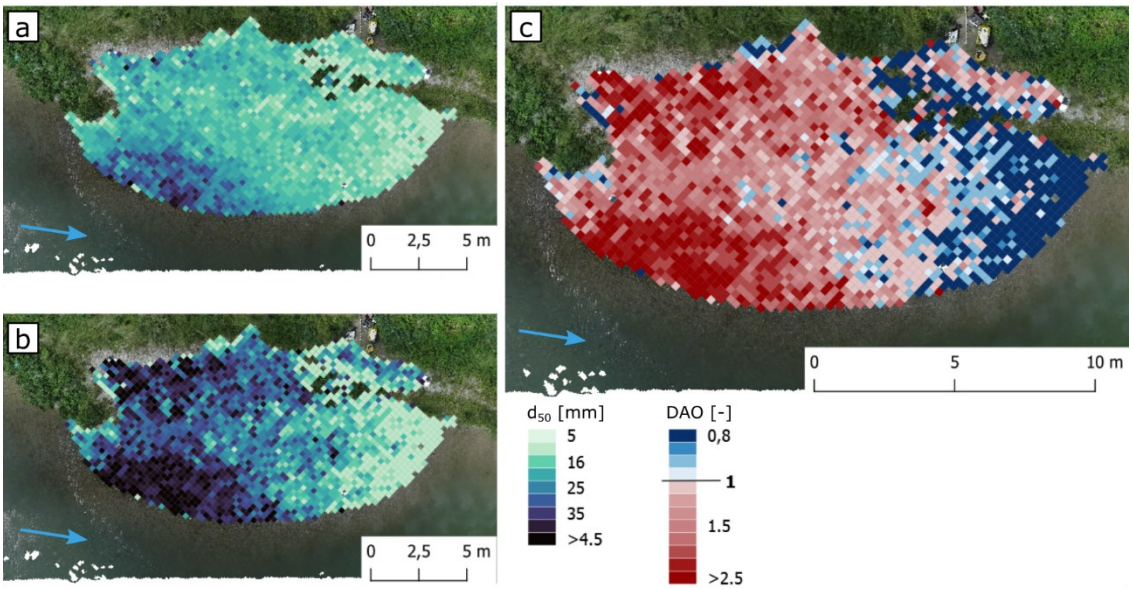

Figure 3.5 Orthophotos with the spatial distribution of different grain size parameters of the surface layer of a natural gravel bar at the Sarine River calculated by *GALET*. a: Median particle diameter (d_{50}) by number. b: d_{50} by weight. c: Degree of armouring (DOA). The resolution of the results is $0.25m \times 0.25m$. The blue arrows indicate the direction of flow.

The d_{50} of the sub-surface sample is $18mm$. The armour layer is most pronounced near the parallel waterline, with a d_{50} by weight up to four times the d_{50} of the subsurface sample. The area of highest DOA coincides well with the location of the initial mid-channel bar before the artificial flood of 2016 and the area of the adjacent riverbank on the upstream side. A DOA below 1.5 is calculated along the longitudinal centre axis. The DOA generally decreases towards the tail. The lowest DOA (< 1) is found directly at the tail of the bar.

The following questions about the methodology of GALET were addressed:

- What is the accuracy of individual grain size assessment using GALET?

This question addresses the quality of measurement once one grain is successfully detected. *GALET* estimated cobble size from $80mm$ to $290mm$ with a RAE of 0.29. A linear regression shows that the model overestimates the lower range of tested cobbles. The small number of samples (40) reduces the reliability of the findings. The low resolution of the orthoimages ($3mm$ per pixel) can lead to poorer results than high-resolution images. For the quality of grain size measurements in the range of pebbles from $10mm$ to $80mm$, these results can only indicate the order of magnitude. In addition, *GALET* only has the image information of the orthogonal projection of each grain. Three-dimensional orientation and coverage by other grains inevitably lead to errors. To which degree these errors impact the accuracy of the results has yet to be investigated for *GALET*.

- What is the accuracy of grain size distribution assessment by GALET?

The highest deviation is found for the smallest grain size class. GALET detects fewer pebbles from $10mm$ to $20mm$ than recorded by the reference measurements. This trend is reversed for pebbles from $30mm$ to $60mm$. The two types of resolution of orthoimages tested yield similar results, with a small deviation only in the medium-size classes. The two resolutions tested were relatively high, with a maximum value of $1.5mm$ per pixel. The $median\ \Delta RO$ for the largest size classes from $80mm$ to $120mm$ equals 0 because there were often no cobbles in the test patches around the transects. The d_m from *GALET* agrees well with the d_m from the 25 analogue reference counts. The MAE and the $RMSE$ are $6.1mm$ and $8.9mm$. This result is good compared to similar models. The model *GRAINet*, for example, was tested against human performance on 17 random tiles ($1.25m \times 0.5m$) and yielded a $RMSE$ of $17mm$ (Lang et al., 2021). However, their test is based on digital line samples from different experts and orthoimages with lower resolution ($2.5mm$ per pixel). Here, the comparison between GSD from *Fehr line counts* and *GALET* is based on a conversion from grid- to area sampling. The different sampling spaces can reduce comparability. All samples were taken at locations of relatively homogeneous GSD with few to no outliers. It is therefore assumed that the used method of comparison provides representable results.

- What are the differences between GALET and analogue methods for grain size distribution assessment?

A GSD from a limited number of analogue sample measurements is commonly biased. In their paper on evaluating the accuracy of in-situ, analogue grain size measurements using Wolman's methodology (Wolman 1954), (Rice and Church 1996) estimated that biases depend on the grain size, the number of samples taken, and the quantile measured. Their work showed that the measurement of a d_{50} is accompanied by a relative error ranging from $\pm 20\%$ to $\pm 50\%$ for a survey of 100 grains, with larger errors on the finest classes. It can be supposed that a model with a global detection scheme like *GALET* is much less biased. The number of samples is significantly higher, and the complete mapping of natural heterogeneities in the surface layer is ensured. The measurements are also 100% reproducible for the same input data and model parameters. The quality of the GSD depends again on the segmentation mask and the vectorisation algorithm.

- What parameters can influence the accuracy of grain size distribution assessment by GALET?

No sensitivity analysis was performed to quantify the effect of different input parameters on the quality of the outcome GSD. From experience, the quality of orthoimages presents a critical parameter. On the one side, the quality depends on the accuracy of the assembly of the drone photos. If not georeferenced correctly, drone photos can cause deficient image reconstruction and blurry or displaced strips in the overlap zones. On the other side, the resolution of the orthoimage determines the smallest detectable grain size. If the

resolution is too low, small grains are not detectable. Other impact parameters are supposed to be environmental noise factors like shadow, reflection, and vegetation and grain appearance factors like size, shape, surface exposure and geology. Those could lead to no or false detection if the deep learning mask were not sufficiently trained to integrate them.

- What findings has GALET made possible for assessing armouring at the Sarine?

GALET was used to calculate the spatial distribution of the DOA and the GSD of a natural gravel bar at the Sarine River. It could show where on the bar the DOA was highest. As expected, fining of the surface occurred towards the bar's tail. This phenomenon was also observed along the upstream and downstream thirds of compound gravel bars of a large gravel river (Rice & Church, 2010). Another interesting finding was that the area of highest DOA coincided well with the location of the initial mid-channel bar before the flood. This result yields insides on bar formation and transformation process in sediment starved reaches from artificial flooding. Where the DOA is high on parts of existing gravel bars, they may be more resistant to intermediate floods and favour bar expansion rather than shifting and sorting processes. The variables d_m and d_{50} of the captured surface of the gravel bar are $37mm$ and $28mm$.

3.2.3 Flood hydrographs and sediment transport capacity

The *Flood 2016* hydrograph at the study site was part of the existing data from the reference studies. The *Flood 2020* hydrograph at the study site was determined from continuous water level measurements during the flood. A rating curve was established from eight associated point pairs of steady outflows from the dam and calculated water levels from the logger. The coefficient of determination (R^2) is greater than 0.99, and the root mean square error ($RMSE$) is $0.045m$. The rating curve is provided in the appendix (Section A2).

The bedload transport capacity and the threshold of motion for bedload transport were calculated for *Flood 2020* from empirical formulas based on the Shields criterion (Badoux & Rickenmann, 2008; Rickenmann, 2001). For this approach, no limitation of bedload availability was assumed. Grain-form roughness effects were neglected. The presence of an armour layer, with the grain size distribution (GSD) of the augmented sediment, was considered. The GSD of the bedload corresponded to the GSD of the surface layer of a downstream natural gravel bar. It was obtained from drone imagery with the image segmentation model *GALET* (Mörtl et al., 2022). Hydrographs and the average bedload transport capacity of *Flood 2016* and *Flood 2020* are shown in Figure 3.6

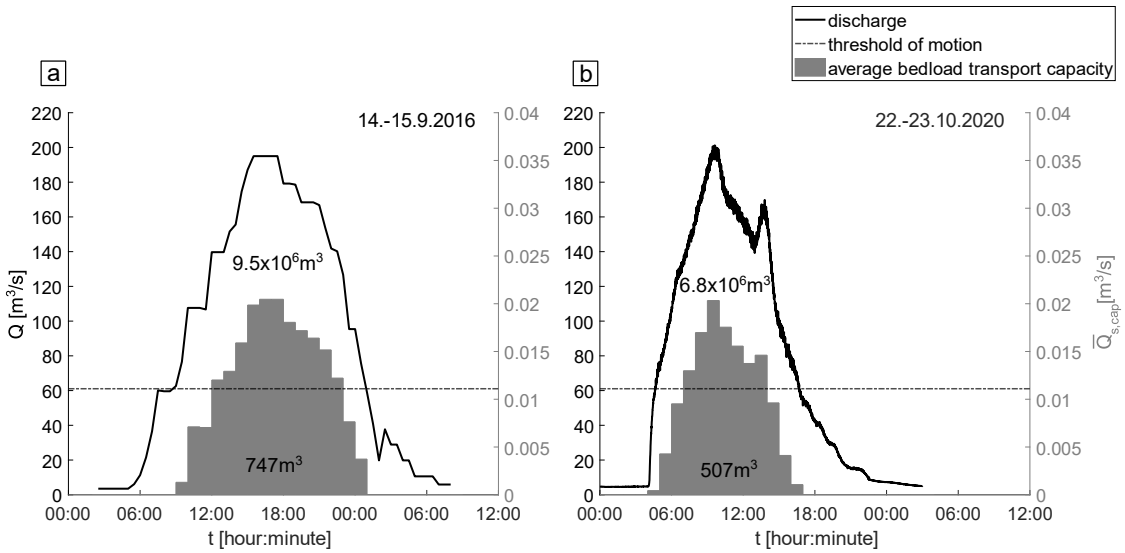

Figure 3.6 Hydrographs and average bedload transport capacity of *Flood 2016* (a) and *Flood 2020* (b). The variable t is the time, Q is the discharge, and $\bar{Q}_{s,cap}$ is the average bedload transport capacity. The horizontal line represents the threshold of motion for bedload transport of the augmented sediment. The label at the top of the hydrographs represents the total flood volume. The label at the bottom of the hydrographs represents the total bedload transport capacity.

This approach only estimates the order of magnitude of the event-based transport capacity It is based on empirical analysis of an extensive laboratory and field data database and results in a simplified calculation, which does not consider local hydromorphological characteristics. In addition, the GSD of the bedload is likely to be finer than the GSD of the natural bar, which can lead to an underestimation of the total transport capacity. The results are highly sensitive to changes in some parameters.

3.2.4 Sediment supply

After decades of interrupted sediment transport continuity by the dam, fine bedload had been largely washed out, and the yearly bedload transport was almost zero (Tonolla et al., 2021). The sediment supply in the study reach during *Flood 2016* and *Flood 2020* was attributed mainly to the augmented sediment from the artificial deposits. The volume loss was estimated from elevation measurements and the change of unwetted area during mean flow (**Figure 3.7**).

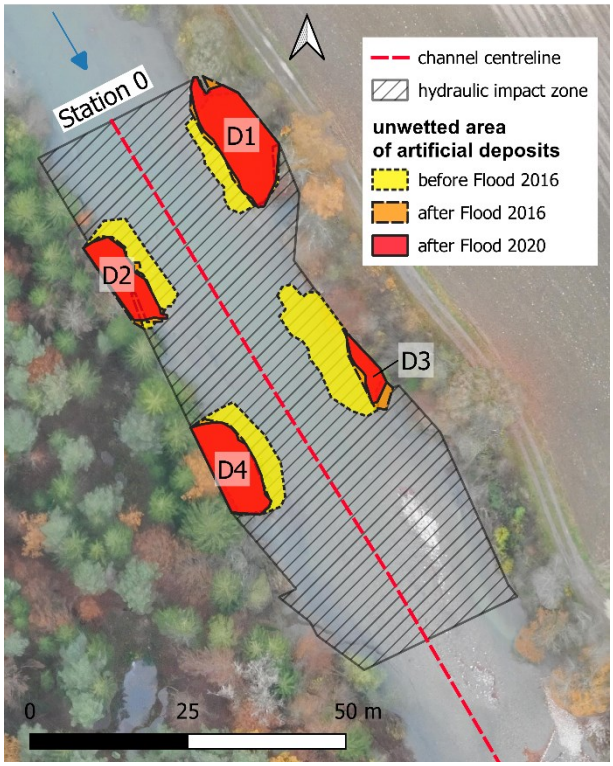

Figure 3.7 Orthophoto with the evolution of the unwetted area of the artificial deposits during mean flow from before *Food 2016* (initial) to after *Flood 2020*. The labels *D1 to D4* identify the deposit number. Background image: November 2020, *Research unit Ecohydrology, Zurich University of Applied Sciences*.

The initially placed artificial deposits contained $1000 m^3$ of sediment and caused a blocking ratio of $1/3\ b_0$ during mean flow. Here, the blocking ratio refers to the ratio of the wetted cross-sectional area of two deposits perpendicular to the main flow direction, divided by the wetted cross-section of the channel without the deposits.

Approximately $708 m^3$ of sediment was eroded from the artificial deposits during *Flood 2016*. Considering the calculated bedload transport capacity of *Flood 2016*, this results in a supply-to-capacity ratio of 95%. During *Flood 2020*, only $11 m^3$ are estimated to have been eroded from the remnants of the artificial deposits. Apart from the shorter flood duration, the smaller blocking ratio reduced the erosive force, and vegetation stabilised the embankment. The low supply-to-capacity ratio (2%) indicates a significant lack of renewed bedload supply compared to the transport capacity of the flood. The erosion rates during both floods varied strongly between the four artificial deposits, which was likely influenced by their alternating positions.

The volume of the artificial deposits was approximated by a cuboid geometry from the mapped perimeter and averaged elevation measurements of the unwetted area. The accuracy of the volume estimation is subject to considerable uncertainty because of the incomplete information on the initial bed topography and the geometrical simplification. The accuracy range was estimated to amount to $\pm 20\%$ based on the existing data.

3.2.5 Mapping of channel geomorphic units

CGUs were mapped during the two measurement campaigns before and after *Flood 2020*, from the initial position of *D1* to $370m$ downstream along the river. The ROE guidelines provide detailed examples of how to identify CGUs according to Table 3.2 in the field. The mapping was performed by Robin Schroff in the framework of his Master Project: *Eco-morphological evaluation of a residual-flow reach restoration measure - Enhancing habitat assessment with a new substrate degradation indicator and digital surveying*. The project was supervised by the author of this thesis.

Table 3.2 Description of channel geomorphic unit (CGU) types. Adapted from (Hunzinger et al., 2019).

CGU type	description
bar	Local sediment deposit, not submerged during low-flow conditions, in the middle of the river or along the bank.
pool	Local deepening of riverbed due to erosion by secondary currents and/or eddies.
glide	Elongated, deep channel section with slow current. Wetted width/depth ratio low (<10–12).
riffle	Broad, elevated portion of the riverbed with slow current and a low gradient. Wetted width/depth ratio higher (>10–12).
run	Steep channel section with swift current, with a high gradient.
backwater	Wetted area with no current during low-flow conditions (“dead end”).
shallows	Low-current zone along the bank or a gravel bar.
step	Natural or artificial drop followed by a plunge pool. The step begins at the point in the upper waters where flow is accelerated towards the drop and ends where the jet enters the lower waters; here the plunge pool begins.
plunge pool	Larger depression following a step.
artificial bed	Local artificial stabilisation of the riverbed, which is not mapped as a step.

CGUs were mapped over the entire active channel width, including the unwetted part of the bed and with a minimum size of $4m^2$. High mapping precision ($< 0.5m$) was achieved thanks to a mobile geographic information system (GIS) application linked to a global navigation satellite system (GNSS) real-time kinematic positioning (RTK) antenna.

3.2.6 Tracking of bedload particles

In the study described by Stähly et al. (2019), 489 tracer stones with RFID PIT tags were distributed equally amongst the four artificial deposits of the 2016 sediment augmentation measure at the time of the initial placement. The tags were placed in three different vertical layers at different depths from the surface. The tracer stones were selected to represent either the mean diameter ($d_m = 57\text{mm}$) or the 90$^{\text{th}}$ percentile diameter ($d_{90} = 113mm$) of the GSD of the augmented sediment. The median grain size diameter (d_{50}) of the augmented sediment is $39mm$. The initial positions of the tracers were recorded, and the positions after *Flood 2016* were mapped in a field campaign by a handheld antenna.

In the scope of this thesis, tracers were searched in a second field campaign from the initial position of *D1* to $650m$ downstream in March 2021, after *Flood 2020*. Since no bed-forming flows occurred during the study period other than *Flood 2016* and *Flood*

2020, tracer stone position and bed morphology are assumed not to have significantly changed outside the time of these two events. Table 3.3 shows the attributes assigned to the tracer stones.

Table 3.3 Attributes of tracer stones. The variable d_m is the mean diameter and d_{90} is the 90th percentile diameter. The acronym CGU means channel geomorphic unit. Attributes marked with an asterisk (*) were recorded with the initial placement and after both floods (*Flood 2016* and *Flood 2020*). Attributes marked with ** are calculated from those attributes (*) after both floods.

attribute	type	range/categories	description
station*	numerical	$[0, 900]m$	Station of the perpendicular projection of a tracer location on the river centre line, which starts at the upstream end of *D1* and runs in the downstream direction.
transport distance**	numerical	$[0, 900]m$	Difference of the station of a tracer before and after a flood.
sphericity	numerical	$[0, 1]$	Calculated from the lengths of its axes (Sneed & Folk, 1958).
zone*	categorical	D1, D2, D3, D4, bar, pool, glide, riffle run, backwater, shallows, step, plunge pool, artificial bed	Zone of the tracer position. Includes the four artificial deposits (*D1* to *D4*) and the CGU types of the riverbed (see Figure 3.2).
movement**	categorical	moved, unmoved	*moved*: transport distance $\geq 2m$ AND zone is a CGU *unmoved*: NOT *moved*
relocation**	categorical	relocated, persistent	*relocated*: changed from a CGU to another *persistent*: remained in the same CGU
size	categorical	dm, d90	*dm*: the diameter is about $d_m = 57\text{mm}$ *d90*: the diameter is about $d_{90} = 113\text{mm}$
layer	categorical	top, middle, bottom	Initial burial depth (h_b) of tracers in the artificial deposits. top: $h_b = 0m$ middle: $h_b = [0.5, 1]m$ bottom: $h_b \approx 1.5m$

Only detected tracers were included in the statistical analysis. The variables developed for the particle analysis do not refer to an absolute tracer number but to a relative change amongst detected tracers. The *mobilisation rate* is the ratio of *moved* to the total number of detected tracers. The *deposit erosion rate* is the *mobilisation rate* for tracers which were detected inside an artificial deposit zone before a flood and outside this zone after the same flood. The probability density function (pdf) of tracer numbers along the channel centreline (*station*) was smoothed with a one-dimensional gaussian kernel density function (kdf) with one-third of the default bandwidth. For the maximum water depth (h_{max}) displayed with the pdf, CS measurements from the reference studies were included, which were spaced much closer in the corresponding section.

Several factors can impact the ability to detect RFID PIT tags. Arnaud et al. (2015) name antenna size and shape, the effect of battery power and the operator as important influencing factors on the detection success. The mobile antenna has a circular electronic loop with a diameter of $0.7m$ and works with a 12v-7Ah battery. The RFID PIT tags work at a frequency of $134.2kHz$. The detection distance with the mobile antenna is up to $0.6m$.

Tracers buried at greater depths under the bed surface could not be detected. In addition, a signal collision can occur for tracers in a range of $0.3m$ (Cassel et al., 2017). These technical limitations can reduce recovery rates in areas where multiple tracers have been deposited. Another limitation is that areas with a water depth deeper than $1.5m$ were not searched. The unsearched area in both campaigns amounts to about 5.9% of the total area of all CGUs identified in 2020. This limitation leads to a lack of data in pools and a substantial limitation of expressiveness concerning this CGU type. Since the material was the same and the operators did not change during a measurement campaign, other limitations that could bias the location of tracer detection are assumed to be minor. In general, the limitations of our particle tracking should lead to an underestimation of the effect of CGUs on bedload transport.

3.2.7 Assessment of hydromorphological changes

Water depth (h) and flow velocity (v) were measured along ten cross-sections (CSs) during mean flow conditions (**Figure 3.2**: c). Data from the reference studies includes a measurement series before and after *Flood 2016*. In the framework of this thesis, a third series of measurements was carried out after *Flood 2020*, including an additional CS (CS1b) at the upstream end of D1.

The measurements are performed with a regular spacing of $1m$ along the ten CSs. Like for the mapping of CGUs, only points along the CS falling inside the active channel were measured. Exposed gravel bars were included. Riverbanks, islands, or gravel bars stabilised by vegetation were excluded. Water depth was measured by the measuring rod of a handheld Acoustic Doppler Velocimeter (ADV; *SonTek FlowTracker*). Flow velocity was measured with the same device at $0.6h$ from the surface to approximate the depth-averaged velocity (e.g. Leopold et al., 1965). Measurements were recorded for $15s$ to $45s$ at $1Hz$. The average of each series was retained as one measurement point.

Bed level profiles were developed from the water depth measurements in reference to the water level during each measurement campaign. Since bed level changes can impact the water level elevation, our approach tends to slightly underestimate vertical bed level changes. This underestimation is due to the fact that the actual water level is lower than the reference level if the CS experiences net erosion. The opposite effect sets in for a net deposition. Apart from that, a standard estimation of the error range in this approach is given by the value of the 84th percentile diameter (d_{84}) of the GSD of the bed substrate. Like the calculation of bedload capacity, the GSD of the armour layer is approximated by the GSD of the augmented sediment. The d_{84} amounts to $84mm$. The error range of the velocity measurements was automatically calculated from the recorded time series. It was typically below $0.01\ m/s$.

The $HMID$ quantifies the hydromorphological diversity on a reach scale and provides a metric to quantify habitat heterogeneity. It is based on the coefficient of variation (COV) of h and v (Gostner et al., 2013). They also developed a relation between $HMID$ and the

variability of hydraulic units and geomorphic patterns (Table 3.4). In a laboratory experiment, Rachelly et al. (2021) showed that the $HMID$ is higher during mean flow in experiments with sediment equilibrium conditions than in supply-limited conditions.

Table 3.4 Categories of the hydromorphological diversity index (HMID; Gostner et al., 2013).

	description
$HMID < 5$	Channelised and morphologically heavily altered sites with only minor hydraulic variability and geomorphic patches.
$5 \leq HMID < 9$	Limited variability of hydraulic units, but hydromorphological patches typical to an intact natural state are not developed.
$HMID \geq 9$	Morphologically pristine sites where gravel-bed streams fully develop their spatial dynamics, showing the complete range of hydraulic habitats

The $HMID$ was calculated separately for the *target section* and the *reference section* and together for the entire *study reach*. *CS1b to CS4* lie inside the *target section*, and the remaining CSs (*CS1 & CS5–CS9*) are inside the *reference section*.

The locations of the CSs were selected to comprise all hydromorphological units present at the site. This approach tends to produce overrated $HMID$ reference results because the spacing is adapted in a way which favours existing structural diversity.

3.2.8 Assessment of habitat diversity

Indicator set 1 of the *guideline for evaluating the outcome of restoration projects* (EOR1) was applied to assess habitat diversity. Its six indicators and attributes are listed in Table 3.5. The assessment was performed by Robin Schroff in the framework of his Master Project: *Eco-morphological evaluation of a residual-flow reach restoration measure - Enhancing habitat assessment with a new substrate degradation indicator and digital surveying*. The project was supervised by the author of this thesis.

Table 3.5 Indicator and attributes of *Indicator set 1* of the *Guideline for evaluating the outcome of restoration projects* (EOR) of the Swiss Federal Office of the Environment (2019). The variable σ is the standard deviation, μ the arithmetic mean and COV the coefficient of variation. Indicator 1.6 is distinguished between two attributes because a calculation approach is currently only available for the attribute *mobilisability* (A2).

indicator	type	categories or variable
1.1 Riverbed structures	categorical	**Structure**: 1. bar, 2. pool, 3. glide, 4. riffle, 5. run, 6. backwater, 7. shallows, 8. step, 9. plunge pool, 10. artificial bed (see **Table 2.1**)
1.2 Riverbank structures	categorical	**Profile**: 1. linear, 2. convex, 3. concave; **Composition**: 4. permeable embankment, 5. impermeable embankment, 6. unconsolidated material, 7. root systems, 8. rock; **Slope**: 9. gentle ($\leq 1/2$), 10. steep ($> 1/2$)
1.3 Water depth	numerical	1. σ, 2. μ, 3. COV
1.4 Flow velocity	numerical	1. σ, 2. μ, 3. COV
1.5 Presence of cover	categorical	**Cover type**: 1. submerged stones, 2. non-submerged stones, 3. small organic particles, 4. medium-sized organic particles, 5. large branches/large roots, 6. tree trunks, 7. tree stumps or intact root plates, 8. overhanging vegetation, 9. undercut banks, 10. water plants, 11. grass/reeds, 12. turbulent water zones, 13. pools
1.6 A1 Substrate	categorical	**Composition**: 1. silt/fine sediment ($< 0.2\ mm$), 2. sand ($]0.2, 2]mm$), 3. gravel ($]2, 16]mm$), 4. stones ($]16, 64]mm$), 5. large stones ($]64, 250]mm$), 6. boulders ($> 250mm$), 7. rock, 8. organic material, 9. artificial substrate
1.6 A2 Substrate	categorical	**Mobilisability:** 1. deposits of suspended particles, 2. fine bedload, 3. coarse bedload, 4. bed material mixed with bedload, 5. coarse bed material

Indicators are evaluated based on different calculation approaches from their attributes and range from a standardised value between 0 (degraded or artificial) and 1 (near-natural). Indicators 1.1, 1.2, 1.5 and 1.6 require an area-wide mapping of the study reach. For each of those indicators, homogeneous sections or areas are identified and classified. For example, *bank structures* are classified by the three attributes *profile*, *composition,* and *slope*. Each attribute is assigned a category. A homogeneous riverbank section can, e.g. be classified as a linear *profile* with a *composition* of unconsolidated material and a gentle *slope*. The calculation of indicators 1.3 and 1.4 is based on measurements along CS.

The calculation of indicators 1.1 and 1.2 is based on the number of homogeneous structures in the study reach. Indicator 1.5 is based on comparing the mapped area of *presence of cover* with an expert estimate of the natural reference condition. A Two independent estimates (P. Vonlanthen, *Aquabios Sàrl*; C. Weber, *Eawag*) were averaged at the study site. For indicator 1.6, a calculation approach is currently only available for the attribute *mobilisability* (1.6 A2). The EOR practice documentation (Weber et al., 2019), describes all survey methods and calculation approaches in detail.

3.3 Physical modelling

3.3.1 Experimental flume

Experiments are run in a $34m$-long wooden channel with varying widths and cross-sections (**Figure 3.8**).

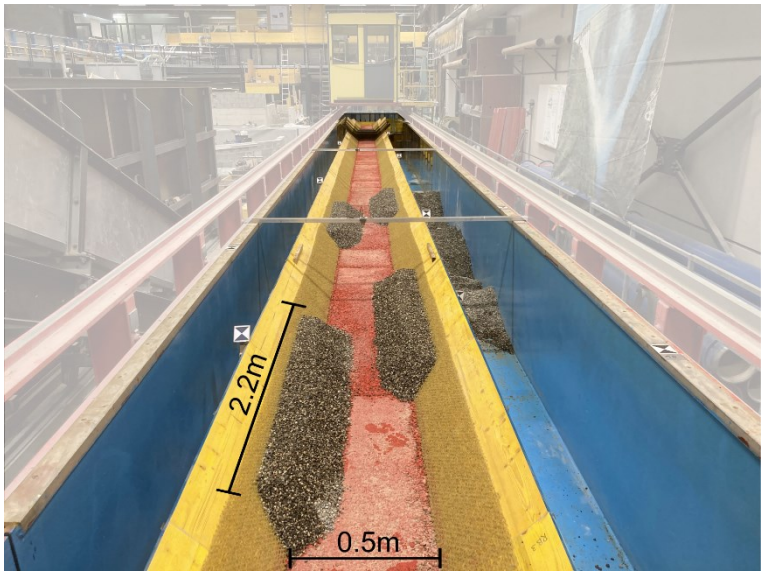

Figure 3.8 Photo of the upstream part of the experimental flume with four initial sediment deposits. View in the downstream direction. © Platform of hydraulic construction of the EPFL (PL-LCH).

The slope of the channel is divided into seven constant sections, each representing one CGU. (**Table 3.6**). The standard bed width (b_0) is $55cm$, and the bank slope is $45°$. The channel width in *section 6* and the bank material varies according to the channel state (**Table 3.7**). The different sections are scaled representations of dominant geomorphic units identified at the reference field site. The bed level profile was obtained from mean bed elevations of cross-section measurements at each section's upstream and downstream edge. For the section length (l) and the bed level profile, a geometrical scaling ratio between the model and field conditions of $(1 \div 10)$ was applied. The bed width (b) was scaled with a geometrical scaling factor of $(1 \div 50)$ to respect the lateral restrictions in the laboratory.

Table 3.6 Attribute table of channel sections of the physical model. The variable l is the length, b the bed width and J the longitudinal slope. A negative sign indicates a rising slope. The standard bed width (b_0) is $55cm$.

		l		b		J
section	bed structure	$[m]$	$[b_0]$	$[m]$	$[b_0]$	$[\%]$
1	start	1.7	3.1	0.55	1	0
2	glide1	6.4	11.6	0.55	1	−0.91
3	riffle1	3.2	5.8	0.55	1	0.16
4	run1	8	14.5	0.55	1	0.54
5	run2	6.9	12.5	0.55	1	0.64
6	*varying*	5.6	10.2		*varying*	
7	glide2	2.5	4.5	0.55	1	0.64

Table 3.7 Attribute table of channel states of the physical model. Variable b is the bed width, z_{min} is the minimum bed elevation, and J is the longitudinal slope. A negative sign indicates a rising slope.

	section 6				
channel state	bed structure	$b\ [m]$	$z_{min}\ [cm]$	$J\ [\%]$	bank material
0	pool	0.55	0	$[8.1;\ 0;\ -5.6]$	wooden planks
1	riffle2	0.81	13	$[8.1;\ 0]$	wooden planks
2	riffle2	0.78	13	$[8.1;\ 0]$	geotextile
3	pool	0.26	5	$[8.1;\ 0;\ -5.6]$	geotextile

The bed layer consists of sediment fixed in place by concrete slurry. The fixed bed is coloured red. In *section 6*, a horizontal layer of mobile sediment is installed, corresponding to the height of z_{min} (**Table 3.7**). Different GSDs were used for the fixed and the mobile sediment (**Figure 3.9**).

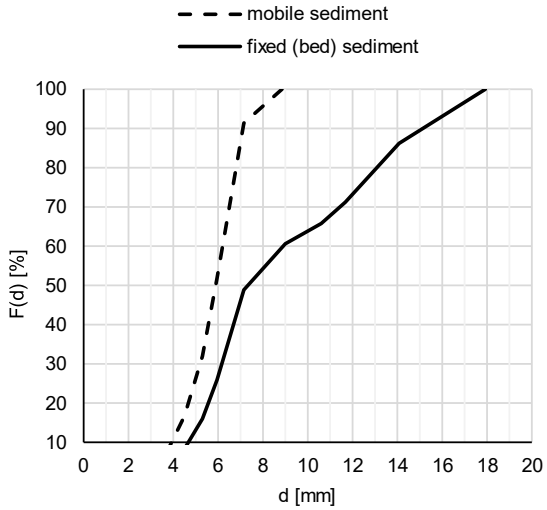

Figure 3.9 Diagram of the grain size distributions (GSDs) of the mobile and the fixed sediment of the physical model. Variable d is the characteristic particle diameter, and $F(d)$ is the weight-based frequency distribution.

The d_{50} of the mobile sediment ($d_{50,mobile}$) is $5.9mm$. The d_{50} of the fixed sediment ($d_{50,bed}$) is $7.3mm$. The GSD of the mobile sediment corresponds to particles in the range of $4cm$ to $8cm$ in field conditions. This distribution lies in the upper range of salmonid spawning gravels (e.g. Kondolf & Wolman, 1993). It represents many restoration projects in lowland rivers and alpine streams (Vonwiller et al., 2017). The GSD of the fixed sediment was selected to represent a coarse armour layer. The mean diameter of the bed ($d_{m,bed}$) corresponds to around $1.6d_{m,mobile}$. The breakup condition of an armour layer, following the approach of Günter (1971), is described by the critical dimensionless shear stress for the breaking up of the armour layer

$$\theta_{c,D} = \theta_c \times \left(\frac{d_{m,D}}{d_m}\right)^{2/3} \tag{3.3}$$

where θ_c is the critical dimensionless shear stress for the initiation of bedload motion, $d_{m,D}$ is the mean particle diameter of the cover layer, and d_m is the mean particle diameter of the bedload. In the experimental flume of this thesis, this would lead to a theoretical breakup condition of an armour layer at $1.34\theta_c$. Further discussions on the limitations are presented in Section 3.3.7.

The Strickler hydraulic roughness (K_{st}) of the bed ($K_{st,bed} = 40\, m^{1/3}s^{-1}$) and the geotextile ($K_{st,gtex} = 25\, m^{1/3}s^{-1}$) were assessed by numerical modelling (Section 3.4). The K_{st} of the wooden planks ($K_{st,wood}$) was estimated at $100\, m^{1/3}s^{-1}$.

The channel instrumentation consists of a 3D laser scanner of type LEICA SCANSTATION P20 (scanner) and seven ultrasonic sensors (USSs) of type Baumer UNAM 30, which are installed in the centre of each channel section (Figure 3.13).

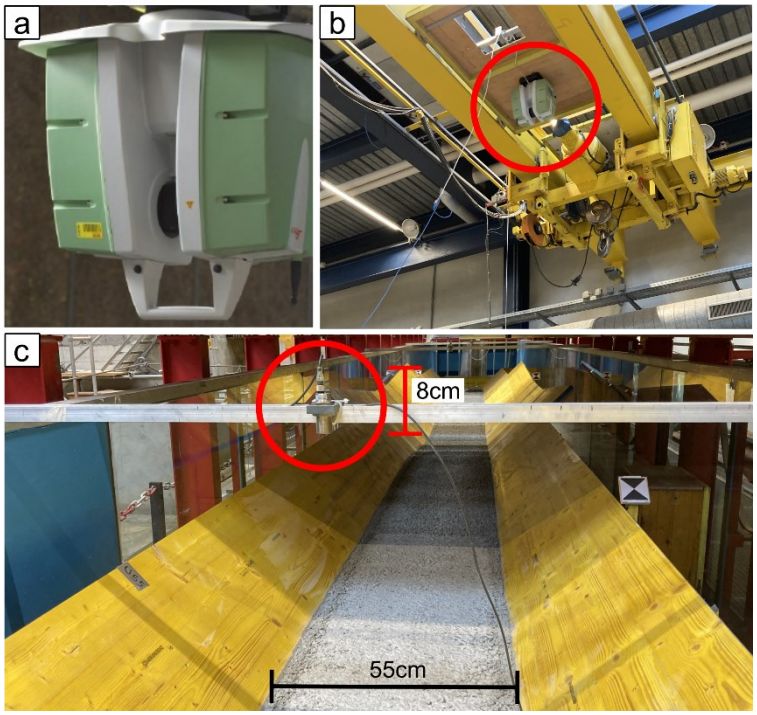

Figure 3.10 Pictures of experimental channel instrumentation, including the laser scanner and an ultrasonic sensor (USS). a: LEICA SCANSTATION P20 (scanner), b: scanner suspended on the bridge crane of the experimental facility, c: one of seven USSs fixed on a rotatable bar above the experimental flume (*state 0*). © Platform of hydraulic construction of the EPFL (PL-LCH).

The scanner has an accuracy of $1.6mm$ at a $10m$ distance, and the USSs have an accuracy of $< 0.3mm$.

3.3.2 Test procedure

Every test run starts with the same initial condition of the experimental channel. During an experimental run, there are four different phases:

- Initial flow phase
- Flood phase
- Emptying phase
- Dry phase

Sediment augmentation and topographic scans are performed in dry conditions. Both actions require emptying and refilling the experimental channel. If none of those two actions is planned, the flood phase is repeated with different discharges according to the experimental planning (**Figure 3.11**).

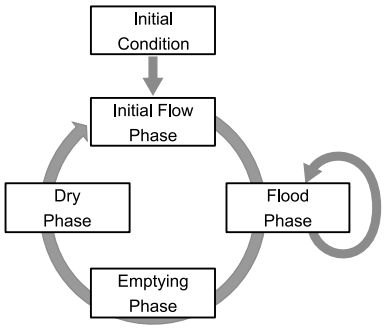

Figure 3.11 Flow chart of the experimental test procedure.

The control elements of the experimental flume are shown in **Figure 3.12**. Pictures of the experimental flume at different test phases are shown in the appendix (**Figure A3.1**).

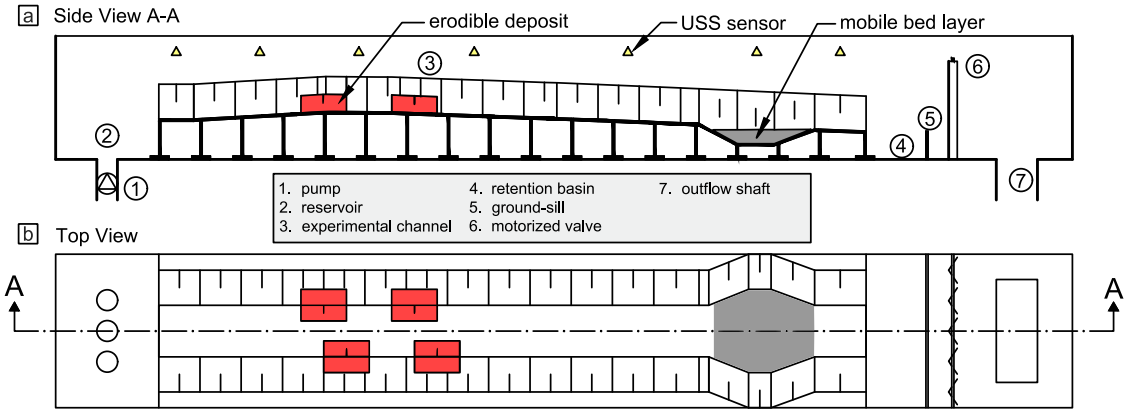

Figure 3.12 Schematic sketch with the control elements of the experimental flume. a: side view (A-A), b.: top view. The grey area represents the mobile bed area.

The inflow to the reservoir is controlled by a pump equipped with a flowmeter (1). Water enters the experimental channel (3) through an open inflow at the upstream end of the flume from a reservoir (2). Downstream of the experimental channel is a retention basin (4) with a ground sill (5). A motorised valve (6) controls the water level in the retention basin and the downstream water level in the experimental channel.

Initial condition

Initially, all mobile sediment is removed from the channel bed outside *section 6*. In *section 6*, a horizontal bed level is created. All characteristics of the flume correspond to the conditions described in Section 3.3.1.

Dry phase

Sediment augmentation and topographic scans are performed in dry conditions. For the augmentation of sediment, mobile sediment is placed in four alternated deposits along the banks. Deposit dimensions are $220cm \times 16cm \times 15cm$ ($length \times width \times height$), which corresponds to a volume of $0.21m^3$. The deposits are shifted half the deposit length in the downstream direction. The blocking ratio is 0.32. This configuration was chosen because previous experiments from Battisacco et al. (2016) have shown that it promotes the formation of morphological patterns in the downstream reach (≤ 20 channel widths) during small morphological flood events, which do not lead to submergence of the deposits greater than 100%. There are two different positions for the initial placement of the artificial deposits. The first starts at $2.5m$ (*Type 1*), and the second one at $6.9m$ (*Type 2*) downstream of the channel inlet (Figure 3.13).

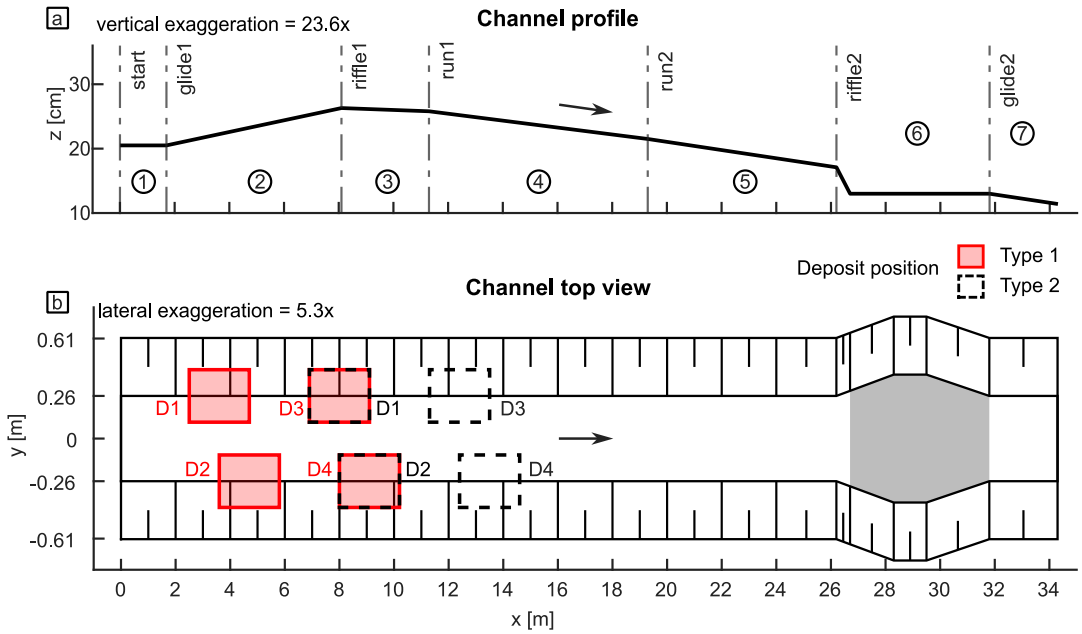

Figure 3.13 Schema of the experimental channel at *state 2* with the two initial deposit positions. a: Channel profile. Variable z is the vertical coordinate, and x is the longitudinal coordinate. The numbers mark the different sections (Table 3.6). b: Channel top view. Variable y is the lateral coordinate. The labels D1 to D4 mark the name of the deposit (D) for the corresponding deposit type. The grey area represents the mobile bed area. The black arrow marks the direction of flow during the experiments.

Consecutive sediment augmentation is performed before a flood by rebuilding all deposits with new sediment to their initial dimensions. Four scans are performed at different positions and with a maximum scan distance of around $10m$ to scan the entire

surface of the flume. The point clouds of those scans are then assembled, and a joint elevation mesh is created.

Initial flow phase

At the beginning of the initial flow phase, water is slowly released into the experimental channel to avoid the mobilisation of mobile sediment. The maximum approach flow is $10\ l/s$. After a few minutes, the initial flow phase is completed once the retention basin is filled with water and the ground sill is overspilled.

Flood phase

With the initial flow phase completed, a constant discharge is set for the pump according to the experimental planning. The downstream water level is adjusted by the outlet gate to approach uniform flow conditions near the channel end ($1.3m$, between the mid-point of *section 7* and the downstream end of the flume) for every change in discharge. The USSs are turned on to record water level fluctuation with a frequency of $3Hz$.

Emptying phase

To empty the channel, the inflow discharge is reduced incrementally within few minutes and the remaining water flow is left to exit the channel.

3.3.3 Data analysis

The metrics of this section were proposed in the framework of this thesis if not stated otherwise. The vertices of the scan clouds are linearly interpolated on a two-dimensional (2D) uniform grid for every scan. The elevation grid is unidirectional with a grid length of $1cm$. A filter of $\pm 7mm$ ($\sim d_{50,bed}$) is applied to subtract two elevation grids.

The *spatial distribution of the vertical change* between two scans, S_a and S_b, is

$$\bigcup z_{S_a - S_b} = \bigcup_{i=1}^{n_{grid}} \mathrm{z}_{S_a,i} - \mathrm{z}_{S_b,i} \tag{3.4}$$

where $\mathrm{z}_{S_a,i}$ and $\mathrm{z}_{S_b,i}$ are the elevation values at cell i from the grid of S_a and S_b, and n_{grid} is the number of cells in the grid. The *volumetric difference* of a zone Z between two scans S_a and S_b is

$$\Delta V_{Z,S_a - S_b} = \mathrm{A}_{\mathrm{grid}} * \sum_{i}^{j} \left(\mathrm{z}_{S_a,i} - \mathrm{z}_{S_b,i}\right), \qquad for\ \forall\ c_i \in \mathrm{Z} \tag{3.5}$$

where A_{grid} is the grid area, and c_i is a grid cell. The *total volume of augmented material* of a scan S is

$$V_{t,S} = \Delta V_{MIZ,S-S_0} + V_{trap,S} \tag{3.6}$$

where $V_{trap,S}$ is the volume in the sediment trap at the time of S. The *volume imbalance* between two scans, S_a and S_b, is

$$\Delta V_{t,S_a-S_b} = \left(\frac{V_{t,S_a}}{V_{t,S_b}} - 1\right) * 100 \tag{3.7}$$

The *erosion rate* of a deposit D between scans S_a and S_b is

$$E_{D,S_a-S_b} = -\left(\frac{\Delta V_{D,S_a-S_0}}{\Delta V_{D,S_b-S_0}} - 1\right) * 100 \tag{3.8}$$

The *dimensionless deposition* is

$$D^* = \frac{V^*_{dep}}{A^*} \tag{3.9}$$

where V^*_{dep} is the deposition volume, normalised by the total volume of the initial deposits, and A^* is the area, normalised by the area of the *MIZ*. The *persistence of mobile sediment* is

$$P^* = \frac{V_{dep,t-1} - V_{ero,t}}{V_{dep,t-1}} \tag{3.10}$$

where $V_{dep,t-1}$ is the deposited volume before a flood and $V_{ero,t-1}$ is the eroded volume after a flood. The *percentage of cover* is

$$POC = \frac{\sum A_{cov}}{A_{oi}} \times 100 \tag{3.11}$$

where A_{cov} is the area of cells covered with augmented sediment (higher elevation than the empty channel) and A_{oi} the total area of interest.

The *Hydromorphological Diversity Index* was calculated after Gostner et al. (2013) and is defined as

$$HMID = \left(1 + \frac{\sigma_v}{\mu_v}\right)^2 \times \left(1 + \frac{\sigma_h}{\mu_h}\right)^2 \tag{3.12}$$

3.3.4 Case study

The case study is one of two studies conducted in the experimental flume in the framework of this thesis. It aims at reproducing the Sarine River case study with the flume experiment. It was used to assess the validity of the physical model. The second study is a parametric model study. It is the main physical model study of this thesis, which directly addresses the first two research questions. It is described in Section 3.3.5.

The configuration of the sediment deposits and two successive floods were scaled in the model according to the field conditions. The physical model was downscaled with a geometrical scaling factor of $1/10$. This scaling approach led to a geometrical distortion of $1/5$ in the lateral direction but no vertical or horizontal distortion. The mobile sediment was scaled with the same λ, which leads to a GSD with d_m equal to $6.3mm$. At the prototype scale, this represents a slightly coarser GSD than the one of the augmented sediment at field conditions with d_m equal to $57mm$ (Stähly et al., 2019).

This study's channel state corresponds to *state 3* (Table 3.7) It means that the surfaces of the banks are covered with a geotextile to represent increased roughness from vegetation and that in *section 6*, the channel is narrowed to about $0.5b_0$ (Figure 3.14). The sediment deposits are always placed in the upstream part of the channel according to placement *Type 1* (Figure 3.13).

Figure 3.14 Photo of the pool section in the downstream part of the experimental flume in channel *state 3* (Table 3.7). View in the downstream direction.

Hydrograph scaling was performed for similitude in relative submergence ratio. The ratio h over $d_{m,mobile}$ is kept similar for model and field conditions. Consequently, the similitude in Re_p, θ and Froude Number (Fr) is relaxed. This model representation was chosen as it required the lowest model discharge over the simulated discharge range. It was the only representation where the peak discharge would not exceed the vertical channel limitations. At the same time, it was considered reasonable since laboratory experiments showed the importance of the submergence ratio for erosion (Friedl et al., 2018) and

deposition patterns (Battisacco et al., 2016) of in-channel sediment deposits. The deposit volume change was compared between model and field conditions (Table 3.8).

Sediment transport conditions in the experimental flume are identical to the parametric study (Section 3.3.5), except for the modified pool section (*section 6*). An analysis of the measured water levels shows that, in this section, the ratio of Shields Number to critical Shields Number (θ/θ_{crit}) with the $d_{50,mobile}$ remained below 1 ($[0.48, 0.72]$) over the full range of simulated flood discharges. Therefore, no sediment transport could be expected across the pool section in the experimental flume.

Table 3.8 Comparison of deposit volume change between model (M) and field conditions (F) for deposit 1 (D1) to D4. Variable $V_{initial}$ is the initial volume, ΔV_{F16} is the volume change after *Flood 2016*, and ΔV_{F20} is the volume change after *Flood 2020*. The values in parentheses show the percentage change compared to the preceding state. All dimensions are given at field scale.

	$V_{initial}[m^3]$		$\Delta V_{F16}[m^3]$		$\Delta V_{F20}[m^3]$	
	M	F	M	F	M	F
D1	270	248	0 (0%)	-103 (-42%)	0 (0%)	+9 (+6%)
D2	215	248	0 (0%)	-200 (-81%)	0 (0%)	+2 (+4%)
D3	240	248	-100 (-42%)	-217 (-88%)	-5 (-4%)	-17 (-56%)
D4	210	248	-170 (-81%)	-188 (-76%)	-5 (-13%)	-5 (-8%)
Total	935	990	-270 (-29%)	-708 (-72%)	-10 (-2%)	-11 (-4%)

In the first flood (*Flood 2016*), the total volume change in the field amounts to an estimate of -72%. The deposit volume change varied significantly between the model and the field. The model representation did not satisfactorily reproduce the erosion pattern of the two upstream deposits (D1 & D2). While no erosion occurred in the model, field measurements showed a substantial volume loss of D1 (-42%) and D2 (-81%). This discrepancy is partly due to the upstream boundary condition, which, in the model, is defined by the static water level of a reservoir. This static water level extends towards the two upstream deposits, where the flow only starts to accelerate. In the field, the flow enters the area of the upstream deposits already with an initial flow velocity and, therefore, a higher-scaled erosive force. In addition, the lateral distortion in the model leads to an increased influence of bank roughness and a reduction of flow velocities at similar relative submergence. Stabilisation by vegetation at the field side is another factor that was not reproduced. Finally, the assumption of an average bed elevation over the channel width cannot reproduce the effect of zones of increased bottom shear stress due to variations in bed elevation. In the second flood (*Flood 2020*), the total volume loss of all deposits was similarly low in the model ($10m^3$) and in the field ($11m^3$), indicating limited availability of sediment in potential erosion zones. The downstream distributions of augmented sediment along the channel are compared between model and field results after *Flood2016* and after *Flood2020* in Figure 3.15.

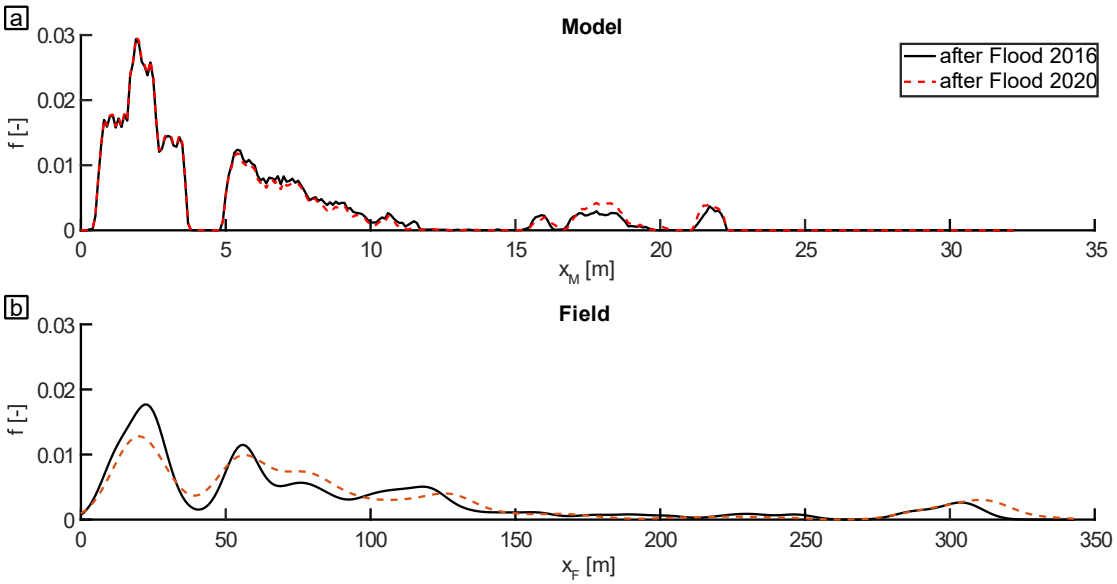

Figure 3.15 Probability density functions (pdf) with the frequency (f) of the amount of augmented sediment along the central channel axis in the model and in the field after *Flood2016* and after *Flood2020*. a: PDF of the augmented sediment volume in the model. Variable x_M is the longitudinal coordinate in the model scale. b: PDF of the tracer stone distribution in the field. The distribution was smoothened by one-dimensional gaussian kernel density estimation with one-third of the default bandwidth. Variable x_F is the coordinate along the channel centre line in the field scale.

After both floods, deposition occurred in the model and field at the downstream end of the initial deposit location ($x_M \approx [10, 12]m$). At this location, the average density is higher in the field (4×10^{-3}) than in the model (1×10^{-3}), and the deposition zone in the field extends twice the length ($x_M \approx [10, 14]m$). In the model and the field, a similar fraction of sediment was transported further than the first deposition zone, suggesting the formation of new sediment patches in the downstream section ($x_M \approx [15, 35]m$) . In the case of the model, this deposition occurred in the run ($x_M \approx [15, 23]m$), whereas in the field, it occurred in the near downstream vicinity of the pool ($x_M \approx [18, 35]m$).

After the second flood (*Flood2020*), deposition patterns in the field indicate a small downstream shift ($[0.5, 1]b_0$) of augmented sediment and a slight growth of the downstream sediment patch (11%). In the model, the only significant change is the growth of a sediment patch in the run (66%; $x_M \approx [15, 19]m$). The model representation could not reproduce sediment transport in the upstream vicinity ($x_M \approx [22, 26]m$) and across the pool ($x_M \approx [26, 32]m$). The upstream edges of the channel walls present a flow obstacle that led to an overproportionate backwater effect and reduction in bottom shear stress upstream of the scour hole. Furthermore, the simplified geometry with a straight channel axis did not cause secondary currents inside the scour section. In the field, these currents are expected to push the bedload towards the main flow along the channel's inner radius, thereby routing sediment across the pool section. In other sections, the model did show reasonable agreement with the measured bedload distribution from the field.

Physical hydraulic models with solid transport can allow for a representation of complex morphological processes. Nevertheless, depending on the target process, the

experimental design requires careful consideration of the site-specific features by precise reproduction or an adequate level of abstraction. This study investigated the evolution of bed morphology for a river reach with diverse bed structures. The difficulty in accurately presenting deposit erosion of the artificial deposits was attributed to the model boundaries and distortion of the physical model representation. Discrepancies in deposition patterns between the model and the field can be partly attributed to the fixed bed assumption. The inability to reproduce sediment transport around the pool section shows the challenge of reproducing the influence of CGUs on bed morphology evolution from SAMs in complex reaches by physical modelling. Further discussions on the limitations are presented in Section 3.3.7.

3.3.5 Parametric study

The parametric study aims at reproducing fluvial processes without being representative of any real case. It is the main physical model study of this thesis, which directly addresses the first two research questions. Froude similarity with a Froude scaling factor (λ) of 10 is assumed to upscale the results to field conditions. In this case, the flume represents a straight, $340m$-long channelised river section with a standard bed width of $5.5\ m$, and the total volume of all four deposits corresponds to $210m^3$ in field conditions. Compared to the standard channel width, this corresponds to the volume of the SAM at the Sarine River in 2016 (Stähly et al., 2019).

Channel configuration

This parametric study's channel state corresponds to *state 2* (Table 3.7). It means that the surfaces of the banks are covered with a geotextile to represent increased roughness from vegetation and that in *section 6*, the channel is widened about $1.4b_0$. The sediment deposits are always placed in the upstream part of the channel according to placement *Type 2* (Figure 3.13).

Ten zones are defined within the channel (Figure 3.16)

- The four initial placement zones of the sediment deposits (D) D1 to D4
- The four zones of interest (ZOI) ZOI1 to ZOI4
- The morphological impact zone (MIZ)
- The scan zone (SZ)

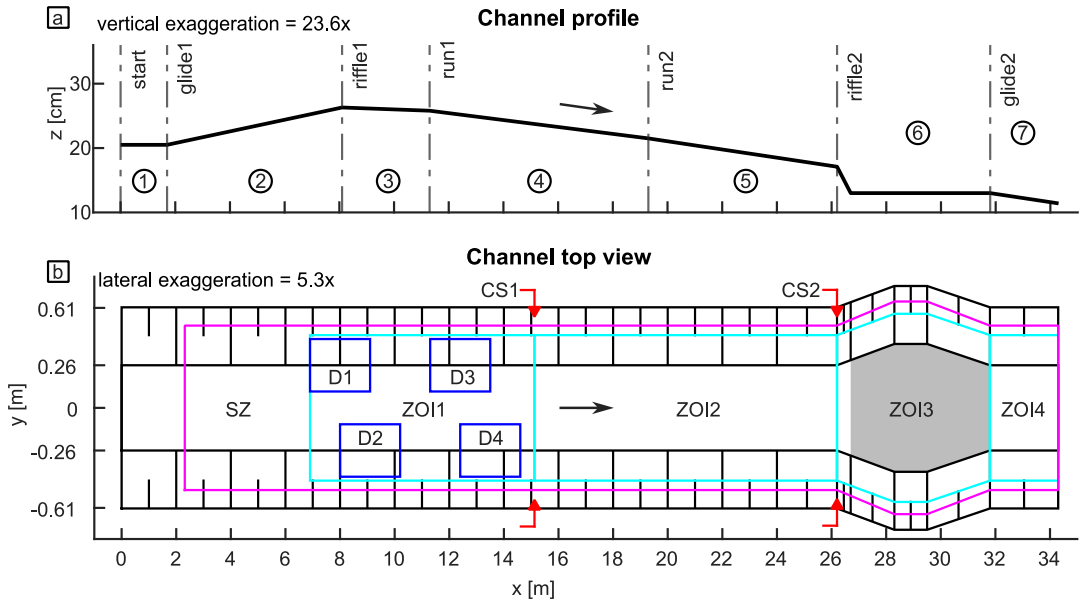

Figure 3.16 Schema of the experimental channel of the parametric study. a: Channel profile. Variable z is the vertical coordinate, and x is the longitudinal coordinate. The numbers mark the different sections (**Table 3.6**). b: Channel top view. Variable y is the lateral coordinate. Blue squares represent the initial placement zones for sediment deposits (Ds) D1 to D4. Cyan polygons represent the zones of interest (ZOI) ZOI1 to ZOI4. The magenta polygon represents the scan zone (SZ). The red arrows mark the two cross-sections (CSs) CS1 & CS2. The grey area represents the mobile bed area. The black arrow marks the direction of flow during the experiments.

ZOI1 extends from the upstream part of *D1* to $1b_0$ downstream of *D4*. It represents the zone of hydraulic impact of the initial sediment deposits. *ZOI2* extends from *ZOI1* to the section of the channel widening. It represents the near downstream target zone. *ZOI3* extends over the zone of varying channel width. It represents the zone of the channel widening. *ZOI4* extends from *ZOI3* to the channel outlet. It represents the downstream end of the target zone. The *MIZ* is the union of *ZOI1* to *ZOI4*, and the *SZ* is the area covered by the topographic scans. Two cross-sections (CSs), *CS1* to *CS2*, are defined at the upstream and downstream ends of *ZOI2*. Sediment is considered *mobilised* once it is transported out of *ZOI1* across *CS1*. The transport rate across *CS1* is also referred to as the *mobilisation rate*.

Experimental Planning

The experiment consists of the six runs *Run_A* to *Run_F* (**Figure 3.17**).

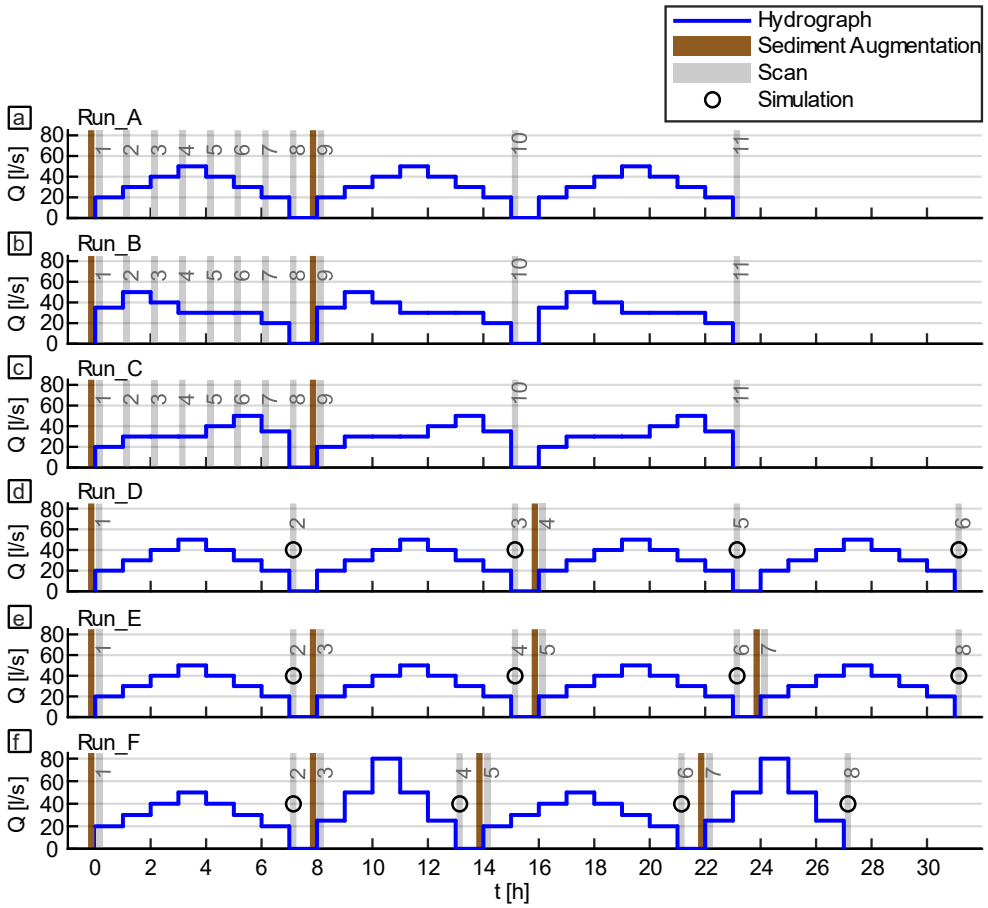

Figure 3.17 Schema of the experimental planning of the parametric study in model scale. a-f: Experimental run A (*Run_A*) to *Run_F*. Variable Q is the discharge, and t is the time. The number on the scan bar describes the scan number. A black circle marks the scans for which a numerical simulation was performed. The flood volume is similar for all hydrograph shapes (±2%).

Each run represents a sequence of floods and interjacent sediment augmentations. Stopping and resuming a flood discharge (requiring emptying and initial phase) for consecutive augmentation or topographic scans does not alter the experimental result and is, therefore, not part of the experimental planning. Fifty-six channel scans were performed at the end of a flood or after a sediment augmentation. *Scan_0* stands for the initial scan of the empty channel. The other scans are labelled according to the corresponding run and in ascending order, starting at 1 for every run (e.g. *Scan_A1*). For thirteen scan topographies, numerical simulations were performed, including one for the empty channel. Simulations are referred to by the corresponding scan (e.g. *Simulation_D2*).

In *Run_A* to *Run_C*, floods with different hydrograph skewness (symmetrical, left-skewed, right-skewed) are released. The peak discharge in the model scale is $50\,l/s$ and corresponds to $15.8\,m^3/s$ in field conditions. For the standard CS and mean channel slope of $2.8‰$, a discharge of $50\,l/s$ results in a flow with 1.2 times the ET and a mean water depth of $35.4 d_{50,mobile}$ ($20.9cm$). The flood volume is similar for all hydrograph shapes (±2%) and corresponds to $0.8 \times 10^6 m^3$ in field conditions. In *Run_D* to *Run_F*, different

repetition frequencies of sediment augmentation (before every or every second mobilising flood) and floods with different peak discharges ($[50;\ 80]\ l/s$) are assessed. For the standard CS and mean channel slope of $2.8‰$, a discharge of $80\ l/s$ results in a flow with 2.5 times the ET and a mean water depth of $38.1 d_{50,mobile}$ ($22.5cm$). The flood volume of both hydrograph types is identical and corresponds to the volume of the floods from *Run_A* to *Run_C*.

Numerical simulations (Section 3.4) are performed with a constant low-flow discharge ($2.2\ l/s$), representing low flow in field conditions. This discharge results in an average water depth of $4.2 d_{50,mobile}$ ($\triangleq 2.5cm$) for the standard CS and mean channel slope. Simulations are run until steady-state conditions are reached. The $HMID$ was calculated for all simulation results from every wetted cell's water depth and absolute velocity.

Hydraulic conditions

The hydraulic conditions along the channel axis for different discharges at the initial channel state were simulated using the numerical model described in Section 3.4. The result for the maximum discharge of $80\ l/s$ is shown in **Figure 3.18**. Supplementary figures for different discharges ($Q_m = [2.2;\ 20;\ 35;\ 45]\ l/s$) are shown in the appendix (Section A4).

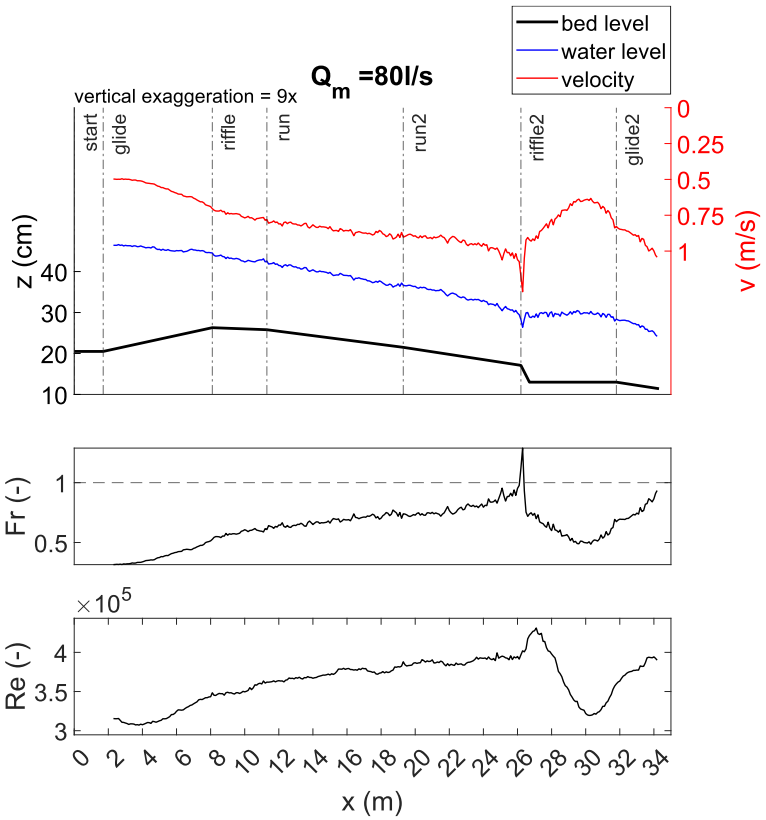

Figure 3.18 Hydraulic conditions along the centre axis of the experimental channel in initial condition for a constant model discharge (Q_m) of $80\ l/s$. Variable x is the longitudinal coordinate, z is the vertical coordinate, v is the absolute flow velocity, Fr is the Froude Number, and Re is the Reynolds Number.

For the full range of discharges released in the physical model ($Q_m = [20, 80]\, l/s$), Fr ranges between 0.1 and 0.8, and Re is greater than 10^4 in most parts of the experimental channel. A hydraulic jump occurs locally, where the initial bed elevation drops by about $4cm$ at the upstream end of the channel widening (*riffle2*). For all discharges, the values for Fr assume a value above 1 on this channel stretch with a length of around $30cm$ ($< 1\%$ of the flume length). Small water level oscillations are observed in the downstream vicinity. With the sediment supply in the experimental runs, this phenomenon quickly disappears during the first flood event, as sediment is deposited in the upstream part of the widening, reducing the bed level difference and raising the local water level elevation.

Sediment transport conditions

The Shields Number θ (Eqn. 2.4) and Particle Reynolds Number Re_p^* (Eqn. 2.5) of characteristic channel conditions were plotted in model scale and field scale in the Shields Diagram to test the correct representation of bedload motion in model scale. Four scenarios were compared with different constant model discharges, ranging from minimum to maximum flow conditions ($Q = [20, 40, 60, 80]\, l/s$). All scenarios apply to the empty experimental flume (initial channel condition). The variables θ and Re_p^* were calculated for the representative particle diameter $d_{50,mobile}$ ($5.9mm$) from USSs water level measurements in the centre of each channel section. The corresponding values for field conditions were calculated with the upscaled hydraulic variables for the selected model representation (Froude Similitude, $\lambda = 10$). The Shields curve was calculated with the explicit formulation of Cao et al. (2006). The results are shown in Figure 3.19. The corresponding data table can be found in the appendix (Table A5.1).

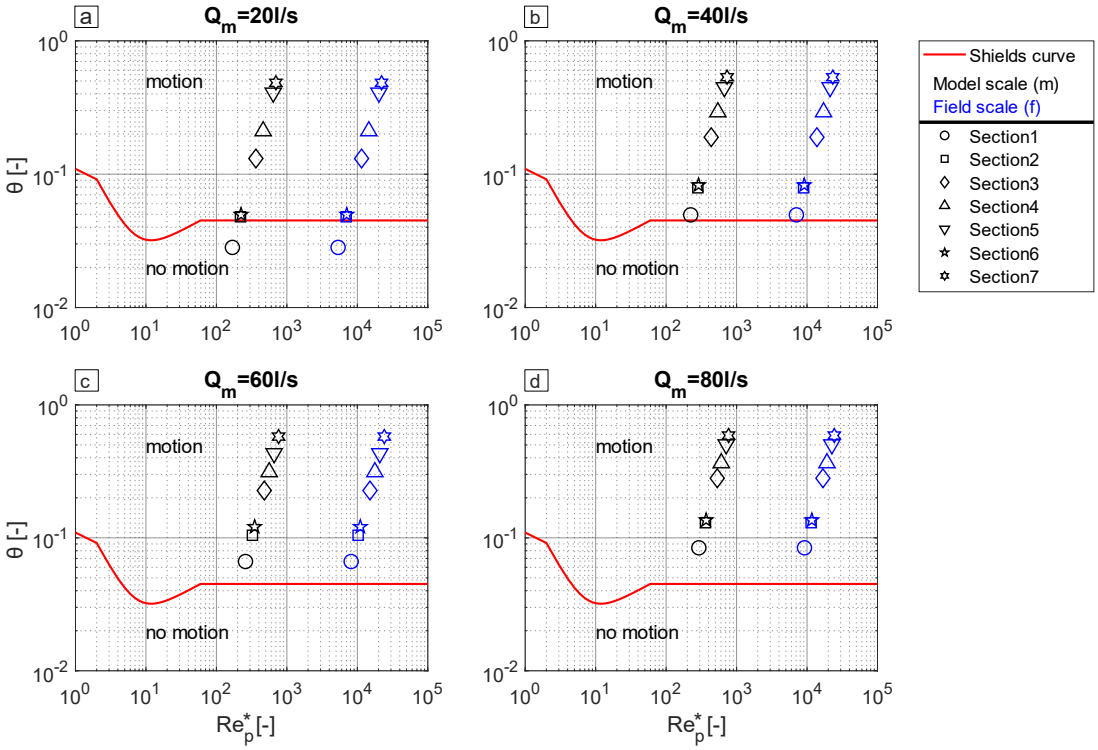

Figure 3.19 Shields diagrams showing the condition of motion for the median particle diameter of the mobile material ($d_{50,mobile}$) in all seven channel sections for four scenarios (a-d) of different constant model discharge (Q_m) in model and field scale. Variable θ is the Shields Number, and Re_p^* is the Particle Reynolds Number.

In the investigated scenarios, sediment transport conditions (motion/ no motion) are similar between model and field conditions. All data points are located at the side of the Shields Diagram where the critical Shields parameter approaches a constant ($Re_p^* > \approx 60$).

The assessed threshold of sediment transport represents the critical condition for the initiation of motion for exposed bedload particles on top of the bed layer. It does not apply to the initiation of the erosion process of the artificial deposits. Because of the narrow grain size distribution of the mobile sediment, selective transport should play a minor role in bedload transport processes in the experimental flume. No longitudinal sediment sorting along the flume was observed after single or multiple sediment augmentations.

Characteristic bar forms

Characteristic bar forms of the represented river section in field conditions are shown in the revised *Da Silva and Yalin's plan* (Ahmari & Da Silva, 2011) in Figure 3.20. The flow depth $h = 0.25m$ represents low-flow conditions, the characteristic diameter $D = 0.06m$ the upscaled $d_{50,mobile}$ and the flow width $B = 5.5m$ the upscaled b_0.

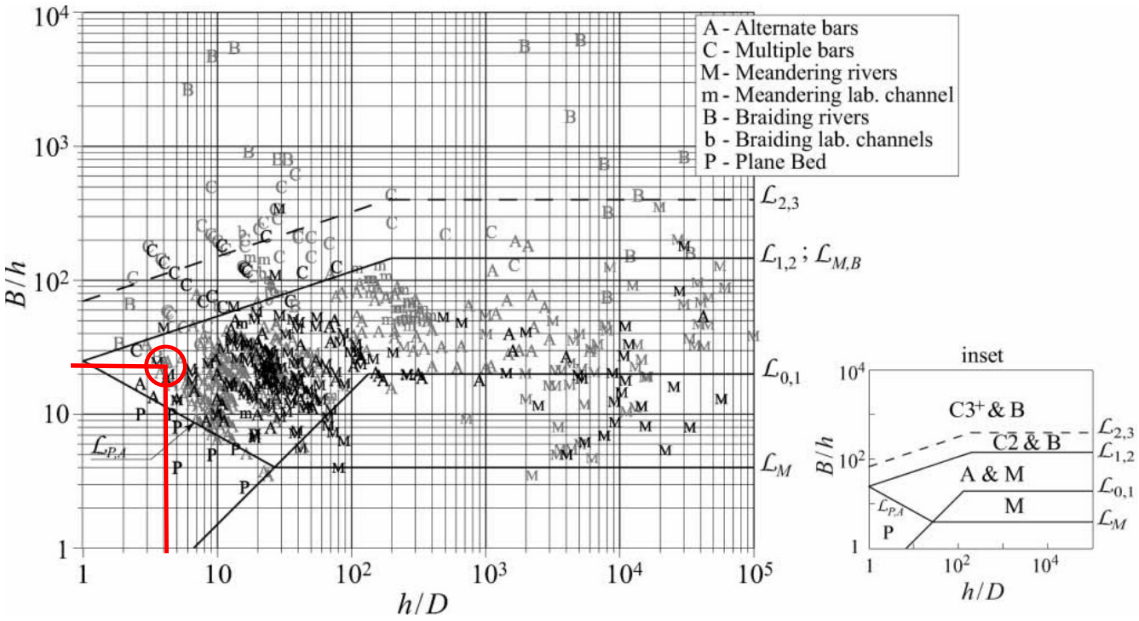

Figure 3.20 Revised version of the *da Silva and Yalin's plan* (Ahmari & Da Silva, 2011), including the characteristic region of the represented river section by the parametric model study. Variable B is the flow width, h is the flow depth, and D is the characteristic grain size diameter. The red circle marks the characteristic region of the represented river section for $B = 5.5m$, $h = 0.25m$ and $D = 0.06m$.

Under sediment equilibrium and low-flow conditions, the represented river section would develop alternate bars with the standard channel width (b_0) in all sections. Alternate bars promote stream meandering (Ahmari & Da Silva, 2011). However, no meandering channel form can evolve since the represented banks are unerodable in the model.

3.3.6 Error assessment

Experimental errors can influence the accuracy and reliability of results. Accuracy measures how close results are to the correct or accepted outcome. Reliability measures how similar the results are when measurements are repeated. The accuracy and reliability of the flume experiment are assessed with the experimental design of the parametric study (Section 3.3.6). The results are part of the methodology, as they provide the groundwork for analysing both studies performed with the experimental flume.

Sources of errors

In all experiments with the presented flume, errors are attributed to a combination of systemic, random, and human errors. Systemic errors can be caused by the inaccuracy of the scan itself or the processing of the scan data. Errors can occur during the assemblage of different scan stations, from undetected mobile grains between coarser grains of the fixed bed or from applying a filter to subtract two scans. A random error occurs, for example, from a change in the moisture content of the deposits during test runs, which impacts cohesion and erosion resistance. Human errors can be caused by

imperfect reconstruction of the deposit geometry or adjustment of the downstream water level.

Accuracy

The accuracy is quantified by calculating the *volume imbalance* (ΔV_t; Eqn. 3.7) after all three floods of *Run_A*. The *volume imbalance* represents the discrepancy between the volume calculated from laser scans and the actual volume of augmented sediment inside the channel. The variable ΔV_t after the first flood ($\Delta V_{t,S_{A8}-S_{A1}}$) is -9.5%. Distributing the volume loss equally among the *MIZ* leads to a lower theoretical average net erosion ($0.8mm$) than in a similar laboratory experiment with a mobile bed (3mm; Rachelly, Friedl, et al., 2021). Variable ΔV_t after the second ($\Delta V_{t,S_{A10}-S_{A9}}$) and third flood ($\Delta V_{t,S_{A11}-S_{A10}}$) takes on a value of -4.2% and -4.5%. It means that the *volume imbalance* of *Run_A* does not go below -10% and decreases with every new sediment augmentation.

Another measure for quantifying accuracy is comparing the elevation difference (ED) of the mean bed elevation along the longitudinal channel axis between the fixed bed and different channel states during the experiment. The range of negative values of the ED represents an error because no erosion is possible below the fixed bed surface. The maximum error of ED in the near downstream section (*ZOI2*) during the first flood of *Run_A* to *Run_C* is equal to $0.6d_{50,mobile}$. Since the vertical error can occur in the negative and positive direction, the corresponding error range is determined to $\pm 0.6d_{50,mobile}$, corresponding to $\pm 3.5mm$.

Reliability

The reliability is quantified by comparing the *erosion rate* (E; Eqn. 3.8) of the deposits after the first flood between *Run_D* to *Run_F* (Table 3.9).

Table 3.9 Erosion rates (E) of deposits (Ds) D1 to D4 after the first flood of experimental run D to F. The initial volumes of the deposits ($V_{initial}$) are compared to those after the first flood (V_{after}). The statistical range ($\bar{R}$), the arithmetic mean (μ) and the standard deviation (σ) of E are calculated for every deposit.

Deposit	D1			D2			D3			D4			Total		
Experimental Run	D	E	F	D	E	F	D	E	F	D	E	F	D	E	F
$V_{initial}$ $[10^{-3}m^3]$	5.6	5.2	5.4	5.3	5.4	5.1	4.8	5.3	5.1	4.8	4.9	4.9	20.5	20.8	20.5
V_{after} $[10^{-3}m^3]$	4.7	4.4	4.5	2.8	3.4	3.4	1.0	1.2	1.4	1.9	1.3	1.5	10.4	10.3	10.8
E [%]	16.1	15.4	16.7	47.2	37.0	33.3	79.2	77.4	72.5	60.4	73.5	69.4	49.3	50.5	47.3
$\bar{R}$ [%]		1.3			13.9			6.7			13.1			3.2	
μ [%]		16.1			39.2			76.4			67.8			49.0	
σ [%]		0.7			7.2			3.5			6.7			1.6	

The highest range of *erosion rates* occurs at *D2* (13.9%) and *D4* (13.1%). The highest standard deviation occurs at *D2* in *Run_D* (7.2%) and *D4* in *Run_D* (6.7%). The standard

deviation of the total *erosion rate* is 1.6%. The erosion rates of all four deposits indicate high reliability, with the standard deviation for each deposit ranging between 0.7% and 7.2%. While the reliability of reproducing erosion rates of multiple, alternated deposits is expected to be lower compared to a single sediment deposit because of their reciprocal influence, our results are comparable to the mean error of erosion rates of a study focusing on deposit erosion processes of a single sediment deposit (<5%; Friedl et al., 2017).

Another approach to qualitatively assess the reliability of results is the comparison of the *spatial distributions of the vertical change* (Eqn. 3.4) between the channel after the first flood of *Run_D* to *Run_F* and the initial empty channel (**Figure 3.21**).

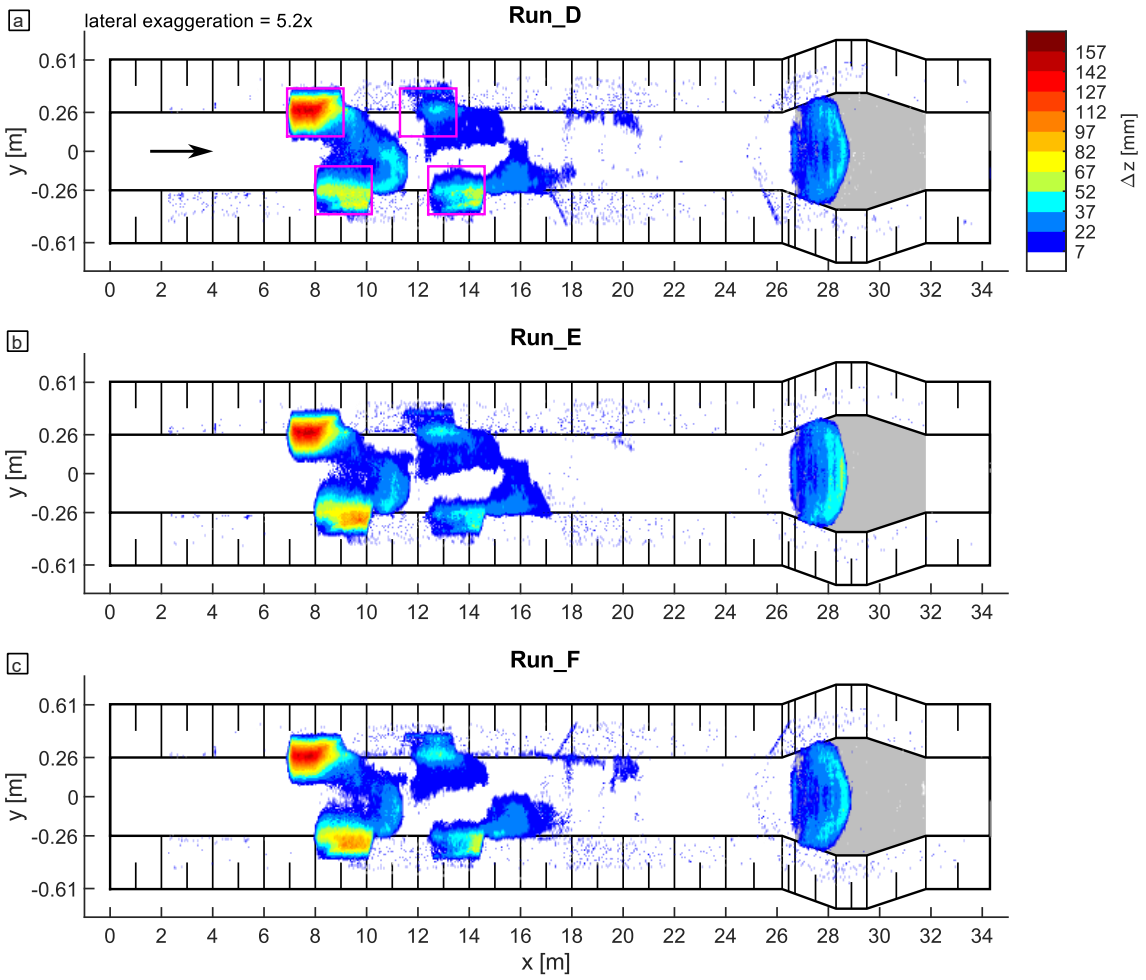

Figure 3.21 Graphic display of the spatial distribution of the vertical change (Δz) between the channel after the first flood of *Run_D* to *Run_F* (a–c) and the initial empty channel. Variable x is the longitudinal channel coordinate, and y is the lateral channel coordinate. The pink squares (a) mark the initial placement of the four deposits. The arrow (a) marks the direction of flow during the experiments. The grey area represents the mobile bed area.

Downstream of *D1* and *D2* ($[10, 11.5]m$), more sediment is deposited in *Run_D* than in *Run_E* and *Run_F* ($+13.6\%$). Downstream of *D3* and *D4* ($[15, 16]m$), sediment is deposited over the entire bed width in *Run_D* and *Run_E,* while in *Run_F*, parts of the channel centre are uncovered. Along the left side of the bed from *D3* to $10b_0$ downstream ($[13.5, 21]m$),

sediment is deposited in *Run_D* and *Run_F* but not in *Run_E*. The deposition pattern is similar in the zone of the channel widening (*ZOI3*, $[26.3, 31.8]m$), and the deposition volume is comparable between *Run_D* to *Run_F* ($\pm 10\%$). Overall, the *spatial distribution of the vertical change* is mainly similar except for the deposition between the initial deposits in *Run_D.* This discrepancy has limited influence on downstream deposition patterns like the volume deposited in the widening section ($\pm 10\%$).

3.3.7 Limitations

A principal limitation of the physical model is the fixed bed assumption. It implies that the initial bed is considered fully immobile throughout the experiment. This limitation causes the experiment to only represent rivers with a cover layer which resists a maximum shear stress of 13.1θ (see Figure 3.19, Table A5.1). It thereby limits the results of the physical model to fully sediment-starved rivers with a highly solidified armour layer. On the other hand, the advantage of the fixed bed assumption is the ability to isolate erosion, transport, and deposition processes of the augmented sediment.

3.4 Numerical modelling

Hydrodynamic modelling is performed with the software *BASEMENT* version 2.8.2. (VAW, 2022). The numerical model is designed for constant flow and steady-state simulations with a constant mesh. The objective of the numerical simulations is to quantify hydromorphological variability for different states of the experimental channel in response to low-flow conditions and thus estimate the impact of different configurations of SAMs on hydromorphological diversity.

3.4.1 Initial conditions

The so-called quality mesh defines the geometry of the simulation mesh. It contains two attributes. Those are the maximum triangle size and the hydraulic roughness (Figure 3.22).

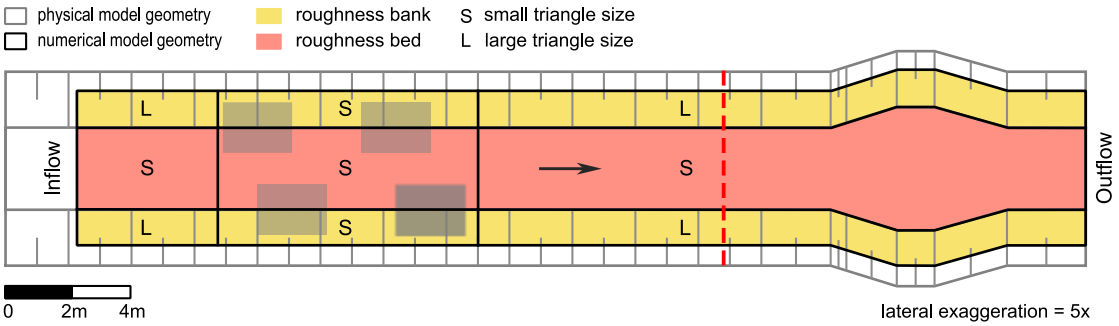

Figure 3.22 Graphic display of the geometry and attributes of the quality mesh. The grey-shaded rectangles represent the initial deposit positions. The red dashed line marks the position of the reference cross-section (CS). The arrow points in the direction of flow during the experiments.

Two categories were defined for the maximum triangle sizes. Their values correspond to an equivalent maximum grid length of $2cm$ (*small*) and $4cm$ (*large*). The higher mesh resolution is implemented at areas of higher topographic complexity, which are the area of the bed surface and the banks' areas at the deposits' initial position. Two categories were equally defined for hydraulic roughness. One is representative of the roughness of the bank, and the other of the roughness of the bed.

The elevation values for the simulation mesh are obtained from the scan topographies of the flume experiment (Section 3.3). The elevation values (z) of the *scan meshes* are interpolated at the location of all points of the *quality mesh* to obtain the simulation mesh for every scan. The initial state of all simulations corresponds to dry conditions. Since no morphodynamical processes were simulated, the *simulation mesh* (attributes and elevation) does not change over time.

3.4.2 Boundary conditions

The upstream boundary condition of the numerical model is a constant inflow at the inlet CS with a slope corresponding to the mean channel slope ($2.8‰$). The downstream boundary condition is a free surface elevation boundary at the outlet CS with a zero-gradient assumption. Numerical simulations are performed with a constant discharge of $2.2\,l/s$, representing low flow in field conditions ($0.7\,m^3/s$). This value is a scaled representation of residual flow at the Sarine River study site. Simulations are run until a steady state is reached. In initial simulations, the standard simulation time (t_s) for steady-state conditions was determined and set to $320s$.

3.4.3 Model calibration

The numerical model is designed for constant flow and steady-state simulations with a constant mesh. The calibration is therefore performed with different scenarios of constant flow releases. The most important calibration variable is hydraulic roughness.

The bed's hydraulic roughness and the banks' geotextile were calibrated with Ultrasonic Velocity Profiling (UVP) and water level measurements. The calibration measurements were conducted by Lionel Julien Pattaroni in the framework of his Master Project: *Influence of bank roughness and bed structure on riverbed morphology*. The project was supervised by the author of this thesis. The measurements were performed in the experimental flume at ten equally spaced measurement points across a reference CS (Figure 3.22).

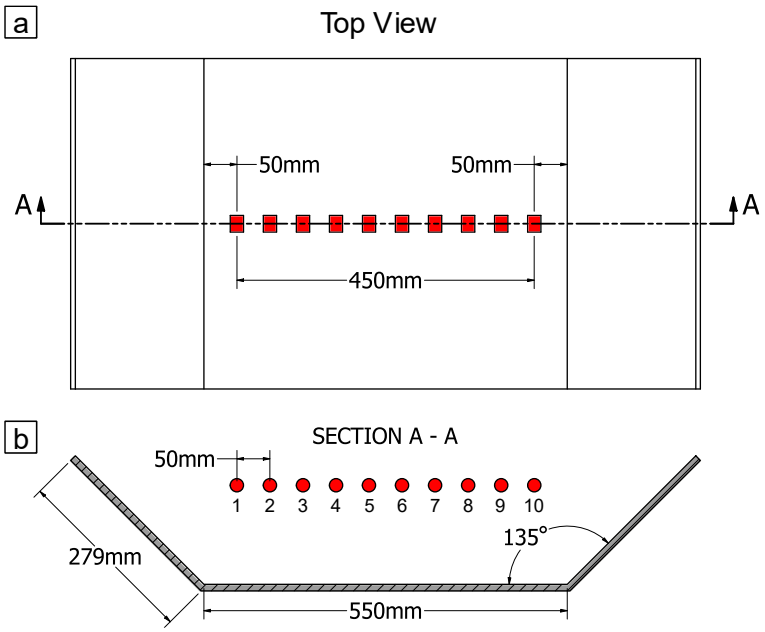

Figure 3.23 Location of the ten measurement points of the Ultrasonic Velocity Profiling (UVP) and water level measurements at the reference cross-section (CS) in the experimental channel. a: top view, b: cross-section A-A. The red points mark the location of the measurement points with the corresponding number labels below.

The location of the CS was fixed in the middle of the downstream run section (*section 5*, Figure 3.16). This location was selected because it has the steepest slope in the flume (0.64%, Table 3.6) and flow conditions are considered uniform in its upstream and downstream vicinity.

UVP measurements were performed with a UBERTONE UB-Lab profiler. Surface flow velocity was not measured because the UVP sensor was hallway submerged, facing downwards in the direction of the bed. For every vertical velocity profile, the average velocity in the flow direction (v) was obtained at $0.6h$ from the surface (e.g. Leopold et al., 1965). Therefore, the first two centimetres below the water surface were truncated. UVP measurements were only performed in the context of numerical model calibration. Water level measurements were performed with a hand-held measuring gauge.

The model was calibrated in two calibration phases. Photos of the different states of the physical model during the two calibration phases are shown in Figure 3.24.

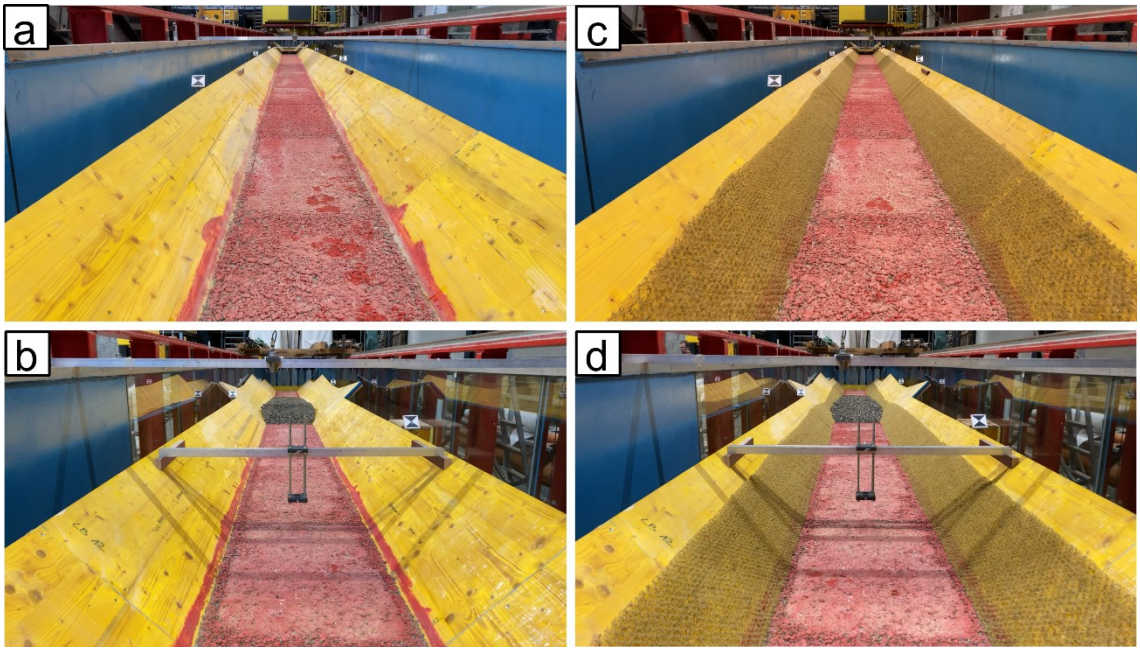

Figure 3.24 Photos of the physical model in flow direction during different calibration phases of the numerical model. a, b: Calibration phase 1 was performed with the experimental model *state 1* (**Table 3.7**). c, d: Calibration phase 2 was performed with the experimental model *state 2*. The pictures in a and c show the upstream part of the experimental channel. The pictures in b and d show the reference cross-section with the slidable mounting of the UVP sensor.

In the first calibration phase, constant discharges ($[20;\ 40;\ 60;\ 80]\ l/s$) were released into the empty channel *state 1* of the physical model. In this model state, no geotextile is installed on the banks. Calibration measurements were conducted for all four discharges. Then, three numerical simulations of the channel geometry in the same state and with the same constant discharges were performed. The roughness of the bank was set to $100\ m^{1/3}s^{-1}$ because the wooden planks have a very smooth surface. For the roughness of the bed, three different values for K_{st} were tested ($[30;\ 40;\ 50] m^{1/3}s^{-1}$) by the three simulations. The mean values of h and v of the calibration measurements were compared between the physical and numerical models **Table 3.10**.

Table 3.10 Mean values (μ) of depth-averaged velocity (μ_v) and water level measurements (μ_h) over the reference cross-section (CS) in calibration phase 1. The values were calculated by numerical simulations with different values of hydraulic bed roughness ($K_{st,bed}$) and by physical model measurements. Physical model measurements were performed by Ultrasonic Velocity Profiling (UVP) and with a hand-held measurement gauge. The reference CS is located at the centre of *section 5* (**Figure 3.22**).

	$\mu_v\ [m/s]$				$\mu_h\ [cm]$			
acquisition method	Q_{20}	Q_{40}	Q_{60}	Q_{80}	Q_{20}	Q_{40}	Q_{60}	Q_{80}
numerical model calculation, $K_{st,bank} = 30 m^{1/3}s^{-1}$	0.53	0.66	0.76	0.85	6.3	9.6	12.2	15.4
numerical model calculation, $K_{st,bank} = 40 m^{1/3}s^{-1}$	**0.61**	**0.79**	**0.95**	**1.06**	**5.4**	**7.9**	**9.6**	**12.0**
numerical model calculation, $K_{st,bank} = 50 m^{1/3}s^{-1}$	0.69	0.88	1.07	1.22	4.7	6.9	8.3	10.2
physical model measurement	0.63	0.75	0.98	1.04	5.2	7.8	9.5	11.5

Numerical simulations with $K_{st,bed}$ equal to 40 resulted in the closest representation of $\mu(v)$ and $\mu(h)$ at the reference CS. The *Pearson Correlation Coefficient* (PCC) is 0.985. The value 40 was therefore assigned to $K_{st,bed}$ in the following simulations.

In the second calibration phase, the channel state of the physical model was changed to *state 2*, which implies the installation of a geotextile along its banks. The procedure of comparing numerical model calculation with physical model measurements for different constant discharges was repeated. For the roughness of the bank, three different values of K_{st} were tested ($[20;\ 25;\ 30]m^{1/3}s^{-1}$). The resulting values of $\mu(v)$ are shown in Table 3.11.

Table 3.11 Mean values (μ) of depth-averaged velocity μ_v and water level measurements μ_h over the reference cross-section (CS) in calibration phase 2. The values were calculated by numerical simulations with different values of hydraulic bed roughness ($K_{st,bed}$) and by physical model measurements. Physical model measurements were performed by Ultrasonic Velocity Profiling (UVP). Water levels were calculated from UVP measurements using the continuity equation in this phase. The reference CS is located at the centre of *section 5* (Figure 3.22).

	$\mu_v\ [m/s]$				$\mu_h\ [cm]$			
acquisition method	Q_{20}	Q_{40}	Q_{60}	Q_{80}	Q_{20}	Q_{40}	Q_{60}	Q_{80}
numerical model calculation, $K_{st,bank} = 20m^{1/3}s^{-1}$	0.46	0.55	0.67	0.73	7.0	11.0	13.1	15.5
numerical model calculation, $K_{st,bank} = 25m^{1/3}s^{-1}$	**0.52**	**0.65**	**0.80**	**0.86**	**6.3**	**9.5**	**11.3**	**13.6**
numerical model calculation, $K_{st,bank} = 30m^{1/3}s^{-1}$	0.57	0.71	0.85	0.90	5.8	8.8	10.7	13.1
physical model measurement	0.51	0.64	0.78	0.85	6.4	9.7	11.6	13.7

Numerical simulations with $K_{st,bank}$ equal to 25 resulted in the closest representation of $\mu(v)$ at the reference CS. The *Pearson Correlation Coefficient* (PCC) is 0.999. The value 25 was therefore assigned to $K_{st,bank}$ in all future simulations of the physical channel with geotextile installed at its banks (*state 2* & *state 3*).

3.4.4 Limitations

With the assumption of uniform hydraulic roughness for the bed, the numerical model does not consider any change in roughness between mobile sediment patches and uncovered parts of the bed. However, this variation should favour hydromorphological diversity. It is therefore assumed that the $HMID$ tends to be underestimated in channel states with increased topographic complexity from mobile sediment deposition.

The physical model was calibrated at a single cross-section in steady-state flow conditions. This simplification leads to uncertainty about the model performance in other parts of the channel and unsteady flow conditions. The calculation of hydromorphological variability ($HMID$) from steady-state low-flow simulations is assumed to be little affected by this limitation.

Chapter 4
Influence of hydrograph shape on sediment transport dynamics of alternating in-channel sediment deposits

In this chapter, the first research question is addressed. The analysis is based on the parametric study of the physical model. Floods with different hydrograph skewness (symmetrical, left-skewed, right-skewed) were released to mobilise alternating in-channel sediment deposits. The erosion patterns of the artificial deposits reproduced well the case study at the Sarine River. Bedload transport rates at two downstream cross-sections were influenced by hydrograph skewness while always exhibiting a clockwise hysteresis. Pulse evolution occurred by a combination of translation and dispersion and was similar for floods with different hydrograph shapes.

4.1 Introduction

This chapter addresses the issue raised in the first research question.

- RQ1: What is the influence of the mobilising flow hydrograph on emerging bed forms from alternating sediment deposits?

The geomorphological terms relevant to restoration projects have been developed in Chapter 2 on background and literature research. "*Emerging*" forms refer to morphological features created from mobilised sediment of the augmentation measure. The term bedform, used in RQ1, is typically associated with in-channel mesoscale morphological features such as dunes, antidunes or riffles. While bedforms are known to influence bedload transport rates in gravel-bed rivers during constant discharge (e.g. Dhont & Ancey, 2018; Pascal et al., 2021), the motivation of research of this thesis is to predict bed morphology evolution in response to sediment augmentation coupled with artificial floods in bedload-starved reaches. Preliminary physical model experiments have shown that a single SAM does not lead to the manifestation of bedforms on a fixed bed representative of a sediment-depleted armour layer (Section 3.2.6). At the early stage of restoration, sediment pulse behaviour determines the deposition pattern of augmented sediment. The augmented sediment was observed to accumulate in patches at different CGUs, leaving large parts of the fixed bed surface uncovered. With multiple repetitions of SAMs, the bedload availability may be restored to a point where bedforms can develop on a mobile bed layer.

This chapter focuses on the influence of hydrograph shape on sediment transport dynamics of alternating in-channel sediment deposits to investigate the design of floods

for mobilising SAMs at an early restoration stage. In a previous flume experiment with a similar deposit configuration, the influence of transient flow releases with different peak times on bed morphology evolution was studied (Battisacco, 2016). The following experiments are run in a channel with a flatter, changing slopes in the impact reach ($[0, 0.64]\%$) compared to the previous study (1.5%). Bed morphology evolution is calculated and displayed from 3D laser scans, allowing for visual analysis of the vertical change of the bed elevation. Bedload transport rates are calculated at two CS at different distances from the deposits. Pulse evolution behaviour is derived from a temporal sequence of the elevation difference along the channel axis.

4.2 Test configuration

The experiments on the topic of this chapter include *Run_A* to *Run_C* of the parametric study. The related methodology is explained in Section 3.3.5. The dataset of the experimental results is publicly available (Mörtl & De Cesare, 2022b). The extract of the experimental planning and the relevant definitions for the experiments are presented in Figure 4.1.

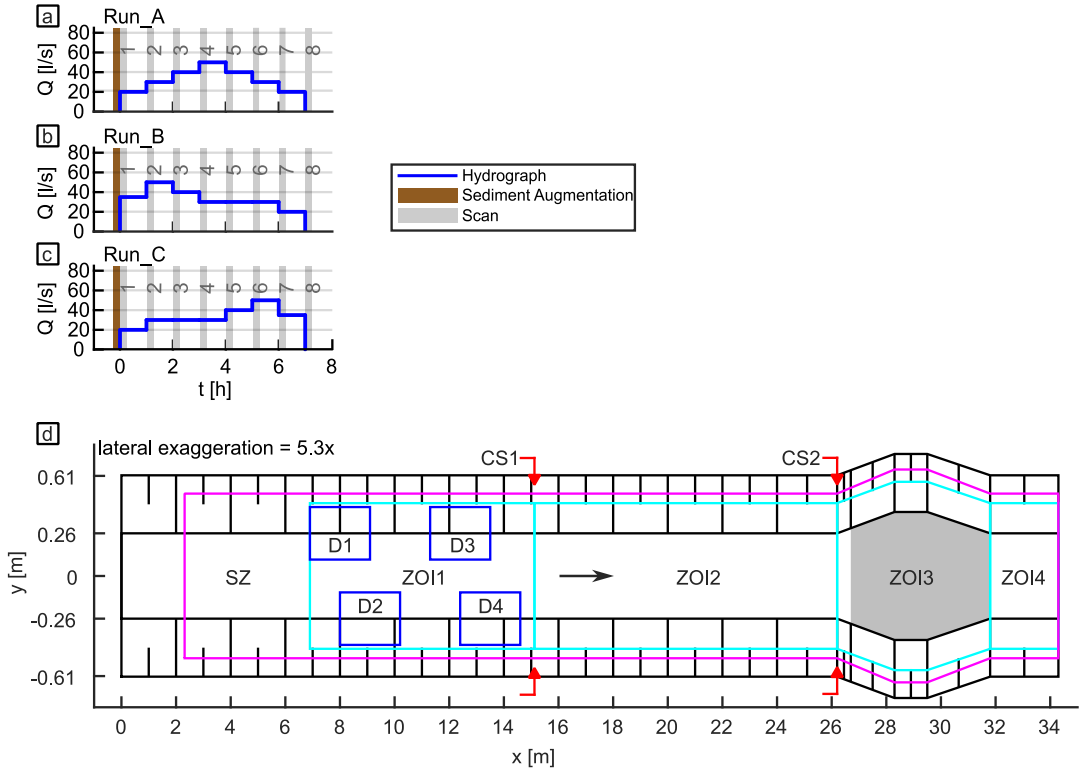

Figure 4.1 Schema of the experimental planning and the experimental channel relevant to the experiments of Chapter 4. The dimensions are given at the model scale. a–c: Experimental planning of run A (*Run_A*) to *Run_C*. Variable Q is the discharge, and t is the time. The number on the scan bar describes the scan number. The flood volume is similar for all hydrograph shapes ($\pm 2\%$). d: Schema of the experimental channel in the top view. Variable x is the longitudinal coordinate, and y is the lateral coordinate. Blue squares represent the initial placement zones for sediment deposits (Ds) D1 to D4. Cyan polygons represent the zones of interest (ZOI) ZOI1 to ZOI4. The magenta polygon represents the scan zone (SZ). The red arrows mark the two cross-sections (CSs), CS1 & CS2. The grey area represents the mobile bed area. The black arrow marks the direction of flow during the experiments.

4.3 Bed morphology evolution

The vertical change between different timesteps during the first flood of *Run_A*, *Run_B* and *Run_C*, and the empty channel is shown in Figure 4.2 to Figure 4.4. The graphic displays of scan topographies were designed to visually analyse the 2D distribution of augmented sediment on the fixed bed surface. Using the empty channel as a reference results in only the deposition of mobile material above the initial bed elevation is calculated. This result is intentional when analysing the resulting bed morphology. The temporal process of erosion and deposition between the corresponding timesteps is displayed in Figure A6.1 to Figure A6.3 in the appendix.

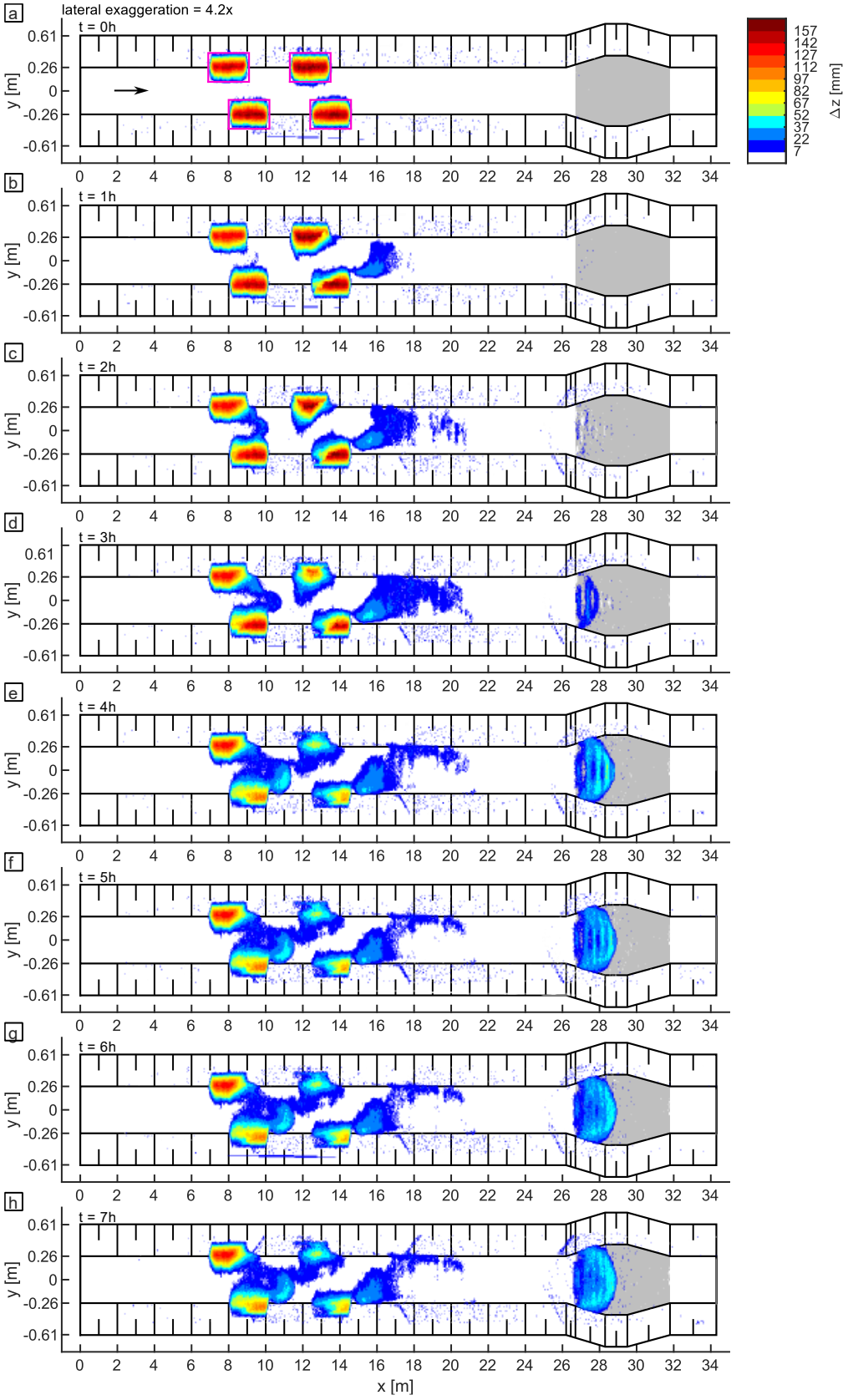

Figure 4.2 Graphic display of the vertical change (Δz) during the first flood of *Run_A*. a-h: Difference between Scan 1 to Scan 8 and the empty channel. Variable x is the longitudinal channel coordinate, and y is the lateral channel coordinate. The label t indicates the experimental time. The pink squares (a) mark the initial placement of the four deposits. The arrow (a) marks the direction of flow during the experiments. The grey area represents the mobile bed area.

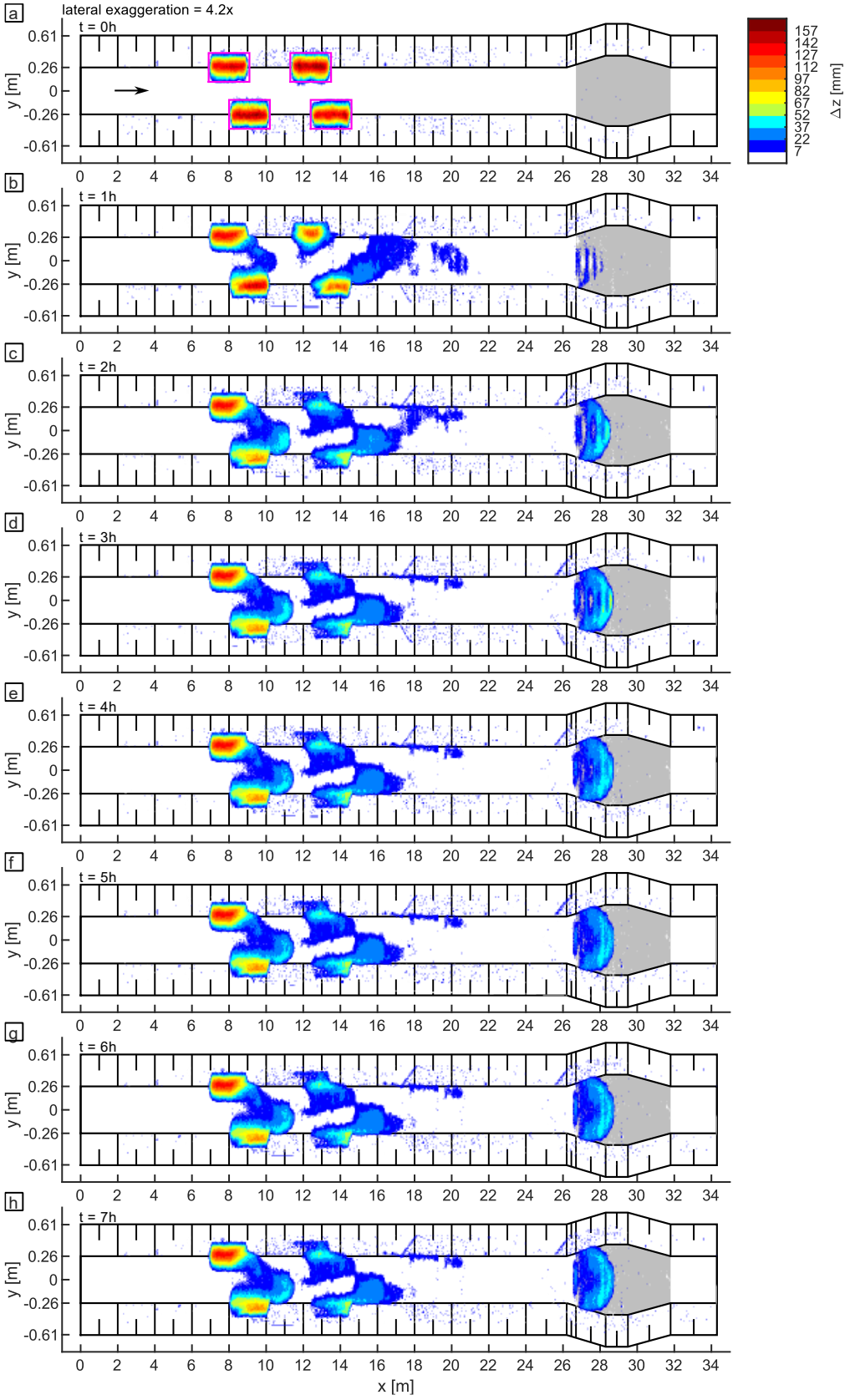

Figure 4.3 Graphic display of the vertical change (Δz) during the first flood of *Run_B*. a-h: Difference between Scan 1 to Scan 8 and the empty channel. Variable x is the longitudinal channel coordinate, and y is the lateral channel coordinate. The label t indicates the experimental time. The pink squares (a) mark the initial placement of the four deposits. The arrow (a) marks the direction of flow during the experiments. The grey area represents the mobile bed area.

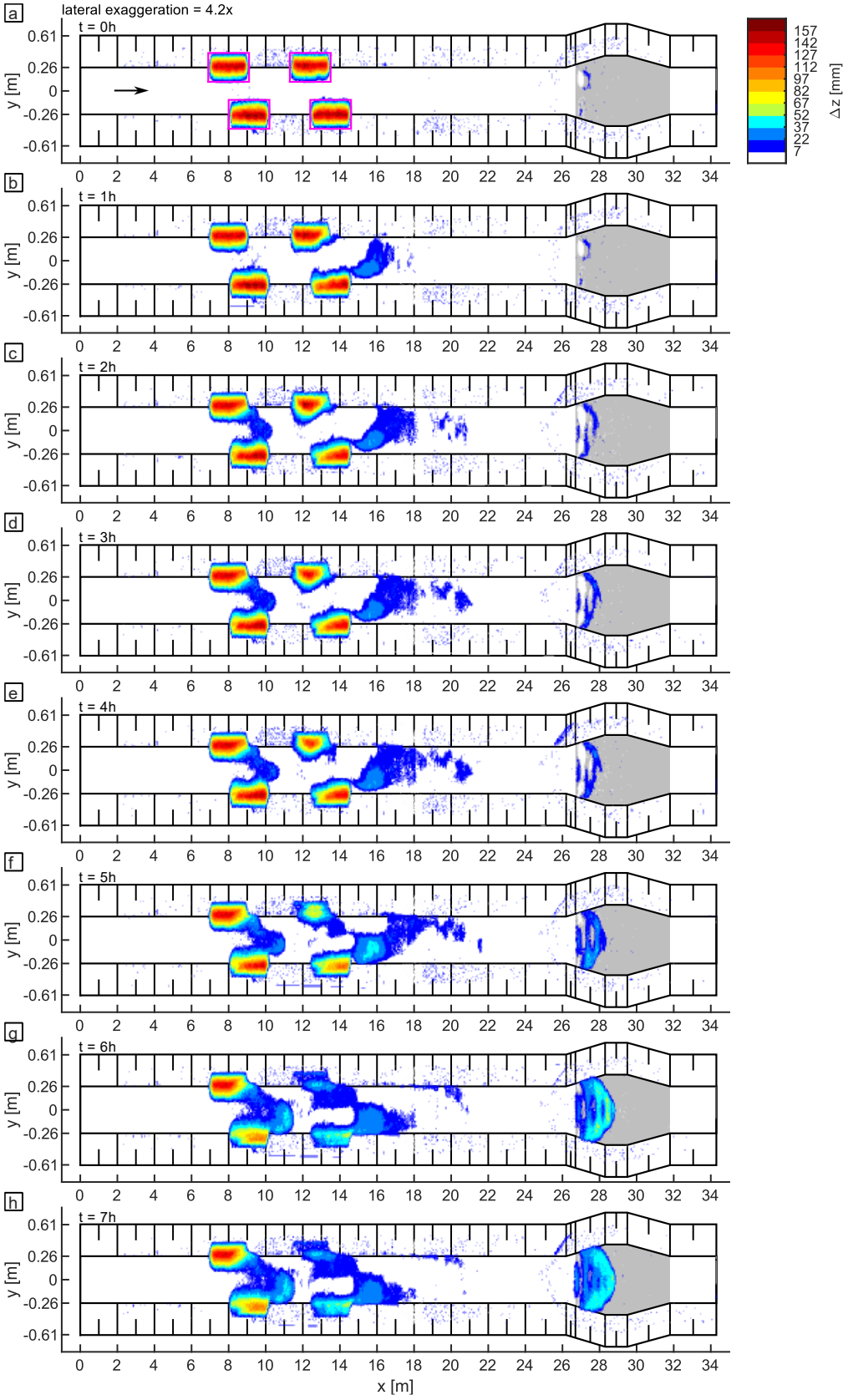

Figure 4.4 Graphic display of the vertical change (Δ*z*) during the first flood of *Run_C*. a-h: Difference between Scan 1 to Scan 8 and the empty channel. Variable x is the longitudinal channel coordinate, and y is the lateral channel coordinate. The label t indicates the experimental time. The pink squares (a) mark the initial placement of the four deposits. The arrow (a) marks the direction of flow during the experiments. The grey area represents the mobile bed area.

No sediment ($< 0.1\%$) was transported out of the channel in all experiments. The upstream deposit (D1) remains mainly uneroded during the first flood, independent of the hydrograph shape. A thin layer of mobile surface cover ($[1, 2]d_{50,mobile}$) forms in the near downstream vicinity of the deposits ($[15, 20]m$) during the rising limb of all hydrograph shapes. This area is then reduced by partial erosion during the falling limb. Once washed out from the near downstream vicinity, sediment is deposited in the zone of the channel widening. No sediment patches manifest in the steeper run section (*section 5*, $[20, 26]m$) at any time during the first flood.

4.4 Bedload transport rates

Sediment transport rates are compared for the first floods of *Run_A* to *Run_C* across *CS1* and *CS2* (Figure 4.5). The corresponding data table can be found in the appendix (Table A9.1).

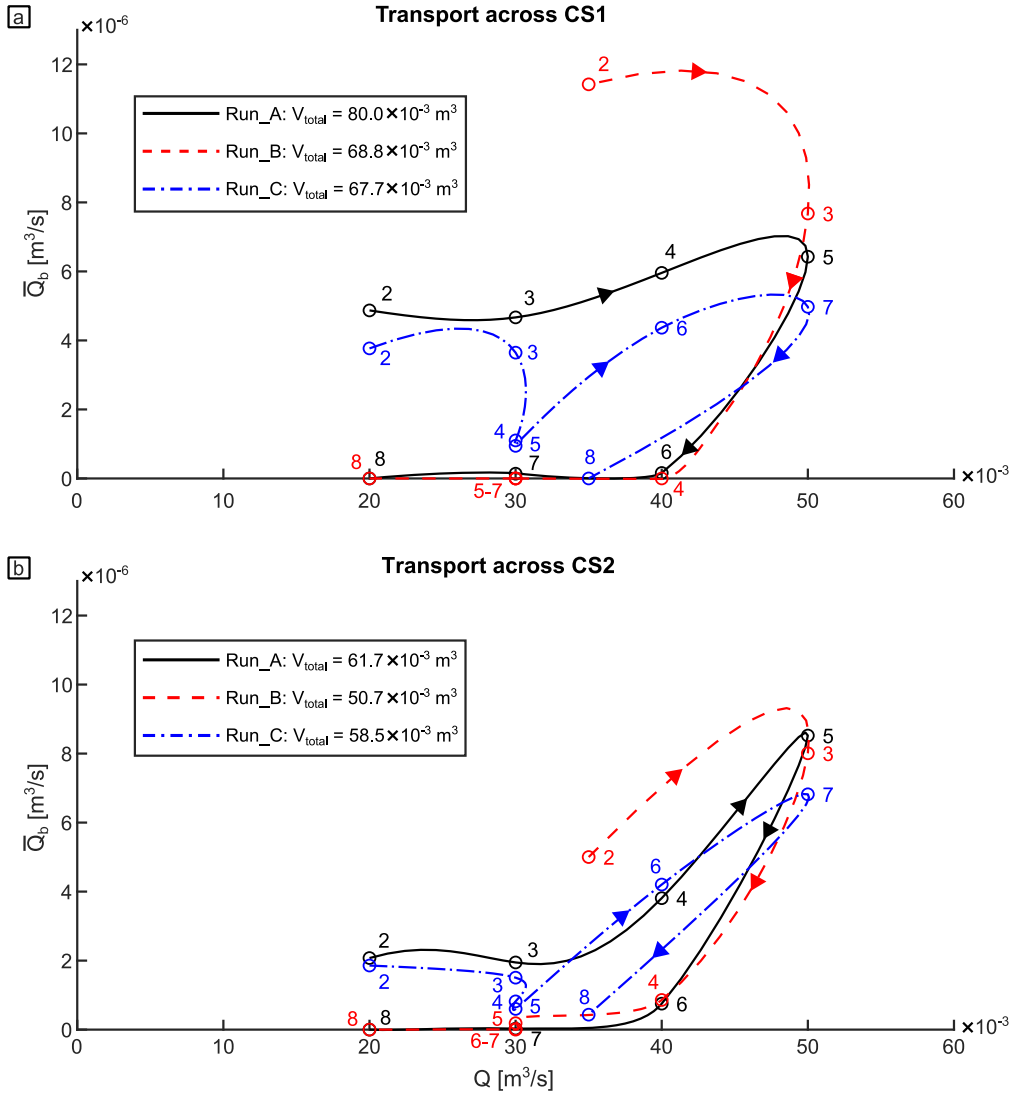

Figure 4.5 Graphs of the average bedload transport rates ($\bar{Q}_b$) during periods of constant discharge (Q) for cross-section (CS) CS1 (a) and CS2 (b). The circles represent the calculated values. The numbers represent the scan number of the corresponding runs. The lines, represented by cubic splines and arrows, indicate the temporal sequence.

The total transport volume across *CS1* and *CS2* is higher in *Run_A* than in *Run_B* and *Run_C*. The total transport volume in *Run_B* compared to *Run_C* is higher across *CS1* and lower across *CS2*. All floods produce a clockwise hysteresis. The transport rate in *Run_A* remains relatively constant from the rising limb until the peak across *CS1* ($[4.7,\ 6.4] \times 10^{-6}\ m^3/s$) and increases quite strongly across *CS2* ($[2.0,\ 8.6] \times 10^{-6}\ m^3/s$). Transport rates during a period of equal discharge in *Run_B* and *Run_C* decrease stronger on average across *CS1* ($1.7 \times 10^{-6}\ m^3/s$) than across *CS2* ($1.0 \times 10^{-6}\ m^3/s$). Therefore, transport rates decrease by 70% more near the artificial deposits (1 channel width) than at 20 channel widths further downstream. Across *CS1* and *CS2*, the peak discharge of all floods corresponds to the highest transport rates, except in *Run_B* across *CS1*.

Results suggest that symmetrical hydrographs cause higher bedload transport near the deposits ($1b_0$; *CS1*) and further downstream ($20b_0$; *CS2*) than asymmetrical hydrographs. It highlights that symmetrical hydrographs can promote the mobilisation of alternated, in-channel deposits. Experiments in a steeper flume (Battisacco, 2016) have led to a complete erosion of deposits independent of the hydrograph shape. The partial erosion of upstream deposits in the experiment presented in this chapter agrees well with observations in the reference case study (Stähly et al., 2019).

The direction of skewness can influence the length of the impact section. The results suggest that right-skewed hydrographs cause higher bedload transport near the deposits ($1b_0$) and lower bedload transport further downstream ($20b_0$) than left-skewed hydrographs. It is attributed to the fact that during low discharge ($\leq 30\ l/s$), the hydrodynamic force is sufficiently high to erode the deposits due to the local channel restriction but insufficient to mobilise mobile sediment in most parts of the downstream section. The later peak of the left-skewed hydrograph increases the time of downstream sediment transport, and thus the mean transport distance, after the partial erosion of the deposits.

The experiment shows that transport rates during a period of equal discharge decrease stronger near the deposits ($1b_0$) than further downstream ($20b_0$). The decrease in transport rates with longer floods was also experienced in a straight flume experiment with constant sediment feed and mobile bed (Plumb et al., 2020). The authors attributed this to the insufficient time for the channel to adjust to changing flow conditions (Plate, 1994). Our results seem to confirm this hypothesis. The stronger decrease close to the deposits ($1b_0$) is attributed to a shorter distance from the sediment source and, thus, a shorter time lag for the adaptation of transport rates.

During all tested hydrograph shapes, bedload transport rates exhibited a clockwise hysteresis. Clockwise bedload hysteresis was also experienced in laboratory experiments with mobile bed and pulse injection (Humphries et al., 2012) and continuous sediment feed for long-duration hydrographs (Plumb et al., 2020). In our experiment, high transport rates during the rising limbs are attributed to the deposits' relatively rapid erosion and the fixed bed's low roughness. Lower transport rates during the falling limbs can be explained by reduced sediment availability from the deposits and higher macro-roughness from morphological complexity.

4.5 Pulse evolution

Pulse evolution is compared by the analysis of the elevation difference (ED) and the cumulative ED (CED) during the first flood of *Run_A* to *Run_C* along *ZOI2* (Figure 4.6).

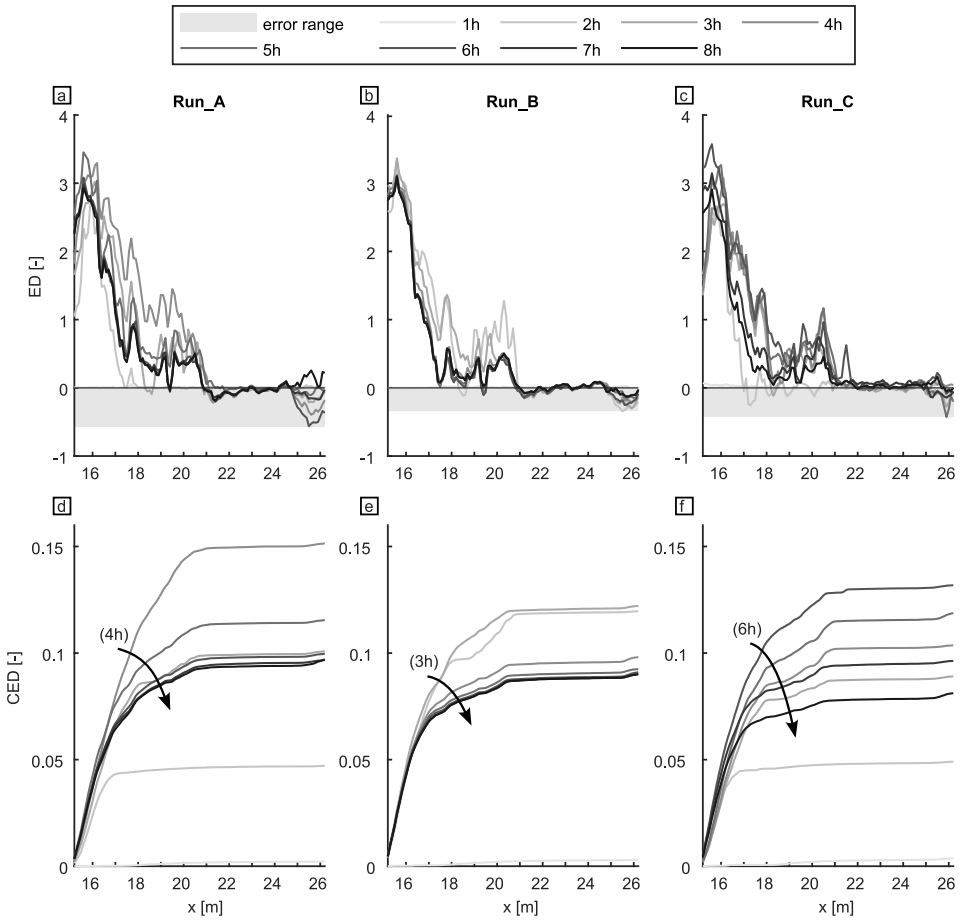

Figure 4.6 Graphs of the elevation difference (ED, a–c) and the cumulative elevation difference (CED, d–f) in the near downstream zone (ZOI2) between different channel states during the first floods of Run A to Run C and the empty channel state (S0). Variable x is the longitudinal channel coordinate. The ED is normalised by the weight-based median grain size diameter (d_{50}) of the mobile sediment ($d_{50,mobile}$). The CED is normalised by the total volume of the sediment augmentation of each run. The arrows indicate the direction of pulse evolution after the highest CED curve. The label of the arrow indicates the time of the highest CED curve.

The range of negative values of ED represents the error range because no erosion is possible below the fixed bed surface. The maximum ED error in *Run_A* to *Run_C* corresponds to $0.6d_{50,mobile}$ ($0.4cm$). The ED is near zero in the lower downstream section ($[21, 25]m$) during the entire flood of *Run_A* to *Run_C*. In the upstream section ($[16, 21]m$), the CED curves are rotated clockwise after the peak discharge in *Run_A* (4h) and *Run_C* (6h) and 1 hour later in *Run_B* (3h). The CED curves in the downstream section ($[21, 25]m$) are nearly horizontal in *Run_A* to *Run_C*.

In this experiment, pulse evolution behaviour is similar for symmetrical and asymmetrical hydrographs in the near downstream zone of the deposits ($< 20b_0$). Different hydrograph shapes cause clockwise rotation of the CED curves directly downstream of the hydraulic impact zone of the deposits ($< 12b_0$). This behaviour is characteristic of dispersion-dominated pulse evolution (Sklar et al., 2009). A combination of translation and dispersion along the entire channel occurred in flume experiments with fixed bed and continuous sediment augmentation (Sklar et al., 2009). The domination of dispersion in

our experiment is attributed to the sediment supply in the form of multiple deposits instead of a constant feed rate. A tongue-shaped deposition front is shaped downstream of the deposits during the rising limb, and its leading edge is dispersed during the falling limb. The horizontal behaviour of the CED in the downstream section ($[21, 25]m$) for all hydrograph shapes indicates a section of transition, where sediment is routed through without the formation of persistent patches on the channel bed. Our results, which suggest a combination of translational and dispersional pulse evolution from alternated in-channel deposits, agree with previous laboratory experiments (Battisacco et al., 2016).

4.6 Conclusion

The findings of this chapter refer to sediment augmentation measures in the form of alternating in-channel deposits, which are shifted half of the deposit length (configuration B; Battisacco et al., 2016) and placed along an elevated portion of the riverbed (riffle). The reach type is restricted to low-gradient ($< 1\%$), sediment-starved, gravel-bed rivers.

The results suggest the following statements for the mobilisation of the artificial deposits:

- Floods with symmetrical hydrograph cause on average 15% higher bedload transport rates than floods with asymmetrical hydrographs.
- Floods with right-skewed hydrographs cause 2% higher bedload transport rates near the artificial deposits (1 channel width) and 13% lower bedload transport further downstream (20 channel widths) than left-skewed hydrographs.
- During periods of equal discharge, transport rates decrease on average 70% more near the artificial deposits (1 channel width) than further downstream (20 channel widths).
- Bedload transport exhibits a clockwise hysteresis.
- Pulse evolution occurs by a combination of translation and dispersion.

The results confirm the initial hypothesis H1 that the hydrograph skewness of the mobilising flood influences sediment transport dynamics from in-channel sediment deposits. Furthermore, it was found that the hydrograph shape of floods with similar volume influences bedload transport rates differently at varying distance from the deposits. The main erosion- and transport patterns remain similar and independent of the hydrograph shape.

Chapter 5
Influence of sediment augmentation repetition frequency on bed morphology evolution

In this chapter, the second research question is addressed. The analysis is based on the results of the physical model. Different scenarios with varying sediment augmentation repetition frequencies (before every or every second mobilising flood) coupled with floods with varying peak discharge (1.2 and 2.5 times the entrainment threshold) are tested. The persistence of mobile sediment patches, deposition rates, and percentage of cover was influenced by sediment augmentation repetition frequency. Consecutive sediment augmentations combined with floods with varying peak discharges did not improve hydromorphological diversity more than in combination with identical floods with lower peak discharge.

5.1 Introduction

This chapter addresses the issue raised in the second research question.

- RQ2: How can the persistence of the resulting bed forms be estimated on a morphologic timescale for a given hydrologic pattern?

The term bedform was discussed in the previous chapter. It was clarified that the research motivation for this thesis is to predict bed morphology evolution on the channel and reach scale. Respectively in this chapter, the persistence of morphological features from SAMs refers to the total volume of augmented sediment in an area rather than a specified feature type. The temporal impact scale of SAMs was addressed in Chapter 2 on background and literature research (Figure 2.3). A prediction can only be made of the morphological impact of SAMs on a defined timescale with the prediction of flow variability and sediment availability. Here, three different hydrological scenarios are developed, similar to the approach of Plumb et al. (2020), who derived different hydrological conditions from measured hydrometric field data. It is assumed that no significant morphological changes occur between the floods, so the time of occurrence and, thereby, the temporal impact scale is neglected in this investigation.

This chapter focuses on the influence of sediment augmentation repetition frequency on bed morphology evolution to investigate the efficiency of consecutive SAMs in combination with different hydrological scenarios. In a previous flume experiment with a similar deposit configuration, the influence of a single repetition of a SAM on bed morphology evolution was investigated (Bösch et al., 2016). The following experiments are run with up to four repetitions and varying flood scenarios. Bed morphology evolution is

calculated and displayed from 3D laser scans, allowing for visual analysis of the vertical change of the bed elevation. Deposition and percentage of cover are calculated for the near downstream target zone and compared between different scenarios. At the same time, the persistence of augmented sediment is considered for the discussion. The hydromorphological diversity of the resulting channel morphologies is calculated from numerical model results.

5.2 Test configuration

The experiments on the topic of this chapter include *Run_D* to *Run_F* of the parametric study. The related methodology is explained in Section 3.3.5. The dataset of the experimental results is publicly available (Mörtl & De Cesare, 2022b). The extract of the experimental planning and the relevant definitions for the experiments are presented in Figure 5.1.

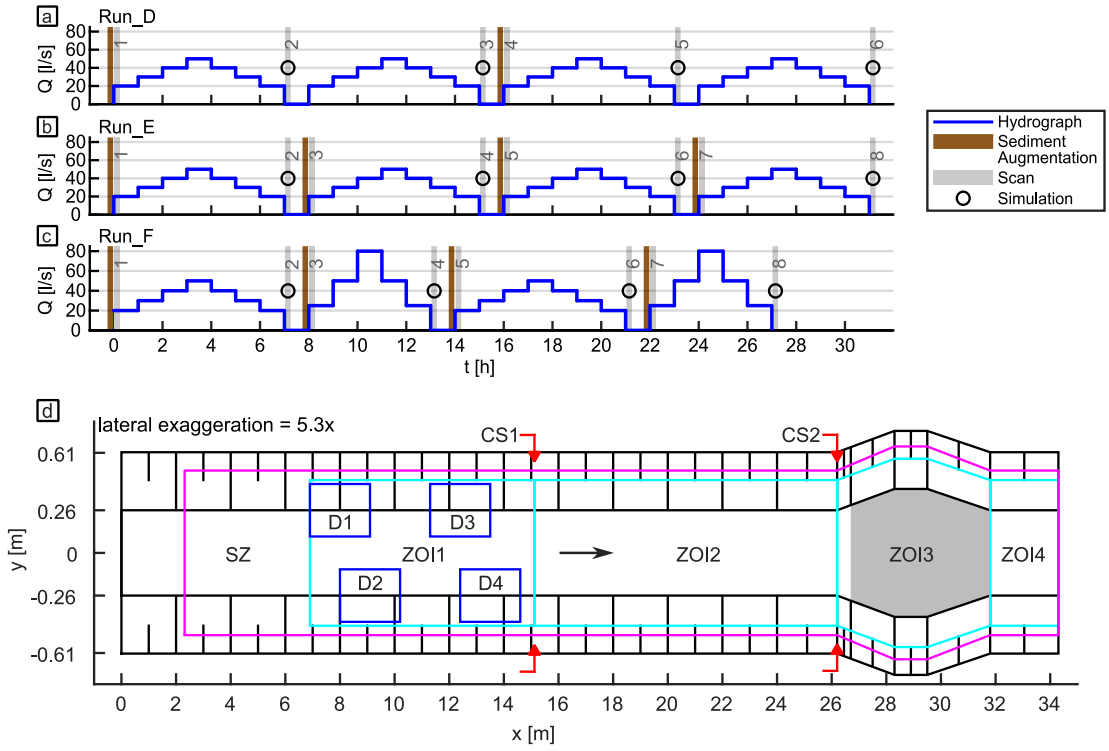

Figure 5.1 Schema of the experimental planning and the experimental channel relevant to the experiments of Chapter 5. The dimensions are given at the model scale. a–c: Experimental planning of run D (*Run_D*) to *Run_F*. Variable Q is the discharge, and t is the time. The number on the scan bar describes the scan number. The flood volume is similar for all hydrograph shapes ($\pm 2\%$). d: Schema of the experimental channel in the top view. Variable x is the longitudinal coordinate, and y is the lateral coordinate. Blue squares represent the initial placement zones for sediment deposits (Ds) D1 to D4. Cyan polygons represent the zones of interest (ZOI) ZOI1 to ZOI4. The magenta polygon represents the scan zone (SZ). The red arrows mark the two cross-sections (CSs), CS1 & CS2. The grey area represents the mobile bed area. The black arrow marks the direction of flow during the experiments.

5.3 Bed morphology evolution

The vertical change between different timesteps after every flood of *Run_D*, *Run_E* and *Run_F*, and the empty channel is shown in Figure 4.2 to Figure 4.4. The temporal process of erosion and deposition between the floods is displayed in Figure A7.1 to Figure A7.3 in the appendix.

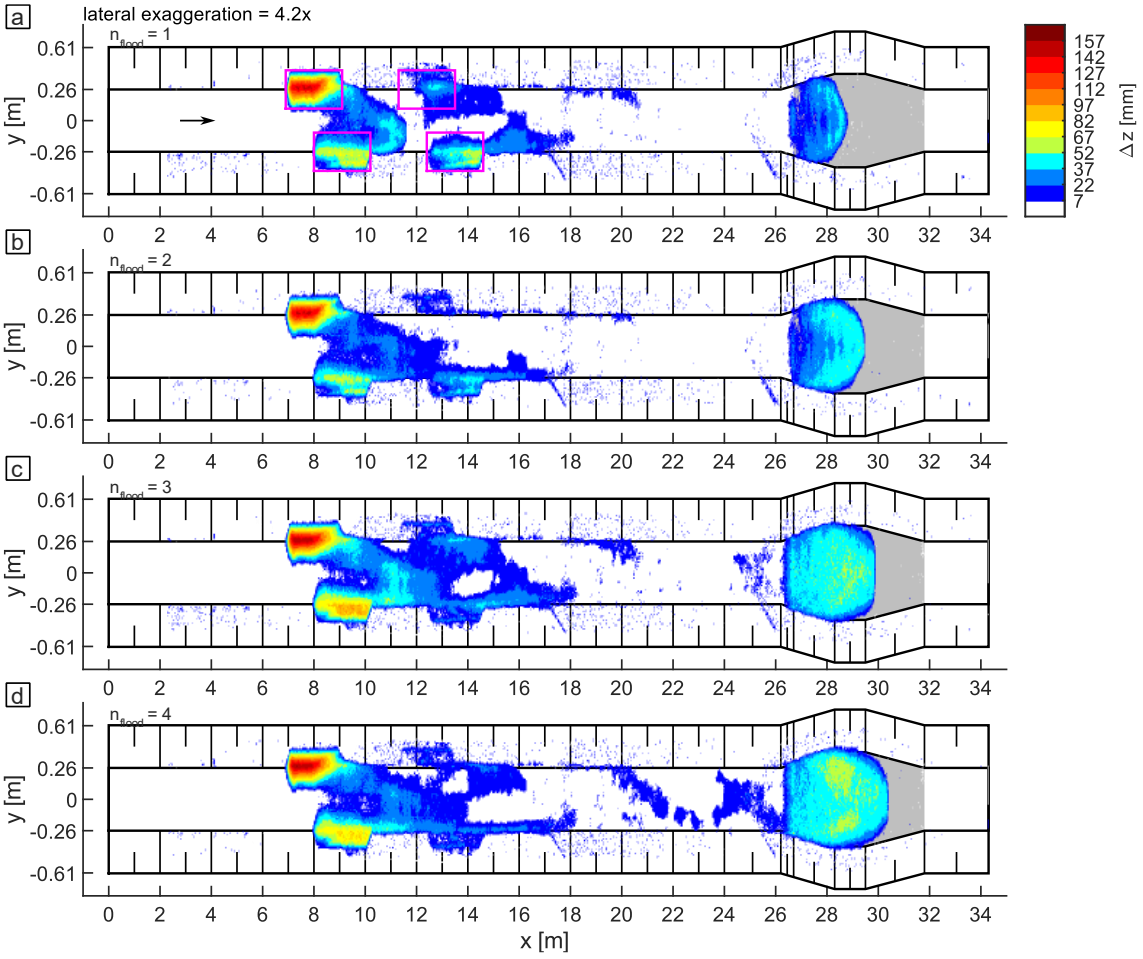

Figure 5.2 Graphic display of the vertical change (Δz) after every flood of *Run_D*. a-d: Difference between the scans after 1 to 4 floods (n_{flood}), and the empty channel. Variable x is the longitudinal channel coordinate, and y is the lateral channel coordinate. The pink squares (a) mark the initial placement of the four deposits. The arrow (a) marks the direction of flow during the experiments. The grey area represents the mobile bed area.

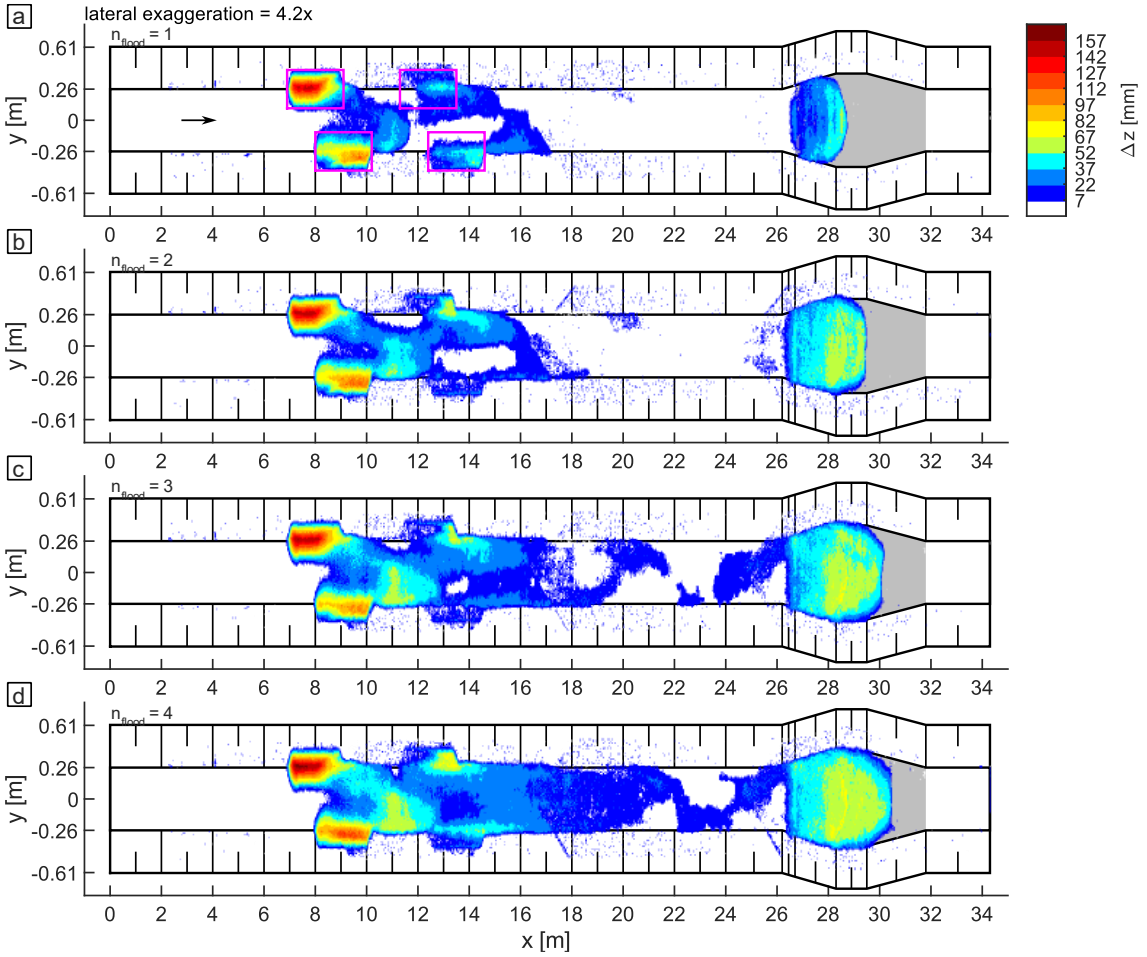

Figure 5.3 Graphic display of the vertical change (Δ*z*) after every flood of *Run_E*. a-d: Difference between the scans after 1 to 4 floods (n_{flood}) and the empty channel. Variable x is the longitudinal channel coordinate, and y is the lateral channel coordinate. The pink squares (a) mark the initial placement of the four deposits. The arrow (a) marks the direction of flow during the experiments. The grey area represents the mobile bed area.

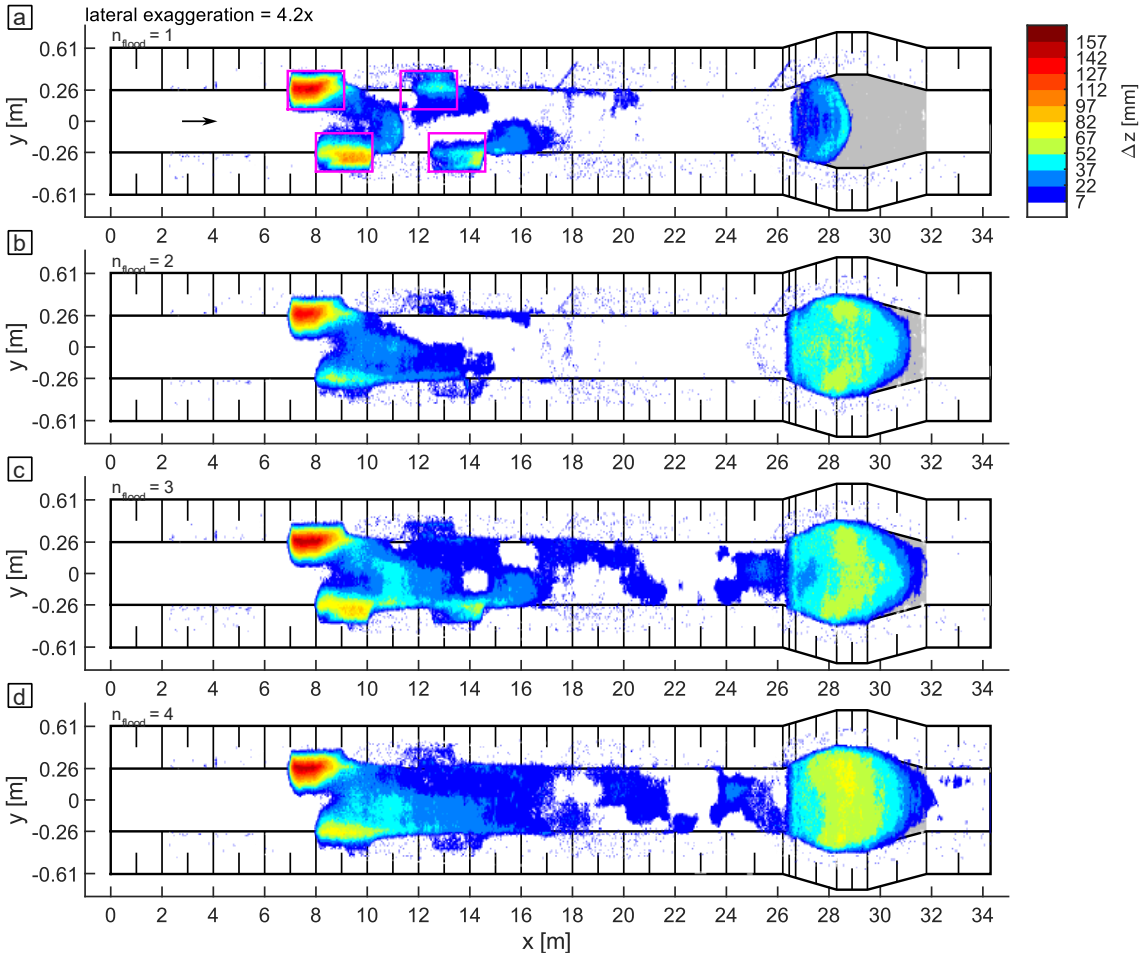

Figure 5.4 Graphic display of the vertical change (Δz) after every flood of *Run_F*. a-d: Difference between the scans after 1 to 4 floods (n_{flood}) and the empty channel. Variable x is the longitudinal channel coordinate, and y is the lateral channel coordinate. The pink squares (a) mark the initial placement of the four deposits. The arrow (a) marks the direction of flow during the experiments. The grey area represents the mobile bed area.

The total volume added was compared to the initial volume of the deposits ($V_{initial}$) for all three runs. The total volume added corresponds to $1.4V_{initial}$ in *Run_D*, $2.2V_{initial}$ in *Run_E* and $2.7V_{initial}$ in *Run_F*. Sediment was transported outside the channel only during *Run_F*. The sediment volume in the trap (V_{trap}) corresponds to less than $0.01\ V_{initial}$ after the second and third floods and to $0.15\ V_{initial}$ after the fourth flood. The upstream deposit (D1) remains largely uneroded during all floods.

In *Run_D*, increased accumulations of sediment patches form only after four floods in the downstream target zone ($[15, 26]m$; *ZOI2*) in the channel centre. In *Run_E*, a cover layer of mobile sediment across the entire channel width emerges after three floods coupled with sediment augmentation in the upstream part of the target section ($[15, 18]m$). It expands further downstream after the fourth flood ($[15, 21]m$). Alternating sediment patches manifest in the downstream section until the channel widening ($x = 26m$). In *Run_F*, sediment patches in the downstream target section (*ZOI2*) were in the channel centre rather than in alternating formation along the banks after four floods. In the widening section (*ZOI3*), the deposition front developed across the entire section and sediment was

released to the downstream end of the target zone ($[32, 34]m$; *ZOI4*) during the fourth flood.

5.4 Deposition and percentage of cover

The dimensionless deposition (D^*; Eqn. 3.9) and the percentage of cover (POC) are compared for the zones of interest *ZOI1* to *ZOI3* after all floods of *Run_D* to *Run_F* (Figure 5.5). The corresponding data table can be found in the appendix (Table A9.2).

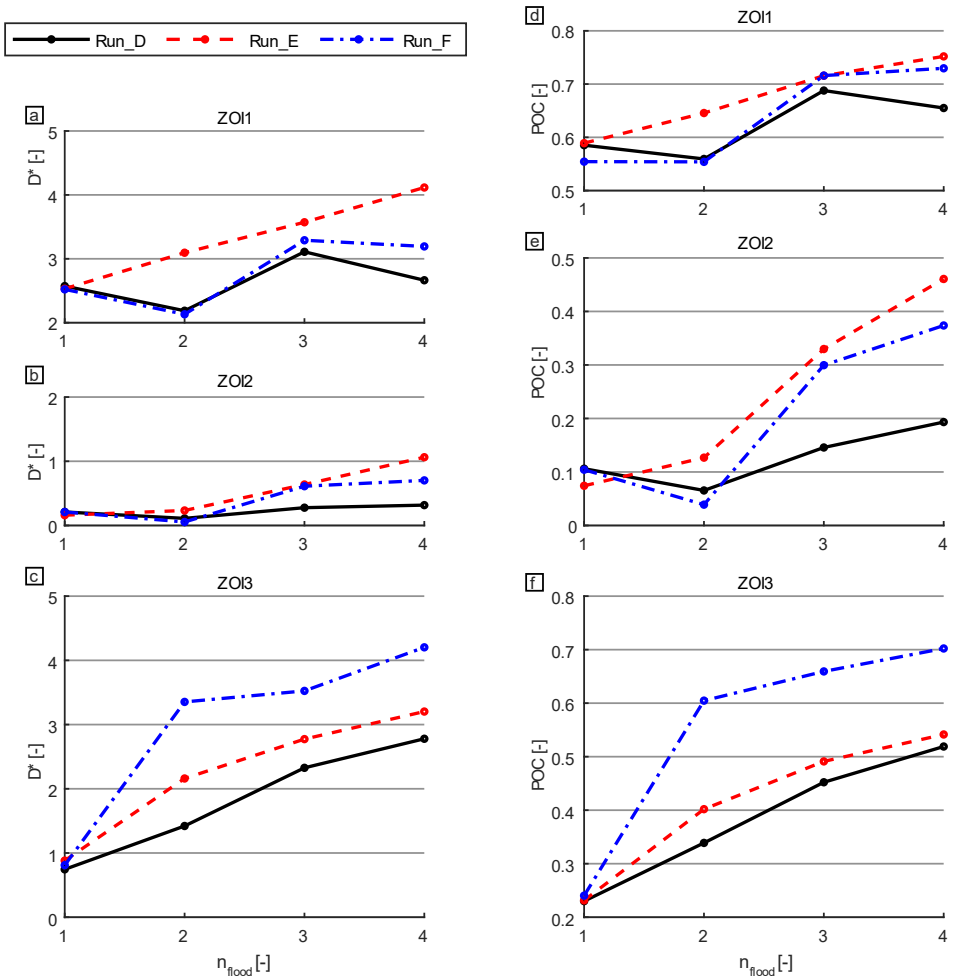

Figure 5.5 Graphs of the dimensionless deposition (D^*, a–c) and the percentage of cover (POC, d–f) for the number of released floods (n_{flood}) of *Run_D* to *Run_F* in the three zones of interest (ZOI) *ZOI1* to *ZOI3*. The scaling of the ordinate is consistent for both parameters (a–c & d–f).

In *Run_D* to *Run_F*, D^* and POC are close to zero in *ZOI4*, except after the last flood of *Run_F* ($D^* = 0.1$; $POC = 6.4\%$). For all floods, the highest D^* in *ZOI1* and *ZOI2* occurs in *Run_E*, and the highest D^* in *ZOI3* occurs in *Run_F*. After four floods, the average D^* of *Run_D* to *Run_F* is 3.3 in *ZOI1*, 0.7 in *ZOI2* and 3.4 in *ZOI3*. The average D^* in the *MIZ* is 1.55 in *Run_D*, 2.36 in *Run_E* and 2.19 in *Run_F*.

In *Run_D* to *Run_F*, the POC reflects the deposition trend for all *ZOI*. After two floods, the average POC of *Run_D* to *Run_F* is 58.6% in *ZOI1*, 7.7% in *ZOI2* and 44.9% in *ZOI3*. After four floods, the average POC of *Run_D* to *Run_F* is 71.2% in *ZOI1*, 34.3% in *ZOI2* and 58.7% in *ZO3*. After four floods, the average POC in the *MIZ* is 38.6% in *Run_D*, 52.4% in *Run_E* and 52.7% in *Run_F*.

These results confirm that deposition and POC are higher for consecutive augmentation measures and floods if sediment augmentation is performed with every flood than if only with every second. This result is expected, as feeding more material in similar flood scenarios in a channel with a fixed bed leads to a net increase in the amount of sediment available for deposition and surface cover. With every consecutive sediment augmentation, the bedload transport condition in the downstream section changes further from a (sediment) supply-limited condition to a (transport) capacity-limited condition.

In the near downstream zone of the deposits ($< 20b_0$, Figure 5.5:b&e), deposition in *Run_D* remained low after four floods ($D^* = [0.11, 0.32]$). It was observed that fresh sediment patches from previous augmentations were washed out in floods without sediment augmentation. It is concluded that these patches do not exert enough flow resistance on the sediment-depleted bed with low morphological complexity and macro surface roughness if no new upstream sediment is supplied to maintain a minimal patch size. These findings agree with Nelson et al. (2009), which showed that, in a channel with a mobile bed, the abundance of sediment patches is tied to sediment supply, and the complete elimination of sediment supply results in a nearly total loss of bed surface heterogeneity. *Run_E* and *Run_F* produced similar deposition to *Run_D* after the first two floods. Then, contrary to *Run_D*, deposition increased notably for both runs after the third flood ($D^* > 0.6$). This behaviour is attributed to the repeated sediment augmentation of *Run_E* and *Run_F* leads first to a progressive bed level rise in the downstream widening. With the adaptation of the local water level, the gradient of the energy grade line of the upstream section decreases, which leads to a reduction of transport capacity and an increase in the deposition.

After four floods, deposition and POC are higher near the deposits ($< 20b_0$) if consecutive sediment augmentations are mobilised with a hydrological flow regime of identical floods close to the ET (*Run_E*) other than with a hydrological flow regime alternated with high peak flow floods (2.5 times the ET) and similar flood volume (*Run_F*). The opposite was observed at a greater distance from the deposits (Figure 5.5:c&f). Near the deposit (Figure 5.5:a&d), the results differ from an experiment with a sinusoidal channel and mobile bed (Humphries et al., 2012), where pulse dispersion and thus POC were highest for floods with 2.5 times the ET.

5.5 Persistence of mobile sediment

The persistence of mobile sediment (P^*; Eqn. 3.10) is calculated for the zone of interest *ZOI2* after two to four floods of *Run_D* to *Run_F* (Figure 5.6). Variable P^* is independent of the sediment supply during a flood event. It relates only to the amount of mobile sediment present before the flood in a given section and returns a percentage value of how much of this sediment remained in the same section after the flood.

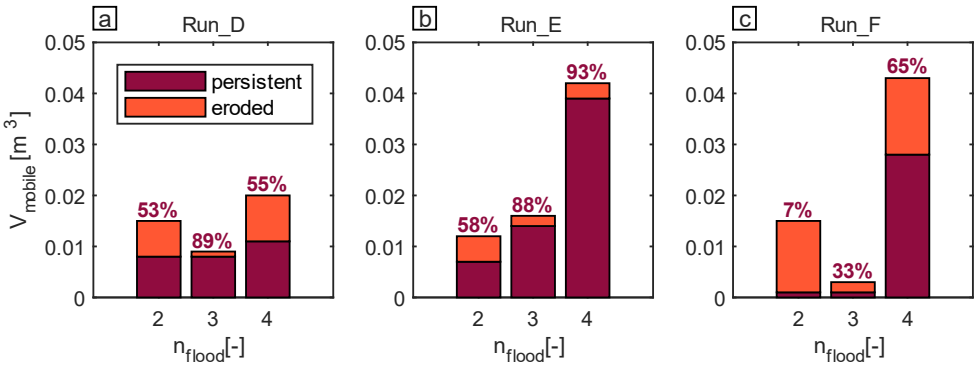

Figure 5.6 Bar plots of the persistence of sediment (P^*) after two to four floods (n_{flood}) of *Run_D* to *Run_F* (a-c) in the zone of interest (ZOI) *ZOI2*. Variable V_{mobile} is the volume of mobile (deposited) sediment before the flood. The value of P^* is shown above each bar. It represents the ratio of persistent sediment (sediment which remained in the section) to V_{mobile} (Eqn. 3.10).

The average P^* after three floods ($n_{Flood} = [2, 4]$) is 66% in *Run_D*, 80% in *Run_E* and 35% in *Run_F*. In *Run_D*, P^* is higher after the third flood with sediment augmentation (89%) than after the other two floods without sediment augmentation ($[53;\ 55]\%$). In *Run_E*, P^* increases continuously after every flood coupled with sediment augmentation ($[58;\ 88;\ 93]\%$). In *Run_F*, the volume of mobile sediment in *ZOI2* corresponds to an average height of $[0.4;\ 0.1;\ 1.3]d_{50,mobile}$ before the second, third and fourth flood. Variable P^* is very low (7%) after the second flood with its high magnitude. After the third flood, 33% of sediment persisted (remained) in *ZOI2*. However, the absolute volume of persistent sediment is low ($0.001m^3$) because almost no sediment remained in this section after the flood. After the fourth flood with its high magnitude, the variable P^* is lower (65%) compared to the fourth flood of *Run_E* (93%) with a lower magnitude, even though the initial deposited volume after three floods is similar ($\pm 0.001m^3$) in the two runs.

The average persistence of mobile sediment is higher after floods with lower peak discharge ($1.2\tau_c^*$) than after floods with higher peak discharge ($2.5\tau_c^*$). This result is expected because higher shear stress leads to higher erosion. The results also show that the persistence of mobile sediment increases with the repetition of floods with similar hydrographs coupled with sediment augmentation. On the other hand, the persistence of mobile sediment decreases after floods without sediment augmentation. Increased persistence after sediment augmentation is attributed to the higher abundance of existing

sediment patches. Zones of accumulated sediment represent local flow obstacles and promote the trapping of free bedload particles. This process stabilises local patches (fixed patches) and a higher proportion of bedload retention. Additional sediment supply also decreases the energy grade line in *ZOI2* with growing deposition in the widening section (*ZOI3*). During floods with high peak discharge ($2.5\tau_c^*$), existing mobile sediment should have a volume which corresponds to at least an average height of $1.3d_{50,mobile}$ to avoid more sediment from being washed out than remaining in the section.

5.6 Hydromorphological diversity

The results of the low flow simulation ($\bar{Q} = 2.2\ l/s$) of the initial empty channel and after the fourth flood of *Run_D* to *Run_F* are shown in Figure 5.7. It provides a visual example of the result of the numerical simulations. It also presents the data used to analyse the hydromorphological variability described in the last part of this section. Figure A8.1 to Figure A8.3 in the appendix displays the remaining simulation results.

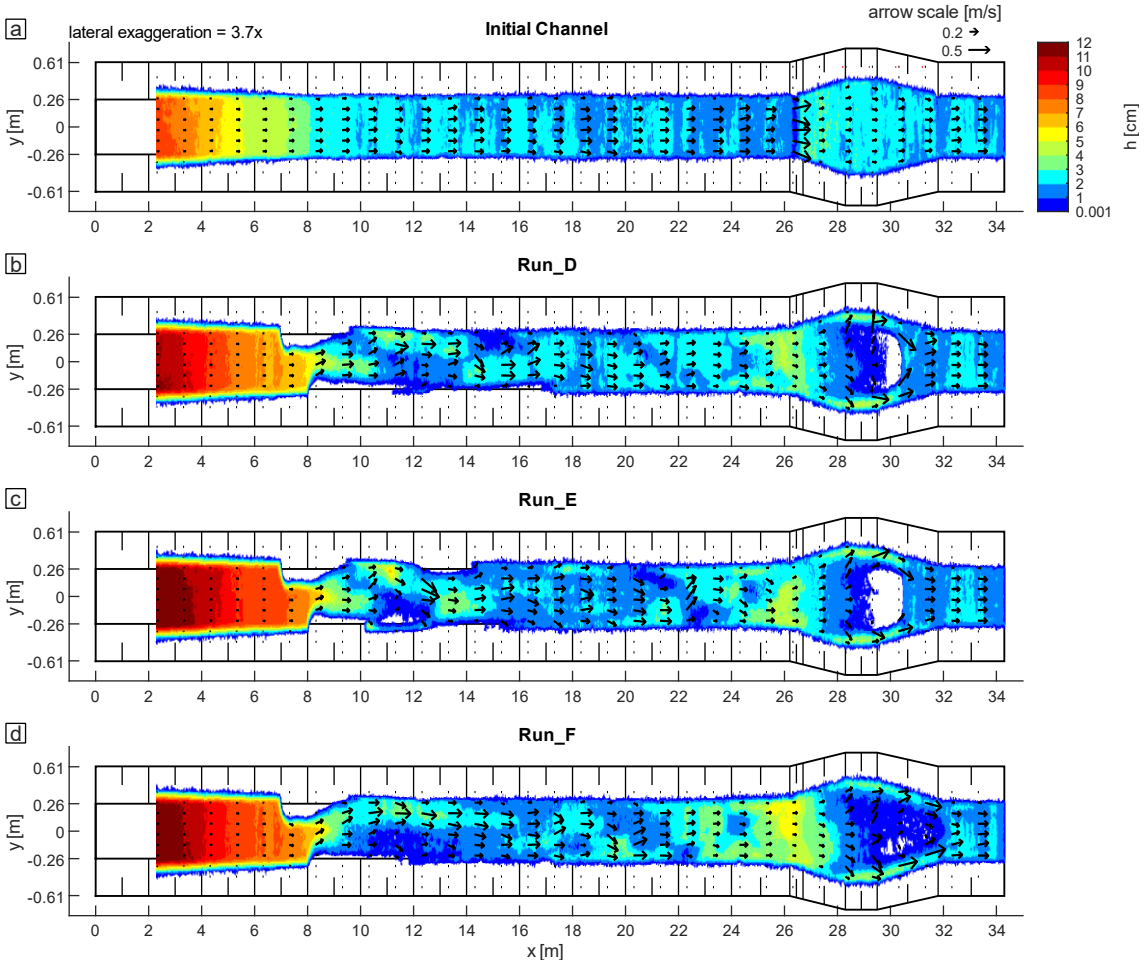

Figure 5.7 Graphic display of the simulated water depth (h) and flow field of the initial channel state (a) and after four floods of *Run_E* to *Run_F* (b-d). Variable x is the longitudinal channel coordinate, and y is the lateral channel coordinate. The black arrows represent the two-dimensional (2D) flow field.

In the result of the initial channel, the 2D local flow field is directed almost everywhere in the main flow direction, parallel to the channel axis. Water depth in the channel centre ranges from $8cm$ ($\triangleq 13.6d_{50,mobile}$) at the upstream backwater to $0.9cm$ ($\triangleq 1.5d_{50,mobile}$) at the drop at the entrance of the widening section (*ZOI3*). After four floods, the flow field is more heterogeneous than in the initial empty channel in *Run_D* to *Run_F*. In *Run_D*, the remnants of the initial upstream deposits concentrate the flow and increase the depth of the upstream backwater. Irregular deposition in the hydraulic impact zone ($[7, 15]m$; *ZOI1*) diversifies the flow field and water depth distribution. The flow field in the downstream target section ($[15, 26]m$; *ZOI2*) is mainly homogeneous.

In the widening section (*ZOI3*), the deposition front creates a small island in the channel centre, which splits the flow into two lateral channels. In *Run_E*, flow field and water depth distribution are the most diverse along the entire channel of all four simulations. The main flow is deflected twice in *ZOI1,* and flow complexity increases in *ZOI2* compared to *Run_D*. Furthermore, the island in *ZOI3* is larger, but the flow pattern is similar in this section. In *Run_F*, the flow is more concentrated in *ZOI1* and more laminar in *ZOI2* than in *Run_E*. No island is formed in *ZOI3* but instead, a large zone of shallow water with an average depth of $0.6cm$ ($\triangleq 1d_{50,mobile}$). While a new bed layer is created progressively with every new sediment augmentation, no alternate bar formation emerges after four repetitions in the low-flow simulations. It is concluded that sediment equilibrium conditions were never reached in the experiment.

The $HMID$ was calculated after every flood of *Run_D* to *Run_F* and compared in Figure 5.8. The corresponding data table can be found in the appendix (Table A9.3).

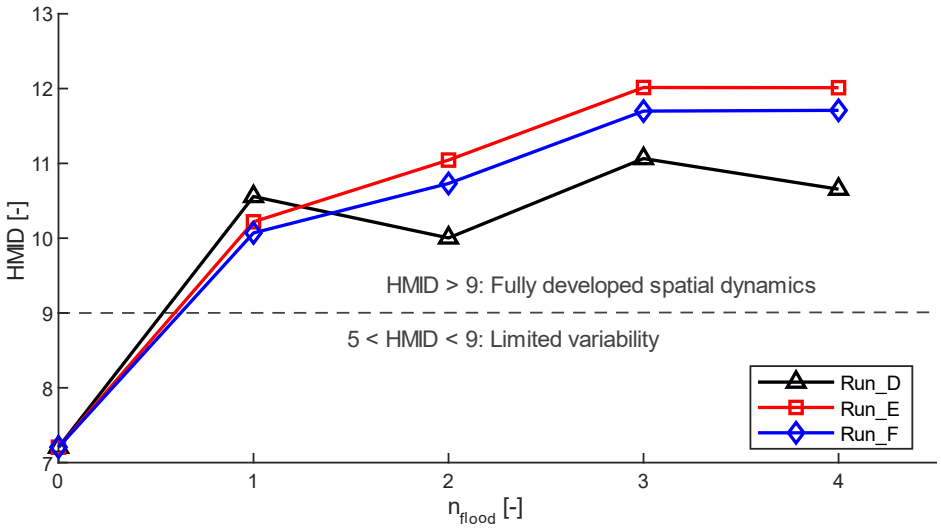

Figure 5.8 Graphs of the hydromorphological index of diversity ($HMID$) for the number of released floods (n_{flood}) of *Run_D* to *Run_F*. A higher $HMID$ represents a higher degree of morphological diversity. The first value of each line represents the $HMID$ of the initial channel state.

A numerical simulation of the empty channel (S_0) indicates a medium $HMID$ (7.2) for a constant low discharge, representing low flow in field conditions. After Gostner et al. (2013), this score indicates a morphologically moderately modified reach with limited variability. The empty channel morphology does not produce a lower $HMID$ in the simulated scenario because the geometrical alteration of CS width and channel slope was designed to represent different channel geomorphic units (e.g. riffle, run) and create pre-existing structural diversity. This value shows to what extent the pre-existing morphological complexity of the experimental flume creates hydromorphological variability in the initial condition and provides the necessary reference for assessing the benefit of each augmentation measure in this regard.

After the first flood, the $HMID$ varies slightly between *Run_D* to *Run_F* with a maximum difference of 0.49. After two to four floods, the $HMID$ is highest in *Run_E* (12.01) and lowest in *Run_D* (10.65). In *Run_D*, the $HMID$ decreases after every flood without sediment augmentation ($n_{flood} = [2, 4]$). In *Run_E* and *Run_F*, the $HMID$ increases less after the second and after the fourth flood. In *Run_F*, the HMID increases less after shorter floods with higher peak discharge ($n_{flood} = [2, 4]$).

The $HMID$ increased after floods coupled with sediment augmentation and decreased after floods without sediment augmentation. Similar experience was made in the field in a sediment-starved residual-flow reach (Schroff et al., 2022). It is also consistent with the findings of increased bed level changes. In the early stage of restoration, the washed-out bed exhibits little topographic complexity. Hydromorphological variability is governed by channel form and geomorphic unit pattern. In such conditions, sediment supply is shown to impact the hydromorphological variability directly. Higher deposition in macro-scale sediment patches or channel scale aggradation zones increases hydromorphological variability. On the other hand, successive morphological floods can wash out exposed sediment patches and reduce the hydromorphological variability again towards initial conditions if no new sediment is resupplied.

The $HMID$ increased stronger compared to initial conditions if consecutive sediment augmentations were mobilised with a hydrological flow regime of identical floods close to the ET (*Run_E,* Figure 5.8: red line) than with a hydrological flow regime alternated with high peak flow floods (2.5 times the ET) and similar flood volume (*Run_F,* Figure 5.8: blue line). This result suggests that altering the discharge regime with high peak floods does not necessarily increase the hydromorphological diversity if the target reach is initially highly sediment-depleted. While larger floods (> 1.5 times the ET) are known to have a positive effect on the restructuring of a mobile bed (Rachelly, Friedl, et al., 2021), our results suggest that they can lead to higher erosion and greater entrainment of sediment out of a target reach under sediment starved conditions, compared to lower peak morphological floods. his effect can then disadvantage the $HMID$ of a target reach for alternated flow regimes at an early bedload restoration phase.

In both scenarios (*Run_E* & *Run_F*), the $HMID$ increases less after the second and fourth repetition of sediment augmentation. The results of these two test runs indicate that hydromorphological variability does not further improve after four consecutive sediment augmentations.

5.7 Conclusion

The findings of this chapter refer to sediment augmentation measures in the form of alternating, in-channel deposits, which are shifted half of the deposit length (configuration B; Battisacco et al., 2016) and placed along an elevated portion of the riverbed (riffle). The reach type is restricted to low-gradient ($< 1\%$), sediment-starved, gravel-bed rivers. The prediction of short-term morphological evolution from sediment augmentation by a limited number of floods in space and time might be strongly influenced by the system's initial conditions, for example, the size and distance of the artificial deposits. This sensitivity might affect the portability and upscaling of the results.

The results suggest the following statements for the evolution of bed morphology from consecutive augmentation:

- Sediment augmentation with every mobilising flood, instead of every second, causes higher deposition and percentage of cover.
- Mobilisation of consecutive sediment augmentations after four consecutive floods with a hydrological flow regime of identical floods close to the entrainment threshold, instead of with a hydrological flow regime alternated with higher peak floods (2.5 times the entrainment threshold) and similar flood volume, causes 51% higher deposition and 24% higher percentage of cover near the deposits (20 channel widths) and a 3% higher hydromorphological diversity index.
- The persistence of augmented sediment patches is higher after floods with a peak flow close to the entrainment threshold than after floods with a higher peak flow (2.5 times the entrainment threshold) and similar flood volume.
- The persistence of augmented sediment patches decreases after floods without sediment augmentation.
- The hydromorphological diversity increases after floods coupled with sediment augmentation and decreases after floods without sediment augmentation.

The results partly confirm the initial hypothesis H2, that sediment augmentation before every-, instead of every second mobilising flood, is beneficial for creating morphological diversity. It was discovered that on a sediment-depleted riverbed, consecutive sediment augmentation with every flood is beneficial for increasing the persistence of mobile sediment patches, which leads to higher deposition and percentage of cover. Even though less pronounced, sediment augmentation before every second mobilising flood can still increase hydromorphological diversity. For mobilising artificial sediment deposits in sediment-starved conditions, alternating the hydrological flow regime with higher peak floods does not benefit the hydromorphological diversity.

With the progressive creation of an active bedload cover layer by consecutive augmentation, the repetition frequency of sediment augmentation becomes less critical for improving hydromorphological diversity. In this scenario, the alternation of the flow regime can increasingly benefit the restructuring of the riverbed.

Chapter 6
Influence of channel geomorphic units on river morphology evolution during artificial floods coupled with sediment augmentation

In this chapter, the third research question is addressed. The analysis is based on observations of the field experiment. Hydromorphological changes are investigated in response to a secondary, low-magnitude flood after a sediment augmentation measure in a residual-flow reach. The channel geomorphic unit type of the riverbed influenced the spatial distribution and persistence of tracers. Hydromorphological diversity increased locally at the channel scale but decreased on the reach scale after a flood with a low supply-to-capacity bedload ratio.

Note: This chapter is based on an article submitted to a peer-reviewed journal[1].

6.1 Introduction

This chapter addresses the issue raised in the third research question.

- RQ3: What are typical emerging bed forms from alternating sediment deposits in different longitudinal riverbed structures (e.g. pools, channels, riffles)?

The term *bedform* was discussed in Section 4.1, and the *term longitudinal riverbed structure* refers to what was defined as channel geomorphic units (CGUs) in Chapter 2 on background and literature research. The reproduction of the Sarine River case study with the experimental flume (Section 3.3.4) has shown the challenge of reproducing the influence of CGUs on bed morphology evolution from SAMs in complex reaches by physical modelling. To best reply to the issue raised in RQ3, the analysis is solely based on observations of the field experiment at the Sarine River (Section 3.2).

This chapter focuses on the influence of channel geomorphic units on river morphology evolution during artificial floods coupled with sediment augmentation to investigate site-specific design recommendations for SAMS in different morphologies. Thompson et al. (1996) linked particle transport to different CGU types in an unregulated reach with a medium slope ($> 1\%$). In this thesis, the investigation focuses on low-gradient ($< 1\%$) sediment-starved, gravel-bed rivers. Descriptive statistics of bedload particle location before and after a flood provide information on the sediment pulse evolution behaviour.

[1] "Influence of channel geomorphic units on the evolution of river morphology during low magnitude bed-forming floods coupled with sediment augmentation" by C. Mörtl, R. Schroff, S. Stähly and G. De Cesare, under review in *Earth Surface Processes and Landforms*. Contribution of the doctoral candidate according to the *CRediT*: conceptualisation; data curation; formal analysis; investigation; methodology; resources; software; validation; visualisation; writing – original draft; writing – reviewing and editing.

The observed distribution of tracers is compared against expected distributions, following different assumptions, to test hypothesis H3, that CGU type influences bedload transport. The relocation of detected tracers before and after *Flood 2020* is analysed to reveal trends of different retention capacities of individual CGU types. Hydromorphological changes are assessed at the channel scale by a qualitative description of CGU organisational patterns and at the reach scale by the change of $HMID$ from ten cross-section measurements. The transferability of results regarding alternative explanatory factors at the study site is discussed.

6.2 Bedload particle transport

This section describes the results of the bedload particle tracking. Descriptive statistics of RFID PIT tags are shown in Table 6.1.

Table 6.1 Descriptive statistics of RFID PIT tags (tracer). The subsamples refer to the three channel states before *Flood 2016* (T_0), after *Flood 2016* (T_{F16}) and after *Flood 2020* (T_{F20}) or the change compared to pre-flood conditions*. The total number of samples N is 489. Variable n is the number of subsamples, μ is the arithmetic mean, max is the maximum value, and σ is the standard deviation. The letters F,D,M and E denote the subsamples. The subscript $(t-1)$ denotes pre-flood conditions.

Subsample	Variable	Definition / Statistics	T_0	T_{F16}	T_{F20}
Detected tracers (D)	Sample number	$n_D[-]$	489	276	200
	Recovery rate	$\frac{n_D}{N}[-]$	1	0.56	0.41
	Station	$max[m]$	56	311	334
Detected tracers in *zone* artificial deposits ($S \subset D$)	Sample number	$n_S[-]$	489	124	46
Moved tracers* ($M \subset D$)	Sample number	$n_M[-]$	-	152	37
	Mobilisation rate	$\frac{n_M}{n_D}[-]$	-	0.55	0.19
	Transport distance	$\mu_M[m]$	-	93	39
		$max_M[m]$	-	300	117
		$\sigma_M[m]$	-	82	34
Detected tracers, which were in *zone* artificial deposits in pre-flood conditions* ($A \subset \{D; S_{t-1}\}$)	Sample number	$n_A[-]$	-	276	55
Moved tracers from an artificial deposit* ($E \subset A$)	Sample number	$n_E[-]$	-	152	9
	Erosion rate	$\frac{n_E}{n_A}[-]$	-	0.55	0.16

Before *Flood 2016*, the maximum *station* of all tracers was $56m$, which corresponds to the perpendicular projection of artificial deposit $D4$ on the centreline.

After *Flood 2016*, fewer tracers from the *base* layer (33) were *moved* than tracers from the *middle* (116) and the *top* layer (127). The mean transport distance was the smallest for *moved* tracers from the *base* layer ($84m$), compared to *moved* tracers from the *middle* ($98m$) and the *top* layer ($92m$).

After *Flood 2020,* the mean and maximum *transport distance* of *moved* tracers outside the artificial deposit zones (28) was $44m$ and $117m$. Considering the time above the

threshold of motion ($12h$), those 28 tracers travelled with an average velocity of $1 \times 10^{-3}\ m/s$. Only 9 of 55 detected tracers inside the artificial deposits before *Flood 2020* were *moved*. The greatest distance from the artificial deposits (maximum *station*) for all tracers increased from $311m$ to $334m$.

As expected, tracer stones with *size* category *dm* travelled on average further after *Flood 2016* ($113m$) and *Flood 2020* ($41m$) than tracer stones from type *d90* ($[79;\ 36\ ]m$). The Pearson coefficient (R) of tracer *sphericity* and *transport distance* for both floods was 0.15.

The position of tracer stones and CGUs are shown in Figure 6.1.

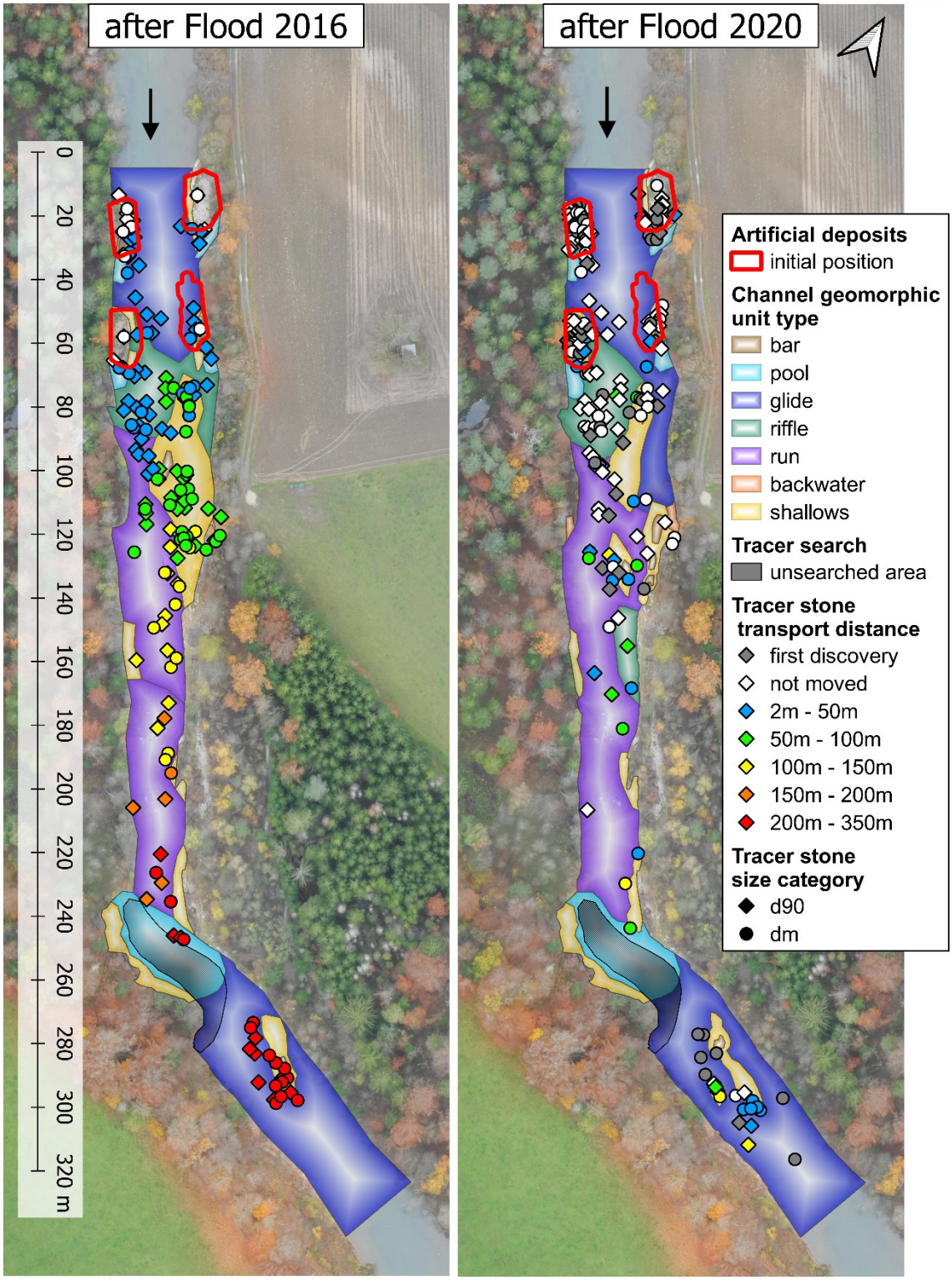

Figure 6.1 Orthophotos with channel geomorphic units (CGUs) and tracer stone positions after *Flood 2016* and *Flood 2020*. The unsearched area marks areas with water depths greater than $1.5m$. Background image: November 2020, *Research unit Ecohydrology, Zurich University of Applied Sciences*.

After *Flood 2016*, tracer density was highest in the *riffle* and *shallows* zones in the direct downstream vicinity of the artificial deposits ($[70, 130]m$). Along this area, the main tracer concentration shifted from the right side towards the left side of the river onto the *shallows*

zone. Along the *run*, tracers were relatively evenly distributed with a lower density ($16.1 \times 10^{-3} m^{-2}$) compared to the average density inside the *target section* ($19.1 \times 10^{-3} m^{-2}$). At the edge of the *pool, three* tracers were found. No information about the number of tracers at the pool's centre is available, but many are expected to accumulate in this CGU. A large cluster of tracers was discovered in the channel centre around the *shallows* zone downstream of the exit slope of the *pool* ($[300, 310]m$).

After *Flood 2020*, the bed was partly reshaped downstream of the artificial deposits ($[70, 170]m$) by the flood coupled with the artificial sediment supply. On the right side of the river ($[70, 110]m$), many tracers had stayed in place and were possibly overtopped by newly deposited sediment. The *riffle* zone ($[70, 90]m$) had increased moderately in size. The bed was incised on the left side of the river, and a new *shallows* zone had formed in the channel centre about $2b_0$ further downstream ($[70, 110]m$). Tracer density had decreased along the *run*. Downstream of the *pool*, tracers were mainly shifted by a small distance ($< 2b_0$) in the downstream direction and previously undetected tracers were found.

A frequency analysis of tracer distribution along the channel centreline is shown in Figure 6.2.

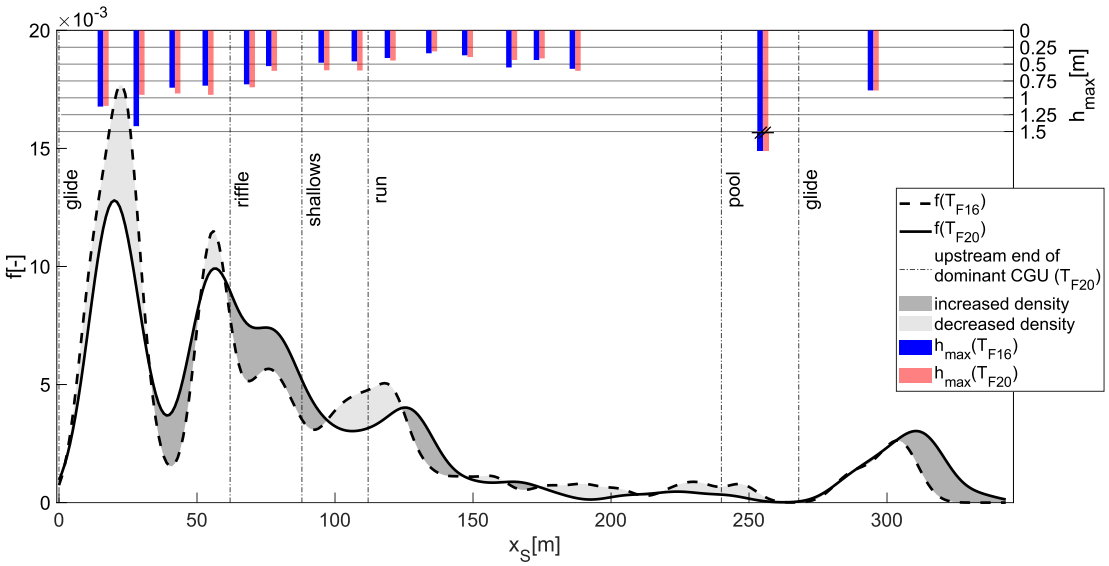

Figure 6.2 Probability density function (pdf) of RFID PIT tags (tracer) positions along the channel centreline. Variable x_S is the station along the channel centreline, f is the frequency of detected tracers, and h_{max} is the maximum water depth at a measured cross-section (CS). Results are given for the two channel states after *Flood 2016* (T_{F16}) and *Flood 2020* (T_{F20}). The acronym CGU means channel geomorphic unit. At the pool, h_{max} was greater than $1.5m$. Areas with h great than $1.5m$ were not searched for tracers.

After *Flood 2020*, tracer density had increased in the *hydraulic impact zone* between opposite artificial deposits ($[0, 35]m$), in the *riffle* zone ($[64, 92]m$), in the upstream part of the *run* ($[125, 148]m$) and at the downstream end of the *study reach* ($[305, 340]m$). A general downstream shift of tracer density of about $1b_0$ was observed.

Chi-square goodness-of-fit tests (χ^2-tests) were performed to test whether the spatial distribution of tracers is determined alone by the proximity to the artificial deposits or, alternatively, is influenced by CGU types in the downstream section. Since the unbiased tracer distribution is unknown, two null hypotheses (H_0) were developed:

- $H_{0,1}$: If not influenced by CGU type, the spatial distribution of tracers is uniformly distributed over the range of detected tracer positions.
- $H_{0,2}$: If not influenced by CGU type, the spatial distribution of tracers is normally distributed along the channel axis, with a mean corresponding to the centroid position of the tracer distribution and the standard deviation corresponding to three times this value.

This assumption of $H_{0,2}$ is based on the results of a case study with 1500 RFID PIT tracers placed in an artificial deposit in a large ($B = 100m$), low-gradient (0.1%) river (Arnaud et al., 2017). The alternative hypothesis (H_A) $H_{A,1\text{-}2}$ in both cases is that the CGU types influence the spatial distribution of tracers in the downstream section of the artificial deposits.

Two χ^2-tests were performed separately for the two channel states after *Flood 2016* and after *Flood 2020* to test $H_{0,1}$. The null hypothesis $H_{0,2}$ was only tested for the channel state after *Flood 2016*. Only tracers detected outside the initial artificial deposits were considered. For each CGU type, the observed numbers of tracers were compared to the expected numbers, following $H_{0,1}$ or $H_{0,2}$. To calculate the expected number of tracers for $H_{0,2}$, the study reach was divided into sections of $10m$ spacing. For each section, the number of expected tracers was calculated. Then, each CGU type was assigned the fraction of the calculated tracer number corresponding to its percentage area within the section. Finally, the assigned tracer numbers were summed up for all CGU types. An example of the expected tracer distribution and the complete data table for the χ^2-tests are shown in the appendix (**Figure A10.1**, **Table A10.1**). The statistical p-values (p) indicate an extremely low probability ($< 10^{-19}$) for $H_{0,1}$ or $H_{0,2}$ to hold. Therefore, $H_{A,1\text{-}2}$ is accepted.

The percentage change in the number of detected tracers and CGU area by CGU type is shown in **Figure 6.3**. Together, these two variables account for tracer density. All tracers detected in CGUs after *Flood 2016* (152) and after *Flood 2020* (154) are used for the following analysis.

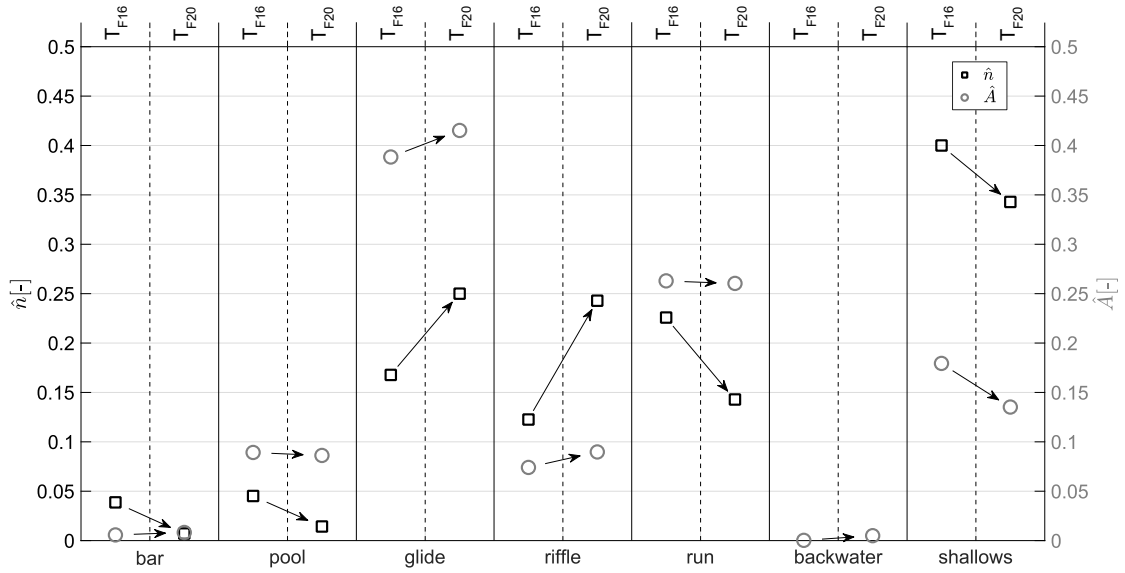

Figure 6.3 Relative number of RFID PIT tags (tracers) and joint area of channel geomorphic units (CGUs) by CGU type for the two channel states after *Flood 2016* (T_{F16}) and after *Flood 2020* (T_{F20}). Variable $\hat{n}$ is the number of detected tracers of a CGU type normalised by the total number of detected tracers, and $\hat{A}$ is the sum of all areas of a CGU type normalised by the total area of all CGUs. The arrows indicate the direction of change.

Compared to the total area of CGU types, the highest number of tracers after *Flood 2016* and after *Flood 2020* were detected in *riffles* ($[19;\ 34]$) and *shallows* ($[62;\ 48]$). Relatively few tracers were found on *glides* after *Flood 2016* (26) and after *Flood 2020* (35), where the total area of *glides* is on average 4.8 times greater than the area of *riffles*. The average tracer number was lowest in *bars* (4) and *backwater* zones (0).

After *Flood 2020*, the ratio of the cumulative area of a CGU type to the total CGU area ($\hat{A}$) remained similar in *bars*, *pools*, *runs* and *backwaters* ($\pm 0.5\%$). It decreased significantly in *shallows* (4.4%), which experienced an absolute area loss of 20.8%. For all CGU types, except *bars* and *pools*, the direction of change in total area was identical to that in the corresponding tracer number. Tracer density increased in *glides* (19.9%) and *riffles* (40.7%) and decreased in *bars* (88.9%), *pools* (71.8%), *runs* (45.0%) and *shallows* (2.2%).

The relocation of individual tracers between different CGU types during *Flood 2020* is shown in Table 6.2. Only individual tracers detected in CGUs after *Flood 2016* and after *Flood 2020* (86) are used for the following analysis.

Table 6.2 Absolute number of RFID PIT tags (tracer) by channel geomorphic unit (CGU) type for the two channel states after *Flood 2016* (T_{F16}) and after *Flood 2020* (T_{F20}).

T_{F16} \ T_{F20}	bar	pool	glide	riffle	run	shallows	total
bar	0	0	0	0	0	2	2
pool	0	0	1	1	0	0	2
glide	0	0	12	0	1	2	15
riffle	0	0	1	16	0	1	18
run	0	1	3	5	9	1	19
shallows	0	0	3	3	6	18	30
total	0	1	20	25	16	24	86

If tracers were detected in *glides* or *riffles* after *Flood 2016*, they remained mostly in the same CGU type during *Flood 2020* ($[80;\ 89]\%$). If those tracers were detected in *runs* or *shallows* after *Flood 2016*, around half were relocated to a different CGU type during *Flood 2020* ($[53;\ 40]\%$). The highest number of tracers were relocated from *shallows* to *runs* (6) and from *runs* to *riffles* (5). The tracer numbers in *pools* and *bars* after *Flood 2016* ($[2;\ 2]$) were too low to derive relocation patterns.

The discussion of the results of Section 6.2 is addressed in Section 6.4: Influence of CGUs on bedload transport.

6.3 Hydromorphological changes

This section describes the results of the cross-section measurements. CS profiles from three measurement campaigns are shown in Figure 6.4. All profiles are shown as a function of water depth because it is the variable used together with the flow velocity to assess hydromorphological changes by the $HMID$. Individual plots of the CS profiles, including velocity measurements and all error ranges, are provided in the appendix (Section A10).

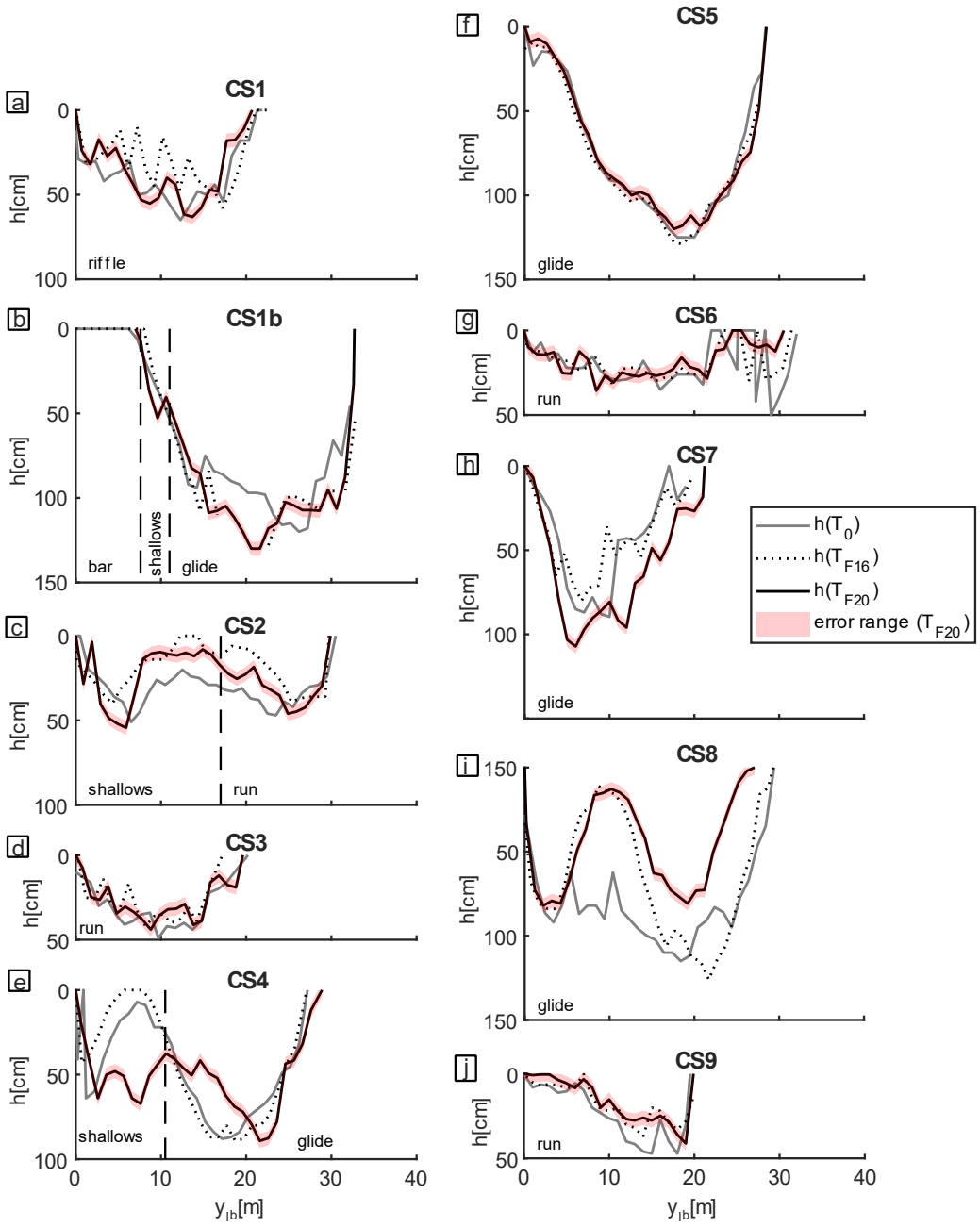

Figure 6.4 Cross-section (CS) profiles for the three channel states before *Flood 2016* (T_0), after *Flood 2016* (T_{F16}) and after *Flood 2020* (T_{F20}). a-j: CS profiles of CS1 to CS9. Variable h is the water depth, and y_{lb} is the distance from the left bank. The label of the channel geomorphic unit (CGU) at T_{F16} was added to every profile. The dashed vertical line separates different CGU types along a CS. The error range is the same for all measurements and is only indicated at T_{F20} for reasons of clarity. In the measurement campaign at T_{F16}, the residual flow discharge ($2.5\ m^3/s$) and the reference water level were lower than during the other two measurement series ($3.5\ m^3/s$).

No significant bed level change had occurred at *CS1*, *CS3*, *CS5*, *CS6* and *CS9*. During the *study period*, the most pronounced morphological changes at the CSs occurred on *shallows*, *glides* and CSs with multiple CGUs. At the location of the initial artificial deposits, incision occurred at the channel centre (*CS1b*). Further downstream in the *target section*, erosion and deposition occurred along *CS2* and *CS4*. In the *glide* zone at the downstream

reference section, erosion occurred at *CS7* and deposition at *CS8*. At both CSs, the vertical change affected almost the entire channel width.

The $HMID$ was calculated separately for the *target* and *reference section* and jointly for the entire *study reach* (Table 6.3).

Table 6.3 Hydromorphological diversity index ($HMID$) of different channel sections for the three channel states before *Flood 2016* (T_0), after *Flood 2016* (T_{F16}) and after *Flood 2020* (T_{F20}). Variable n_p is the total number of measurement points considered. In the measurement campaign at T_{F16}, the residual flow discharge ($2.5\ m^3/s$) and the reference water level were lower than during the other two measurement series ($3.5\ m^3/s$).

	target section			*reference section*			*study reach* (total)		
	T_0	T_{F16}	T_{F20}	T_0	T_{F16}	T_{F20}	T_0	T_{F16}	T_{F20}
n_p [−]	100	90	102	142	145	143	242	235	245
$HMID$ [−]	8.1	11.1	9.2	9.3	11.6	10.1	8.9	11.1	9.7

The $HMID$ is lower for all measurements in the *target section* than in the *reference section*. In both the *target and the reference section*, the $HMID$ increased after *Flood 2016* and decreased during *Flood 2020*. However, the change is more pronounced in the *target section* than in the *reference section*. For the *study reach*, the $HMID$ increased by 25% after *Flood 2016* and decreased by 13% after *Flood 2020*.

The discussion of the results of Section 6.3 is addressed in Section 6.5: Evolution of CGU organisational patterns and reach scale hydromorphological diversity.

6.4 Influence of CGUs on bedload transport

The following analysis is based on field observations from a sediment-starved residual-flow reach. The peak discharge of the two observed floods corresponds to floods with a one to two years return period in pre-dam conditions (Leite Ribeiro et al., 2014). This return period represents the average return period of bankfull discharge in unregulated reaches (Agouridis, 2014).

To test the hypothesis that existing CGUs influence bedload transport, the bedload tracer particle distribution was analysed. Based on a χ^2-test, the null hypothesis $H_{0,1}$, that the spatial distribution of tracer on the riverbed is uniformly distributed, can be rejected ($p < 10^{-19}$). In a high-gradient, pool-riffle stream, Thompson et al. (1996) performed the same test with the observed distribution of coloured pebbles after several low-magnitude bed-forming floods with a return smaller than three years. They also calculated a low probability for this null hypothesis ($p = 5 \times 10^{-5}$). The difference in statistical significance is attributed to the fact that they placed their tracers at different locations and that their study reach contains several sequences of recurring CGU types. The second null hypothesis $H_{0,2}$, that the spatial distribution of tracers is normally distributed, with a mean corresponding to the centroid position of the tracer distribution and the standard deviation corresponding to three times this value, could also be rejected ($p = 10^{-175}$). The low probability is partly

attributed to the assumption being based on a case study with a single deposit injection (Arnaud et al., 2017). On the other hand, it provides strong support for the alternative hypothesis $H_{A,1\text{-}2}$, that the spatial distribution of tracer is influenced by CGU type.

Whether the persistence of tracers during a flood event depends on the CGU type was assessed by comparing the relocation of detected tracers after *Flood 2020* between different CGU types (Table 6.2). The analysis revealed that the persistence of augmented sediment was highest in *riffles* (89%). During a flood, shear stress is relatively low in *riffles* due to reduced water depth on the elevated portion of the riverbed and favours bedload deposition. Existing studies have already concluded that riffles in riffle-pool morphologies tend to be subject to aggradation during bankfull discharge and act as transit zones for fine bedload during low flow (Thompson & MacVicar, 2022). Because bed level changes along the measured CSs were quite pronounced in *riffles*, it can be supposed that tracers got quickly overtopped by newly deposited sediment in zones of aggradation, increasing the persistence of augmented sediment in this CGU type.

On the other hand, the highest relocation of tracers to other CGU types during *Flood 2020* was experienced in *runs* (53%). In *runs*, the steep slope increases shear stress and vertical mixing processes are limited on the stabilised bed with its characteristically coarse bed substrate composition. The translational behaviour of the pulse migration in the long *run* section was therefore attributed to a locally increased transport capacity and reduced effect of bedload overtopping during the two floods. The highest number of tracers were relocated from *shallows* to *runs* and from *runs* to *riffles*. These relocation patterns resulted from the reshaping of CGUs in the downstream vicinity of the artificial deposits after *Flood2020*. Parts of the *shallows* transformed into a *run* while the *riffle* expanded into the former *run* zone.

CS profiles with the most pronounced morphological changes (*CS2*, *CS4*, *CS7* & *CS8*) were each located at the downstream vicinity ($< 2b_0$) of *bars*, *shallows*, *riffles,* and *pools*. This length corresponds to the average downstream shift of augmented sediment patches observed after *Flood 2020*. It was inferred that these types of CGUs can act as important storage units for dynamic bedload. During the falling limb of a flood hydrograph, *bars*, *shallows,* and *riffles* are characterised by low water depth, favouring sediment deposition. It was concluded that these depositions then provide a potential sediment source during the subsequent flood. In *pools*, flood flows can accelerate scour, while continuous deposition of upstream sediments in the scour hole may also occur (Gazi et al., 2019). *Pools* can thereby act as a sink and source for bedload during flood flow because *pools* can accumulate and periodically release waves of sediments (Dhont & Ancey, 2018).

The results about the influence of CGU order and position on bedload transport depend on the assumption of the unbiased tracer distribution. Considering $H_{0,1}$, the order and position of CGUs have no influence. Considering $H_{0,2}$, the order and position of CGUs bias the results of tracer numbers in individual CGU types, favouring deposition in *runs* and *shallows* (see Table A10.1).

6.5 Evolution of CGU organisational patterns and reach scale hydromorphological diversity

The evolution of CGUs in response to a low-magnitude bed-forming flood with a low bedload supply-to-capacity ratio (2%) was analysed for their organisational patterns. After *Flood 2020*, the evolution of CGUs was characterised by a moderate change in size or small downstream displacement rather than dispersion and new emergences. The probability distribution of the tracer positions along the *centreline* indicated no major dispersion of tracer density. Instead, a small downstream shift of about $1b_0$ of existing sediment patches from the initial sediment pulse was observed. An exception was the emergence of a new *glide* zone inside the *hydraulic impact zone* of the artificial deposits. This evolution was traced back to the fact that during *Flood 2020*, the main flow was concentrated between the remnants of the initial artificial deposits and deflected towards the bank. It led to local incision from a lack of upstream sediment supply (Schroff et al., 2022).

Channel sections of a single CGU remained mainly of the same CGU type. It supports the theory of deterministic organisational pattern of channel units (Wyrick & Pasternack, 2014). Patterns of physical channel characteristics, like slope and width-to-depth ratio, favour the grouping and collocation of certain CGU types. The observed flood did not lead to a significant diversification of the organisational patterns of CGUs. Floods of significantly higher magnitude (six to nine times bankfull flow) in a river segment with a coarser GSD mainly caused shrinkage and fragmentation of CGUs and a general shift towards a low relief morphology (Woodworth & Pasternack, 2022). It was concluded that the rearrangement and diversification of static, organisational patterns of CGUs, which are characteristic of highly regulated reaches requires higher flood magnitude and bedload supply than in the conditions of the observed flood event.

The $HMID$ increased across the *study reach* by 24% to 11.1 after *Flood 2016* and decreased by 13% to 9.7 after *Flood 2020*. While the score of the $HMID$ cannot be linked directly to the ecological state of a reach, it provides a measure of the diversity of the physical habitat. Successive assessment of the $HMID$ allows for determining the trend of habitat evolution. Natural variations are thereby site-specific and require a long-term record to be eliminated. Nevertheless, the $HMID$ can indicate the effect of river engineering projects (Gostner et al., 2013), like sediment augmentation measures (Stähly et al., 2019). Inside the study reach, the change of $HMID$ was greater in the *target section* than in the *reference section*. This result indicates the positive effect of the additional bedload supply after *Flood 2016*. The decrease after *Flood 2020* was attributed to fresh patches of augmented sediment on the armoured bed or outcropping bedrock from the previous flood was washed out without renewed upstream bedload supply. This finding agrees with the result of the previous study that evaluated the change in $HMID$ for the same event at a smaller stretch in the upstream end of our study reach ($[0, 200]m$) with a shorter CS spacing ($[10, 20]m$) (Schroff et al., 2022). The results of $HMID$ of our study over

a section of five times the length and with reference data before and after two floods suggest that the abundance of CGUs alone cannot explain reach scale hydromorphological diversity. This result agrees with Rosenfeld et al. (2011), who showed that the variation of the hydraulic characteristics h and v depend on CGU type and flow rate.

6.6 Transferability of results

To assess the transferability of this study, alternative explanatory factors at the study site, which can bias the results of bedload transport and bed morphology evolution, are highlighted. The topographic confinement of the Sarine in the *study reach* is believed to have impacted bedload transport and the evolution of CGUs. The outcropping alluvial bedrock along the left bank at the upstream part of the *study reach* restricted the channel's evolution laterally and vertically. The *pool* in the *reference section* was located at the deflection point, where the Sarine hit the cliff of molasse rock. Its geometry was forced by the rock, and it was unlikely to migrate or disperse. Another potential explanatory factor for bedload transport during the observed floods is riparian vegetation. At the site, vegetated banks limit lateral channel evolution by bank stabilisation since plant roots and rhizomes generally increase erosion resistance. Riparian vegetation can also change the flow field by causing increased flow resistance near the banks. A reduction in flow velocity near the banks can impact morphodynamics (Camporeale et al., 2013). However, no lateral tendency of erosion or deposition across the channel width was observed at the measured CSs. It was therefore estimated that the impact of riparian vegetation on bedload transport and CGU evolution was relatively low.

6.7 Conclusion

The findings of this chapter refer to morphological processes in response to low-magnitude, bed-forming floods coupled with sediment augmentation. The reach type is restricted to low-gradient ($< 1\%$), sediment-starved, gravel-bed rivers. The assessment of the statistical significance of the channel geomorphic units' influence on bedload transport strongly depends on the choice of estimation function for the null hypothesis. The uncertainty of the selected estimation functions might affect the validity of the results.

The results suggest the following statements for bed morphology evolution:

- Channel geomorphic units influence bedload transport.
- The persistence of bedload particles during a flood event depends on the channel geomorphic unit type.
- The abundance of channel geomorphic units does not represent reach-scale hydromorphological diversity.

The results confirm the initial hypothesis H3, that channel geomorphic units influence bedload transport during low-magnitude, bed-forming floods coupled with sediment

augmentation. Furthermore, it was found that some CGU types have a higher bedload retention capacity during a flood than others and can thereby act as important storage units for dynamic bedload in the target section of a SAM. The results of this chapter provide rare field observations of the interaction of bedload transport with channel geomorphic units. A more extensive database is required to reduce the uncertainty and better quantify and assess this interaction.

Chapter 7
Impact assessment of sediment augmentation measures on habitat diversity

In this chapter, the fourth research question is addressed. The analysis is based on field observations combined with literature research. Six indicators of Indicator set 1 of the Guidelines for Evaluating the Outcome of Restoration Projects of the Swiss Federal Office of the Environment are assessed at the Sarine River study site. Categorical indicators are mapped and spatially analysed regarding the impact of the 2016 sediment augmentation measure. The scores of categorical- and numerical indicators are calculated, and their validity is discussed. The four indicators, (i) riverbed structures, (ii) substrate mobilisability, (iii) water depth and (iv) flow velocity, were judged to have the highest validity for the impact quantification of sediment augmentation measures on habitat diversity.

Note: This chapter is based on two articles published in different technical journals[1,2] and an article submitted to a technical journal[3].

7.1 Introduction

This chapter addresses the issue raised in the fourth research question.

- RQ4: How can the eco-morphological effectiveness of sediment augmentation measures be quantified?

The literature research in Chapter 2 summarises existing approaches for eco-geomorphological assessment in the riverine environment. It also highlights the lack of application of integral assessment strategies in the context of SAM. With the publication of the *guideline for evaluating the outcome of restoration projects* (EOR) of the FOEN (2019) and its guide for the impact monitoring of bedload remediation measures still under development, the motivation of research was to assess the validity of the EOR for the impact assessment of the 2016 SAM on habitat diversity at the study site of the Sarine

[1] Wirkungskontrolle einer Sedimentzugabe: Habitatvielfalt und Kolmation [Eco-morphological evaluation of a sediment augmentation measure] by R. Schroff, C. Mörtl and G. De Cesare, published in *Wasserwirtschaft*. Contribution of the doctoral candidate according to the *CRediT*: conceptualisation; investigation; project administration; resources; supervision; writing – reviewing and editing.

[2] Impacts et enjeux de charriage d'une crue artificielle – Exemple de la Petite Sarine 2020 [Effects and bedload related challenges of an artificial flood - Example of the Petite Sarine 2020] by R. Schroff, C. Mörtl, P. Vonlanthen and G. De Cesare, published in *Wasser Energie Luft - Eau Energie Air*. Contribution of the doctoral candidate according to the *CRediT*: resources; writing – reviewing and editing.

[3] Sediment continuity and augmentation measures by C. Mörtl, R. Schroff and G. De Cesare, submitted to *FactSheet Collection of the project Riverscape – sediment dynamics and connectivity*. Contribution of the doctoral candidate according to the *CRediT*: conceptualisation; data curation; formal analysis; investigation; methodology; resources; software; validation; visualisation; writing – original draft; writing – reviewing and editing.

River. The assessment of biological indicators was neglected because it exceeded the scope of this thesis.

This chapter focuses on the validity of the EOR indicator set 1 (EOR1) for the impact assessment of a SAM. The EOR1 was recorded after two floods in the main study reach and a reference section. The results are discussed regarding habitat diversity changes at the study site. The assessment method is compared to other assessment methods from literature and practice, and its validity is discussed. The novelty consists in the detail of the physical habitat assessment regarding the impact of a sediment augmentation measure, making the field investigation one of its first kind and high value for the practice of SAM and sediment management in general.

7.2 Study framework

The EOR1 assessment was performed in a $200m$ section around the artificial sediment deposits from 2016 (see Figure 3.2), called *restoration reach* (RR), and a suitable upstream *control reach* (CR) of the same length (Figure 7.1). The RR was subdivided into the $80m$-long *intervention section* (IS) and $120m$-long *downstream section* (DS) to allow a differentiated evaluation.

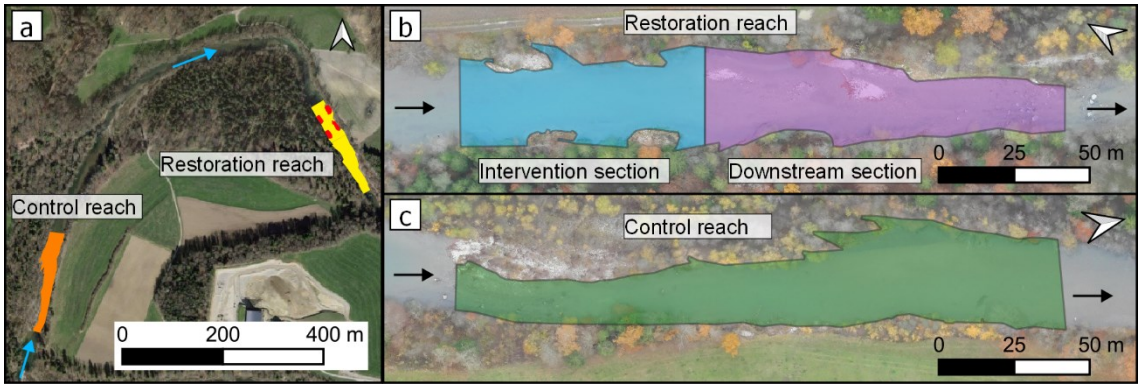

Figure 7.1 Map of the study sections used for the physical habitat assessment. a: Overview. The orange polygon marks the *control reach* (CR), the yellow polygon the *restoration reach* (RR) and the red polygons the initial artificial deposit positions. b: RR. The blue polygon marks the *intervention section* (IS), and the violet polygon is the *downstream section* (DS). c: CS. Arrows mark the direction of flow. Background images: © swisstopo (a) and research unit ecohydrology, Zurich University of Applied Science (b, c).

The EOR1 assessment was performed twice in both the *restoration* and *control reach* (Figure 7.2).

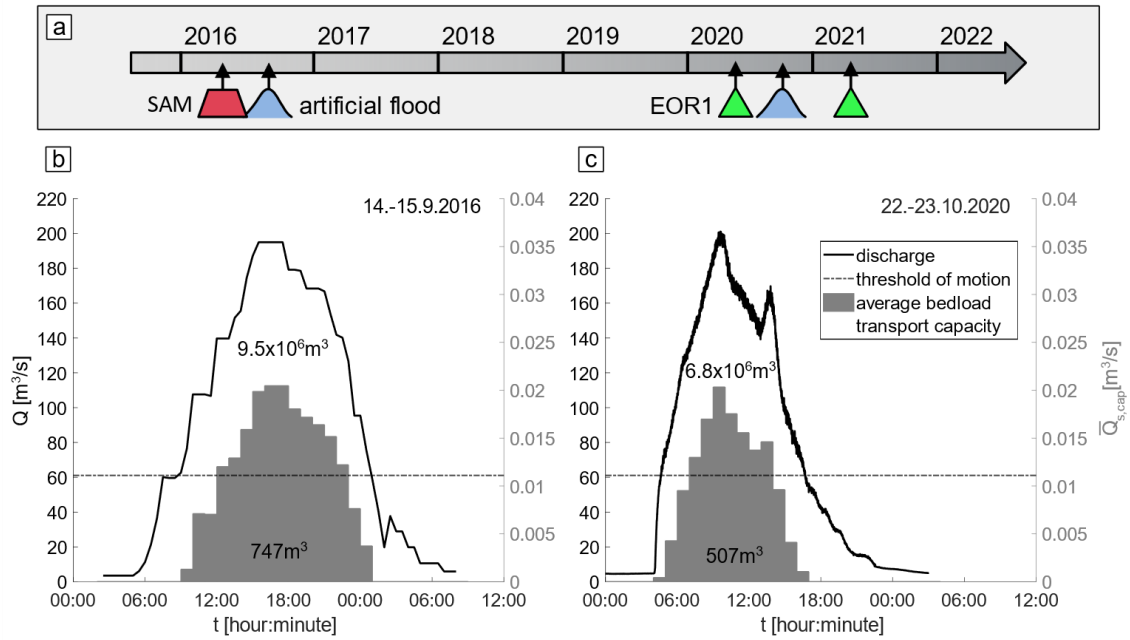

Figure 7.2 Assessment timeline (a) and hydrographs and transport capacity of *Flood 2016* (b) and *Flood 2020* (c). The red trapezium marks the time of the sediment augmentation measure (SAM), the blue curve symbols the time of the artificial floods and the green triangles the time of the assessment of the first indicator set of the guideline for evaluating the outcome of restoration projects of the Swiss Federal Office of the Environment (EOR1). Variable t is the time, Q is the discharge, and $\bar{Q}_{s,cap}$ is the average bedload transport capacity.

7.3 Indicators of habitat diversity

The results of all indicators of the EOR1 assessment from 2020 and 2021 for the *restoration reach* and the *control reach* are summarised in **Table 7.1**

Table 7.1 Results of the assessments of the first indicator set of the guideline for evaluating the outcome of restoration projects of the Swiss Federal Office of the Environment (EOR1). Acronym RR is the *restoration reach*, CR is the *control reach*, and ER is an estimated reference by an expert. Categories or variables are referred to by number and described in **Table 3.5**. Their values refer to statistical values for indicators 1.3 and 1.4. Otherwise: For each category, the percentage of the feature relative to the total length of the bank line (Indicator 1.2), the wetted bed area (Indicator 1.5) or the entire bed width from bank toe to bank toe (Indicators 1.1, 1.6 A1, 1.6 A2).

				Category or variable number												
	Reach	Year	Score	1	2	3	4	5	6	7	8	9	10	11	12	13
Indicator 1.1 Riverbed structure	RR	2020	0.50	0.8%	2.6%	30.2%	12.3%	32.0%	0.1%	21.9%	0.0%	0.0%	-	-	-	-
		2021	0.50	1.1%	2.8%	36.5%	14.7%	29.8%	1.4%	13.8%	0.0%	0.0%	-	-	-	-
	CR	2020	0.50	0.0%	0.0%	24.4%	47.0%	15.4%	0.0%	13.1%	0.0%	0.0%	-	-	-	-
		2021	0.50	0.1%	0.0%	20.5%	54.1%	14.7%	2.1%	8.4%	0.0%	0.0%	-	-	-	-
Indicator 1.2 Riverbank structure	RR	2020	1.00	58.2%	31.1%	10.6%	0.0%	0.0%	50.5%	48.2%	1.3%	66.8%	33.2%	-	-	-
		2021	1.00	57.4%	28.4%	14.2%	0.0%	0.0%	55.6%	39.7%	4.7%	48.3%	51.7%	-	-	-
	CR	2020	1.00	80.3%	0.7%	19.0%	0.0%	0.0%	26.3%	69.8%	3.9%	35.6%	64.4%	-	-	-
		2021	1.00	75.9%	4.7%	19.4%	0.0%	0.0%	57.6%	40.9%	1.6%	41.7%	58.3%	-	-	-
Indicator 1.3 Water depth	RR	2020	0.48	0.31 m	0.66 m	0.48	-	-	-	-	-	-	-	-	-	-
		2021	0.39	0.26 m	0.66 m	0.39	-	-	-	-	-	-	-	-	-	-
	CR	2020	0.40	0.40 m	0.99 m	0.40	-	-	-	-	-	-	-	-	-	-
		2021	0.35	0.34 m	0.97 m	0.35	-	-	-	-	-	-	-	-	-	-
Indicator 1.4 Flow velocity	RR	2020	0.72	0.33 m/s	0.42 m/s	0.79	-	-	-	-	-	-	-	-	-	-
		2021	0.69	0.34 m/s	0.45 m/s	0.76	-	-	-	-	-	-	-	-	-	-
	CR	2020	1.00	0.34 m/s	0.31 m/s	1.11	-	-	-	-	-	-	-	-	-	-
		2021	0.85	0.31 m/s	0.34 m/s	0.93	-	-	-	-	-	-	-	-	-	-
Indicator 1.5 Presence of cover	RR	2020	0.25	1.4%	0.3%	0.0%	0.2%	2.4%	3.7%	0.0%	3.2%	0.1%	0.1%	2.8%	0.7%	2.5%
		2021	0.25	0.8%	0.9%	0.0%	0.4%	0.0%	2.9%	0.0%	4.2%	0.1%	0.3%	1.4%	0.0%	2.1%
	CR	2020	0.25	2.8%	0.4%	0.0%	0.2%	2.1%	1.5%	0.0%	6.5%	1.1%	1.0%	4.8%	1.4%	0.0%
		2021	0.25	0.5%	0.3%	1.7%	1.3%	1.2%	3.7%	0.1%	4.4%	1.5%	0.1%	4.1%	0.7%	0.0%
	ER		-	1.0%	1.0%	1.5%	0.5%	2.3%	3.8%	2.3%	0.5%	0.5%	0.0%	0.0%	14.0%	30.0%
Indicator 1.6 A1 Substrate Composition	RR	2020	-	9.7%	0.7%	0.7%	6.0%	58.9%	6.2%	6.4%	11.5%	0.0%	-	-	-	-
		2021	-	9.8%	0.8%	0.1%	2.8%	62.2%	9.7%	10.3%	4.4%	0.0%	-	-	-	-
	CR	2020	-	19.6%	0.0%	1.9%	9.6%	54.8%	10.3%	0.0%	3.7%	0.0%	-	-	-	-
		2021	-	14.5%	0.0%	0.9%	7.5%	58.7%	10.7%	0.1%	7.6%	0.0%	-	-	-	-
Indicator 1.6 A2 Substrate Mobilisability	RR	2020	0.25	16.2%	1.1%	3.0%	71.3%	8.3%	-	-	-	-	-	-	-	-
		2021	0.25	13.9%	0.3%	3.5%	50.8%	31.5%	-	-	-	-	-	-	-	-
	CR	2020	0.25	22.6%	1.9%	2.0%	55.3%	18.2%	-	-	-	-	-	-	-	-
		2021	0.25	22.0%	1.2%	7.2%	29.1%	40.5%	-	-	-	-	-	-	-	-

The indicator scores are identical for *restoration* and *control reach* in both assessments for all indicators with categorical attributes (1.1, 1.2, 1.5, 1.6A2). The indicator scores of *flow velocity* and *water depth* declined in both reaches from the assessment in 2020 to the assessment in 2021. The indicators are analysed separately in the following sections.

7.3.1 Riverbed structures

The results of the mapped riverbed structures at the *restoration* and *control reach* are shown in **Figure 7.3**. Consistent with the definition in Section 2.1.1, riverbed structures are referred to as channel geomorphic units (CGUs) in the analysis of results.

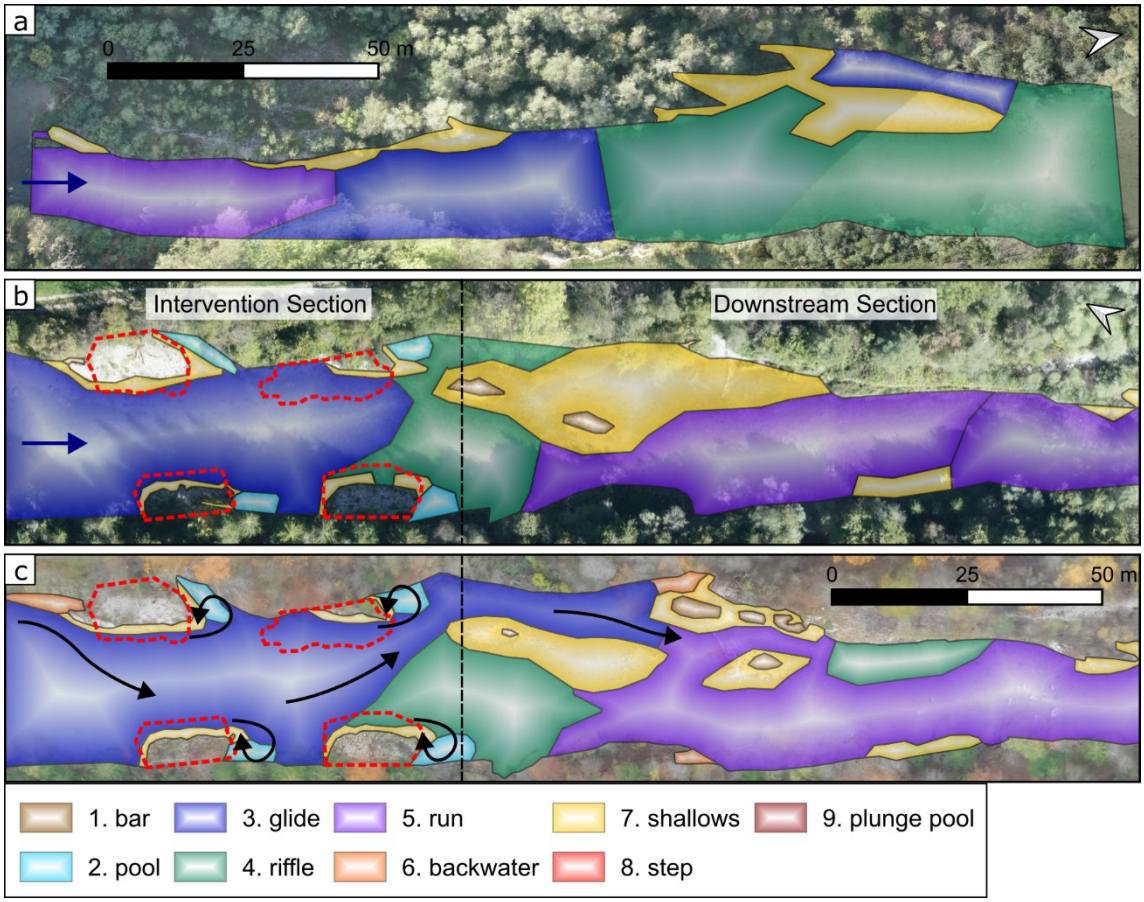

Figure 7.3 Mapped riverbed structures (CGUs) at different study reaches and assessment times. a: *Control reach*, 2020. b: *Restoration reach*, 2020. c: *Restoration reach*, 2021. The red dashed line indicates the initial artificial deposit positions. The black dashed line separates the *intervention section* and the *downstream section*. Blue arrows indicate the direction of flow. Black arrows indicate basic flow patterns during *Flood 2020*. The number in the legend indicates the category number (see **Table 7.1**). Background images: © research unit ecohydrology, Zurich University of Applied Science.

In 2020, the number of CGUs was higher in the *restoration reach* (18) than in the *control reach* (7). *Bars* (6.8%) and *pools* (2.5%) are only present in the *restoration reach*. A large area of *shallows* (20.6%) with two in-channel *bars* was mapped downstream of the artificial deposits. After *Flood 2020*, the most important structural changes occurred in the *downstream section*. *Bars* occurred predominantly at the left bank compared to the channel centre. The glide section penetrated from the *intervention section* into an area previously identified as *shallows*. The extent of the *shallows* decreased significantly (8.1%). A new *riffle* section occurred on the left bank in the *run* section.

After *Flood 2016*, the SAM likely contributed to aggradation in the near downstream vicinity of the artificial deposits, increasing the size of *shallows* and *riffles*. Recirculating flow at the downstream end of the artificial deposits during flood formed scour holes, classified as *pool* sections. In the *intervention section*, the main flow was deviated first towards the right bank by the most upstream artificial deposit and then deflected back towards the left bank, leading to an almost complete erosion of the downstream artificial deposit. During *Flood2020*, the flow was deviated by the artificial deposits' remnants, similar to *Flood2016*. It led to sediment entrainment along the left bank downstream of the artificial deposits,

which manifested in the growth of the *glide* section and the formation of *bars* in a downstream deposition zone, where the channel starts to narrow.

According to the EOR1, the score of Indicator 1.1 is evaluated per unit length, defined as 12 times the width of the riverbed. The score increases with the number of CGU types and dominant CGU types of a *glide–riffle–run* or a natural or near-natural *step–pool* sequence. The complete evaluation criteria are provided in the appendix (Table A12.1). The indicator score for both reaches remained unchanged between 2020 and 2021 (0.5).

Sediment supply is a crucial control factor for the morphological evolution of a water course (e.g. Pfeiffer et al., 2017). The mapping of CGUs allows for capturing and quantifying this evolution. The qualitative analysis of the mapped field data showed that several changes to the CGU arrangement could be attributed to the sediment augmentation measure. While the EOR1 score represents the diversity of CGUs, it does not consider the importance of shifting CGU organisational patterns (Stanford et al., 2005). A diverse but static pattern may reflect a high score with limited long-term ecological benefit. The importance of dominant CGUs for the calculation method of the EOR1 indicator 1.1 allows for a good comparison to a near-natural reference state. However, it can underestimate the ecological benefit of other CGUs in regulated reaches.

7.3.2 Riverbank structures

The results of the mapped riverbank structures at the *restoration* and *control reach* are shown in Figure 7.4.

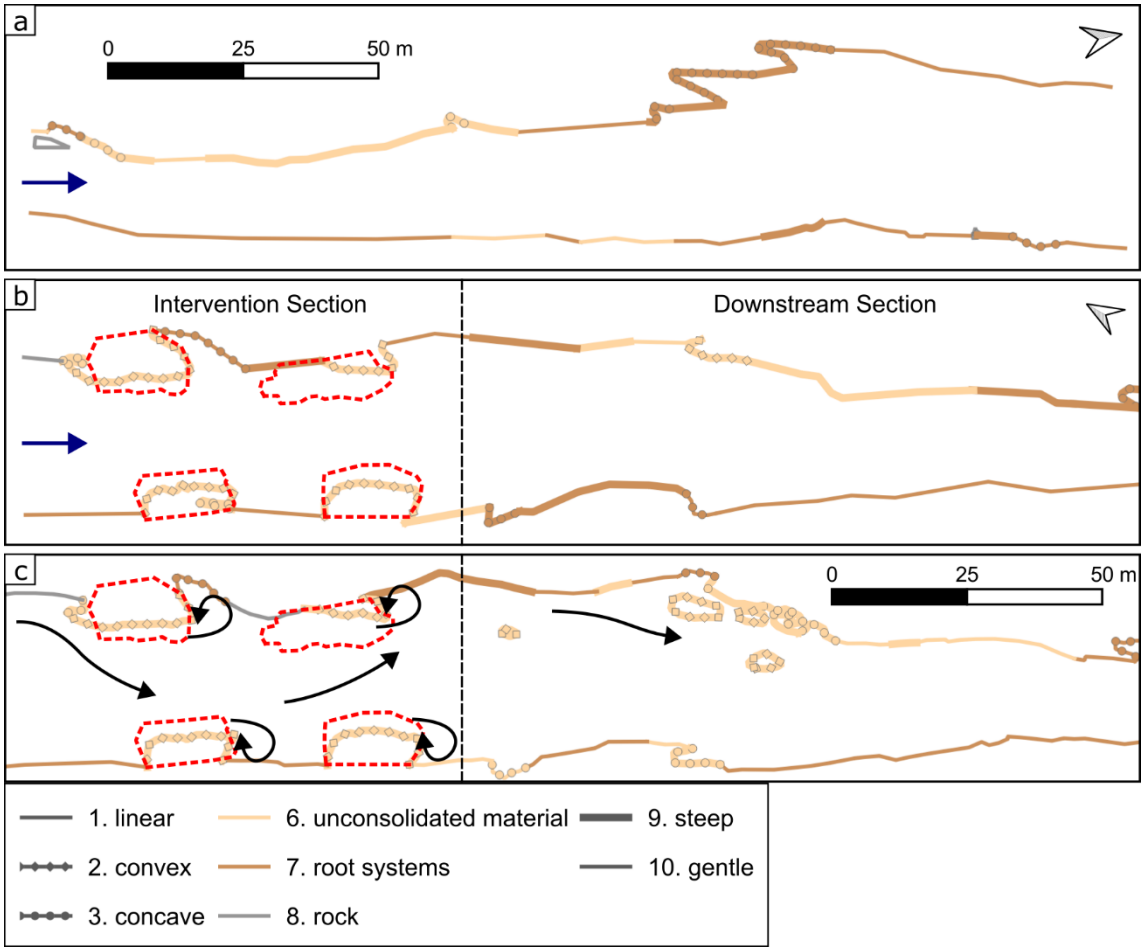

Figure 7.4 Mapped riverbank structures at different study reaches and assessment times. a: *Control reach*, 2020. b: *Restoration reach*, 2020. c: *Restoration reach*, 2021. The red dashed line indicates the initial artificial deposit positions. The black dashed line separates the *intervention section* and the *downstream section*. Blue arrows indicate the direction of flow. Black arrows indicate basic flow patterns during *Flood 2020*. The number in the legend indicates the category number (see **Table 7.1**).

In 2020, the highest number of bank structures was identified in the control reach (27). The highest density of bank structures was mapped in the *intervention section*. No embankment (artificial bank protection) was present in both reaches. The bank structures of the *downstream section* consisted of similar types and heterogeneity as the bank structures of the *control reach*. In 2021, the number of individual bank structures doubled from 11 to 22 in the *downstream section*, and the bank line increased from $263m$ to $339m$.

After *Flood* 2016, the remnants of the artificial deposits themselves contributed to the diversity of riverbank structures by creating additional *steep*, *convex* bank lines of *unconsolidated material*. Where supplementary sediment from the SAM was deposited near the banks, the bank tends to consist of *unconsolidated material* and the slope to be rather *gentle* than *steep*. This distribution is the case in large parts along the left bank in the *downstream section*. After *Flood 2020*, the deviation of the main flow caused sediment erosion from the left bank downstream of the artificial deposits until the uncovering of the root *systems*. The alluvial bars created new bank lines in the downstream deposition zone.

According to the EOR1, the score of Indicator 1.2 is evaluated per unit length, similar to Indicator 1.1. The score increases with a lower proportion of linear embankment and higher structural diversity. The complete evaluation criteria are provided in the appendix (Table A12.2). The indicator score for both reaches remained unchanged between 2020 and 2021 (1).

Changes in channel form, and thus significant changes in riverbank structures, occur during channel-forming flow combined with sufficient sediment supply (e.g. Montgomery & Buffington, 1998). The impact of the SAM on the evolution of riverbanks without channel-forming flow is limited to small-scale changes from local erosion and deposition along unprotected bank lines.

7.3.3 Hydromorphological diversity

Indicators 1.3 and 1.4 are calculated from depth and velocity measurements across fourteen cross-sections in the *restoration reach* and five cross-sections in the *control reach*. The scores are standardised from the CoV, where a value greater than 1 for Indicator 1.3 and greater than 1.1 for Indicator 1.4 corresponds to a score of 1, with the score function being linear. The indicator score of water depth (Ind. 1.3) decreases in the *restoration reach* from 0.48 to 0.39 and from 0.40 to 0.35 in the *control reach*. The indicator score of flow velocity (Ind. 1.4) decreases in the *restoration reach* from 0.72 to 0.69 and from 1.00 to 0.85 in the *control reach*.

The higher score of water depth (Ind. 1.3) in the *restoration reach* compared to the *control reach* was likely impacted by the channel incision between the artificial deposits and the aggradation in their near downstream vicinity. Nevertheless, the low number of cross-sections in the *control reach* leads to a lower representability of this indicator score. After *Flood 2020*, both hydromorphological indicators (Ind. 1.3 & 1.4) decreased. With no supplementary sediment supply, the washing out of the remaining bedload and the incision of the main channel can lead to a homogenisation of the bed morphology and the flow field.

SAM can impact hydromorphological diversity by promoting topographic and hydraulic variability through artificial sediment supply (e.g. Arnaud et al., 2017; Gaeuman, 2014; Stähly, 2019). Physical habitat heterogeneity is vital for river biodiversity and ecosystem function (Allan & Castillo, 2007). Therefore, water depth and flow velocity are valid indicators for physical habitat assessment. Other than, for example, the $HMID$, Indicator 1.3 of the EOR1 includes only the maximum water depth of every cross-section. It generally yields higher scores for elevation differences between homogeneous cross-section profiles than the $HMID$, which can be expected in highly modified water bodies. The absolute scores cannot be compared, but both indicators are equally valid for the impact assessment of SAMs when used in a before-after analysis.

7.3.4 Presence of cover

The results of the mapped presence of cover at the *restoration* and *control reach* are shown in Figure 7.5.

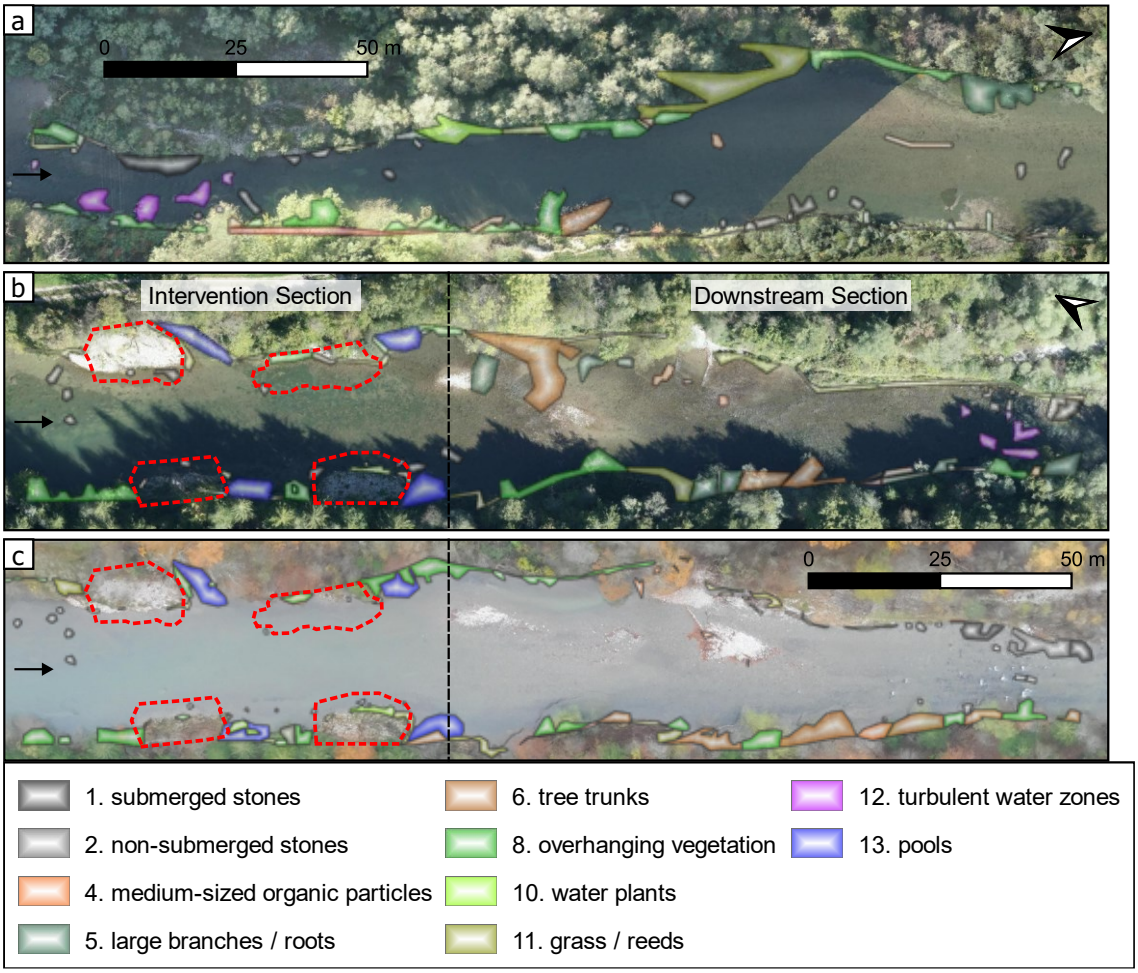

Figure 7.5 Mapped presence of cover at different study reaches and assessment times. a: *Control reach*, 2020. b: *Restoration reach*, 2020. c: *Restoration reach*, 2021. The red dashed line indicates the initial artificial deposit positions. The black dashed line separates the *intervention section* and the *downstream section*. The number in the legend indicates the category number (see Table 7.1). Background images: © research unit ecohydrology, Zurich University of Applied Science.

In 2020, nine types of cover existed in the *control reach*, with *overhanging vegetation* (6.5%) and *grass/reeds* (4.8%) presenting the largest proportion of the wetted area. In the *restoration reach*, *pools* existed on top of all cover types of the *control reach*, accounting for 2.5% of the wetted area. In 2021, *overhanging vegetation* increased (1.0%), *grass/reeds* decreased (1.4%), and the proportion of *pools* remained relatively similar (−0.4%). A paired t-test showed that the expected change in the presence of cover after *Flood 2020* observed in the *control reach* was not significantly different from the actual change in the *restoration reach* ($p = 0.77$). In both reaches, there was a substantial deviation from the reference estimation for the two types of *turbulent water zones* (14.0%) and *pools* (30.0%).

After *Flood 2016,* the scour holes (*pools*) created by the artificial deposits increased the presence of cover. Apart from this, there is no evidence of the direct influence of the SAM. This result is supported by the statistical t-test, which did not allow to reject the hypothesis that the SAM had an influence on the presence of cover during *Flood 2020*.

According to the EOR1, the score of Indicator 1.5 is evaluated by comparing the presence of all cover types against an expert reference estimation for the river type. The score increases with a lower deviation from the reference estimation. The complete evaluation criteria are provided in the appendix (Table A12.3). The indicator score for both reaches remained unchanged from 2020 to 2021 (0.25).

The presence of cover in the habitat mosaic is crucial for the diversity of fish species (Smokorowski & Pratt, 2007). Frequent bedload transport is required to sustain a large abundance of turbulent water and pools and thus provide vital cover for different fish species. Other categories of the EOR1 Indicator 1.5 are not created by SAM other than from structural diversity around the intervention zone. Since bedload equilibrium is not obtained from a single SAM and many cover types are independent of sediment supply, the EOR1 Indicator 1.5 is not valid for the impact assessment of the 2016 SAM.

7.3.5 Substrate quality

The results of the mapped substrate mobilisability at the *restoration* and *control reach* are shown in Figure 7.6. The results of the mapped substrate composition are provided in the appendix (Figure A12.1).

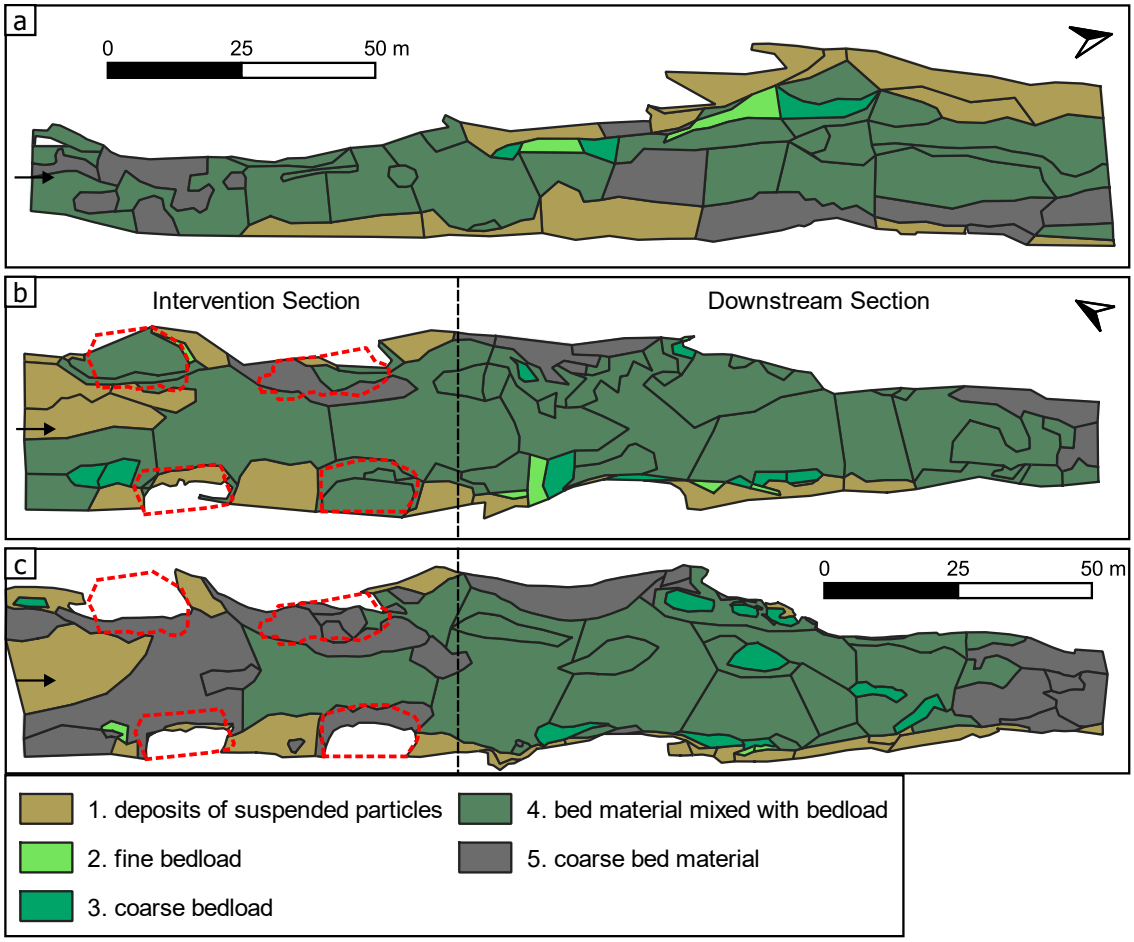

Figure 7.6 Mapped substrate mobilisability at different study reaches and assessment times. a: *Control reach*, 2020. b: *Restoration reach*, 2020. c: *Restoration reach*, 2021. The red dashed line indicates the initial artificial deposit positions. The black dashed line separates the *intervention section* and the *downstream section*. The number in the legend indicates the category number (see **Table 7.1**).

In 2020, the distributions of substrate composition and mobilisability of the *restoration reach* and *control reach* were very similar. More than 50% of the bed area was dominated by large stones ($]64, 250]mm$). Concerning the mobilisability, more substrate was classified as *bed material mixed with bedload* in the *restoration reach* (71.3%) than in the *control reach* (55.3%). *Coarse bedload* (3.0%) and *fine bedload* (1.1%) only existed in small patches along the right bank at the restoration reach. In 2021, a large substrate area previously classified as *bed material mixed with bedload* degraded to *coarse bed material* ($\sim 20\%$).

After Flood 2016, the SAM has likely contributed to increasing the mobilisability of the substrate in the *restoration reach* by providing additional *gravel* and *stones*. That only a small fraction of areas was classified as *coarse bedload* or *fine bedload* can be attributed to the fact that the assessment was performed four years after the last bed-forming flow and that clogging has decreased the mobilisability across the entire residual-flow reach. The degradation of substrate mobilisability after *Flood 2020* is attributed to the fact that no new sediment was added, and the existing bedload was further washed out during the flood.

According to the EOR1, the score of substrate mobilisability (Ind. 1.6.A2) is evaluated by distribution type. The score is highest for a symmetrical distribution of categories 1 to 5, representing the predominance of bedload deposits and no or limited areas of coarse, armoured bed material. The complete evaluation criteria are provided in the appendix (Table A12.4). The indicator score for both reaches remained unchanged between 2020 and 2021 (0.25).

Degradation of substrate quality by bedload deficit and clogging can be one possible consequence of insufficient hydromorphological dynamics in regulated reaches (Hauer, Wagner, et al., 2018) and can diminish the biological diversity of the aquatic fauna (e.g. Bo et al., 2007; Mathers et al., 2019). SAMs are designed to increase the amount of bedload in a restoration reach. The attribute *mobilisability* of the EOR1 Indicator 1.6 (A2) provides an essential proxy of substrate quality and is therefore valid for the impact assessment of SAMs on habitat diversity. Even though the indicator score might not represent the impact of a SAM on a sufficiently high resolution, the mapped areas can still quantify the amount of improved substrate quality. The calculation method for the attribute *composition* (Indicator 1.6, A1) is yet to be developed. However, it already presents an essential variable for sampling and interpreting biological indicators (Hunzinger et al., 2019).

7.4 Conclusion

The findings of this chapter suggest the following statements for the impact assessment of a single sediment augmentation measure coupled with low-magnitude, bed-forming flood events on habitat diversity in a residual-flow reach:

- Riverbed structures, substrate mobilisability, water depth, and flow velocity are valid indicators.
- Riverbank structures and substrate composition cannot indicate small-scale morphological changes in response to low-magnitude, bed-forming flood events.
- The presence of cover is not a valid indicator.

The results partially confirm the hypothesis H4 that *Indicator set 1* of the *Swiss Guideline for Evaluating the Outcome of Restoration Projects* is valid for assessing the impact of sediment augmentation measures on habitat diversity. Some indicators are essential for the impact assessment, but their score alone can often not explain small-scale impacts, especially in the case of categorical indicators. Beyond the mandatory indicator set 1, indicator set 2 (*dynamics*) is also highly relevant and can be an effective assessment tool for sediment augmentation measures. Its three indicators, *riverbed structure dynamics*, *riverbank structure dynamics*, and *bed position evolution*, are directly linked to a properly functioning sediment regime. The suitability of the remaining abiotic and biotic indicator sets, such as indicator set 7 (fish), can be assessed case-by-case and depend on the restoration objectives. Ultimately, detailed eco-geomorphological assessment of sediment augmentation measures requires expert judgement and site-specific interpretation.

Chapter 8
Recommendations for sediment augmentation measures

In this chapter, practical recommendations for sediment augmentation measures are derived from the research of this thesis. It outlines how design measures can be adapted to site-specific restrictions and restoration- and management objectives. The potential impact of sediment augmentation measures is highlighted in a discussion about the choice of the sediment source. Conflicts and synergies for the design of artificial floods show that the recommendations of the laboratory experiments need to be complemented with, or weight against, ecological- and operational demands. An objective-based, conceptual design framework is introduced, providing a hands-on tool for pre-designing sediment augmentation measures. Examples of long-term restoration strategies give an idea about the feasibility of different measures and the scale of the required commitment.

Note: This chapter is based on an article published in a peer-reviewed journal[1] and a translated article published in a technical journal[2].

8.1 Introduction

This chapter breaks down the scientific results and discussions of the previous chapters to provide concise information for stakeholders and application-oriented recommendations for practitioners.

From the literature review (Chapter 2), the idea was developed to distinguish SAM by the four primary restoration and management objectives (i) *Bedload Budget*, (ii) *Channel Dynamics*, (iii) *Riverbed Structure* and (iv) *Interstitial (Spawning) Habitat* (Figure 2.3). The following chapter discusses possible restrictions for those objectives within the target reach based on experience from the literature. Morphologic site conditions that influence the implementation of the SAM are derived from the field experiment (Chapter 6). Then, background information on the origin of the sediment is provided. Design recommendations for mobilising SAMs by artificial floods are derived from laboratory studies (Chapter 4 and Chapter 5). Critical points for assessment strategies are elaborated from the study described in Chapter 7. Essential criteria for the pre-design of

[1] "Sediment augmentation for river rehabilitation and management - a review" by C. Mörtl and G. De Cesare, published in 2021 in *Land* (Mörtl & De Cesare, 2021). Contribution of the doctoral candidate according to the *CRediT*: conceptualisation; data curation; investigation; validation; visualisation; writing – original draft; writing – reviewing and editing.

[2] "Sedimentzugaben in Fliessgewässern. Überblick über Methoden und Fallbeispiele [Sediment augmentation in flowing waters. Overview of methods and case studies]" by C. Mörtl and G. De Cesare, published in 2022 in *Ingenieurbiologie* (Mörtl & De Cesare, 2022a). Contribution of the doctoral candidate according to the *CRediT*: conceptualisation; data curation; investigation; resources; validation; visualisation; writing – original draft; writing – reviewing and editing.

SAMs are summarised in a conceptual framework. This chapter ends with a section on long-term restoration strategies providing examples of standard application cases.

8.2 Restrictions

The restoration and management objective of SAM should depend on the target section and vice versa. A possible restriction for sediment augmentation is the flow regime. At constant low flow discharge, stream power is insufficient to mobilise considerable amounts of bedload material if the flow is below the entrainment threshold (Gintz et al., 1996). Discharge variations shape channel patterns (Leopold & Wolman, 1957). In river reaches with no recurring morphological discharges, the hydrogeomorphic processes are restricted to a point where channel dynamics are largely impaired, e.g. (Kondolf, 1997; Sear, 1995; Tonolla et al., 2021).

Sediment discontinuities, like dams or sediment traps, can restrict or prevent the effectiveness of SAM aimed for bedload restoration. Hydropower structures affect the bedload budget in many ways. Complete and long-term retention and continuous routing are possible (Schälchli & Kirchhofer, 2012). To enhance channel dynamics by SAM, the river corridor and the bank structure should allow lateral migration. Downstream of dams, the encroachment of alluvial vegetation can stabilise channel banks (P. R. Wilcock et al., 1996) and lead to substantial narrowing of the active channel width (Tonolla et al., 2021) if no recurring floods and sufficient bedload transport rates cause the dynamic reshaping of the riparian zone. In populated areas, artificial bank protection for flood protection or channelisation equally impairs channel evolution.

The required conditions for a successful SAM can be a limiting factor, or otherwise, be the target of a secondary restoration measure and used to create possible synergies (Schälchli & Kirchhofer, 2012). For example, where a lack of recurring morphological discharges restricts channel dynamics, a regular flushing scheme can be introduced as a secondary measure. Such an additional measure can provide both the required flow discharge and the necessary transport capacity to progressively enhance channel dynamics and promote a regular shifting and declogging of the riverbed.

8.3 Morphologic site conditions

The results of Chapter 6 showed that different channel geomorphic units can locally impact pulse evolution. Therefore, assessing existing riverbed structures at the target site is recommended for the design of a SAM. The placement or constant injection should be performed at sections where shear stress is high during a flood for a high mobilisation rate. It includes sections with a small channel width and steep slope, as in *riffles*. The placement can also be adapted to whether the goal is to increase the impact length and counter incision along the thalweg or replenish local sediment sources for future floods. A schematic example is provided in Figure 8.1. The prediction of deposition patterns is qualitative and derived from the results of Chapter 6.

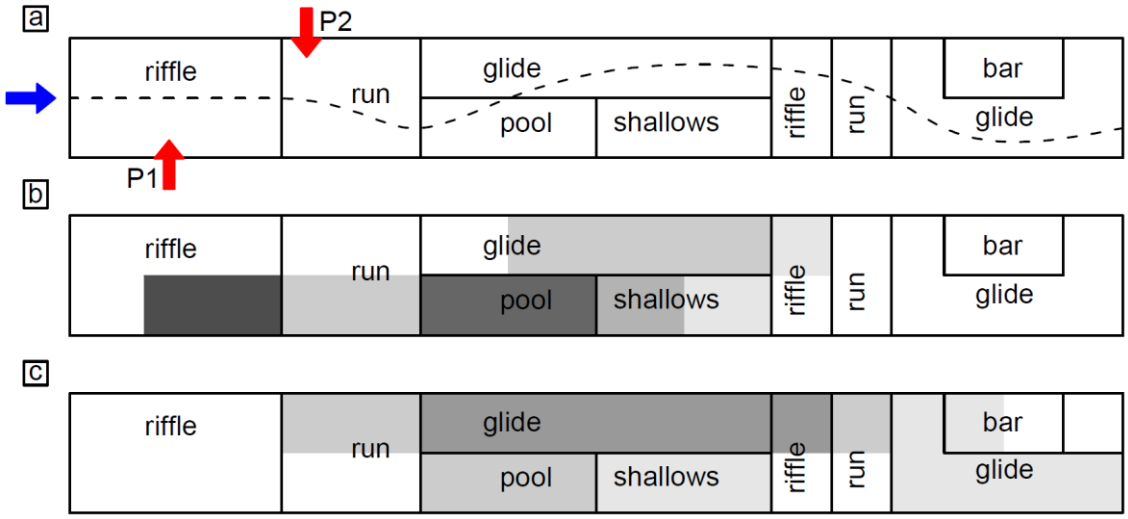

Figure 8.1 Schematic sketch of sample organisational pattern of channel geomorphic units (CGUs) in a restoration reach and predicted deposition from indirect sediment augmentation at two different locations after a low-magnitude bed-forming flood. a: restoration reach. The red arrows mark two possible placements (P1 & P2) with different implementation objectives. The blue arrow indicates the direction of flow. The dashed line is the thalweg. b: Deposition pattern in response to P1. c: Deposition pattern in response to P2. The grayscale represents the density of the predicted deposition.

Placement P1 favours a replenishment of sediment in *pools, shallows, and riffles*, which can act as local sediment sources (**Figure 8.1** b). Placement P2 favours the mitigation of channel incision and the re-establishment of an active layer in *glides and runs*, which exerts a high transport capacity during a flood (**Figure 8.1** c). Placement P2 also favours the increase of the impact length and sediment transport towards downstream reaches. When evaluating different locations of placement for a SAM, the consequence of a rise of the backwater curve and local incision from flow deviation should be considered.

Another important site specification is the depth of the active layer. It determines the existing “budget” of bedload during a flood. The laboratory tests of this thesis have shown that continuous repetitions of SAM in successive floods with augmentation volumes, which satisfy the full transport capacities, are vital for the recreation of an active layer in sediment-starved reaches. When an active layer has been partially restored, repetition frequency, augmentation volume and flood intensity can be altered to promote a natural diversification of the river morphology.

8.4 Origin of sediment

The sediment for the SAM can be excavated from the alluvial plain or an external source, like a gravel pit. In a residual-flow reach, the sediment can be extracted from the upstream zone of the reservoir or upstream of a check dam (**Figure 8.2**).

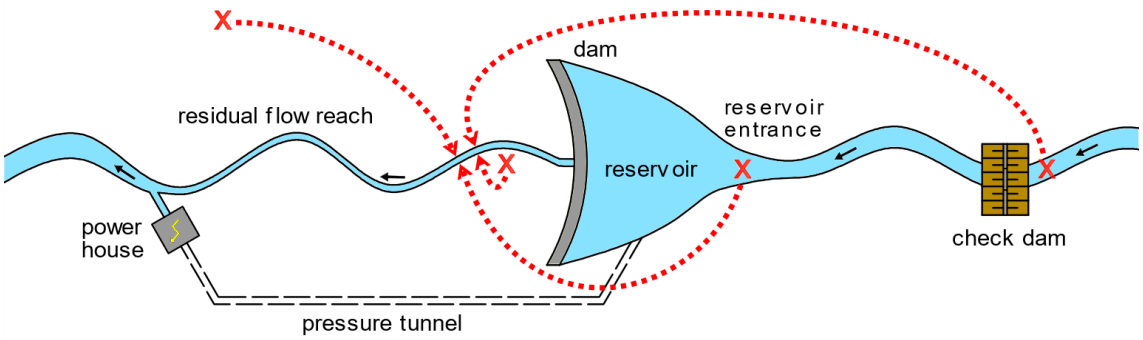

Figure 8.2 Schematic sketch of possible extraction sites for sediment augmentation in a residual-flow reach. The red cross marks the extraction site, and the arrow symbolises the transport to the sediment augmentation site.

For accessible sediment sources, sediment properties and transport distance are important decision factors. Sediment properties are discussed in Section 2.3.2. The transport distance is consequential because it can cause significantly increasing economic, ecological, and social impacts. Direct costs are caused by the transport by truck or the building of temporary construction roads. Indirect costs can be caused, for example, by traffic restrictions. The environmental impact consists of carbon and noise emissions by the trucks or the densification of soils by transporting heavy loads. Social impact is caused by transport noise, increased danger, of injury or access restrictions.

Excavating sediment at the adjacent floodplain is a common sediment source for SAM because it minimises transport distance. In case of reaches that have been regulated over decades, the GSD of the excavated material usually represents bedload in pre-dam conditions. It is not suited for mobilisation in small artificial flood events. In areas where the alluvial plain is covered by hardwood forest, the amount of organic material is usually high, which can have adverse ecological effects when introduced in disproportionate quantities to the river. Dredged sediment from a reservoir or a check dam is suited for downstream augmentation if the percentage of fines is low, and the GSD allows for a large proportion of augmented sediment to be mobilised in artificial flood events. External sediment sources such as gravel pits allow for a choice of GSD by design and excluding organic material. On the other side, adverse side effects from long transport distances can increase unintended negative impacts of the restoration project.

8.5 Artificial floods

8.5.1 Hydrograph shape

The laboratory experiments of this thesis have shown that the hydrograph shape of an artificial flood can influence sediment transport dynamics from a SAM. The recommendations of this chapter apply to sediment augmentation measures in the form of alternating, in-channel deposits, which are shifted half the deposit length (configuration B; Battisacco et al., 2016) and placed along an elevated portion of the riverbed (riffle). The

reach type is restricted to low-gradient (< 1%), sediment-starved, gravel-bed rivers. The following section summarises the main hydrograph characteristics and their influence.

Symmetry

A flood with symmetrical hydrographs can promote the mobilisation of artificial deposits. It can be beneficial where vegetation encroachment has stabilised the deposits. It also helps to reduce the risk of flooding at the augmentation site by the swift reduction of the blocking ratio of the artificial deposits and the corresponding lowering of the backwater curve. In cases where the deposits themselves are designed to contribute to a diversification of reach morphology, asymmetrical hydrographs can cause them to become only partially eroded.

Skewness

Left-skewed hydrographs, characterised by a sharper falling limb than the rising limb (Figure 8.3), can increase the mean transport distance. This effect can be beneficial in cases with large augmentation volumes or where an active layer already exists in the restoration reach to increase the length of the impact section. It can also promote the transportation of augmented sediment to a target zone not located in the close downstream vicinity of the sediment injection point. This effect can be beneficial if such a target section is inaccessible or establishing a closer injection point would cause a disproportional high economic, ecological, or social impact (Section 8.4). On the other hand, when the augmented volume is small compared to the expected transport capacity and the degree of armouring is high, right-skewed hydrographs allow for increasing deposition in the downstream vicinity of the injection point.

Periods of equal discharge

In the event of a flood coupled with sediment augmentation, sediment transport rates decrease over time during periods of equal discharge. This effect is more pronounced near the artificial deposits (1 channel widths) than further downstream (20 channel widths). It suggests that for the design of an artificial flood downstream of a hydraulic structure, maintaining a constant discharge over a long period (e.g. 30% of the flood duration) can reduce the transport of eroded sediment out of the hydraulic impact zone of the artificial deposits while the distribution of augmented sediment continues further downstream of the sediment source. This process can be desired for the successive supply and distribution of sediment in a series of smaller floods coupled with a single sediment augmentation measure.

Flashiness

Longer duration floods with lower peak discharge can benefit efforts to distribute sediment in the near downstream vicinity of the artificial deposits and restore a mobile bed layer. On the contrary, the alternation with shorter duration floods with higher peak

discharge leads to higher sediment erosion and transport and can be used to restructure a static bed morphology.

8.5.1 Ecological design

Artificial floods can be performed for multiple purposes with contradicting design requirements. Morphogenic floods are performed for reservoir management purposes, with the most common goal being to flush out fine sediment from the reservoir to reduce reservoir sedimentation (Schleiss et al., 2016). Environmental floods are designed to improve the ecological state of the river, e.g. for detaching nuisance algae or floodplain management (Loire et al., 2021). While reservoir flushing aims to mobilise sediment through the rapid opening of gates and steep flood limbs, ecological adverse effects can be limited with gradually rising and falling flood hydrographs. Aquatic fauna requires time to seek shelter in refugia during up-ramping phases and risks stranding during rapid down-ramping periods (Greimel et al 2018). It is recommended to decrease the steepness of the rising and falling limb at the beginning and the end of the flood below the threshold of coarse bedload motion to mitigate such ecological adverse effects during artificial floods designed to mobilise a SAM (Figure 8.3). The addition of the ecological flood volume intended to reduce the ramping rate of the artificial flood is a qualitative design recommendation based on studies about hydropeaking mitigation measures (e.g. Greimel et al., 2018).

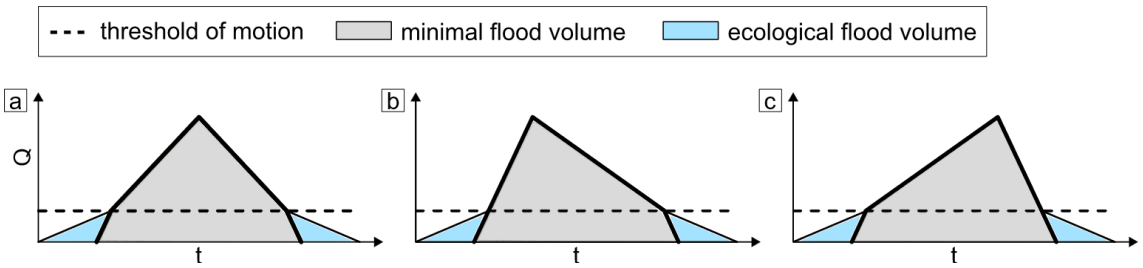

Figure 8.3 Schematic sketch of different hydrograph shapes with minimal and ecological flood volume. Variable Q is the discharge, and t is the time. a: symmetrical hydrograph. b: right-skewed hydrograph. c: left-skewed hydrograph.

8.6 Assessment strategies

Evaluation in the context of SAM should distinguish between the components of *implementation* and *outcome evaluation*. Implementation evaluation describes what was done, and outcome evaluation what was achieved. Both components are essential for quantifying the success of a SAM. The eco-geomorphological assessment of a SAM focuses on outcome evaluation. The assessment strategy should be defined in the early planning stage and be based on the dimensions and the objective of the SAM.

In Chapter 7, a study described the validity of indicators of *Indicator Set 1* of the *Guideline for the Outcome of Restoration Projects* of the Swiss Federal Office of the Environment

(EOR1). Figure 8.4 provides an overview of an objective-based indicator selection for the eco-geomorphological assessment of SAM.

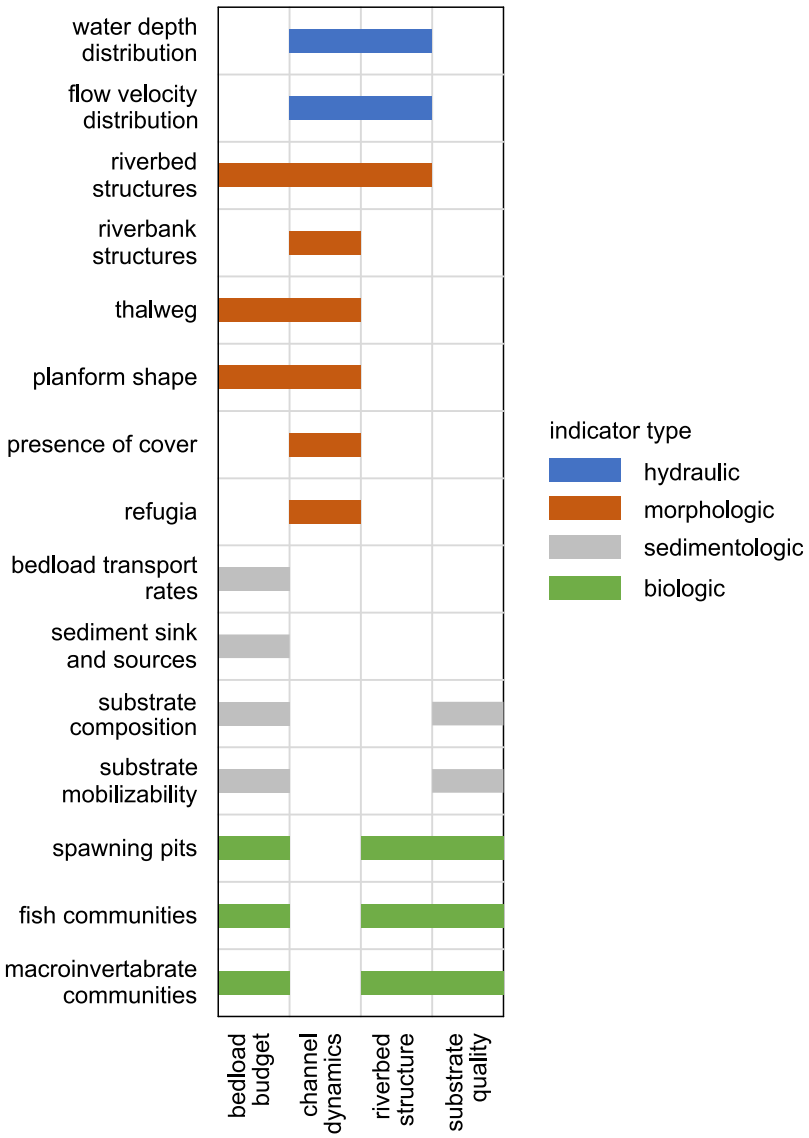

Figure 8.4 Indicator for eco-geomorphological assessment of sediment augmentation measures (SAMs) with different primary objectives. A bar at the intersection between an indicator (row) and the primary objective of a SAM (column) indicates a relevant combination.

Hydraulic indicators like *flow velocity* and *water depth* can indicate channel dynamics and riverbed structure changes. They are used to calculate the $HMID$, and Indicators 1.3 and 1.4 of the EOR1, which quantify habitat diversity.

Morphologic indicators can be recorded at different levels of detail, either on a sub-reach scale through field mapping or on a larger scale by topographic or image analysis of air-borne or satellite imagery. They are most relevant for assessing SAMs in the context of bedload balancing and the promotion of channel dynamics. For example, the bedload

volume of a historic, near-natural reference state can be estimated based on the *planform shape*, which includes river type and average channel width, or the distribution of the *riverbed structure* type of gravel bars (Schälchli & Hunzinger, 2018).

Sedimentologic indicators like bedload transport rate and sediment sink and sources are essential in the context of an eco-geomorphological assessment to compare the actual state of the bedload budget to a near-natural reference state. *Substrate composition* and *substrate quality* are direct indicators for assessing substrate quality. Together with hydraulic characteristics, they can be used for the assessment of reproduction suitability, for example, by the indicator for reproduction suitability based on substrate degradation (IRS; Schroff et al., 2021b), or for the aquatic habitat diversity, for example by the indicator for the attractiveness of river morphology (IAM; Vonlanthen et al., 2018).

Biologic indicators, like *fish communities* or *macroinvertebrate communities*, provide a holistic representation of ecosystem functioning. Those indicators can represent changes in physiology, behaviour, and morphology to changes in survival and mortality of single species or communities (Pander & Geist, 2013). Since many environmental conditions influence the living fauna, it is difficult to isolate the impact of SAMs on such indicators. In this context, *spawning pits* can provide a suitable indicator to relate changes in physical habitat from SAM more directly to ecological changes.

8.7 Conceptual design framework

Based on the research of this thesis, a conceptual framework was developed pre-assessing potentially relevant restrictions, design approaches and assessment methods for different primary objectives of SAMs (Table 8.1).

First, existing restrictions at the target reach are identified from the list of restrictions. Second, the objectives, which are relevant to all the selected restrictions, are identified. Third, relevant design approaches and assessment methods are similarly identified for the selected set of objectives in the corresponding lists. The design approaches and assessment methods are discussed in Section 2.3.2, and the restrictions are discussed in Section 8.2.

Table 8.1 Conceptual framework for identifying relevant restrictions, design approaches and assessment methods for four primary restoration and management objectives of sediment augmentation measures. The four objectives are *Bedload Budget* (B), *Channel Dynamics* (C), *Riverbed Structure* (R), and Interstitial (Spawning) Habitat (I). Thy symbol x marks a relevant objective.

		Primary objectives			
		B	C	R	I
Restrictions *1. Identify relevant primary objectives for existing restrictions*					
	Constant low residual flow discharge			x	x
	No recurring major morphological discharges	x		x	x
	Sediment discontinuities		x	x	x
	Lateral limitations for river widenings	x		x	x
	None of the above	x	x	x	x
Design Approaches *2. Identify relevant design approaches for defined objectives*					
Sediment Properties	Spawning substrate				x
	Sediment mix		x	x	
	Bedload material	x	x	x	
Volume	Missing spawning substrate				x
	Morpho-dynamically required volume		x	x	
	Bedload deficit	x	x		
Injection Method	In-channel injection			x	x
	Stockpile	x	x	x	x
	High-flow constant injection	x	x	x	x
	Induced riverbank erosion	x	x	x	
	Reactivation of old side channels	x			
Mobilisation Event	*None*			x	x
	Natural flood	x	x	x	
	Environmental flow release	x	x	x	x
	Reservoir flushing	x	x	x	
Period	Before the spawning period of target fish species				x
	Before the flood season	x	x	x	
Frequency	One/two years	x			x
	Based on constant assessment	x	x	x	x
Assessment Methods *3. Identify relevant assessment methods for defined objectives*					
	Biotic indicators	x	x	x	x
	Abiotic indicators	x	x	x	
	Topographic survey	x	x	x	
	Bedload tracing	x			

8.8 Long-term restoration strategies

This section aims to provide examples of long-term restoration strategies using SAMs.

A typical case of application is the diversification of incised channel sections. A sufficient bedload supply, which compensates for the existing deficit, should be ensured to diversify such homogeneous sections. This supply can be provided by the injection of artificial deposits, dynamic river widenings, or induced bank erosion. Low-magnitude bed-forming flows (~Q2) of extended duration ($> 24h$) can then restore a mobile, dynamic bed layer.

With sufficient repetition, aggradation, and the emergence of new CGUs, like alternating *bar*s, can occur. At this stage, flood events of medium magnitude (Q10), which can control active floodplain width and erosion of vegetated areas (Tonolla et al., 2021), can lead to the emergence of diverse CGUs.

Another case of application is the hydromorphological enhancement of channel sections of heterogeneous but static CGUs downstream of dams, such as at the Sarine River residual-flow reach. A complete restructuring requires, on the one hand, sufficient bedload supply that exceeds the corresponding transport capacity until the existing deficit has been compensated. On the other hand, it requires at least the flow of a medium flood event to alter physical channel characteristics and completely reorganise CGU arrangement. Suppose the complete restructuring of the reach morphology is either unfeasible or not proportionate. In that case, hydromorphological diversity can be kept at a high level and basic morphodynamical processes maintained if continuous migration of upstream bedload across the section is ensured. This process can be promoted by regular, at least low-magnitude bed-forming floods that mimic a more natural discharge distribution and sediment augmentation in the order of the corresponding transport capacity. Flood releases without any bedload supply can decrease hydromorphological diversity (Schroff et al., 2022).

For the direct restructuring of the riverbed through in-channel rehabilitation works, the pre-condition of physical channel characteristics and the interaction between individual CGU types and sub-reach morphological evolution in response to different sediment and discharge regime disturbances should be considered.

An objective-based concept at different restoration stages is shown in Figure 8.5.

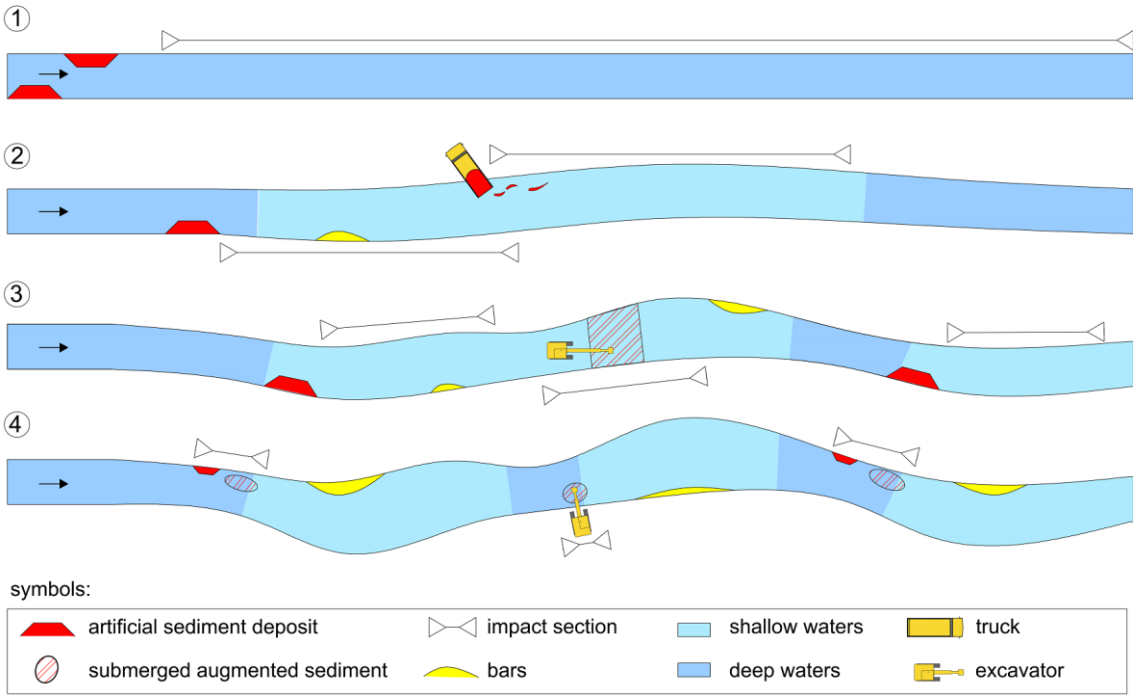

Figure 8.5 Schematic sketch of promoting the evolution of an impaired river reach towards a near-natural state by sediment augmentation measures (SAMs). 1: Balancing of the bedload budget. 2: Promotion of channel dynamics. 3: Diversification of riverbed structures. 4: Improvement of interstitial habitat

The above figure visualises the concept of decreasing temporal and spatial impact scale of SAMs with the eco-geomorphological state of a watercourse (Figure 2.3). With the removal of lateral channel restrictions, a near-natural flow and sediment regime will re-establish favourable ecological conditions over time. Intervening at different stages with well-adapted SAMs can accelerate this evolution or help to maintain essential ecological functions in impaired reaches.

This integral restoration approach can be applied for the eco-geomorphological enhancement of the Sarine River residual-flow reach by means of sediment augmentation. In the first phase of a few years, bedload should be added in multiple injection points along the reach and mobilised by low-magnitude morphological floods with a minimum frequency, corresponding to their return period, to restore a reach-wide mobile bed layer. At the same time, spawning gravel should seasonally be added or declogged by the mechanical loosening in locations of potential spawning grounds. In the second phase, sediment augmentations should focus on stretches with static geomorphic units and areas for potential channel widenings. In these areas, channel dynamics should be promoted by removing vegetation along the banks, dredging side arms, or creating artificial islands for induced bank erosion. The low-magnitude floods should be altered with channel-forming flood events to trigger processes of natural channel dynamics. Through periodic eco-geomorphological assessment, sediment augmentation and artificial floods should be adapted to the response of the reach and ecology.

Chapter 9
Conclusion and Outlook

This chapter summarises the findings of the four research topics and describes the benefits for practitioners. In an outlook, it is suggested to dedicate future research efforts about sediment augmentation measures towards more advanced restoration- and management stages, considering lateral channel migration and the interaction with a mobile bed layer.

9.1 Overview

This thesis investigates the hydromorphological impact of sediment augmentation in gravel-bed rivers. The research focuses on sediment augmentation in the form of alternating, in-channel deposits in low-gradient ($< 1\%$), sediment-starved reaches. Data analysis and testing are based on field observations and physical- and numerical modelling.

A field experiment was performed at the Sarine River residual-flow reach downstream of the Rossens Dam in Switzerland. The study site served as a reference field site for the design of a flume experience. The flume was constructed at the Platform of Hydraulic Constructions of the Ecole Polytechnique Fédérale de Lausanne. Hydrodynamic simulations of the flume experiment were performed with the software BASEMENT from the Laboratory of Hydraulics, Hydrology and Glaciology (VAW) of ETH Zürich. Four research questions were formulated and treated in a separate chapter. For each question, an initial hypothesis was formulated.

9.2 Influence of hydrograph shape on sediment transport dynamics of alternating in channel sediment deposits

A flume experiment was designed in a straight, wooden channel with a trapezoidal cross-section and varying slopes and channel widths. Each channel section represents a channel geomorphic unit identified at the reference field site. The bed level is fixed in most parts, and mobile sediment is placed in four, alternating deposits in the upstream part of the channel bed. Floods with different hydrograph skewness (symmetrical, left-skewed, right-skewed) are released to mobilise the mobile deposits. The initial hypothesis was that the mobilising flood's hydrograph skewness influences sediment transport dynamics from in-channel sediment deposits.

The results confirm the initial hypothesis. Symmetrical hydrographs led to increased overall bedload mobilisation, and transport rates and skewness influenced the impact length. Left-skewed hydrographs increased the mean transport distance. The influence of hydrograph shape was attributed to the time-dependent process of deposit erosion and bedload transport. At the beginning of the erosion process, a low discharge is

sufficient to erode the artificial deposits, while the erosion efficiency of the flow discharge decreases over time. With the artificial deposits already partially eroded at the time of high flow in tests with left-skewed hydrographs, bedload was transported further than during tests with right-skewed hydrographs. This result allows practitioners to consider the adaptation of the mobilising hydrograph with the options of focusing either on replenishing substrate in a limited downstream section or increasing the impact length of the restoration measure.

9.3 Influence of sediment augmentation repetition frequency on bed morphology evolution

In the same flume, symmetrical floods were repeated and coupled with consecutive sediment augmentation measures (SAMs). Different scenarios with varying sediment augmentation repetition frequencies (before every- or every second mobilising flood) coupled with floods with varying peak discharge (1.2- and 2.5 times the entrainment threshold) were tested. The initial hypothesis was that sediment augmentation before every-, instead of every second mobilising flood, is beneficial for creating morphological diversity.

The results confirm the initial hypothesis. Deposition and percentage of cover in the downstream section were higher in tests where sediment augmentation was performed with every- than if only with every second mobilising flood. With every consecutive sediment augmentation, the bedload transport condition in the downstream section changed further from a supply-limited sediment condition to a capacity-limited transport condition. The persistence of sediment patches decreased after floods without sediment augmentation. It increased after floods with lower peak discharge (1.2 times the entrainment threshold) coupled with sediment augmentation, progressively establishing an active layer of mobile sediment in the downstream vicinity of the artificial deposits. Numerical simulations of low-flow discharge for the resulting morphologies of the physical model showed that the index of hydromorphological diversity ($HMID$) increased after SAMs. Results showed that hydromorphological diversity did not benefit from altering the discharge regime with higher peak floods (2.5 times the entrainment threshold) at an early restoration stage. This information helps designing consecutive SAMs and artificial floods more effectively in highly sediment-starved reaches.

9.4 Influence of channel geomorphic units on river morphology evolution during artificial floods coupled with sediment augmentation

In a field experiment, bedload particles from a SAM were tracked with passive integrated transponder (PIT) tags (tracer) after the second major flood event following their installation. The positions of detected tracers were compared to their previous positions assessed in a reference study. In addition, channel geomorphic units (CGUs) were

mapped before and after the same flood. Data on tracer movement and the evolution of CGUs were combined and statistically analysed. The initial hypothesis H3 was that CGUs influence bedload transport from sediment augmentation during low-magnitude, bed-forming floods.

It could be rejected with high confidence ($p < 10^{-19}$) that the distribution of tracers is determined by the proximity to the artificial deposits alone. Instead, the alternative hypothesis $H_{A,1\text{-}2}$ was accepted that CGU types influence the spatial distribution of tracers in the downstream section of the artificial deposits. The persistence of tracers was higher in *shallows* and *riffles* than in *runs* and *glides*, where tracers were disproportionally prone to be relocated to another CGU type during a flood event. High tracer persistence in *riffles* (89%) was attributed to reduced shear stress due to low water depth during periods of low-flood discharge and tracers getting quickly overtopped by newly deposited sediment in aggradation zones. Low persistence in *runs* (47%) was attributed to a locally increased transport capacity on the characteristically steep slope. The investigated flood did not lead to a significant restructuring of CGU organisational patterns, suggesting that, for their restructuring, higher flow rates and sediment supply are required. The recommendations provided in this thesis outline how assessing existing CGUs at an early planning stage of a SAM can help practitioners optimising placement location and predicting deposition patterns.

9.5 Impact assessment of sediment augmentation measures on habitat diversity

A detailed assessment of habitat diversity was performed at the Sarine River study site. In addition to the study reach, an upstream control reach was assessed as a representative reference section. All indicators of *Indicator Set 1* of the Swiss *Guideline for Evaluating the Outcome of Restoration Projects* (EOR1) were mapped before and after the artificial flood. The initial hypothesis was that the EOR1 is valid for assessing the impact of sediment augmentation measures on habitat diversity.

The results can only partially confirm the initial hypothesis. The indicator *riverbed structure* (1.1) and *substrate mobilisability* (1.6A2) showed changes that could be attributed to the impact of the SAM. The score of the indicators *maximum water depth* (1.3) and *flow velocity* (1.4) represented well the observed hydromorphological changes at the measured cross-sections and results of the $HMID$. The indicators *riverbank structures* (1.2), *presence of cover* (1.5) and *substrate composition* (1.6A1) could not represent distinct changes caused by the SAM and are consequently not judged valid for the assessment of the impact of a SAM during low-magnitude, bed-forming floods. Based on these results and complementary literature research, a summary for objective-based indicator selection for the eco-geomorphological assessment of SAMs was developed for practitioners.

9.6 Future work

The research of this thesis has focused on the initial phase of restoration in sentiment-starved conditions with an armoured riverbed and stabilised channel forms, common in residual-flow reaches. In the next step, a later restoration phase with a re-established active layer should be investigated to see how CGUs can be restructured and their diversity established or maintained through effective sediment augmentation measures. Another step is to extend the research to less regulated reaches with erodible banks to investigate the promotion of channel dynamics by sediment augmentation measures.

A numerical model can be developed to estimate bedload distribution based on (i) main channel slope, (ii) CGU organisational pattern, (iii) active layer depth and in response to (i) sediment augmentation volume and (ii) placement, and (iii) flood hydrographs. Elaborating empirical resistance functions for different channel geomorphic unit types with and without an active layer would allow for a low-calculation-cost simulation for a rough estimation of the morphological impact of SAM in regulated reaches in response to low-magnitude artificial floods. The calibration can be performed with data from case studies using particle tracking. Combined with drone-based automated image detection of CGU types and a user-friendly GIS plugin, this tool could provide a quick and simple assessment and planning tool for practitioners.

The following research questions remain unanswered:

- Can sediment augmentation measures promote the mobilisation and the vertical exchange of an active layer?
- Can sediment augmentation measures promote channel dynamics in a sinusoidal channel with mobile banks?
- How do channel geomorphic units' organisational patterns evolve in response to bedload supply from sediment augmentation measures coupled with channel-forming flood events?

Future work on sediment augmentation measures should provide practitioners with objective-based and site-specific design recommendations to intervene effectively at different restoration and management stages.

Bibliography

Acreman, M. C., & Ferguson, A. J. D. (2010). Environmental flows and the European Water Framework Directive. *Freshwater Biology*, *55*(1), 32–48. https://doi.org/10.1111/j.1365-2427.2009.02181.x

Agouridis, C. (2014). Bankfull Frequency in Rivers. In S. Eslamian (Ed.), *Handbook of Engineering Hydrology - Modelling, Climate Change and Variability* (pp. 35–51). CRC Press. https://doi.org/10.1201/b16683-4

Ahmari, H., & Da Silva, A. M. F. (2011). Regions of bars, meandering and braiding in da Silva and Yalin's plan. *Journal of Hydraulic Research*, *49*(6), 718–727. https://doi.org/10.1080/00221686.2011.614518

Allan, D. J., & Castillo, M. M. (2007). *Stream Ecology - Structure and function of running waters* (Second). Springer International Publishing.

Arnaud, F., Piégay, H., Béal, D., Collery, P., Vaudor, L., & Rollet, A.-J. (2017). Monitoring gravel augmentation in a large regulated river and implications for process-based restoration. *Earth Surface Processes and Landforms*, *42*(13), 2147–2166. https://doi.org/10.1002/esp.4161

Arnaud, F., Piégay, H., Vaudor, L., Bultingaire, L., & Fantino, G. (2015). Technical specifications of low-frequency radio identification bedload tracking from field experiments: Differences in antennas, tags and operators. *Geomorphology*, *238*, 37–46. https://doi.org/10.1016/j.geomorph.2015.02.029

Badoux, A., & Rickenmann, D. (2008). Berechnungen zum geschiebtransport während der Hochwasser 1993 und 2000 im Wallis [Calculations of bedload transport during the floods of 1993 and 2000 in Valais]. *Wasser, Energie, Luft*, *100*(3), 217–226.

BAFU (Hrsg.). (2017). *Geschiebe- und Habitatsdynamik. Merkblatt-Sammlung Wasserbau und Ökologie [Bedload and habitat dynamics. Fact Sheet Collection Hydraulic Engineering and Ecology]*. https://www.rivermanagement.ch/en/products-publications/practice-tools/

Bakker, M., Gimbert, F., Geay, T., Misset, C., Zanker, S., & Recking, A. (2020). Field Application and Validation of a Seismic Bedload Transport Model. *Journal of Geophysical Research: Earth Surface*, *125*(5), 1–23. https://doi.org/10.1029/2019JF005416

Battisacco, E. (2016). *Replenishment of sediment downstream of dams: erosion and transport processes* (Vol. 7239) [Thesis, EPFL]. https://doi.org/10.5075/epfl-thesis-7239

Battisacco, E., Franca, M. J., & Schleiss, A. J. (2016). Sediment replenishment: Influence of the geometrical configuration on the morphological evolution of channel-bed. *Water Resources Research*, *52*(11), 8879–8894. https://doi.org/10.1002/2016WR019157

Belletti, B., Rinaldi, M., Bussettini, M., Comiti, F., Gurnell, A. M., Mao, L., Nardi, L., & Vezza, P. (2017). Characterising physical habitats and fluvial hydromorphology: A new system for the survey and classification of river geomorphic units. *Geomorphology*, *283*, 143–157. https://doi.org/10.1016/j.geomorph.2017.01.032

Benke, A. C. (2001). Importance of flood regime to invertebrate habitat in an unregulated river–floodplain ecosystem. *Journal of the North American Benthological Society*, *20*(2), 225–240. https://doi.org/10.2307/1468318

Bo, T., Fenoglio, S., Malacarne, G., Pessino, M., & Sgariboldi, F. (2007). Effects of clogging on stream macroinvertebrates: An experimental approach. *Limnologica*, *37*(2), 186–192. https://doi.org/10.1016/j.limno.2007.01.002

Bösch, L., Battisacco, E., Franca, M. J., & Schleiss, A. J. (2016). Influence of consecutive sediment replenishment on channel bed morphology. In G. Constantinescu, M. Garcia, & D. R. Hanes (Eds.), *River Flow - Proceedings of the International Conference on Fluvial Hydraulics, RIVER FLOW 2016* (pp. 1147–1155). CRC Press, Taylor & Francis Group.

Breitenstein, M., & Kirchhofer, A. (2010). Förderung der litho-rheophilen Fischarten der Schweiz [Promotion of litho-rheophilic fish species of Switzerland]. In *Factsheets zu Biologie und Förderungsmassnahmen*. Bundesamt für Umwelt BAFU. https://www.bafu.admin.ch/dam/bafu/de/dokumente/biodiversitaet/externe-studien-berichte/foerderung_der_litho-rheophilenfischartenderschweiz.pdf.download.pdf/foerderung_der_litho-rheophilenfischartenderschweiz.pdf

Brousse, G., Arnaud-Fassetta, G., Liébault, F., Bertrand, M., Melun, G., Loire, R., Malavoi, J., Fantino, G., & Borgniet, L. (2020). Channel response to sediment replenishment in a large gravel-bed river: The case of the Saint-Sauveur dam in the Buëch River (Southern Alps, France). *River Research and Applications*, *36*(6), 880–893. https://doi.org/10.1002/rra.3527

Buffington, J. M., & Montgomery, D. R. (2022). Geomorphic Classification of Rivers: An Updated Review. In J. Shroder (Ed.), *Treatise on Geomorphology* (2nd ed., pp. 1143–1190). Elsevier. https://doi.org/10.1016/B978-0-12-818234-5.00077-8

Bundi, U., Liechti, P., Ueli, S., von Blücher, U., Willi, H. P., Frutiger, A., Hütte, M., Peter, A., Göldi, C., Kupper, U., Meier, W., & Niederhauser, P. (1998). Methoden zur Untersuchung und Beurteilung der Fliessgewässer in der Schweiz: Modul-

Stufen-Konzept [Methods for the investigation and assessment of watercourses in Switzerland: Modular Stepwise Procedure]. In *Mitteilungen zum Gewässerschutz* (Issue 26). http://www.modul-stufen-konzept.ch/index_EN

Bunte, K. (2004). Gravel Mitigation and Augmentation Below Hydroelectric Dams : A Geomorphological Perspective. In *State of the Science Review Gravel* (Issue October). https://doi.org/10.13140/2.1.1094.3361

Buscombe, D. (2020). SediNet: a configurable deep learning model for mixed qualitative and quantitative optical granulometry. *Earth Surface Processes and Landforms*, *45*(3), 638–651. https://doi.org/10.1002/esp.4760

Camenen, B., & Melun, G. (2021). *Guide pour la mesure et la modélisation du transport solide [Guide for measuring and modeling solid transport]* (French national agency for biodiversity (OFB), Ed.). http://oai.afbiodiversite.fr/cindocoai/download/PUBLI/1298/1/33092_OFB_Guide transport solide_BD.pdf_23872Ko

Camporeale, C., Perucca, E., Ridolfi, L., & Gurnell, A. M. (2013). Modeling the interactions between river morphodynamics and riparian vegetation. *Reviews of Geophysics*, *51*(3), 379–414. https://doi.org/10.1002/rog.20014

Cao, Z., Pender, G., & Meng, J. (2006). Explicit Formulation of the Shields Diagram for Incipient Motion of Sediment. *Journal of Hydraulic Engineering*, *132*(10), 1097–1099. https://doi.org/10.1061/(ASCE)0733-9429(2006)132:10(1097)

Cassel, M., Dépret, T., & Piégay, H. (2017). Assessment of a new solution for tracking pebbles in rivers based on active RFID. *Earth Surface Processes and Landforms*, *42*(13), 1938–1951. https://doi.org/10.1002/esp.4152

Cepello, S., Kennedy, S., Manwaring, M., & Pasternack, G. B. (2009). Spawning riffle gravel supplementation for anadromous spring-run chinook salmon and steelhead. *Waterpower XVI*, *July 2009*, 1–18.

Chapman, D. W. (1988). Critical Review of Variables Used to Define Effects of Fines in Redds of Large Salmonids. *Transactions of the American Fisheries Society*, *117*(1), 1–21. https://doi.org/10.1577/1548-8659(1988)117<0001:CROVUT>2.3.CO;2

Chardon, V., Schmitt, L., Arnaud, F., Piégay, H., & Clutier, A. (2021). Efficiency and sustainability of gravel augmentation to restore large regulated rivers: Insights from three experiments on the Rhine River (France/Germany). *Geomorphology*, *380*, 107639. https://doi.org/10.1016/j.geomorph.2021.107639

Church, M., & Haschenburger, J. K. (2017). What is the "active layer"? *Water Resources Research*, *53*(1), 5–10. https://doi.org/10.1002/2016WR019675

Coelho, C., Ferreira, M., & Marinho, B. (2020). Numerical Modelling of Artificial Sediment Nourishment Impacts. *Journal of Coastal Research*, *95*(sp1), 209–213. https://doi.org/10.2112/SI95-041.1

Crisp, D. T., & Carling, P. A. (1989). Observations on siting, dimensions and structure of salmonid redds. *Journal of Fish Biology*, *34*(1), 119–134. https://doi.org/10.1111/j.1095-8649.1989.tb02962.x

Czapiga, M. J., Blom, A., & Viparelli, E. (2022). Sediment Nourishments to Mitigate Channel Bed Incision in Engineered Rivers. *Journal of Hydraulic Engineering*, *148*(6), 1–10. https://doi.org/10.1061/(asce)hy.1943-7900.0001977

Darby, S. E., Rinaldi, M., & Dapporto, S. (2007). Coupled simulations of fluvial erosion and mass wasting for cohesive river banks. *Journal of Geophysical Research*, *112*(F3), F03022. https://doi.org/10.1029/2006JF000722

Detert, M., & Weitbrecht, V. (2012). Automatic object detection to analyze the geometry of gravel grains – a free stand-alone tool. In R. Murillo Munoz (Ed.), *River Flow 2012* (1st Editio, Vol. 1, pp. 595–600). CRC Press. https://doi.org/10.1201/b13250

Detert, M., & Weitbrecht, V. (2013). User guide to gravelometric image analysis by BASEGRAIN. In S. Fukuoka, H. Nakagawa, T. Sumi, & H. Zhang (Eds.), *Advances in River Sediment Research* (1st Editio, Issue January, pp. 1789–1796). CRC Press. https://doi.org/10.1201/b15374

Dhont, B., & Ancey, C. (2018). Are bedload transport pulses in gravel bed rivers created by bar migration or sediment waves? *Geophysical Research Letters*, *45*(11), 5501–5508. https://doi.org/10.1029/2018GL077792

Döring, M., Tonolla, D., Robinson, C. T., Schleiss, A. J., Stähly, S., Gufler, C., Geilhausen, M., & Di Cugno, N. (2018). Künstliches Hochwasser an der Saane – Eine Massnahme zum nachhaltigen Auenmanagement [Artificial flood at the Sarine - A measure for sustainable floodplain management]. *Wasser Energie Luft*, *2*, 119–127.

du Boys, M. P. (1879). Études du régime du Rhone et l'action exercée par les eaux sur un lit a fond de graviers indéfiniment affouiable. *Annales Des Ponts et Chaussees*, *5*(18), 141–195.

Dubuis, R., & De Cesare, G. (2023). The clogging of riverbeds: A review of the physical processes. *Earth-Science Reviews*, *239*(October 2022), 104374. https://doi.org/10.1016/j.earscirev.2023.104374

Eaton, B. C., & Church, M. (2004). A graded stream response relation for bed load–dominated streams. *Journal of Geophysical Research*, *109*(F3), F03011. https://doi.org/10.1029/2003JF000062

Eaton, B. C., & Church, M. (2009). Channel stability in bed load–dominated streams with nonerodible banks: Inferences from experiments in a sinuous flume. *Journal of Geophysical Research*, *114*(F01024), 1–17. https://doi.org/10.1029/2007JF000902

Ehrbar, D., Schmocker, L., Doering, M., Cortesi, M., Bourban, G., Boes, R. M., & Vetsch, D. F. (2018). Continuous seasonal and large-scale periglacial reservoir sedimentation. *Sustainability (Switzerland)*, *10*(9), 1–16. https://doi.org/10.3390/su10093265

Eizel-Din, M., Bui, M. D., El Tahawy, T., & Rutschmann, P. (2010). Numerical Investigation of Grain Size Effect on Bed Deformation in Meandering Channel. *Proceedings of the First European IAHR*, *1*.

Elgueta-Astaburuaga, M. A., & Hassan, M. A. (2017). Experiment on temporal variation of bed load transport in response to changes in sediment supply in streams. *Water Resources Research*, *53*(1), 763–778. https://doi.org/10.1002/2016WR019460

Espa, P., Brignoli, M. L., Crosa, G., Gentili, G., & Quadroni, S. (2016). Controlled sediment flushing at the Cancano Reservoir (Italian Alps): Management of the operation and downstream environmental impact. *Journal of Environmental Management*, *182*, 1–12. https://doi.org/10.1016/j.jenvman.2016.07.021

Fehr, R. (1987). Einfache Bestimmung der Korngrössenverteilung von Geschiebematerial mit Hilfe der Linienzahlanalyse [Simple determination of the grain size distribution of bedload material using line count analysis]. *Schweizer Ingenieur Und Architekt*, *105*(38), 1104–1109.

Feld, C. K., Sousa, J. P., da Silva, P. M., & Dawson, T. P. (2010). Indicators for biodiversity and ecosystem services: towards an improved framework for ecosystems assessment. *Biodiversity and Conservation*, *19*(10), 2895–2919. https://doi.org/10.1007/s10531-010-9875-0

Friedl, F. (2017). *Laboratory Experiments on Sediment Replenishment in Gravel-bed Rivers* (Issue 24826) [Thesis, ETH Zurich]. https://doi.org/doi.org/10.3929/ethz-b-000161430

Friedl, F. (2018). Laboratory Experiments on Sediment Replenishment in Gravel-Bed Rivers. In R. M. Boes (Ed.), *VAW Mitteilung 245*. Laboratory of Hydraulics, Hydrology and Glaciology (VAW). https://www.ethz.ch/content/dam/ethz/special-interest/baug/vaw/vaw-dam/documents/das-institut/mitteilungen/2010-2019/245.pdf

Friedl, F., Weitbrecht, V., & Boes, R. M. (2017). Laboratory experiments on gravel deposit erosion. In S. Wieprecht, S. Haun, K. Weber, M. Noack, & K. Terheiden (Eds.), *River Sedimentation - Proceedings of the 13th International Symposium*

on River Sedimentation, ISRS 2016 (pp. 603–610). Taylor & Francis. https://doi.org/10.1201/9781315623207-109

Friedl, F., Weitbrecht, V., & Boes, R. M. (2018). Erosion pattern of artificial gravel deposits. *International Journal of Sediment Research*, *33*(1), 57–67. https://doi.org/10.1016/j.ijsrc.2017.08.003

Frings, R. M., Döring, R., Beckhausen, C., Schüttrumpf, H., & Vollmer, S. (2014). Fluvial sediment budget of a modern, restrained river: The lower reach of the Rhine in Germany. *CATENA*, *122*, 91–102. https://doi.org/10.1016/j.catena.2014.06.007

Frings, R. M., Gehres, N., Promny, M., Middelkoop, H., Schüttrumpf, H., & Vollmer, S. (2014). Today's sediment budget of the Rhine River channel, focusing on the Upper Rhine Graben and Rhenish Massif. *Geomorphology*, *204*, 573–587. https://doi.org/10.1016/j.geomorph.2013.08.035

Frings, R. M., Hillebrand, G., Gehres, N., Banhold, K., Schriever, S., & Hoffmann, T. (2019). From source to mouth: Basin-scale morphodynamics of the Rhine River. *Earth-Science Reviews*, *196*(January), 102830. https://doi.org/10.1016/j.earscirev.2019.04.002

Frissell, C. A., Liss, W. J., Warren, C. E., & Hurley, M. D. (1986). A hierarchical framework for stream habitat classification: Viewing streams in a watershed context. *Environmental Management*, *10*(2), 199–214. https://doi.org/10.1007/BF01867358

Fuller, R. L., Dennison, J., Doyle, S., Levy, L., Owen, J., Shope, E., Swarr, G., Vo, L., Weichert, K., DiCesare, E., & Doyle, M. W. (2014). Influence of flood history and hydrology on transport of organic matter in a frequently flooded river. *Journal of Freshwater Ecology*, *29*(1), 37–51. https://doi.org/10.1080/02705060.2013.812045

Gaeuman, D. (2014). High-flow gravel injection for constructing designed in-channel features. *River Research and Applications*, *30*(6), 685–706. https://doi.org/10.1002/rra.2662

Gaeuman, D., Stewart, R., Schmandt, B., & Pryor, C. (2017). Geomorphic response to gravel augmentation and high-flow dam release in the Trinity River, California. *Earth Surface Processes and Landforms*, *42*(15), 2523–2540. https://doi.org/10.1002/esp.4191

Gazi, A. H., Afzal, M. S., & Dey, S. (2019). Scour around piers under waves: Current status of research and its future prospect. *Water*, *11*(11), 2212. https://doi.org/10.3390/w11112212

Gintz, D., Hassan, M. A., & Schmidt, K.-H. (1996). Frequency and magnitude of bedload transport in a mountain river. *Earth Surface Processes and Landforms*,

21(5), 433–445. https://doi.org/10.1002/(SICI)1096-9837(199605)21:5<433::AID-ESP580>3.0.CO;2-P

Gostner, W., Alp, M., Schleiss, A. J., & Robinson, C. T. (2013). The hydro-morphological index of diversity: a tool for describing habitat heterogeneity in river engineering projects. *Hydrobiologia*, *712*(1), 43–60. https://doi.org/10.1007/s10750-012-1288-5

Greimel, F., Schülting, L., Graf, W., Bondar-Kunze, E., Auer, S., Zeiringer, B., & Hauer, C. (2018). Hydropeaking Impacts and Mitigation. In S. Schmutz & J. Sendzimir (Eds.), *Riverine Ecosystem Management* (pp. 91–110). Springer. https://doi.org/10.1007/978-3-319-73250-3_5

Grimardias, D., Guillard, J., & Cattanéo, F. (2017). Drawdown flushing of a hydroelectric reservoir on the Rhône River: Impacts on the fish community and implications for the sediment management. *Journal of Environmental Management*, *197*, 239–249. https://doi.org/10.1016/j.jenvman.2017.03.096

Günter, A. (1971). Die kritische mittlere Sohlenschubspannung bei Geschiebemischungen unter Berücksichtigung der Deckschichtbildung und der turbulenzbedingten Sohlenschubspannungsschwankungen. In *Nr. 3 Mitteilungen der Versuchsanstalt für Wasserbau, Hydrologie und Glaziologie*.

Halwas, K. L., Church, M., & Richardson, J. S. (2005). Benthic assemblage variation among channel units in high-gradient streams on Vancouver Island, British Columbia. *Journal of the North American Benthological Society*, *24*(3), 478–494. https://doi.org/10.1899/02-075.1

Harrison, L. R., Legleiter, C. J., Wydzga, M. A., & Dunne, T. (2011). Channel dynamics and habitat development in a meandering, gravel bed river. *Water Resources Research*, *47*(4), 1–21. https://doi.org/10.1029/2009WR008926

Hartmann, S. (2009). Sustainable sediment management of Alpine reservoirs considering ecological and economical aspects. In S. Hartmann, H. Knoblauch, G. De Cesare, & C. Steinich (Eds.), *ALPRESERV* (Vol. 7). Institut für Wasserwesen Universität der Bundeswehr München. https://www.alpine-space.org/2000-2006/uploads/media/ALPRESERV_Recommendation_and_best_practice_EN.pdf

Hauer, C., Leitner, P., Unfer, G., Pulg, U., Habersack, H., & Graf, W. (2018). The Role of Sediment and Sediment Dynamics in the Aquatic Environment. In *Riverine Ecosystem Management* (pp. 151–169). Springer International Publishing. https://doi.org/10.1007/978-3-319-73250-3_8

Hauer, C., Wagner, B., Aigner, J., Holzapfel, P., Flödl, P., Liedermann, M., Tritthart, M., Sindelar, C., Pulg, U., Klösch, M., Haimann, M., Donnum, B. O., Stickler, M., & Habersack, H. (2018). State of the art, shortcomings and future challenges for a

sustainable sediment management in hydropower: A review. *Renewable and Sustainable Energy Reviews*, *98*(January), 40–55. https://doi.org/10.1016/j.rser.2018.08.031

Heckmann, T., Haas, F., Abel, J., Rimböck, A., & Becht, M. (2017). Feeding the hungry river: Fluvial morphodynamics and the entrainment of artificially inserted sediment at the dammed river Isar, Eastern Alps, Germany. *Geomorphology*, *291*, 128–142. https://doi.org/10.1016/j.geomorph.2017.01.025

Hemond, H. F., & Fechner, E. J. (2015). Chapter 2 - Surface Waters. In H. F. Hemond & E. J. Fechner (Eds.), *Chemical Fate and Transport in the Environment* (Third Edit, pp. 75–218). Academic Press. https://doi.org/10.1016/B978-0-12-398256-8.00002-5

Hillman, M., & Brierley, G. (2005). A critical review of catchment-scale stream rehabilitation programmes. *Progress in Physical Geography: Earth and Environment*, *29*(1), 50–76. https://doi.org/10.1191/0309133305pp434ra

Hilton, J., O'Hare, M., Bowes, M. J., & Jones, J. I. (2006). How green is my river? A new paradigm of eutrophication in rivers. *Science of The Total Environment*, *365*(1–3), 66–83. https://doi.org/10.1016/j.scitotenv.2006.02.055

Huet, M. (1949). Aperçu des relations entre la pente et les populations piscicoles des eaux courantes. *Schweizerische Zeitschrift Für Hydrologie*, *11*(3–4), 332–351. https://doi.org/10.1007/BF02503356

Humphries, R., Venditti, J. G., Sklar, L. S., & Wooster, J. K. (2012). Experimental evidence for the effect of hydrographs on sediment pulse dynamics in gravel-bedded rivers. *Water Resources Research*, *48*(1), 1–15. https://doi.org/10.1029/2011WR010419

Hunzinger, L., Peter, A., & Schweizer, S. (2019). Indicator-Set 1 – Habitat diversity. In Federal Office for the Environment (Ed.), *Evaluating the outcome of restoration projects – collaborative learning for the future* (V1.04). Suisse Federal Office of the Environment.

Hütte, M., & Niederhauser, P. (1998). Methoden zur Untersuchung und Beurteilung der Fliessgewässer in der Schweiz - Ökomorphologie Stufe F [Methods for the investigation and assessment of watercourses in Switzerland: Ecomorphology Level F]. In *Mitteilungen zum Gewässerschutz* (Vol. *27*). http://www.modul-stufen-konzept.ch/download/oekomorphologie-f.pdf

Juez, C., Battisacco, E., Schleiss, A. J., & Franca, M. J. (2016). Assessment of the performance of numerical modeling in reproducing a replenishment of sediments in a water-worked channel. *Advances in Water Resources*, *92*, 10–22. https://doi.org/10.1016/j.advwatres.2016.03.010

Kantoush, S. A., & Sumi, T. (2010). River morphology and sediment management strategies for sustainable reservoir in Japan and European Alps. *Ann Disas Prev Res Inst Kyoto Univ*, *53*(B), 821–839.

Kantoush, S. A., & Sumi, T. (2011). Sediment replenishing measures for revitalization of Japanese rivers below dams. In E. M. Valentine, C. J. Apelt, J. Ball, H. Chanson, R. Cox, R. Ettema, G. Kuczera, M. Lambert, B. W. Melville, & J. E. Sargison (Eds.), *Proceedings of the 34th World Congress of the International Association for Hydro- Environment Research and Engineering: 33rd Hydrology and Water Resources Symposium and 10th Conference on Hydraulics in Water Engineering* (Issue July, pp. 2838–2846). Engineers Australia.

Kantoush, S. A., Sumi, T., & Kubota, A. (2010). Geomorphic response of rivers below dams by sediment replenishment technique. In A. Dittrich, K. Koll, J. Aberle, & P. Geisenhainer (Eds.), *Proceedings of the River Flow 2010 Conference* (pp. 1155–1163).

Kantoush, S. A., Sumi, T., Kubota, A., & Suzuki, T. (2010). Impacts of Sediment Replenishment Below Dams on Flow and Bed Morphology of River. *First International Conference on Coastal Zone Management of River Deltas and Low Land Coastlines*, *285*(March), 285–303.

Kantoush, S., Suzuki, T., Takemon, Y., El Kadi Abderrezzak, K., Ata, R., Sumi, T., & Saber, M. (2018). Numerical study on reservoir sediment management through adding excavated sediment downstream of dams in Japan. *E3S Web of Conferences*, *40*, 1–8. https://doi.org/10.1051/e3sconf/20184003033

King, J., Brown, C., & Sabet, H. (2003). A scenario-based holistic approach to environmental flow assessments for rivers. *River Research and Applications*, *19*(5–6), 619–639. https://doi.org/10.1002/rra.709

Klösch, M., Hornich, R., Baumann, N., Puchner, G., & Habersack, H. (2011). Stream Restoration in Dynamic Fluvial Systems: Scientific Approaches, Analyses, and Tools. In A. Simon, S. J. Bennett, & J. M. Castro (Eds.), *Geophysical Monograph Series* (Fist Editi, Vol. 194). American Geophysical Union. https://doi.org/10.1029/GM194

Kondolf, G. M. (1997). Hungry water: Effects of dams and gravel mining on river channels. *Environmental Management*, *21*(4), 533–551. https://doi.org/10.1007/s002679900048

Kondolf, G. M., Gao, Y., Annandale, G. W., Morris, G. L., Jiang, E., Zhang, J., Cao, Y., Carling, P., Fu, K., Guo, Q., Hotchkiss, R., Peteuil, C., Sumi, T., Wang, H.-W., Wang, Z., Wei, Z., Wu, B., Wu, C., & Yang, C. T. (2014). Sustainable sediment management in reservoirs and regulated rivers: Experiences from five

continents. *Earth's Future*, *2*(5), 256–280. https://doi.org/10.1002/2013EF000184

Kondolf, G. M., & Wilcock, P. R. (1996). The flushing flow problem: Defining and evaluating objectives. *Water Resources Research*, *32*(8), 2589–2599. https://doi.org/10.1029/96WR00898

Kondolf, G. M., & Wolman, M. G. (1993). The sizes of salmonid spawning gravels. *Water Resources Research*, *29*(7), 2275–2285. https://doi.org/10.1029/93WR00402

Korpak, J., Łapuszek, M., Lenar-Matyas, A., & Mączałowski, A. (2019). Effect of Riffle Sequences on Discharge and Sediment Transport in a Mountain Stream. *Journal of Ecological Engineering*, *20*(3), 157–166. https://doi.org/10.12911/22998993/99747

Lamouroux, N., Olivier, J.-M., Persat, H., PouilLy, MarC., Souchon, Y., & Statzner, B. (1999). Predicting community characteristics from habitat conditions: fluvial fish and hydraulics. *Freshwater Biology*, *42*(2), 275–299. https://doi.org/10.1046/j.1365-2427.1999.444498.x

Lang, N., Irniger, A., Rozniak, A., Hunziker, R., Wegner, J. D., & Schindler, K. (2021). GRAINet: mapping grain size distributions in river beds from UAV images with convolutional neural networks. *Hydrology and Earth System Sciences*, *25*(5), 2567–2597. https://doi.org/10.5194/hess-25-2567-2021

Leite Ribeiro, M., Wampfler, S., & Schleiss, A. J. (2014). Morphodynamic changes in a natural river confluence due to a hydropower modified flow regime. In A. J. Schleiss, G. De Cesare, M. J. Franca, & M. Pfister (Eds.), *River Flow 2014* (1st ed., pp. 191–199). CRC Press. https://doi.org/10.1201/b17133

Leopold, L. B., & Wolman, M. G. (1957). River Channel Patterns - Braided, Meandering and Straight. *The Professional Geographer*, *9*, 39–85.

Leopold, L. B., Wolman, M. G., & Miller, J. P. (1965). Fluvial Processes in Geomorphology. In *Geographical Review* (Dover edit, Vol. 55, Issue 3). Dover Publications, INC. https://doi.org/10.2307/213147

Liro, M., Ruiz-Villanueva, V., Mikuś, P., Wyżga, B., & Bladé Castellet, E. (2020). Changes in the hydrodynamics of a mountain river induced by dam reservoir backwater. *Science of the Total Environment*, *744*. https://doi.org/10.1016/j.scitotenv.2020.140555

Loire, R., Piégay, H., Malavoi, J.-R., Kondolf, G. M., & Bêche, L. A. (2021). From flushing flows to (eco)morphogenic releases: evolving terminology, practice, and integration into river management. *Earth-Science Reviews*, *213*(December 2020), 103475. https://doi.org/10.1016/j.earscirev.2020.103475

Louhi, P., Mäki-Petäys, A., & Erkinaro, J. (2008). Spawning habitat of Atlantic salmon and brown trout: general criteria and intragravel factors. *River Research and Applications*, *24*(3), 330–339. https://doi.org/10.1002/rra.1072

Madej, M. A., Sutherland, D. G., Lisle, T. E., & Pryor, B. (2009). Channel responses to varying sediment input: A flume experiment modeled after Redwood Creek, California. *Geomorphology*, *103*(4), 507–519. https://doi.org/10.1016/j.geomorph.2008.07.017

Manso, P. A., Vorlet, S. L., & De Cesare, G. (2018). Evolution of reservoir flushing and emptying practices in a cascade of large reservoirs across several decades. *HYDRO 2018*.

Marteau, B., Gibbins, C., Vericat, D., & Batalla, R. J. (2020a). Geomorphological response to system-scale river rehabilitation II: Main-stem channel adjustments following reconnection of an ephemeral tributary. *River Research and Applications*, *36*(8), 1472–1487. https://doi.org/10.1002/rra.3682

Marteau, B., Gibbins, C., Vericat, D., & Batalla, R. J. (2020b). Geomorphological response to system-scale river rehabilitation I: Sediment supply from a reconnected tributary. *River Research and Applications*, *36*(8), 1488–1503. https://doi.org/10.1002/rra.3683

Mathers, K. L., Hill, M. J., Wood, C. D., & Wood, P. J. (2019). The role of fine sediment characteristics and body size on the vertical movement of a freshwater amphipod. *Freshwater Biology*, *64*(1), 152–163. https://doi.org/10.1111/fwb.13202

Merz, J. E., & Ochikubo Chan, L. K. (2005). Effects of gravel augmentation on macroinvertebrate assemblages in a regulated California River. *River Research and Applications*, *21*(1), 61–74. https://doi.org/10.1002/rra.819

Mesick, C. (2001). Studies of spawning habitat for fall-run Chinook salmon in the Stanislaus River between Goodwin Dam and Riverbank from 1994 to 1997. In R. L. Brown (Ed.), *Fish Bulletin 179* (Vol. 2, Issue July, pp. 217–252). Department of Fish and Game. http://www.sjbfish.com/srfg/docs/Spawning_Surveys_1994-1997_Fish_Bulletin.pdf%0Apapers3://publication/uuid/0200911E-91D5-4AEC-961D-2A0C8C35DF0F

Meyer-Peter, E., & Müller, R. (1948). Formulas for bed-load transport. *2nd Meeting of the International Association of Hydraulic Structures Research*, 39– 64. https://doi.org/1948-06-07

Miwa, H., & Parker, G. (2012). Numerical simulation of low-flow channel evolution due to sediment augmentation. *International Journal of Sediment Research*, *27*(3), 351–361. https://doi.org/10.1016/S1001-6279(12)60040-7

Miwa, H., & Parker, G. (2017). Effects of sand content on initial gravel motion in gravel-bed rivers. *Earth Surface Processes and Landforms*, *42*(9), 1355–1364. https://doi.org/10.1002/esp.4119

Mizuyama, T., Laronne, J., Nonaka, M., Sawada, T., Satofuka, Y., Matsuoka, M., Yamashita, S., Sako, Y., Tamaki, S., Watari, M., Yamaguchi, S., & Tsuruta, K. (2010). Calibration of a passive acoustic bedload monitoring system in Japanese mountain rivers. *Bedload-Surrogate Monitoring Technologies*, 296–318.

Moir, H. J., & Pasternack, G. B. (2008). Relationships between mesoscale morphological units, stream hydraulics and Chinook salmon (Oncorhynchus tshawytscha) spawning habitat on the Lower Yuba River, California. *Geomorphology*, *100*(3–4), 527–548. https://doi.org/10.1016/j.geomorph.2008.02.001

Montgomery, D. R., & Buffington, J. M. (1997). Channel-reach morphology in mountain drainage basins. *Geological Society of America Bulletin*, *109*(5), 596–611. https://doi.org/10.1130/0016-7606(1997)109<0596:CRMIMD>2.3.CO;2

Montgomery, D. R., & Buffington, J. M. (1998). Channel Processes, Classification, and Response. In R. J. Naiman & R. E. Bilby (Eds.), *River Ecology and Management* (pp. 13–42). Springer New York. https://doi.org/10.1007/978-1-4612-1652-0_2

Mörtl, C., Baratier, A., Berhet, J., Duvillard, P.-A., & De Cesare, G. (2022). GALET: A deep learning image segmentation model for drone-based grain size analysis of gravel bars. In M. Ortega-Sánchez (Ed.), *Proceedings of the 39th IAHR World Congress—From Snow To Sea* (pp. 5326–5335). IAHR. https://doi.org/10.3850/IAHR-39WC2521716X2022procd

Mörtl, C., & De Cesare, G. (n.d.). Continuous monitoring of morphological changes from sediment augmentation by field measurements and flume experiments (accepted on 23.09.2022). *Riverflow 2022*.

Mörtl, C., & De Cesare, G. (2021). Sediment Augmentation for River Rehabilitation and Management—A Review. *Land*, *10*(12), 1309. https://doi.org/10.3390/land10121309

Mörtl, C., & De Cesare, G. (2022a). Sedimentzugaben in Fliessgewässern. Überblick über Methoden und Fallbeispiele [Sediment augmentation in running waters. Overview of methods and case studies]. *Ingenieurbiologie*, *22*(4), 21–26.

Mörtl, C., & De Cesare, G. (2022b). *Dataset for a flume experiment on sediment augmentation [Data set]*. https://doi.org/10.5281/ZENODO.7299705

Mörtl, C., Vorlet, S. L., Manso, P. A., & De Cesare, G. (2020). The sediment challenge of Swiss river corridors interrupted by man-made reservoirs. In W. Uijttewaal, M.

J. Franca, D. Valero, V. Chavarrias, C. Y. Arbós, R. Schielen, & A. Crosato (Eds.), *Riverflow 2020* (1st Editio, pp. 1764–1773). Taylor & Francis Group. https://doi.org/10.1201/b22619

Nelson, P. A., Brew, A. K., & Morgan, J. A. (2015). Morphodynamic response of a variable-width channel to changes in sediment supply. *Water Resources Research*, *51*(7), 5717–5734. https://doi.org/10.1002/2014WR016806

Nelson, P. A., Venditti, J. G., Dietrich, W. E., Kirchner, J. W., Ikeda, H., Iseya, F., & Sklar, L. S. (2009). Response of bed surface patchiness to reductions in sediment supply. *Journal of Geophysical Research*, *114*(F2), F02005. https://doi.org/10.1029/2008JF001144

Newcomer, M. E., Hubbard, S. S., Fleckenstein, J. H., Maier, U., Schmidt, C., Thullner, M., Ulrich, C., Flipo, N., & Rubin, Y. (2016). Simulating bioclogging effects on dynamic riverbed permeability and infiltration. *Water Resources Research*, *52*(4), 2883–2900. https://doi.org/10.1002/2015WR018351

Ock, G., Gaeuman, D., McSloy, J., & Kondolf, G. M. (2015). Ecological functions of restored gravel bars, the Trinity River, California. *Ecological Engineering*, *83*, 49–60. https://doi.org/10.1016/j.ecoleng.2015.06.005

Ock, G., Kondolf, G. M., Takemon, Y., & Sumi, T. (2013). Missing link of coarse sediment augmentation to ecological functions in regulated rivers below dams: Comparative approach in Nunome River, Japan and Trinity River, California, US. In S. Fukuoka, H. Nakagawa, T. Sumi, & H. Zhang (Eds.), *Advances in River Sediment Research* (pp. 1531–1538). CRC Press. https://doi.org/10.1201/b15374

Ock, G., Sumi, T., & Takemon, Y. (2013). Sediment replenishment to downstream reaches below dams: implementation perspectives. *Hydrological Research Letters*, *7*(3), 54–59. https://doi.org/10.3178/hrl.7.54

Pander, J., & Geist, J. (2013). Ecological indicators for stream restoration success. *Ecological Indicators*, *30*, 106–118. https://doi.org/10.1016/j.ecolind.2013.01.039

Pascal, I., Ancey, C., & Bohorquez, P. (2021). The variability of antidune morphodynamics on steep slopes. *Earth Surface Processes and Landforms*, *46*(9), 1750–1765. https://doi.org/10.1002/esp.5110

Pasquale, N., Perona, P., Schneider, P., Shrestha, J., Wombacher, A., & Burlando, P. (2011). Modern comprehensive approach to monitor the morphodynamic evolution of a restored river corridor. *Hydrology and Earth System Sciences*, *15*(4), 1197–1212. https://doi.org/10.5194/hess-15-1197-2011

Pasternack, G. B., Baig, D., Weber, M. D., & Brown, R. A. (2018). Hierarchically nested river landform sequences. Part 2: Bankfull channel morphodynamics governed

by valley nesting structure. *Earth Surface Processes and Landforms*, *43*(12), 2519–2532. https://doi.org/10.1002/esp.4410

Petts, G. E., & Gurnell, A. M. (2005). Dams and geomorphology: Research progress and future directions. *Geomorphology*, *71*(1–2), 27–47. https://doi.org/10.1016/j.geomorph.2004.02.015

Pfeiffer, A. M., Finnegan, N. J., & Willenbring, J. K. (2017). Sediment supply controls equilibrium channel geometry in gravel rivers. *Proceedings of the National Academy of Sciences*, *114*(13), 3346–3351. https://doi.org/10.1073/pnas.1612907114

Pizzuto, J. E. (1990). Numerical simulation of gravel river widening. *Water Resources Research*, *26*(9), 1971–1980. https://doi.org/10.1029/WR026i009p01971

Plate, E. J. (1994). The need to consider non-stationary sediment transport. *International Journal of Sediment Research*, *9*, 117–123.

Plumb, B. D., Juez, C., Annable, W. K., McKie, C. W., & Franca, M. J. (2020). The impact of hydrograph variability and frequency on sediment transport dynamics in a gravel-bed flume. *Earth Surface Processes and Landforms*, *45*(4), 816–830. https://doi.org/10.1002/esp.4770

Podschun, S. A., Albert, C., Costea, G., Damm, C., Dehnhardt, A., Fischer, C., Fischer, H., Foeckler, F., Gelhaus, M., Gerstner, L., Hartje, V., Hoffmann, T. G., Hornung, L., Iwanowski, J., Kasperidus, H., Linnemann, K., Mehl, D., Rayanov, M., Ritz, S., … Pusch, M. (2018). RESI - Anwendungshandbuch. *Berichte Des IGB*, *2018*(31). https://doi.org/10.4126/FRL01-006410777

Poff, N. L., Allan, J. D., Bain, M. B., Karr, J. R., Prestegaard, K. L., Richter, B. D., Sparks, R. E., & Stromberg, J. C. (1997). The Natural Flow Regime. *BioScience*, *47*(11), 769–784. https://doi.org/10.2307/1313099

Pulg, U., Barlaup, B. T., Sternecker, K., Trepl, L., & Unfer, G. (2013). Restoration of spawning habitats of brown trout (salmo trutta) in a regulated chalk stream. *River Research and Applications*, *29*(2), 172–182. https://doi.org/10.1002/rra.1594

Rachelly, C., Friedl, F., Boes, R. M., & Weitbrecht, V. (2021). Morphological Response of Channelized, Sinuous Gravel-Bed Rivers to Sediment Replenishment. *Water Resources Research*, *57*(6). https://doi.org/10.1029/2020WR029178

Rachelly, C., Mathers, K. L., Weber, C., Weitbrecht, V., Boes, R. M., & Vetsch, D. F. (2021). How does sediment supply influence refugia availability in river widenings? *Journal of Ecohydraulics*, *6*(2), 121–138. https://doi.org/10.1080/24705357.2020.1831415

Rachelly, C., Vetsch, D. F., Boes, R. M., & Weitbrecht, V. (2022). Sediment supply control on morphodynamic processes in gravel-bed river widenings. *Earth Surface Processes and Landforms*, *2022*, 1–20. https://doi.org/10.1002/esp.5460

Rachelly, C., Weitbrecht, V., Vetsch, D. F., & Boes, R. M. (2018). Morphological development of river widenings with variable sediment supply. *E3S Web of Conferences*, *40*, 02007. https://doi.org/10.1051/e3sconf/20184002007

Reckendorfer, W., Badura, H., & Schütz, C. (2019). Drawdown flushing in a chain of reservoirs—Effects on grayling populations and implications for sediment management. *Ecology and Evolution*, *9*(3), 1437–1451. https://doi.org/10.1002/ece3.4865

Rennie, C. D., Millar, R. G., & Church, M. A. (2002). Measurement of Bed Load Velocity using an Acoustic Doppler Current Profiler. *Journal of Hydraulic Engineering*, *128*(5), 473–483. https://doi.org/10.1061/(asce)0733-9429(2002)128:5(473)

Rice, S. P., & Church, M. (1996). Sampling surficial fluvial gravels; the precision of size distribution percentile sediments. *Journal of Sedimentary Research*, *66*(3), 654–665. https://doi.org/10.2110/jsr.66.654

Rice, S. P., & Church, M. (2010). Grain-size sorting within river bars in relation to downstream fining along a wandering channel. *Sedimentology*, *57*(1), 232–251. https://doi.org/10.1111/j.1365-3091.2009.01108.x

Rickenmann, D. (2001). Comparison of bed load transport in torrents and gravel bed streams. *Water Resources Research*, *37*(12), 3295–3305. https://doi.org/10.1029/2001WR000319

Rickenmann, D. (2017). Bedload transport measurements with geophones, hydrophones, and underwater microphones (passive acoustic methods). In D. Tsutsumi & J. B. Laronne (Eds.), *Gravel-Bed Rivers: Processes and Disasters* (pp. 185–208). John Wiley & Sons, Ltd. https://doi.org/10.1002/9781118971437.ch7

Rinaldi, M., Gurnell, A., Belletti, B., Berga Cano, M. I., Bizzi, S., Bussettini, M., Gonzalez del Tanago, M., Grabowski, R., Habersack, H., Klösch, M., Magdaleno Mas, F., Mosselman, E., Toro Velasco, M., & Vezza, P. (2015). *Final report on methods, models, tools to assess the hydromorphology of rivers, Deliverable 6.2, Part 1, of REFORM (REstoring rivers FOR effective catchment Management), a Collaborative project (large-scale integrating project) funded by the European Comm*.

Rohde, S., Schütz, M., Kienast, F., & Englmaier, P. (2005). River widening: an approach to restoring riparian habitats and plant species. *River Research and Applications*, *21*(10), 1075–1094. https://doi.org/10.1002/rra.870

Rosenfeld, J. S., Campbell, K., Leung, E. S., Bernhardt, J., & Post, J. (2011). Habitat effects on depth and velocity frequency distributions: Implications for modeling hydraulic variation and fish habitat suitability in streams. *Geomorphology*, *130*(3–4), 127–135. https://doi.org/10.1016/j.geomorph.2011.03.007

Sato, T., Kano, Y., Huang, L., Yamashita, T., Li, J., & Shimatani, Y. (2016). Relationships between fish richness, habitat diversity, and channel parameters in gravel-bed streams in the east Tiaoxi Riv. In *11th International Symposium on Ecohydraulics (ISE 2016)* (pp. 195–202). Engineers Australia. https://asnevents.s3.amazonaws.com/Abstrakt-FullPaper/26049-Sato_26049_FINAL.pdf

Schälchli, U. (1992). The clogging of coarse gravel river beds by fine sediment. *Hydrobiologia*, *235–236*(1), 189–197. https://doi.org/10.1007/BF00026211

Schälchli, U. (1993). *Die Kolmation von Fliessgewassersohlen: Prozesse und Berechnungsgrundlagen [Clogging of streambeds: Processes and calculation bases]* (Issue 10293) [Thesis, ETH Zürich]. https://doi.org/10.3929/ethz-a-001322977

Schälchli, U., & Hunzinger, L. (2018). Die erforderliche Geschiebefracht [The required bedload volume]. In *Fachbericht zum Modul «Geschiebehaushalt – Massnahmen» der Vollzugshilfe Renaturierung der Gewässer [Technical report for the module "Reactivation of bed load dynamics - Measures" of the Swiss implementation guide for the revitalisation of water bodies.]*. Bundesamt für Umwelt. https://www.bafu.admin.ch/dam/bafu/de/dokumente/wasser/externe-studien-berichte/die-erforderliche-geschiebefracht.pdf.download.pdf/BAFU-bericht-flussbau-geschiebefracht.pdf

Schälchli, U., & Kirchhofer, A. (2012). Sanierung Geschiebehaushalt - Strategische Planung. Ein Modul der Vollzugshilfe Renaturierung der Gewässer [Reactivation of bed load dynamics - Strategic planning. A module of the implementation guide for the restoration of water bodies.]. In *Umwelt-Vollzug* (Vol. 1226). Bundesamt für Umwelt. www.bafu.admin.ch/uv-1226-d

Scheurer, T., & Molinari, P. (2003). Experimental floods in the River Spöl, Swiss National Park: Framework, objectives and design. *Aquatic Sciences*, *65*(3), 183–190. https://doi.org/10.1007/s00027-003-0667-4

Schleiss, A. J., De Cesare, G., & Althaus, J. J. (2010). Verlandung der Stauseen gefährdet die nachhaltige Nutzung der Wasserkraft. *Wasser Energie Luft*, *102*(1), 31.

Schleiss, A. J., Franca, M. J., Juez, C., & De Cesare, G. (2016). Reservoir sedimentation. *Journal of Hydraulic Research*, *54*(6), 595–614. https://doi.org/10.1080/00221686.2016.1225320

Schroff, R., Mörtl, C., & De Cesare, G. (2021a). Ultrasonic Doppler flow velocity measurements as a co-indicator for the eco-morphological assessment in a residual flow reach. *13th International Symposium on Ultrasonic Doppler Methods for Fluid Mechanics and Fluid Engineering*, *June*.

Schroff, R., Mörtl, C., & De Cesare, G. (2021b). Wirkungskontrolle einer Sedimentzugabe: Habitatvielfalt und Kolmation [Eco-morphological evaluation of a sediment augmentation measure]. *WasserWirtschaft*, *111*(9–10), 68–76. https://doi.org/10.1007/s35147-021-0896-2

Schroff, R., Mörtl, C., Vonlanthen, P., & De Cesare, G. (2022). Impacts et enjeux de charriage d'une crue artificielle – Exemple de la Petite Sarine 2020 [Effects and bedload related challenges of an artificial flood - Example of the Petite Sarine 2020]. *Wasser Energie Luft - Eau Energie Air*, *114*(2–2022), 75–84. https://www.swv.ch/wel/fachzeitschrift-wel/wasser-energie-luft-2-2022

Schumm, S. A. (1977). *The fluvial system*. John Wiley &Sons.

Schwartz, J. (2016). Use of ecohydraulic-based mesohabitat classification and fish species traits for stream restoration design. *Water*, *8*(520), 1–33. https://doi.org/10.3390/w8110520

Schwindt, S., & Pasternack, G. B. (2020). Automating flood-safe ecological river modelling and design. In W. Uijttewaal, M. J. Franca, D. Valero, V. Chavarrias, C. Y. Arbós, R. Schielen, & A. Crosato (Eds.), *Riverflow 2020* (1st Editio, pp. 1359–1367). Taylor & Francis Group. https://doi.org/10.1201/b22619

Schwindt, S., Pasternack, G. B., Bratovich, P. M., Rabone, G., & Simodynes, D. (2019). Hydro-morphological parameters generate lifespan maps for stream restoration management. *Journal of Environmental Management*, *232*(November 2018), 475–489. https://doi.org/10.1016/j.jenvman.2018.11.010

Sear, D. A. (1995). Morphological and sedimentological changes in a gravel-bed river following 12 years of flow regulation for hydropower. *Regulated Rivers: Research & Management*, *10*(2–4), 247–264. https://doi.org/10.1002/rrr.3450100219

SedNet Organisation. (2004). *Contaminated sediments in European river basins* (W. Salomons & J. Brils, Eds.). www.sednet.org

Sellheim, K. L., Watry, C. B., Rook, B., Zeug, S. C., Hannon, J., Zimmerman, J., Dove, K., & Merz, J. E. (2016). Juvenile Salmonid Utilization of Floodplain Rearing Habitat After Gravel Augmentation in a Regulated River. *River Research and Applications*, *32*(4), 610–621. https://doi.org/10.1002/rra.2876

Shields, A. (1936). Anwendung der Ähnlichkeitsmechanik und der Turbulenzforschung auf die Geschiebebewegung [Application of similarity mechanics and turbulence research to bedload motion]. *Mitteilung Der Preussischen Versuchsanstalt Für Wasserbau Und Schiffbau*, *26*.

Sklar, L. S., Fadde, J., Venditti, J. G., Nelson, P., Wydzga, M. A., Cui, Y., & Dietrich, W. E. (2009). Translation and dispersion of sediment pulses in flume experiments simulating gravel augmentation below dams. *Water Resources Research*, *45*(8), 1–14. https://doi.org/10.1029/2008WR007346

Smokorowski, K. E., & Pratt, T. C. (2007). Effect of a change in physical structure and cover on fish and fish habitat in freshwater ecosystems- A review and meta-analysis. *Environmental Reviews*, *15*(December 2007), 15–41. https://doi.org/10.1139/a06-007

Soares-Frazão, S., Le Grelle, N., Spinewine, B., & Zech, Y. (2007). Dam-break induced morphological changes in a channel with uniform sediments: measurements by a laser-sheet imaging technique. *Journal of Hydraulic Research*, *45*(sup1), 87–95–87–95. https://doi.org/10.1080/00221686.2007.9521835

Soloy, A., Turki, I., Fournier, M., Costa, S., Peuziat, B., & Lecoq, N. (2020). A Deep Learning-Based Method for Quantifying and Mapping the Grain Size on Pebble Beaches. *Remote Sensing*, *12*(21), 3659. https://doi.org/10.3390/rs12213659

Spinewine, B., Capart, H., le Grellle, N., Soares-Frazão, S., & Zech, Y. (2002). Experiments and computations of bankline retreat due to geomorphic dam-break floods. *Proceedings of the 1st International. Conference on Fluvial Hydraulics*, *October 2014*, 651–662.

Staentzel, C., Arnaud, F., Combroux, I., Schmitt, L., Trémolières, M., Grac, C., Piégay, H., Barillier, A., Chardon, V., & Beisel, J.-N. (2018). How do instream flow increase and gravel augmentation impact biological communities in large rivers: A case study on the Upper Rhine River. *River Research and Applications*, *34*(2), 153–164. https://doi.org/10.1002/rra.3237

Staentzel, C., Kondolf, G. M., Schmitt, L., Combroux, I., Barillier, A., & Beisel, J. N. (2020). Restoring fluvial forms and processes by gravel augmentation or bank erosion below dams: A systematic review of ecological responses. *Science of the Total Environment*, *706*, 135743. https://doi.org/10.1016/j.scitotenv.2019.135743

Stähly, S. (2019). *Hydraulic-morphological habitat assessment in rivers considering residual flow, sediment replenishment and artificial flood events* [Thesis]. EPFL.

Stähly, S., Franca, M. J., Robinson, C. T., & Schleiss, A. J. (2019). Sediment replenishment combined with an artificial flood improves river habitats

downstream of a dam. *Scientific Reports*, *9*(5176), 1–7. https://doi.org/10.1038/s41598-019-41575-6

Stähly, S., Franca, M. J., Robinson, C. T., & Schleiss, A. J. (2020). Erosion, transport and deposition of a sediment replenishment under flood conditions. *Earth Surface Processes and Landforms*, *45*(13), 3354–3367. https://doi.org/10.1002/esp.4970

Stähly, S., Gostner, W., Franca, M. J., Robinson, C. T., & Schleiss, A. J. (2018). Sampling sufficiency for determining hydraulic habitat diversity. *Journal of Ecohydraulics*, *3*(2), 130–144. https://doi.org/10.1080/24705357.2019.1576021

Stanford, J. A., Lorang, M. S., & Hauer, F. R. (2005). The shifting habitat mosaic of river ecosystems. *SIL Proceedings, 1922-2010*, *29*(1), 123–136. https://doi.org/10.1080/03680770.2005.11901979

Staudt, F., Mullarney, J. C., Pilditch, C. A., & Huhn, K. (2019). Effects of grain-size distribution and shape on sediment bed stability, near-bed flow and bed microstructure. *Earth Surface Processes and Landforms*, *44*(5), 1100–1116. https://doi.org/10.1002/esp.4559

Strahler, A. N. (1957). Quantitative analysis of watershed geomorphology. *Transactions, American Geophysical Union*, *38*(6), 913. https://doi.org/10.1029/TR038i006p00913

Sumi, T., & Kantoush, S. (2011). Sediment management strategies for sustainable reservoir. In A. J. Schleiss & R. M. Boes (Eds.), *Dams and Reservoirs under Changing Challenges* (First Edit, Issue May, pp. 353–362). Taylor & Francis Group. https://doi.org/10.1201/b11669-47

Sumi, T., Kantoush, S., Esmaeili, T., & Ock, G. (2017). Reservoir Sediment Flushing and Replenishment Below Dams. In D. Tsutsumi & J. B. Laronne (Eds.), *Gravel-Bed Rivers* (First Edit, pp. 385–414). John Wiley & Sons, Ltd. https://doi.org/10.1002/9781118971437.ch14

Bundesgesetz über den Schutz der Gewässer [Federal act on the protection of waters], (1991) (testimony of Swiss Confederation).

Thompson, D. M., & MacVicar, B. J. (2022). Pool-Riffle. In J. (Jack) F. Shroder (Ed.), *Treatise on Geomorphology* (2nd ed., pp. 587–608). Elsevier. https://doi.org/10.1016/B978-0-12-409548-9.12087-1

Thompson, D. M., Wohl, E. E., & Jarrett, R. D. (1996). A revised velocity-reversal and sediment-sorting model for a high-gradient, pool-riffle stream. *Physical Geography*, *17*(2), 142–156. https://doi.org/10.1080/02723646.1996.10642578

Thoms, M. C., & Parsons, M. (2002). Eco-geomorphology: An interdisciplinary approach to river science. In F. J. Dyer, M. C. Thompson, & J. M. Olley (Eds.), *IAHS-AISH Publication* (Issue 276, pp. 113–119). International Assosciation of Hydrological Sciences (IAHS).

Tonolla, D., Geilhausen, M., & Doering, M. (2021). Seven decades of hydrogeomorphological changes in a near-natural (Sense River) and a hydropower-regulated (Sarine River) pre-Alpine river floodplain in Western Switzerland. *Earth Surface Processes and Landforms*, *46*(1), 252–266. https://doi.org/10.1002/esp.5017

VAW. (2022). *BASEMENT – Basic Simulation Environment for Computation of Environmental Flow and Natural Hazard Simulation* (2.8.2). Versuchsanstalt für Wasserbau, Hydrologie und Glaziologie (VAW), ETH Zurich.

Venditti, J. G., Dietrich, W. E., Nelson, P. A., Wydzga, M. A., Fadde, J., & Sklar, L. (2010). Mobilization of coarse surface layers in gravel-bedded rivers by finer gravel bed load. *Water Resources Research*, *46*(7), 1–10. https://doi.org/10.1029/2009WR008329

Venditti, J. G., Nelson, P. A., Minear, J. T., Wooster, J., & Dietrich, W. E. (2012). Alternate bar response to sediment supply termination. *Journal of Geophysical Research: Earth Surface*, *117*(2), 1–18. https://doi.org/10.1029/2011JF002254

Vetsch, D., Allen, J., Belser, A., Boes, R., Brodersen, J., Fink, S., Franca, M. J., Juez, C., Nadyeina, O., Robinson, C. T., Scheidegger, C., Schleiss, A., Siviglia, A., Weber, C., & Weitbrecht, V. (2018). Lebensraum Gewässer – Sedimentdynamik und Vernetzung [Water habitat - sediment dynamics and connectivity]. *Wasser Energie Luft*, *1*, 19–24.

Volz, C., Rousselot, P., Vetsch, D., & Faeh, R. (2012). Numerical modelling of non-cohesive embankment breach with the dual-mesh approach. *Journal of Hydraulic Research*, *50*(6), 587–598. https://doi.org/10.1080/00221686.2012.732970

Vonlanthen, P., Périat, G., Kreienbühl, T., Schlunke, D., Morillas, N., Grandmottet, J.-P., & Degiorgi, F. (2018). IAM – Eine Methode zur Bewertung der Habitatvielfalt und -attraktivität von Fliessgewässerabschnitten [IAM – A method for assessing the habitat diversity and attractiveness of stream segments.]. *Wasser Energie Luft*, *110*(3), 201–207.

Vonwiller, L. (2017). *Numerical Modeling of Morphological Response of Gravel-Bed Rivers to Sediment Supply* [Thesis, ETH Zurich]. https://doi.org/10.3929/ethz-b-000479106

Vonwiller, L., Friedl, F., Vetsch, D. F., Weitbrecht, V., Boes, R. M., Battisacco, E., Franca, M. J., & Schleiss, A. J. (2017). Designing gravel additions - What types of gravel

additions in lowland rivers and alpine streams have been implemented so far and what lessons have been learned ? In *Research Program "River Engineering and Ecology" – Project "Sediment and Habitat Dynamics."* Federal Office for the Environment FOEN. https://www.rivermanagement.ch/fileadmin/sites/rivermanagement/produkte_publikationen/hilfsmittel/geschiebe_dynamik/praxisfragen_en/Q04_designing_gravel_additions.pdf

Vonwiller, L., Vetsch, D., & Boes, R. (2018). Modeling Streambank and Artificial Gravel Deposit Erosion for Sediment Replenishment. *Water*, *10*(4), 508. https://doi.org/10.3390/w10040508

Weber, C., Sprecher, L., Åberg, U., Thomas, G., Baumgartner, S., & Haertel-Borer, S. (2019). Summary and content. In *Evaluating the outcome of rehabilitation projects – collaborative learning for the future* (V1.02). Federal Office for the Environment.

Weidemann, M. (2005). Feuille 1205 Rossens [Sheet 1205 Rossens]. In *Notices explicatives de l'Atlas géologique de la Suisse 1:25000 [Explanatory booklet of the Geological Atlas of Switzerland 1:25000]* (Vol. 105). Swiss Federal Office for the Topography.

Wheaton, J. M., Fryirs, K. A., Brierley, G., Bangen, S. G., Bouwes, N., & O'Brien, G. (2015). Geomorphic mapping and taxonomy of fluvial landforms. *Geomorphology*, *248*, 273–295. https://doi.org/10.1016/j.geomorph.2015.07.010

Wheaton, J. M., Pasternack, G. B., & Merz, J. E. (2004a). Spawning habitat rehabilitation - II. Using hypothesis development and testing in design, Mokelumne river, California, U.S.A. *International Journal of River Basin Management*, *2*(1), 21–37. https://doi.org/10.1080/15715124.2004.9635219

Wheaton, J. M., Pasternack, G. B., & Merz, J. E. (2004b). Spawning habitat rehabilitation -I. Conceptual approach and methods. *International Journal of River Basin Management*, *2*(1), 3–20. https://doi.org/10.1080/15715124.2004.9635218

Wilcock, P., Pitlick, J., & Cui, Y. (2009). *Sediment transport primer: estimating bed-material transport in gravel-bed rivers* (Issue RMRS-GTR-226). https://doi.org/10.2737/RMRS-GTR-226

Wilcock, P. R., Kondolf, G. M., Matthews, W. V. G., & Barta, A. F. (1996). Specification of sediment maintenance flows for a large gravel-bed river. *Water Resources Research*, *32*(9), 2911–2921. https://doi.org/10.1029/96WR01627

Wolman, M. G. (1954). A method of sampling coarse river-bed material. *Transactions, American Geophysical Union*, *35*(6), 951. https://doi.org/10.1029/TR035i006p00951

Woodworth, K. A., & Pasternack, G. B. (2022). Are dynamic fluvial morphological unit assemblages statistically stationary through floods of less than ten times bankfull discharge? *Geomorphology*, *403*(108135). https://doi.org/10.1016/j.geomorph.2022.108135

Woolsey, S., Capelli, F., Gonser, T., Hoehn, E., Hostmann, M., Junker, B., Paetzold, A., Roulier, C., Schweizer, S., Tiegs, S. D., Tockner, K., Weber, C., & Peter, A. (2007). A strategy to assess river restoration success. *Freshwater Biology*, *52*(4), 752–769. https://doi.org/10.1111/j.1365-2427.2007.01740.x

Wu, W. (2007). *Computational River Dynamics*. CRC Press. https://doi.org/10.4324/9780203938485

Wyrick, J. R., & Pasternack, G. B. (2014). Geospatial organization of fluvial landforms in a gravel–cobble river: Beyond the riffle–pool couplet. *Geomorphology*, *213*, 48–65. https://doi.org/10.1016/j.geomorph.2013.12.040

Yang, S. L., Zhang, J., & Xu, X. J. (2007). Influence of the Three Gorges Dam on downstream delivery of sediment and its environmental implications, Yangtze River. *Geophysical Research Letters*, *34*(10), L10401. https://doi.org/10.1029/2007GL029472

Zeug, S. C., Sellheim, K., Watry, C., Rook, B., Hannon, J., Zimmerman, J., Cox, D., & Merz, J. (2014). Gravel augmentation increases spawning utilization by anadromous salmonids: a case study from California, USA. *River Research and Applications*, *30*(6), 707–718. https://doi.org/10.1002/rra.2680

Zimmer, M. P., & Power, M. (2006). Brown trout spawning habitat selection preferences and redd characteristics in the Credit River, Ontario. *Journal of Fish Biology*, *68*(5), 1333–1346. https://doi.org/10.1111/j.0022-1112.2006.00995.x

Appendix

A1. Representative case studies

Table A1.1 References for representative case studies of sediment augmentation measures (SAMs), displayed in Figure 2.5. The corresponding bibliography is presented at the end of the appendix.

Number of case study	Reference
1	(S. A. Kantoush, Sumi, & Kubota, 2010)
2	(S. A. Kantoush & Sumi, 2011)
3	(S. A. Kantoush, Sumi, & Kubota, 2010)
4	(Gaeuman et al., 2017)
5	(Gaeuman, 2014)
6	(Gaeuman, 2014)
7	(Stähly et al., 2019)
8	(Brousse et al., 2020)
9	(Arnaud et al., 2017)

A2. Rating curve of the measurement station at the Sarine River

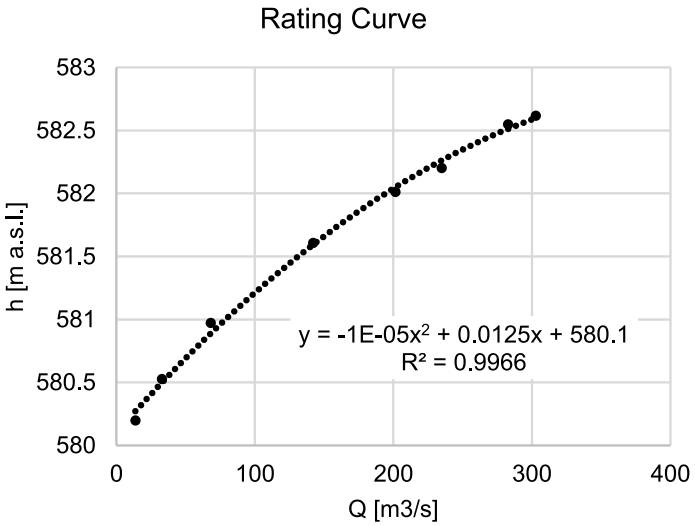

Figure A2.1 Graph of the rating curve at the measurement location, based on the eight calibration points. Variable L is the water level elevation, and Q is the discharge. Calibration points are plotted as black dots.

Table A2.1 Data table for **Figure A2.1**, listing all eight calibration points. Variable L is the water level elevation, and Q is the discharge.

Q $[m^3/s]$	L [m a. s. l.]
302.9	582.615
282.8	582.548
235	582.201
201.6	582.012
142	581.606
68.1	580.972
32.9	580.526
13.8	580.196

A3. Pictures of the experimental flume

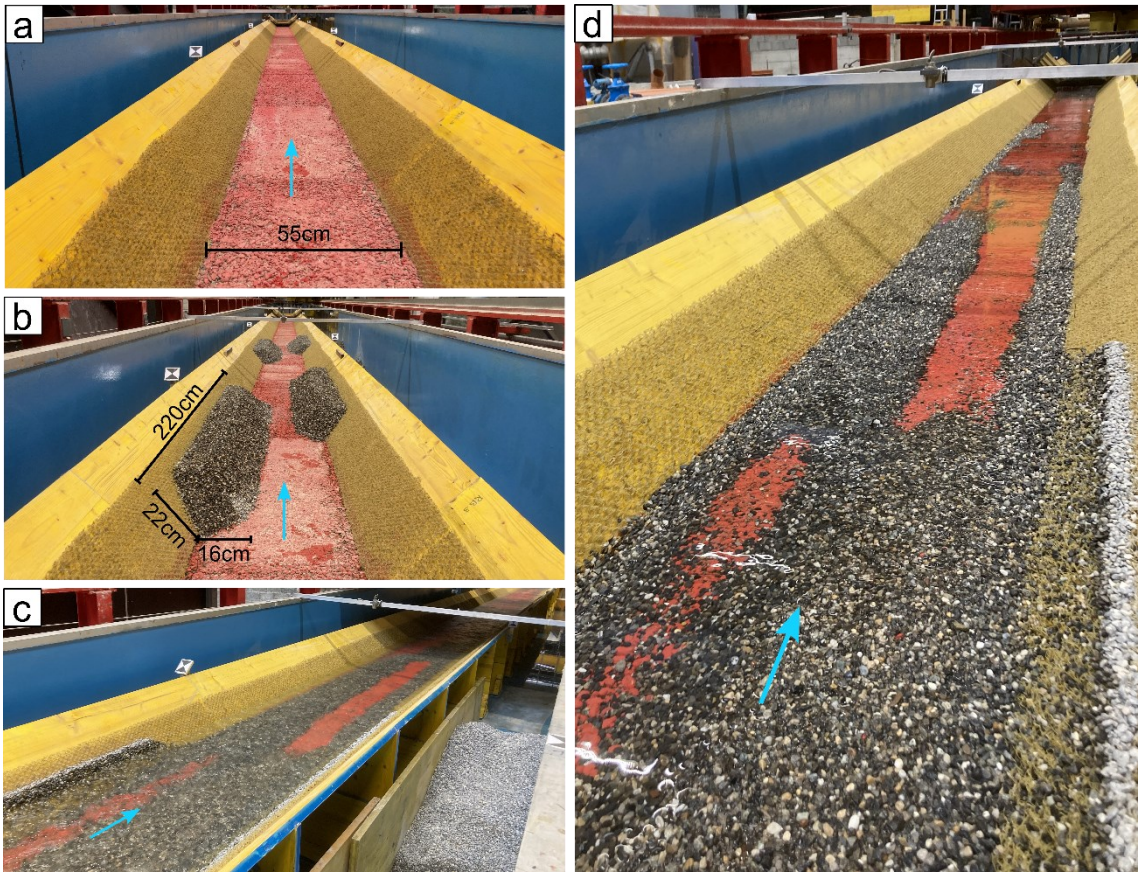

Figure A3.1 Pictures of the experimental flume at different test phases. a: initial condition, b: sediment augmentation in the dry phase: sediment is added in the form of artificial deposits, c: flood phase with constant flow release, d: emptying phase: The discharge is stopped, and the water is flowing out of the channel, leaving behind the bed topography to be scanned. The arrows indicate the direction of flow. © Platform of hydraulic construction of the EPFL (PL-LCH).

A4. Hydraulic conditions in the physical model

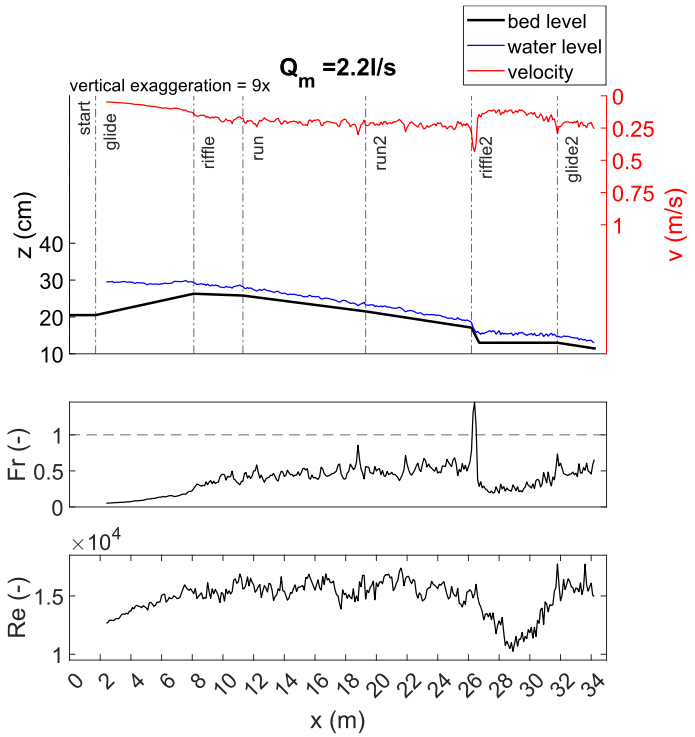

Figure A4.1 Hydraulic conditions along the centre axis of the experimental channel in initial condition for a constant model discharge (Q_m) of $2.2\,l/s$. Variable x is the longitudinal coordinate, z is the vertical coordinate, v is the absolute flow velocity, Fr is the Froude Number, and Re is the Reynolds Number.

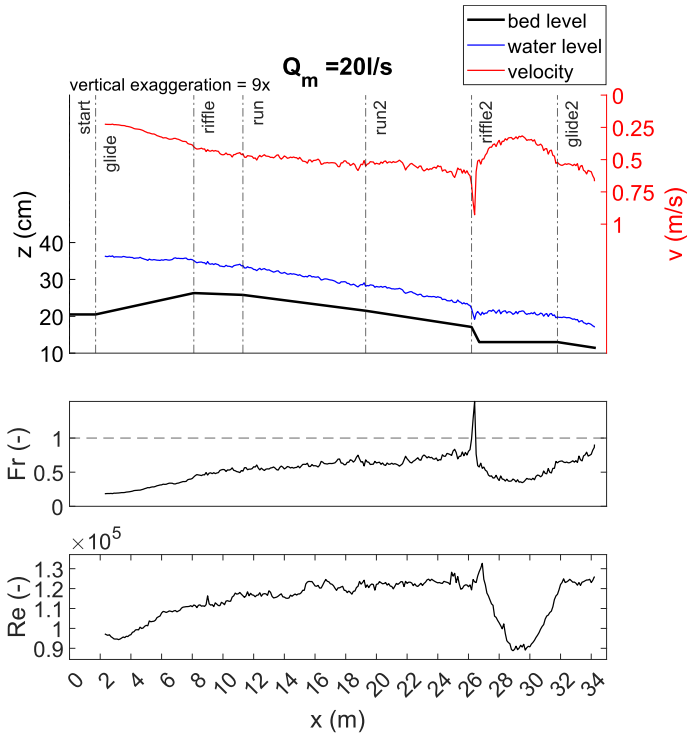

Figure A4.2 Hydraulic conditions along the centre axis of the experimental channel in initial condition for a constant model discharge (Q_m) of $20\,l/s$. Variable x is the longitudinal coordinate, z is the vertical coordinate, v is the absolute flow velocity, Fr is the Froude Number, and Re is the Reynolds Number.

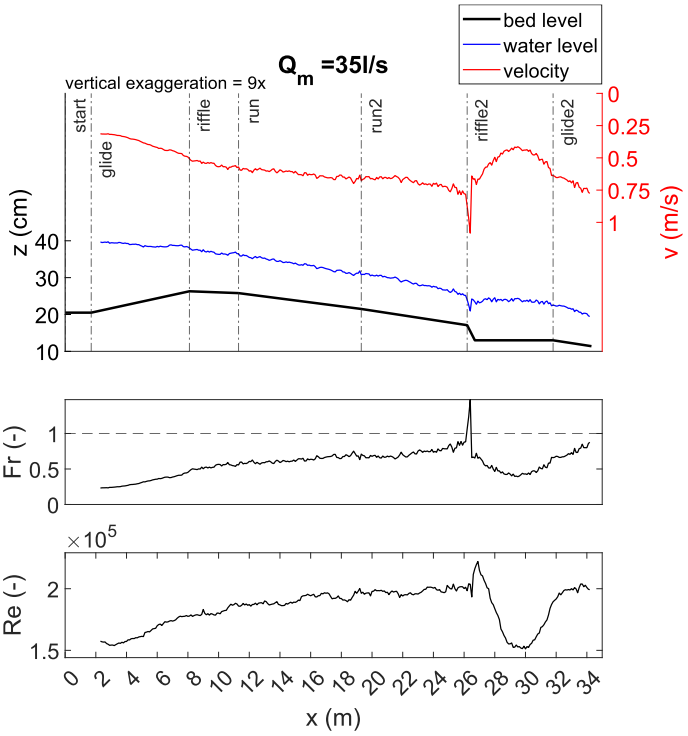

Figure A4.3 Hydraulic conditions along the centre axis of the experimental channel in initial condition for a constant model discharge (Q_m) of $35\ l/s$. Variable x is the longitudinal coordinate, z is the vertical coordinate, v is the absolute flow velocity, Fr is the Froude Number, and Re is the Reynolds Number.

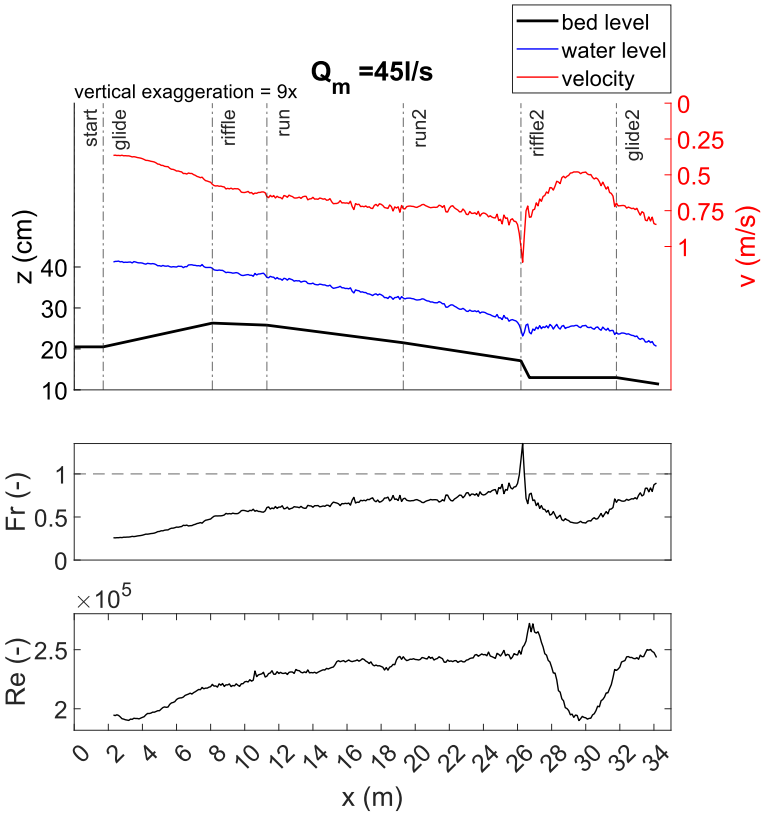

Figure 9.4 Hydraulic conditions along the centre axis of the experimental channel in initial condition for a constant model discharge (Q_m) of $45\ l/s$. Variable x is the longitudinal coordinate, z is the vertical coordinate, v is the absolute flow velocity, Fr is the Froude Number, and Re is the Reynolds Number.

A5. Conditions for bedload transport in the physical model

Table A5.1 Data table for **Figure 3.19**, including a calculation of the ratio of Shields Number (θ) to critical Shields Number ($\theta_c = 0.045$). Variable Q_m is the discharge in the model scale, and Re_p^* is the Particle Reynolds Number.

$Q_m[l/s]$	Section	$Re_p^*[-]$	$\theta[-]$	$\theta/\theta_c\,[-]$
20	1	169	0.028	0.6
20	2	220	0.048	1.1
20	3	363	0.131	2.9
20	4	461	0.211	4.7
20	5	641	0.408	9.1
20	6	224	0.050	1.1
20	7	699	0.484	10.8
40	1	223	0.050	1.1
40	2	282	0.079	1.8
40	3	437	0.189	4.2
40	4	542	0.292	6.5
40	5	671	0.447	9.9
40	6	289	0.083	1.8
40	7	733	0.534	11.9
60	1	259	0.066	1.5
60	2	325	0.105	2.3
60	3	478	0.227	5.0
60	4	561	0.313	6.9
60	5	659	0.432	9.6
60	6	349	0.121	2.7
60	7	763	0.578	12.8
80	1	291	0.084	1.9
80	2	362	0.130	2.9
80	3	532	0.281	6.2
80	4	606	0.365	8.1
80	5	712	0.503	11.2
80	6	370	0.136	3.0
80	7	770	0.589	13.1

A6. Vertical change of successive scans during the first flood of Run_A to Run_C

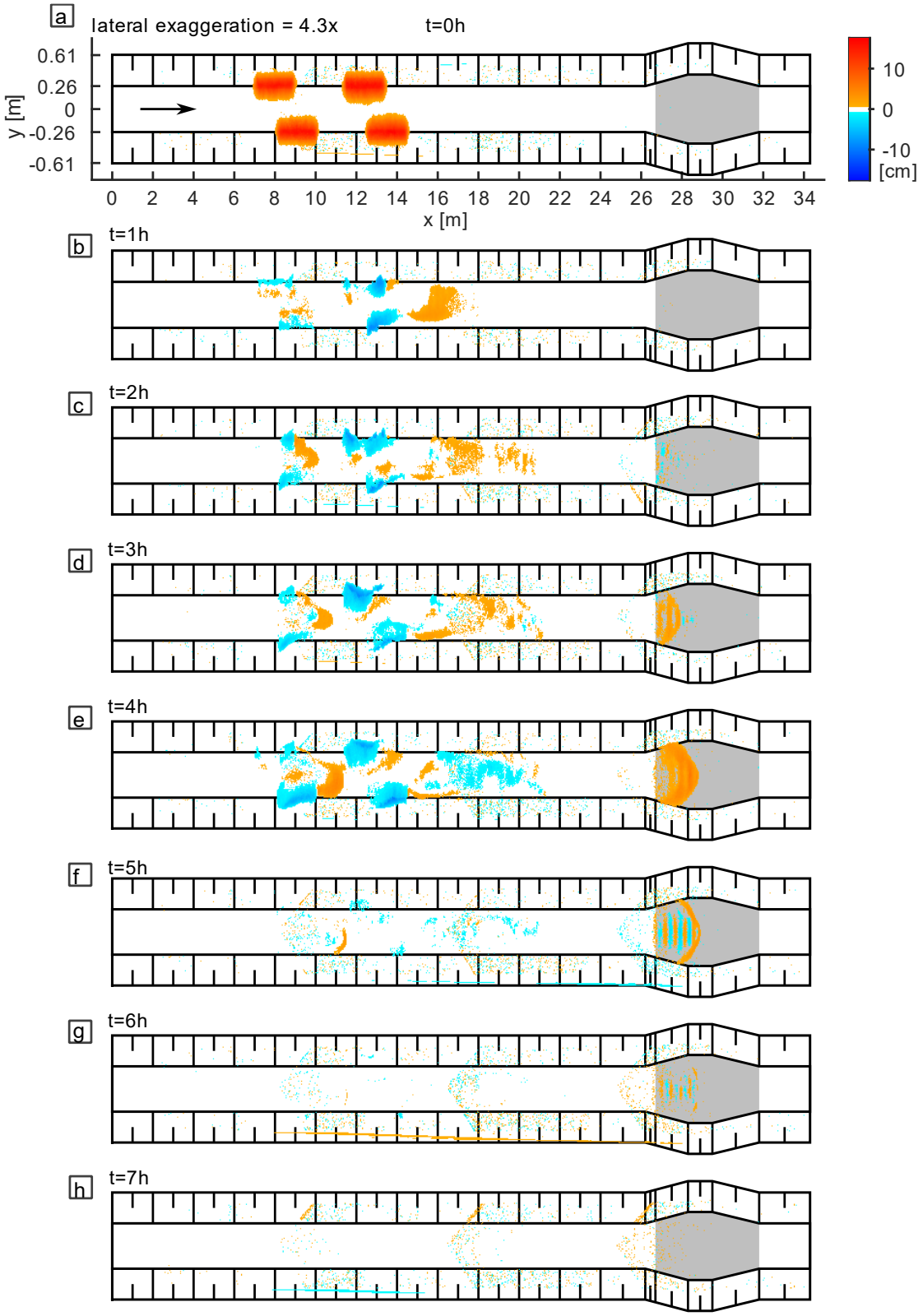

Figure A6.1 Graphic display of the vertical change during the first flood of *Run_A*. a-h: Difference between Scan 1 to Scan 8 and the previous channel state. Variable x is the longitudinal channel coordinate, and y is the lateral channel coordinate. The label t indicates the experimental time. The grey area represents the mobile bed area.

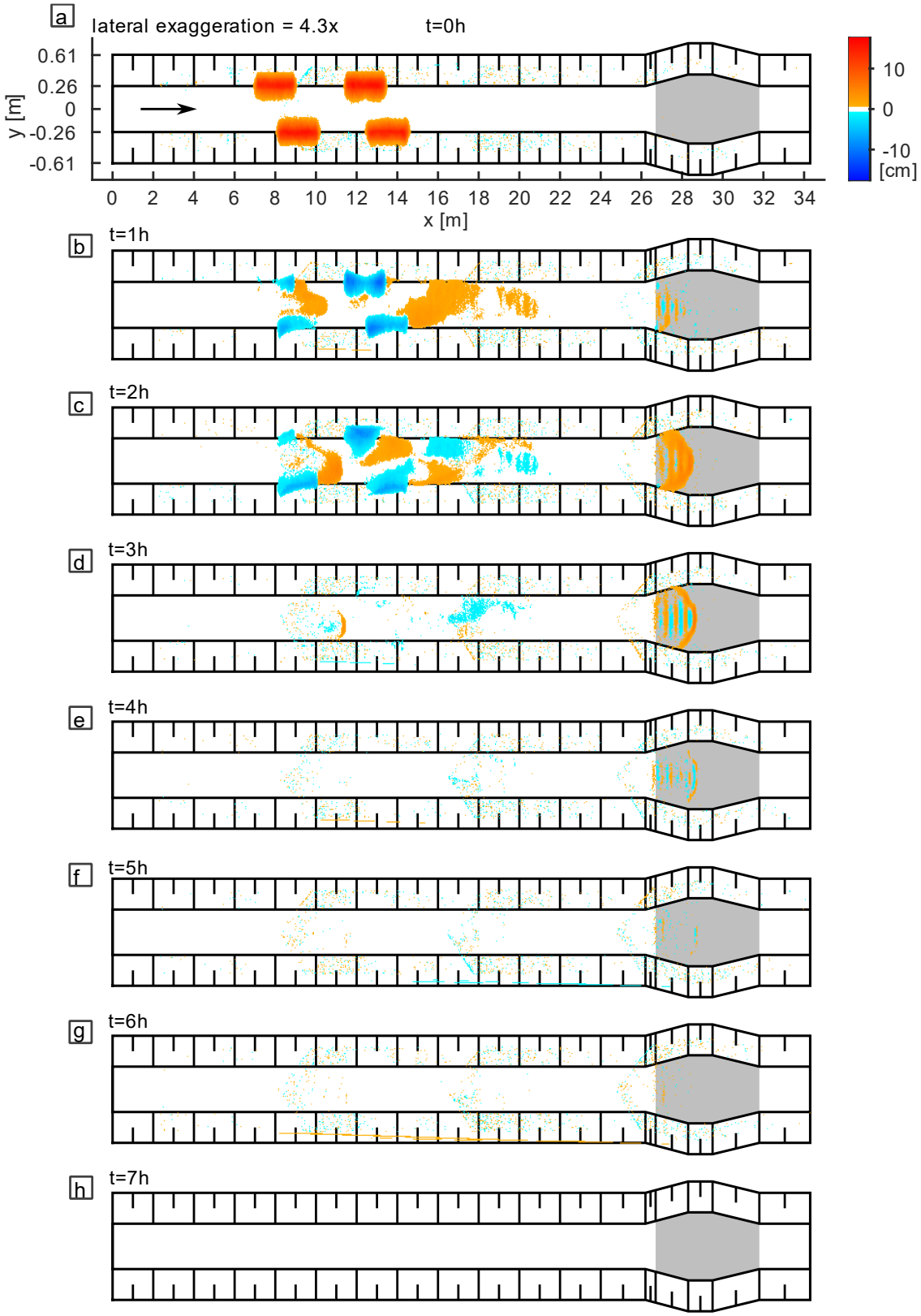

Figure A6.2 Graphic display of the vertical change during the first flood of *Run_B*. a-h: Difference between Scan 1 to Scan 8 and the previous channel state. Variable x is the longitudinal channel coordinate, and y is the lateral channel coordinate. The label t indicates the experimental time. The grey area represents the mobile bed area.

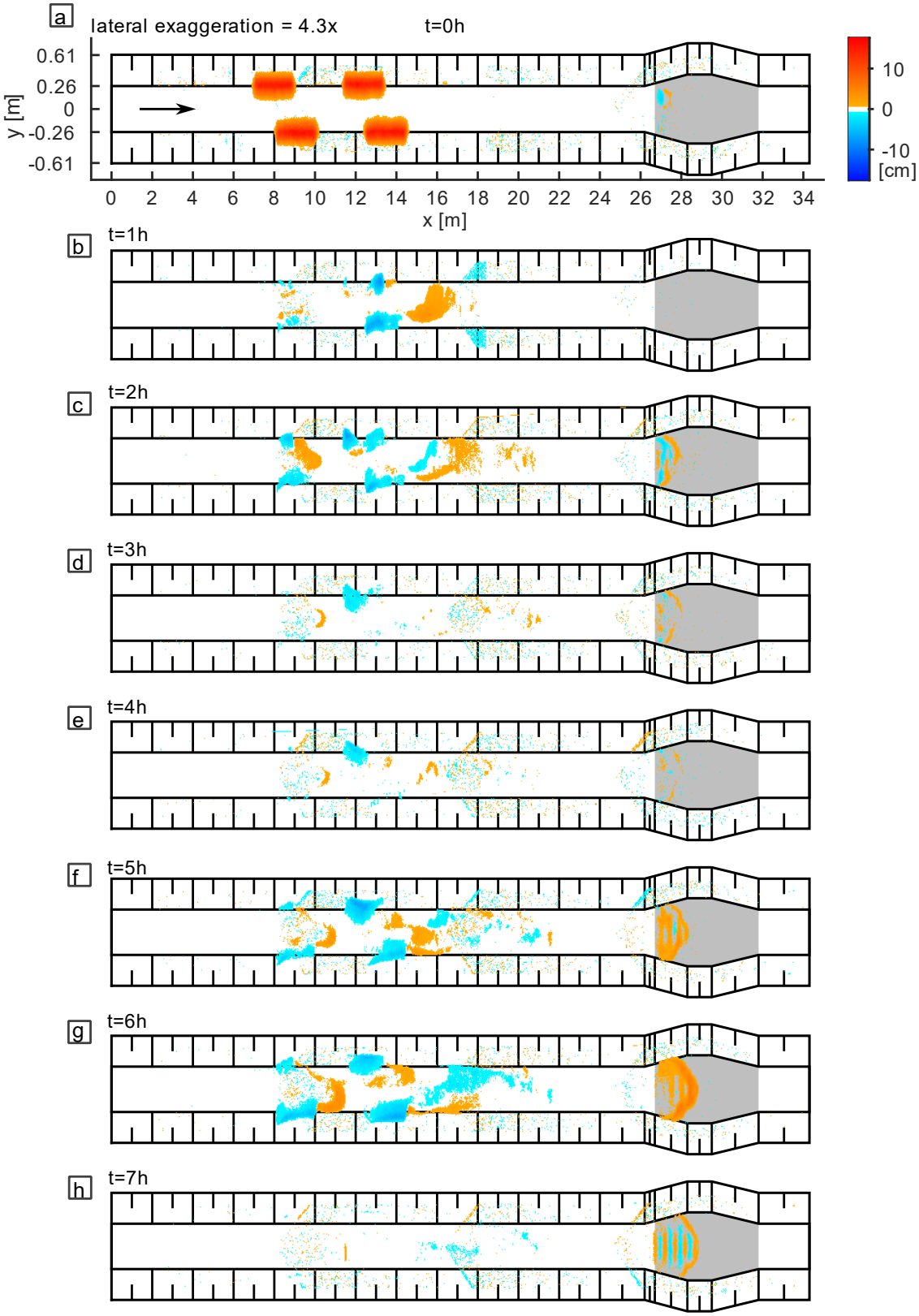

Figure A6.3 Graphic display of the vertical change during the first flood of *Run_C*. a-h: Difference between Scan 1 to Scan 8 and the previous channel state. Variable x is the longitudinal channel coordinate, and y is the lateral channel coordinate. The label t indicates the experimental time. The grey area represents the mobile bed area.

A7. Vertical change between floods of Run_D to Run_F

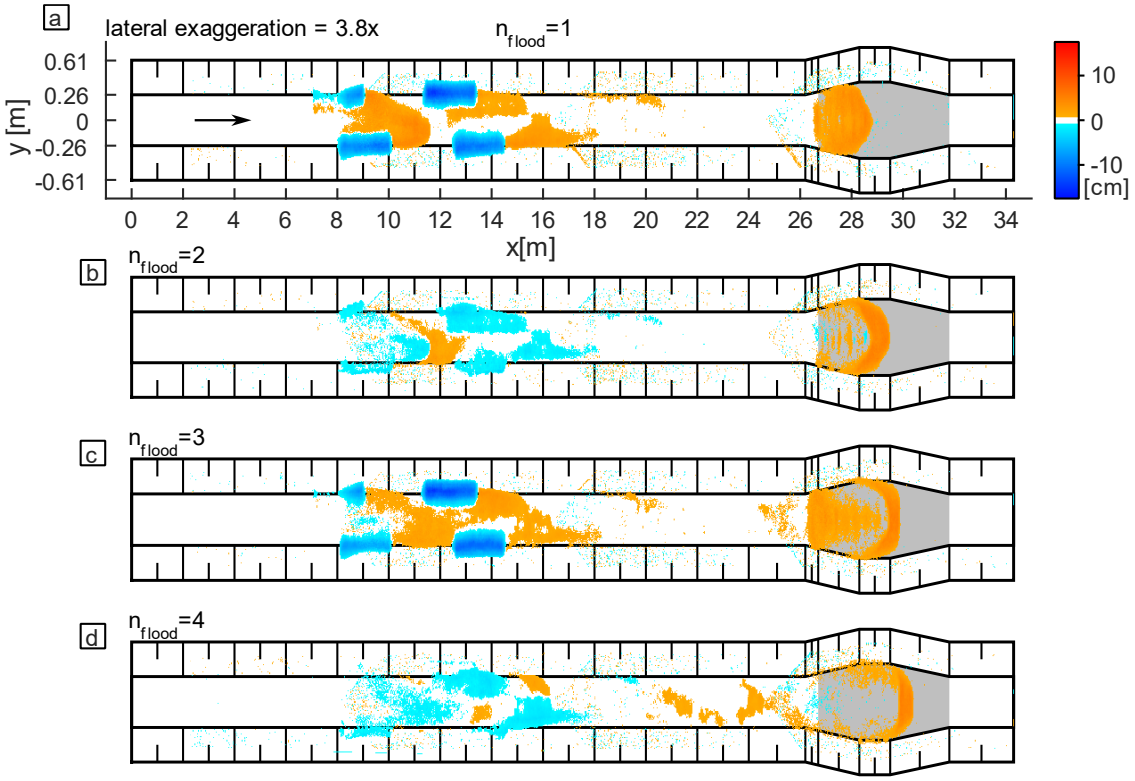

Figure A7.1 Graphic display of the vertical change between every flood of *Run_D*. a-d: Difference between the scans after 1 to 4 floods (n_{flood}) and the previous channel state. Variable x is the longitudinal channel coordinate, and y is the lateral channel coordinate. The grey area represents the mobile bed area.

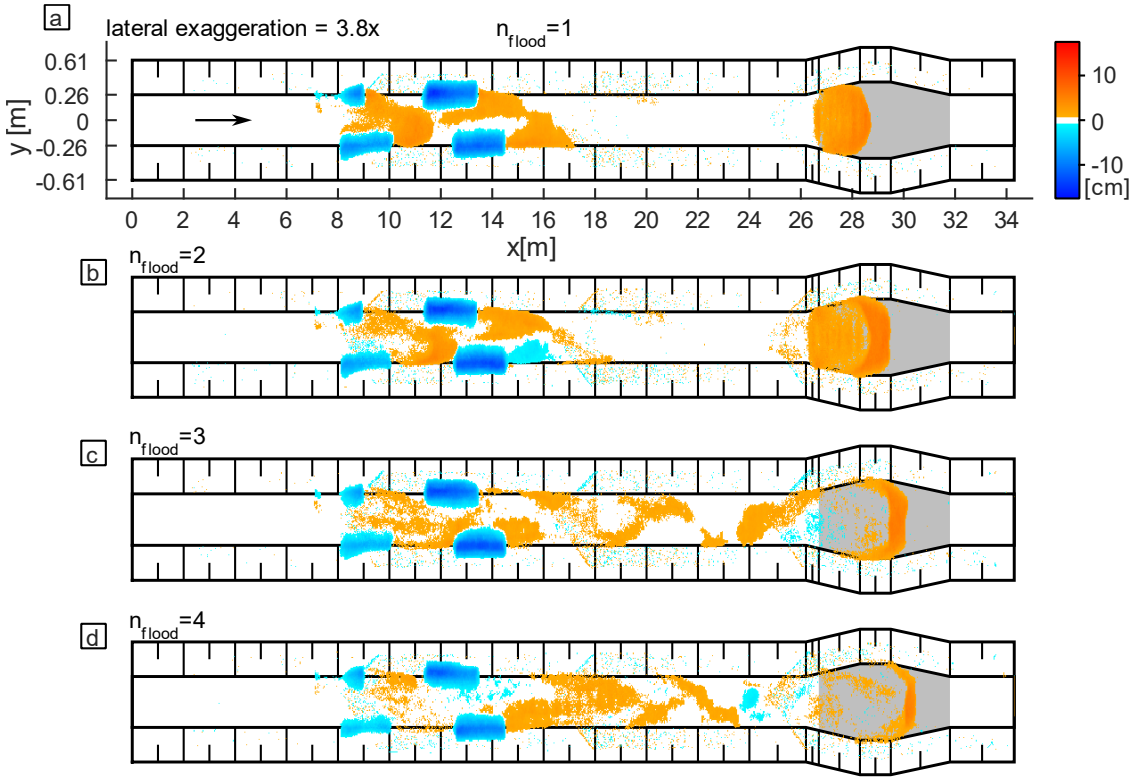

Figure A7.2 Graphic display of the vertical change between every flood of *Run_E*. a-d: Difference between the scans after 1 to 4 floods (n_{flood}) and the previous channel state. Variable x is the longitudinal channel coordinate, and y is the lateral channel coordinate. The grey area represents the mobile bed area.

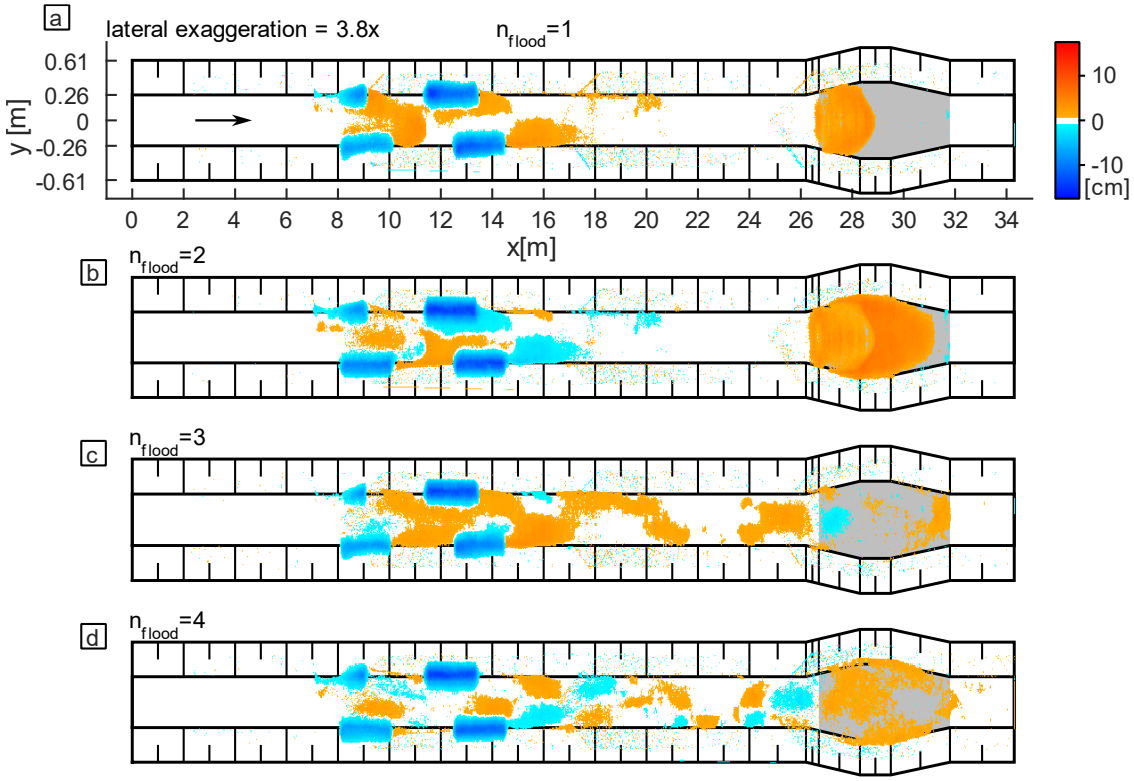

Figure A7.3 Graphic display of the vertical change between every flood of *Run_F*. a-d: Difference between the scans after 1 to 4 floods (n_{flood}) and the previous channel state. Variable x is the longitudinal channel coordinate, and y is the lateral channel coordinate. The grey area represents the mobile bed area.

A8. Low-flow simulations of Run_D to Run_F

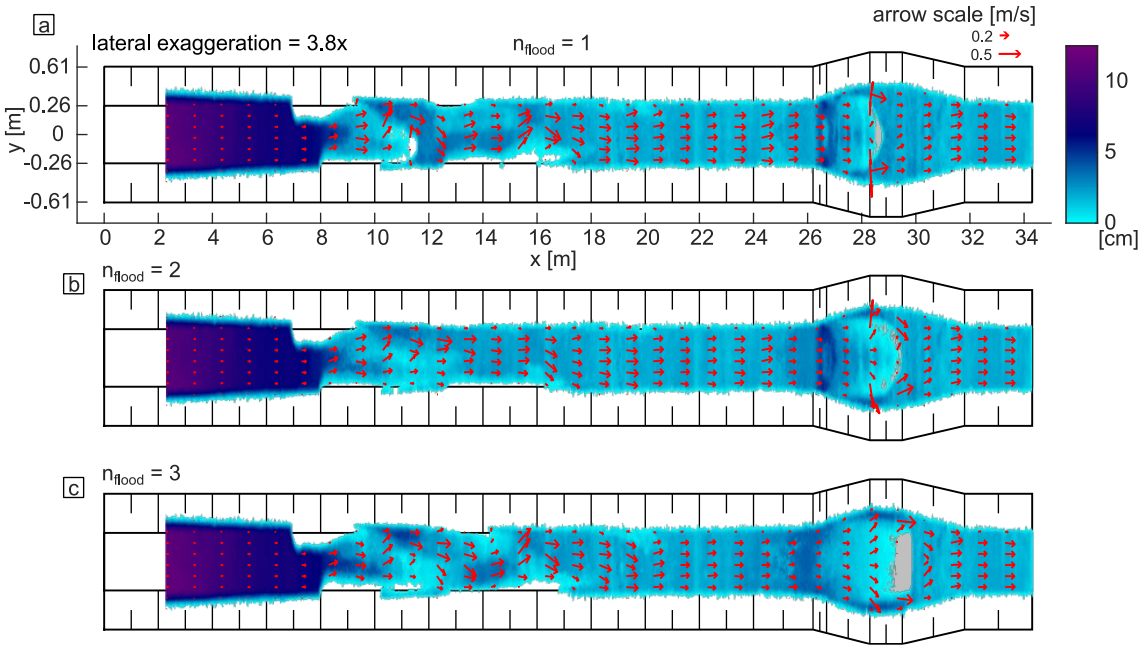

Figure A8.1 Graphic display of the simulated water depth and flow field after the three first floods of *Run_D*. a-c: Simulation results after 1 to 3 floods (n_{flood}). Variable x is the longitudinal channel coordinate, and y is the lateral channel coordinate. The grey area represents the mobile bed area. The colour scale indicates the water depth h. The red arrows represent the two-dimensional (2D) flow field.

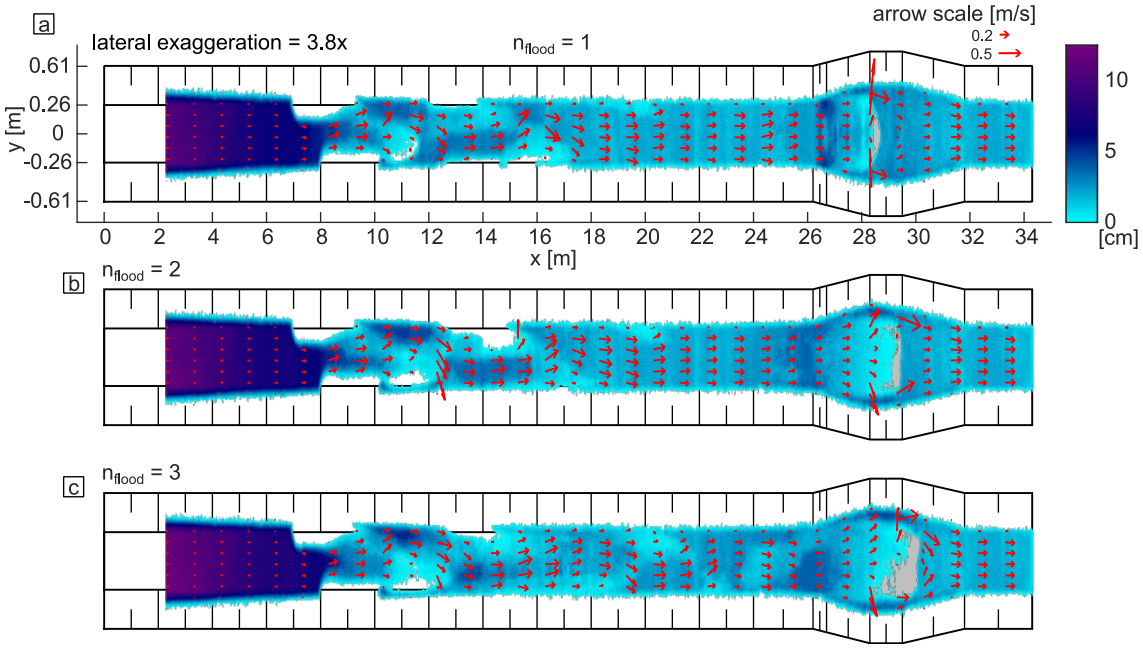

Figure A8.2 Graphic display of the simulated water depth and flow field after the three first floods of *Run_E*. a-c: Simulation results after 1 to 3 floods (n_{flood}). Variable x is the longitudinal channel coordinate, and y is the lateral channel coordinate. The grey area represents the mobile bed area. The colour scale indicates the water depth h. The red arrows represent the two-dimensional (2D) flow field.

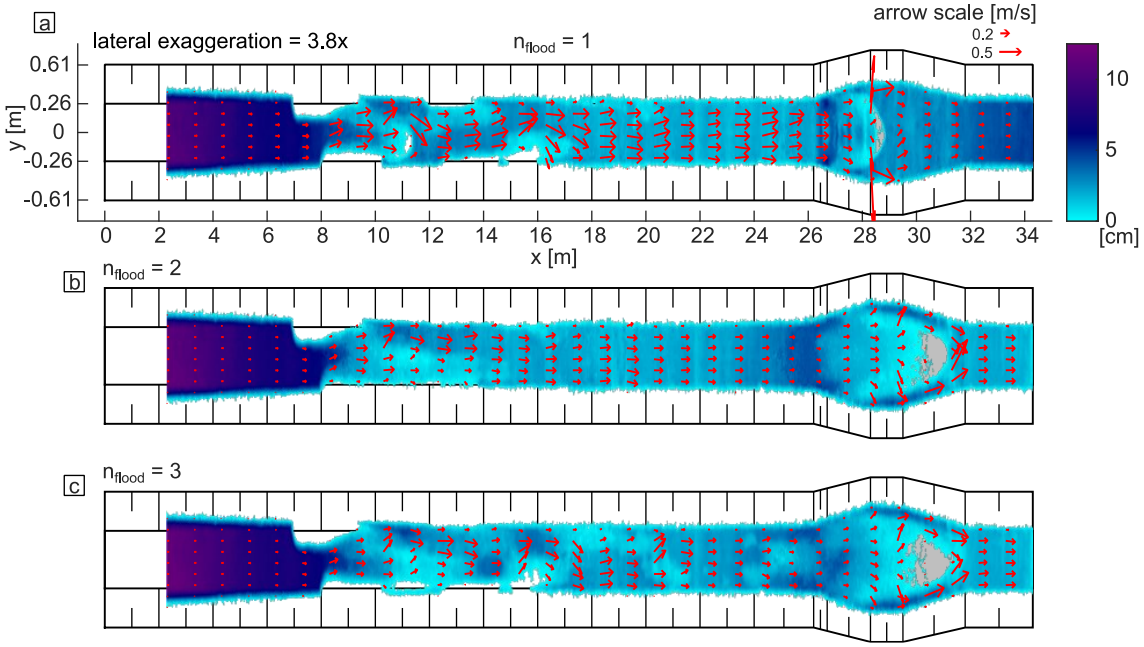

Figure A8.3 Graphic display of the simulated water depth and flow field after the three first floods of *Run_F*. a-c: Simulation results after 1 to 3 floods (n_{flood}). Variable x is the longitudinal channel coordinate, and y is the lateral channel coordinate. The grey area represents the mobile bed area. The colour scale indicates the water depth h. The red arrows represent the two-dimensional (2D) flow field.

A9. Data tables for results of the laboratory parametric study

Table A9.1 Data table for **Figure 4.5**. Variable Q is the constant water discharge, and $\bar{Q}_b$ is the average bedload transport rate. Variable $\bar{Q}_b$ is given for the cross-sections (CSs) *CS1* and *CS2*.

Scan	$Q\left[10^{-3}\ \frac{\mathrm{m}^3}{s}\right]$	$\bar{Q}_b\left[10^{-6}\ \frac{\mathrm{m}^3}{s}\right]$	
		CS1	CS2
A2	20	4.87	2.07
A3	30	4.67	1.95
A4	40	5.96	3.81
A5	50	6.43	8.52
A6	40	0.16	0.75
A7	30	0.14	0.03
A8	20	0.00	0.00
B2	35	11.42	5.00
B3	50	7.68	8.01
B4	40	0.00	0.86
B5	30	0.00	0.19
B6	30	0.00	0.01
B7	30	0.00	0.00
B8	20	0.00	0.00
C2	20	3.77	1.86
C3	30	3.65	1.51
C4	30	1.10	0.82
C5	30	0.94	0.60
C6	40	4.37	4.20
C7	50	4.97	6.82
C8	35	0.00	0.43

Table A9.2 Data table for **Figure 5.5**. Variable n_{flood} is the number of released floods, D^* is the dimensionless deposition, and POC the percentage of cover. Variables D^* and POC are given for the zones of interest (ZOI) *ZOI1* to *ZOI3*.

Run	n_{flood}	$D^*[-]$			$POC[-]$		
		ZOI1	ZOI2	ZOI3	ZOI1	ZOI2	ZOI3
D	1	2.57	0.21	0.75	0.59	0.11	0.23
D	2	2.19	0.11	1.42	0.56	0.07	0.34
D	3	3.11	0.28	2.33	0.69	0.15	0.45
D	4	2.66	0.32	2.78	0.66	0.19	0.52
E	1	2.53	0.16	0.88	0.59	0.07	0.23
E	2	3.09	0.23	2.16	0.65	0.13	0.40
E	3	3.57	0.64	2.77	0.72	0.33	0.49
E	4	4.12	1.06	3.20	0.75	0.46	0.54
F	1	2.52	0.21	0.81	0.55	0.10	0.24
F	2	2.13	0.05	3.35	0.55	0.04	0.60
F	3	3.29	0.61	3.52	0.72	0.30	0.66
F	4	3.19	0.70	4.20	0.73	0.37	0.70

Table A9.3 Data table for **Figure 5.8**. Variable n_{flood} is the number of released floods, and $HMID$ is the hydromorphological index of diversity.

Run	$n_{flood}[-]$	$HMID[-]$
D	0	7.21
D	1	10.56
D	2	10.00
D	3	11.06
D	4	10.65
E	0	7.21
E	1	10.22
E	2	11.04
E	3	12.01
E	4	12.01
F	0	7.21
F	1	10.07
F	2	10.73
F	3	11.70
F	4	11.71

A10. Supplementary information for statistical testing of the field study

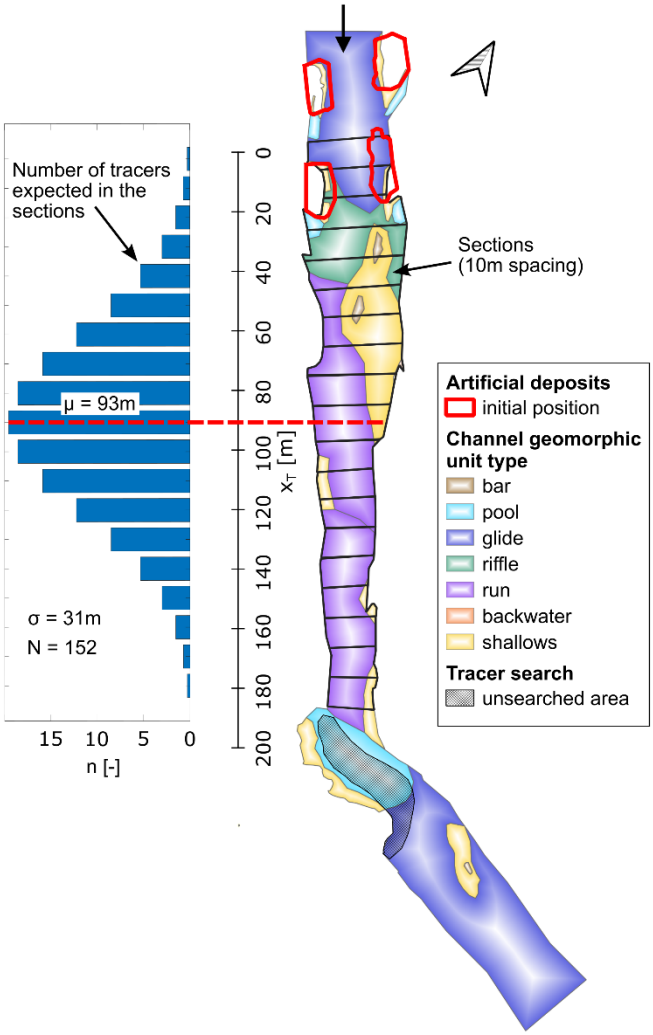

Figure A10.1 Graphic display of channel geomorphic units (CGUs) after *Flood 2016* with the expected tracer distribution along the channel axis, following $H_{0,2}$. Variable x_T is the distance from the centre of the initial position of the four artificial deposits along the channel axis, n is the number of tracers by section, μ is the arithmetic mean, σ the standard deviation, and N the number of tracers detected outside the initial artificial deposits.

Table A10.1 Comparison of observed (O) and expected (E) number of tracers for the null hypotheses (H_0) $H_{0,1}$ and $H_{0,2}$ by channel geomorphic unit (CGU) type for the two channel states after Flood 2016 (T_{F16}) and after Flood 2020 (T_{F20}). Variable $\boldsymbol{n_{total}}$ is the total number of tracers considered, and p is the statistical p-value for the chi-square goodness-of-fit test (χ^2-test).

	$\boldsymbol{T_{F16}}$			$\boldsymbol{T_{F20}}$	
CGU type	O [−]	$E(H_{0,1})$ [−]	$E(H_{0,2})$ [−]	O [−]	$E(H_{0,1})$ [−]
bar	6	0.89	1.02	1	1.15
pool	7	13.83	0.37	2	12.07
glide	26	60.19	1.03	35	58.13
riffle	19	11.48	6.27	34	12.57
run	35	40.76	101.48	20	36.45
backwater	0	0.04	0.17	0	0.70
shallows	62	27.80	41.66	48	18.93
$\boldsymbol{n_{total}}$ [−]	155	155	155	140	140
$\boldsymbol{p}$ [−]	-	10^{-19}	10^{-175}	-	10^{-21}

A11. Cross-section profiles

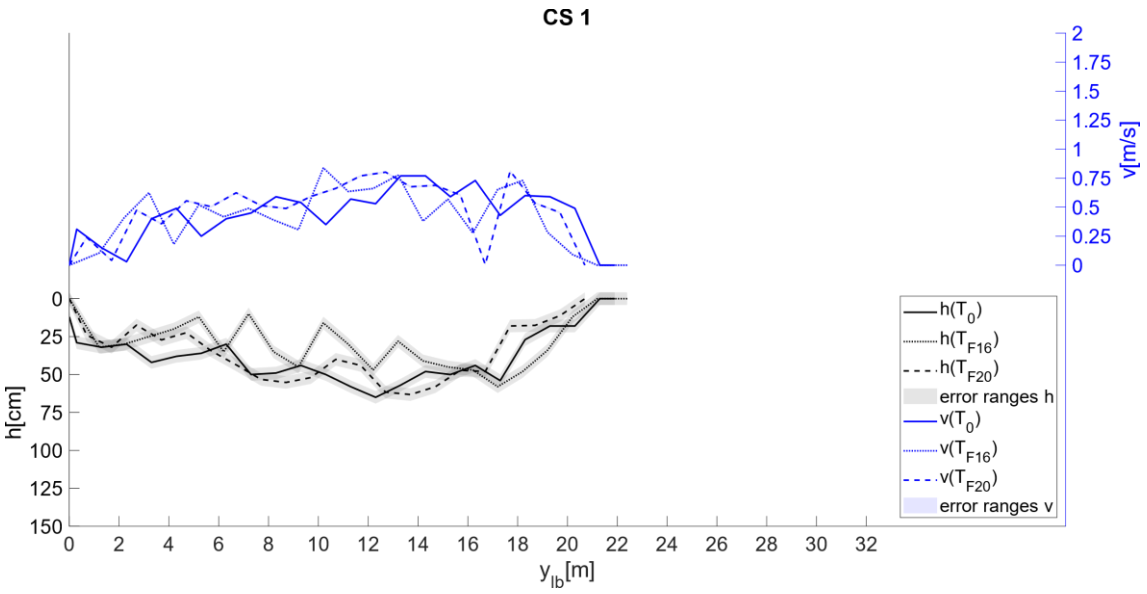

Figure A11.1 Cross-section (CS) profile of CS1 for the three channel states before *Flood 2016* (T_0), after *Flood 2016* (T_{F16}) and after *Flood 2020* (T_{F20}). Variable h is the water depth, v is the velocity measured at $0.6h$ from the surface at each measurement point, and y_{lb} is the distance from the left bank. In the measurement campaign at T_{F16}, the residual flow discharge (2.5 m^3/s) and the reference water level were lower than during the other two measurement series (3.5 m^3/s).

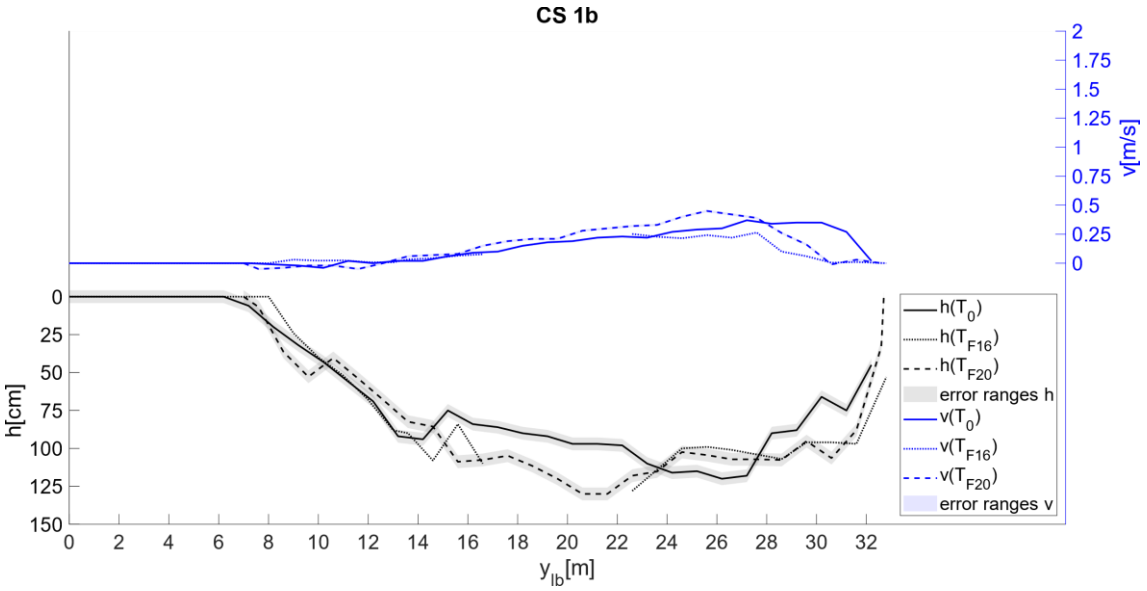

Figure A11.2 Cross-section (CS) profile of CS1b for the three channel states before *Flood 2016* (T_0), after *Flood 2016* (T_{F16}) and after *Flood 2020* (T_{F20}). Variable h is the water depth, v is the velocity measured at $0.6h$ from the surface at each measurement point, and y_{lb} is the distance from the left bank. In the measurement campaign at T_{F16}, the residual flow discharge (2.5 m^3/s) and the reference water level were lower than during the other two measurement series (3.5 m^3/s).

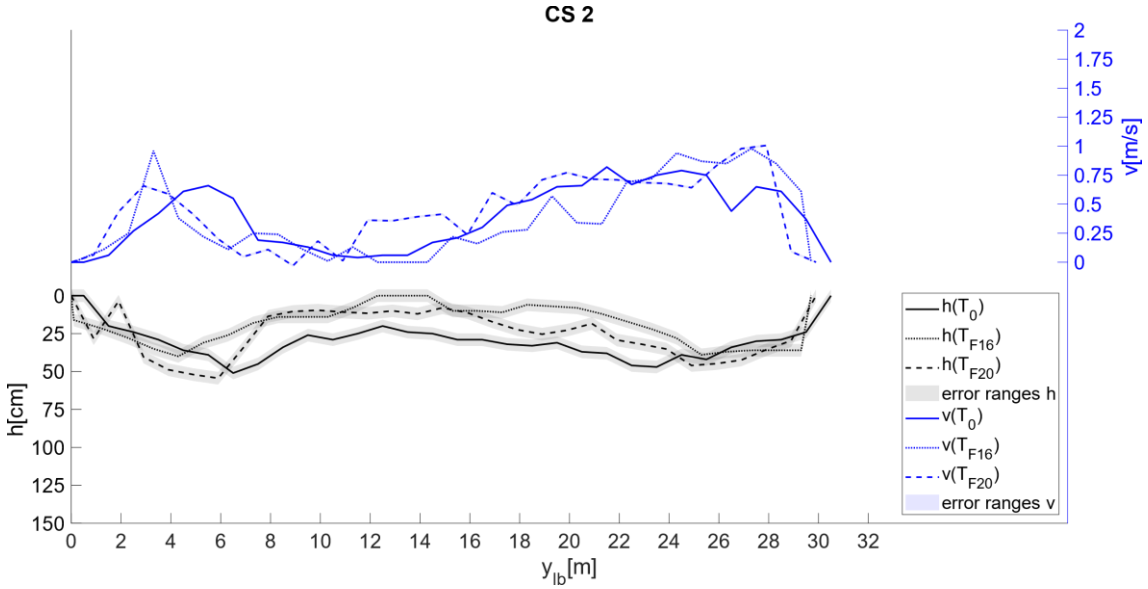

Figure A11.3 Cross-section (CS) profile of CS2 for the three channel states before *Flood 2016* (T_0), after *Flood 2016* (T_{F16}) and after *Flood 2020* (T_{F20}). Variable h is the water depth, v is the velocity measured at $0.6h$ from the surface at each measurement point, and y_{lb} is the distance from the left bank. In the measurement campaign at T_{F16}, the residual flow discharge ($2.5\ m^3/s$) and the reference water level were lower than during the other two measurement series ($3.5\ m^3/s$).

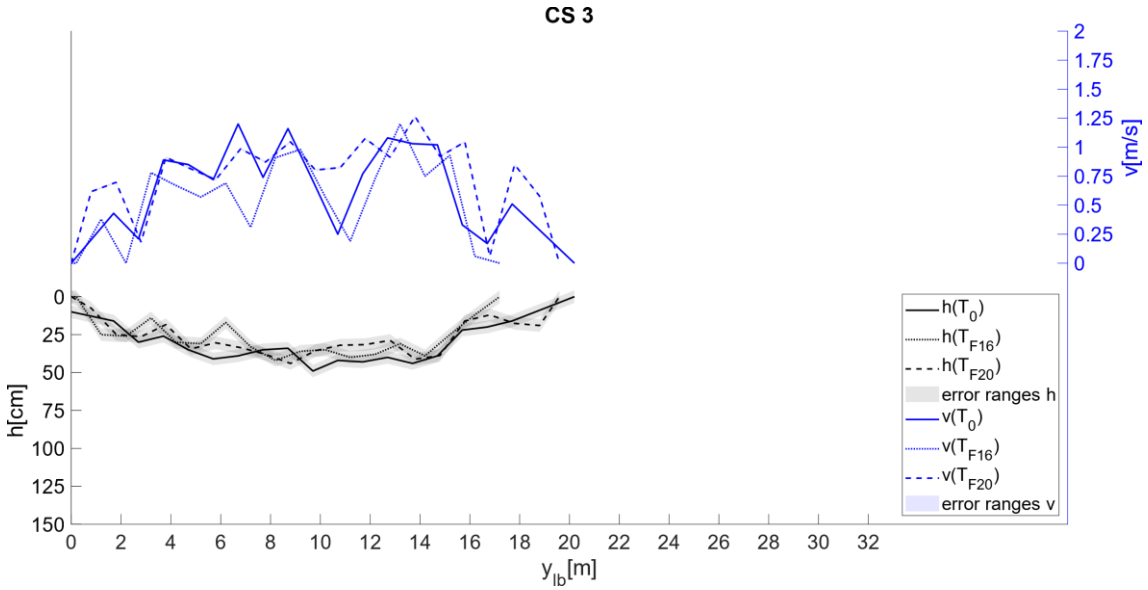

Figure A11.4 Cross-section (CS) profile of CS3 for the three channel states before *Flood 2016* (T_0), after *Flood 2016* (T_{F16}) and after *Flood 2020* (T_{F20}). Variable h is the water depth, v is the velocity measured at $0.6h$ from the surface at each measurement point, and y_{lb} is the distance from the left bank. In the measurement campaign at T_{F16}, the residual flow discharge ($2.5\ m^3/s$) and the reference water level were lower than during the other two measurement series ($3.5\ m^3/s$).

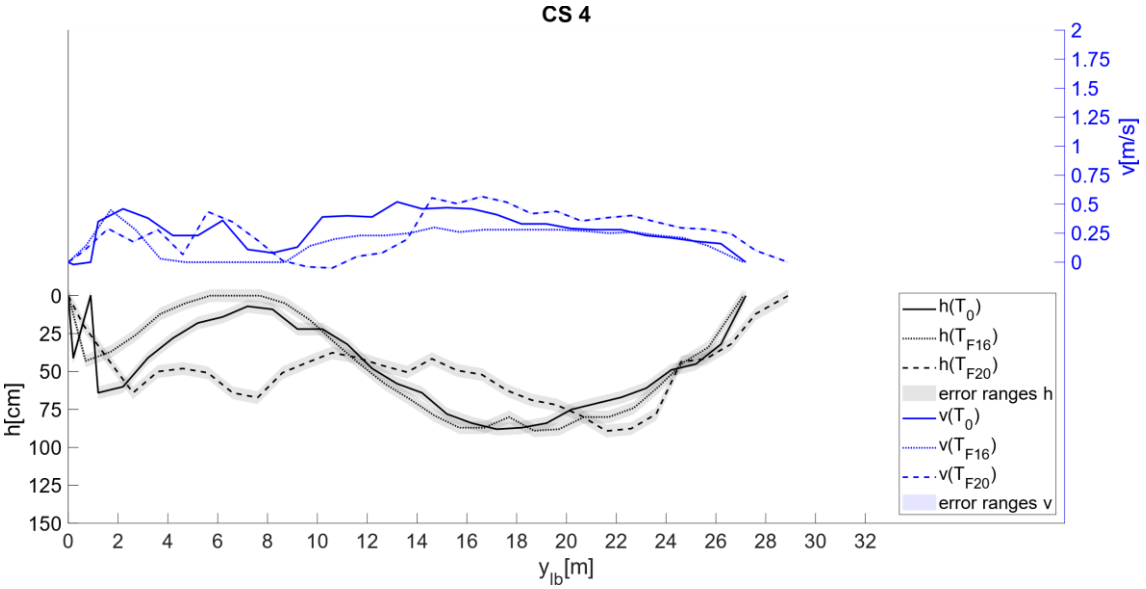

Figure A11.5 Cross-section (CS) profile of CS4 for the three channel states before *Flood 2016* (T_0), after *Flood 2016* (T_{F16}) and after *Flood 2020* (T_{F20}). Variable h is the water depth, v is the velocity measured at $0.6h$ from the surface at each measurement point, and y_{lb} is the distance from the left bank. In the measurement campaign at T_{F16}, the residual flow discharge ($2.5\ m^3/s$) and the reference water level were lower than during the other two measurement series ($3.5\ m^3/s$).

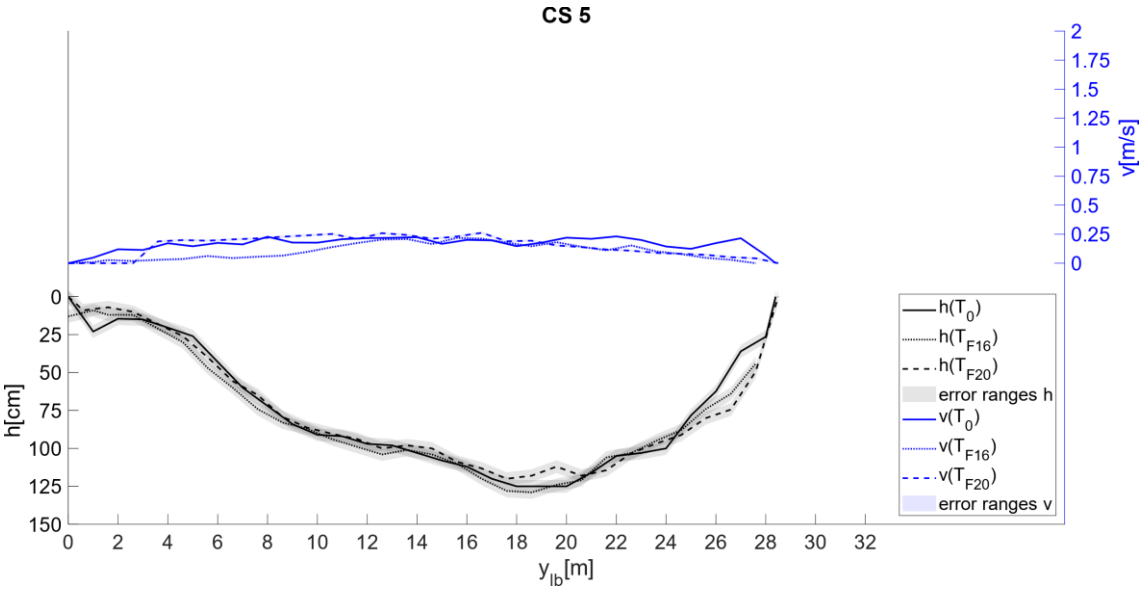

Figure A11.6 Cross-section (CS) profile of CS5 for the three channel states before *Flood 2016* (T_0), after *Flood 2016* (T_{F16}) and after *Flood 2020* (T_{F20}). Variable h is the water depth, v is the velocity measured at $0.6h$ from the surface at each measurement point, and y_{lb} is the distance from the left bank. In the measurement campaign at T_{F16}, the residual flow discharge ($2.5\ m^3/s$) and the reference water level were lower than during the other two measurement series ($3.5\ m^3/s$).

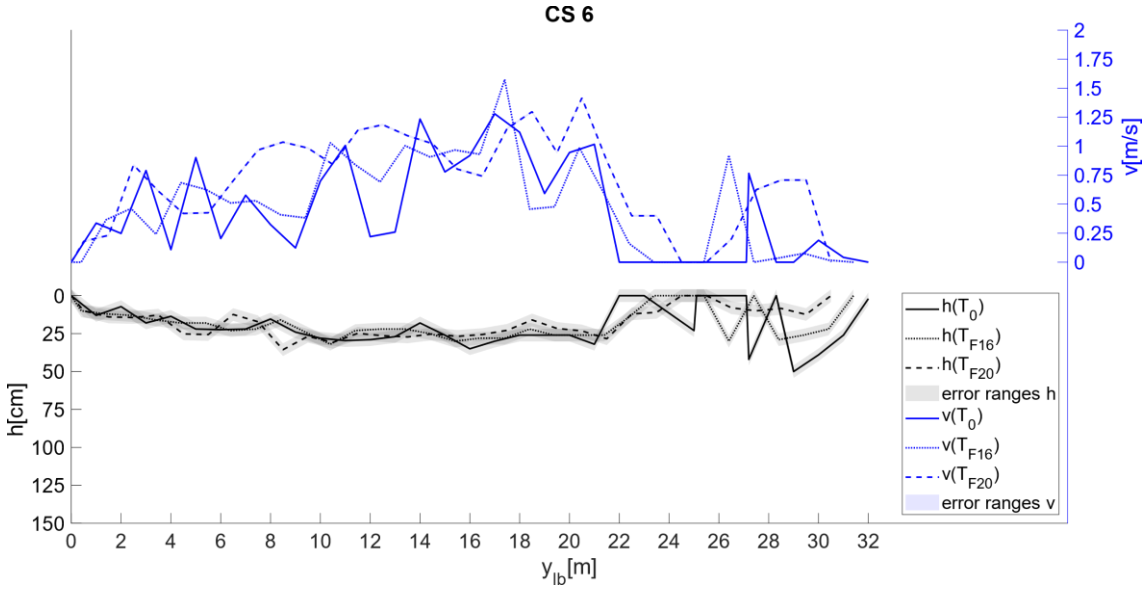

Figure A11.7 Cross-section (CS) profile of CS6 for the three channel states before *Flood 2016* (T_0), after *Flood 2016* (T_{F16}) and after *Flood 2020* (T_{F20}). Variable h is the water depth, v is the velocity measured at $0.6h$ from the surface at each measurement point, and y_{lb} is the distance from the left bank. In the measurement campaign at T_{F16}, the residual flow discharge ($2.5\ m^3/s$) and the reference water level were lower than during the other two measurement series ($3.5\ m^3/s$).

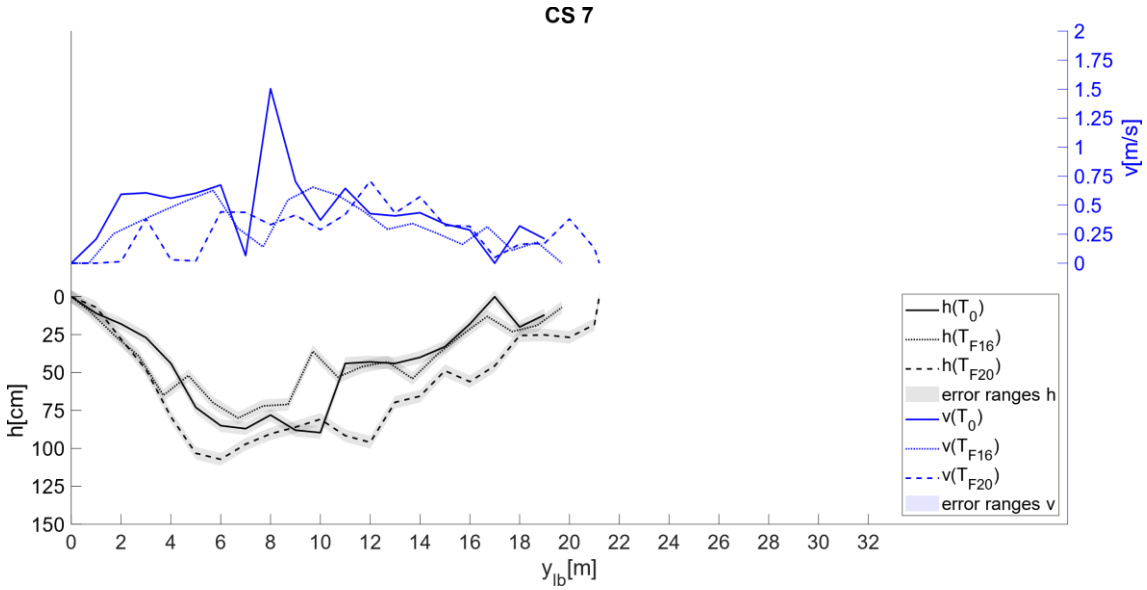

Figure A11.8 Cross-section (CS) profile of CS7 for the three channel states before *Flood 2016* (T_0), after *Flood 2016* (T_{F16}) and after *Flood 2020* (T_{F20}). Variable h is the water depth, v is the velocity measured at $0.6h$ from the surface at each measurement point, and y_{lb} is the distance from the left bank. In the measurement campaign at T_{F16}, the residual flow discharge ($2.5\ m^3/s$) and the reference water level were lower than during the other two measurement series ($3.5\ m^3/s$).

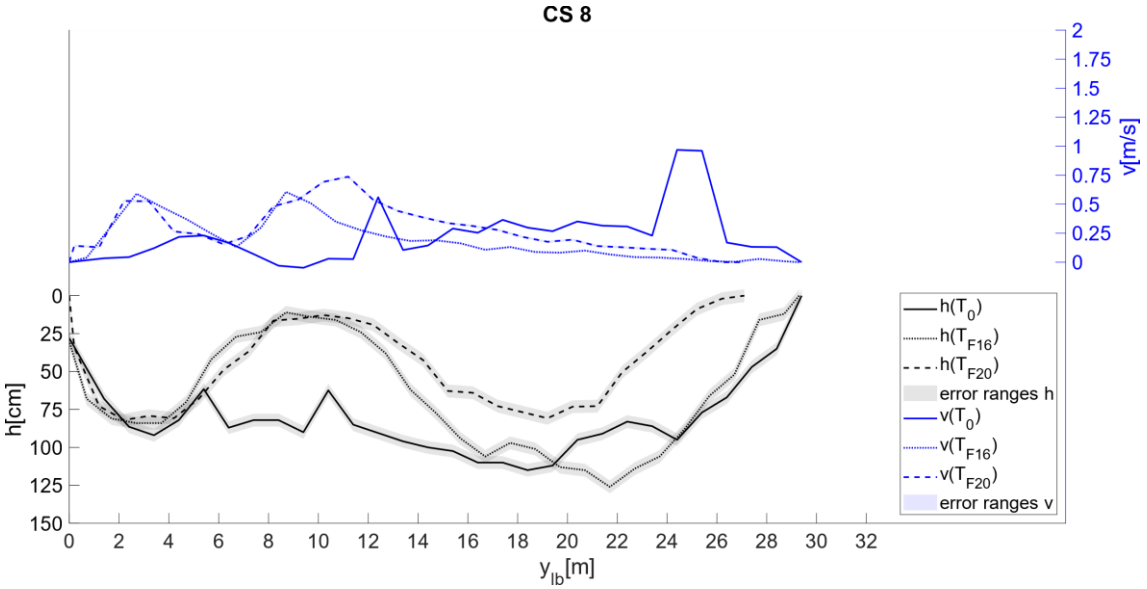

Figure A11.9 Cross-section (CS) profile of CS8 for the three channel states before *Flood 2016* (T_0), after *Flood 2016* (T_{F16}) and after *Flood 2020* (T_{F20}). Variable h is the water depth, v is the velocity measured at $0.6h$ from the surface at each measurement point, and y_{lb} is the distance from the left bank. In the measurement campaign at T_{F16}, the residual flow discharge ($2.5\ m^3/s$) and the reference water level were lower than during the other two measurement series ($3.5\ m^3/s$).

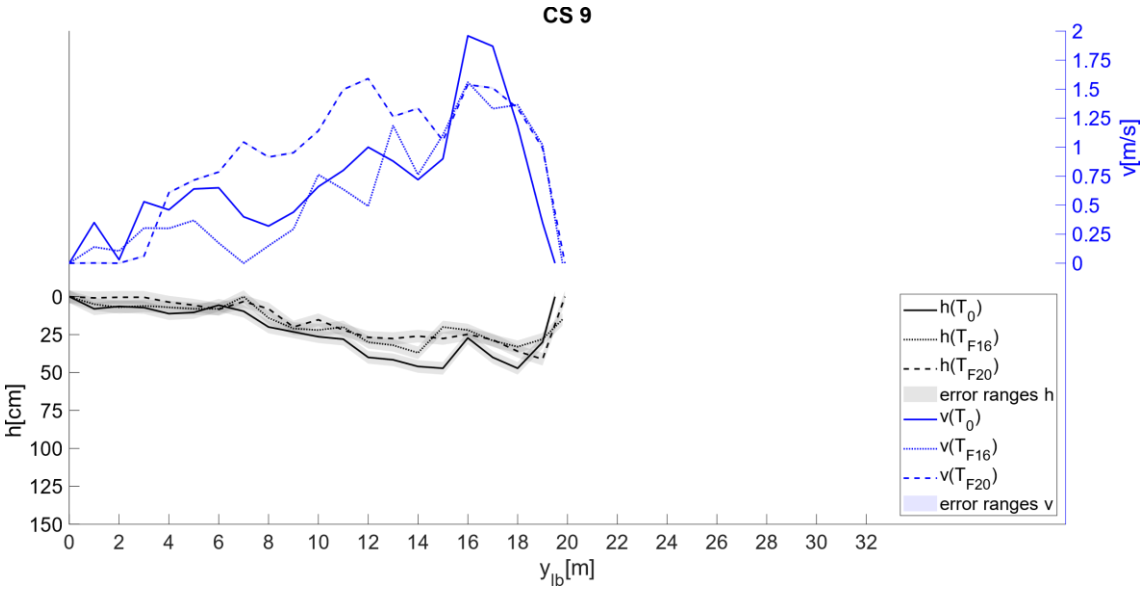

Figure A11.10 Cross-section (CS) profile of CS9 for the three channel states before *Flood 2016* (T_0), after *Flood 2016* (T_{F16}) and after *Flood 2020* (T_{F20}). Variable h is the water depth, v is the velocity measured at $0.6h$ from the surface at each measurement point, and y_{lb} is the distance from the left bank. In the measurement campaign at T_{F16}, the residual flow discharge ($2.5\ m^3/s$) and the reference water level were lower than during the other two measurement series ($3.5\ m^3/s$).

A12. Physical habitat assessment methods

Table A12.1 Evaluation criteria for Indicator 1.1 of the guideline for evaluating the outcome of restoration projects of the Swiss Federal Office of the Environment (Hunzinger et al., 2019).

Evaluation classes	score [-]
Only one structure type present	0
The structure type glide dominates. Other structure types occur with isolated, spatially isolated structures.	0.25
4 or more structure types are present with a density of 4-8 structures per unit length. If the structure type glide dominates, the structures of the remaining structure types locally form a diverse pattern.	0.5
All structure types of a glide-riffle-run or a natural or near-natural step-pool sequence present with a density of 8-11 structures of this sequence per unit length.	0.75
All structure types of a glide-riffle-run or a natural or near-natural step-pool sequence present with a density of 12 structures or more of this sequence per unit length	1

Table A12.2 Evaluation criteria for Indicator 1.2 of the guideline for evaluating the outcome of restoration projects of the Swiss Federal Office of the Environment (Hunzinger et al., 2019).

step	calculation	description
1	$A_{Emb} = \frac{1}{2} \times \left(1 - \frac{L_{lin,imp} - 0.5 L_{lin,perm}}{L_{bank}}\right)$	The linear embankment parameter (A_{Emb}) is calculated by the bank line with linear embankment and impermeable ($L_{lin,imp}$) and permeable embankment ($L_{lin,perm}$) and the total bank line (L_{bank}).
2	$\mathrm{A_{Structure}} = f(\mathrm{n}_{bank})$	The structural elements parameter ($A_{structure}$) is determined by the number of bank structures n_{bank}, where $\mathrm{A_{Structure}} = 0 \quad for\ \mathrm{n}_{bank} < 2$ $\mathrm{A_{Structure}} = (\mathrm{n}_{bank} - 2) \times \frac{1}{12} \quad for\ 2 \leq \mathrm{n}_{bank} \leq 8$ $\mathrm{A_{Structure}} = 0.5 \quad for\ \mathrm{n}_{bank} > 8$
3	$Ind_{1.2} = A_{Emb} + \mathrm{A_{Structure}}$	The normalised value of Indicator 1.2 ($Ind_{1.2}$) is calculated from A_{Emb} and $\mathrm{A_{Structure}}$.

Table A12.3 Evaluation criteria for Indicator 1.5 of the guideline for evaluating the outcome of restoration projects of the Swiss Federal Office of the Environment (Hunzinger et al., 2019). Variable Δ_{ref} is the deviation from the estimated reference condition.

Δ_{ref} [%]	score [-]
> 80	0
$]50, 80]$	0.25
$]30, 50]$	0.5
$]10, 30]$	0.75
< 10	1

Table A12.4 Evaluation criteria for Indicator 1.6 A2 of the guideline for evaluating the outcome of restoration projects of the Swiss Federal Office of the Environment (Hunzinger et al., 2019). The substrate type of the attribution corresponds to the category number of Indicator 1.6 A2 (see **Table 3.5**).

description	distribution	score [-]
Mainly coarse and armoured bed material, locally also mixed with bedload.	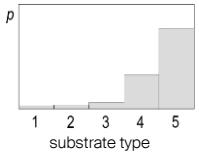	0
Mainly coarse and armoured bed material, partly mixed with bedload. No areas with bedload deposits.	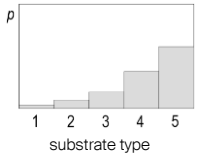	0.25
Mostly coarse substrate mixed with bedload. Some areas with bedload deposits.	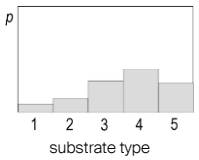	0.5
Balanced distribution of all classes.	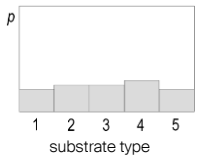	0.75
Bedload deposits predominate. No or limited areas of coarse, armoured bed material. Rather limited fine sediments.	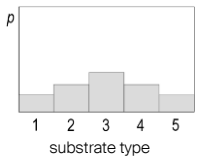	1

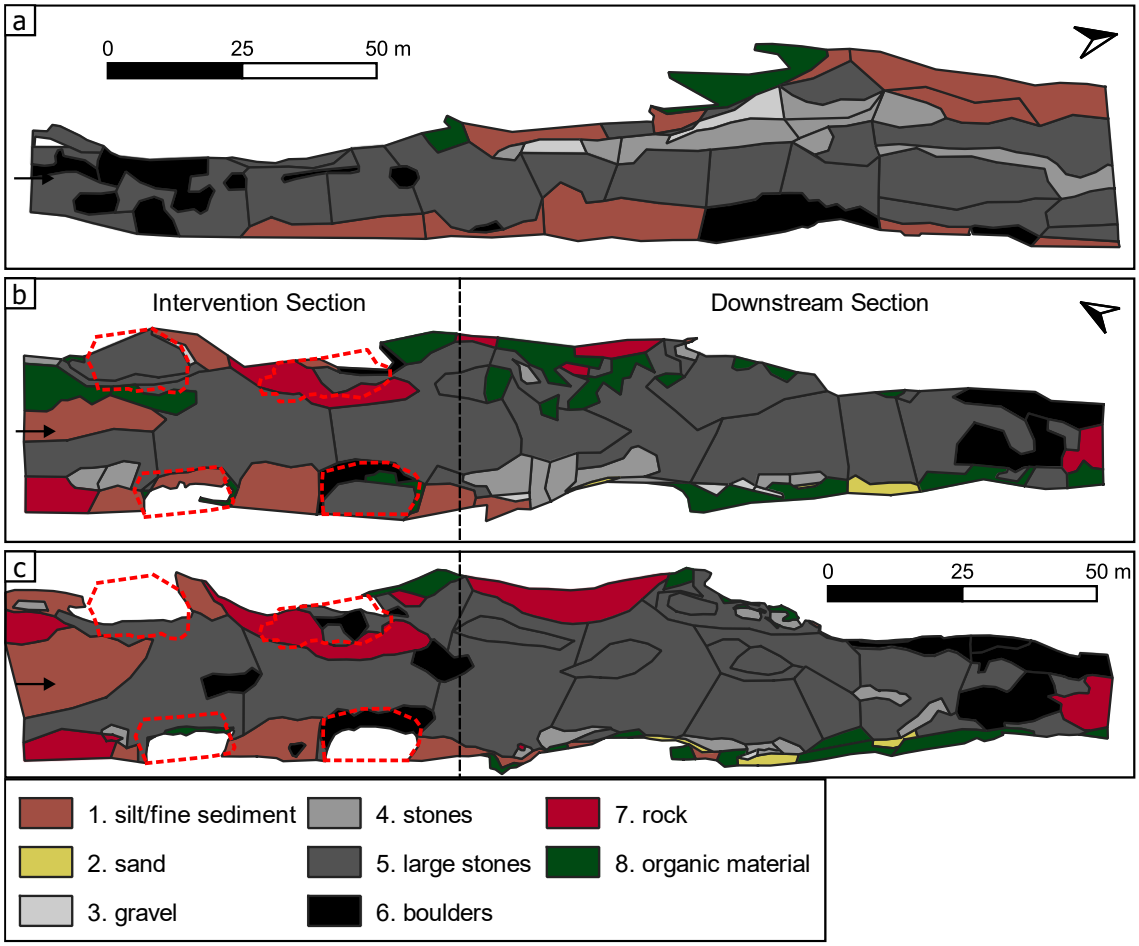

Figure A12.1 Mapped substrate composition at different study reaches and assessment times. a: *Control reach*, 2020. b: *Restoration reach*, 2020. c: *Restoration reach*, 2021. The red dashed line indicates the initial artificial deposit positions. The black dashed line separates the *intervention section* and the *downstream section*. The number in the legend indicates the category number (see **Table 3.5**).

Curriculum Vitae

Christian Mörtl

Nationality: German
Year of birth: 1990
Email: c.moertl@outlook.de

Education

03/2019 – 05/2023 Lausanne	**Hydraulic Construction Lab., PhD (EPFL)** Topic: Hydromorphological assessment of sediment augmentation measures in gravel-bed rivers
10/2014 – 06/2017 Munich	**Environmental Engineer, Master (TUM)** Environmental Hazards and Resource Management Hydraulic-, Geotechnical Eng., Risk Analysis, GIS
10/2010 – 09/2014 Munich	**Environmental Engineer, Bachelor (TUM)** Eng. Basics, Construction, Traffic, Water, Soil

Practical Experiences

10/2017 – 02/2019 Munich *Project Engineer*	**ARCADIS Germany GmbH** Construction planning of flood protection projects, hydraulic calculations and reservoir management
06/2017 – 09/2017 Munich *Research Assistant*	**TUM Research Institute of Hydraulic Eng.** Model development and interface programming of a bed-load transport model (Inn)
10/2015 – 09/2016 Munich *Working Student*	**Obermeyer Planen & Beraten** Department of Water, Wastewater & Development, flood protection (WWA Aschaffenburg), pipe network and test track planning
10/2014 – 05/2015 Munich *Working Student*	**Sustainable AG** Potential analysis, Development of calculation scenarios, Tendering, Development of a CR-Tool (Excel VBA) for MAN SE
01/2014 – 02/2014 Munich *Intern*	**BAH Office for Applied Hydrology** Control of measurement devices, Data processing and treatment, hydrological modelling national park Bavarian Forest
11/2013 – 12/2013 Munich *Intern*	**Geotechnical Laboratory Munich** Geotechnical laboratory testing, sieve analysis, field experiments, construction ground probing and sounding, Further construction and office work
11/2012 – 02/2013 Munich *Student Assistant*	**TUM Chair of Water Hydraulics & Managem.** Assistance in teaching, tutor tasks

Experiences Abroad

2016 8 Mon.	**France** Master Thesis (Geophysics)
2015 2 We.	**Ethiopia** Field Excursion (Hydropower)
2014 2 Mon.	**Greece** Study Project (Soil Dynamics)
2013 2 Mon.	**Norway** Bachelor Thesis (River Eng.)
2012 1 Mon.	**Namibia** Internship (Environm. Educ.)
2009 1 year	**Canada** Work and Travel
2007 6 Mon.	**America** Student Exchange

Language Skills

German: Native Language
English: Business Fluent (C2)
French: Fluent (C1)

Computing Knowledge

Microsoft Office, RIB Arriba

GIS (ArcGIS, QGIS)

CAD (AutoCAD, PROVI, Inventor)

Modelling:
- **hydrological** (ArcEGMO, HEC-RAS)
- **hydraulic** (MODFLOW, BASEMENT)
- **statistical** (GeNIe)

Programming
(Matlab, Python, R, Visual Basic)

Interests/Engagement

Outdoor sports, marathon, volleyball (STV Küttingen), 2 years committee member Association du Corps Intermédiaire de l'EPFL (ACIDE), 3 years action.uni delegate

Mandates

Kariba Dam	Study of plunge pool rehabilitation works at Kariba Dam for the Zambezian River Authority (ZRA). Responsible for project coordination, design of model adaptation, performance and evaluation of the measurements, documentation, and presentation results at the site at the Kariba Joint Mission (July 2019) in Siavonga, Zambia.
Ilarion Dam	Study of plunge pool rehabilitation works at Ilarion Dam for the Public Power Corporation S.A. (PPC). Responsible for the physical model design and construction, and supervision of the physical model study.

Courses

Data Analysis for Science and Engineering (4 ECTS)	Doctoral course for Civil- and Environmental Engineering (EPFL), spring semester 2019, taught by Davison Anthony C., Goldstein Darlene, Morgenthaler Stephan, Panaretos Victor
Experimental design and data analysis with R (2 ECTS)	Master course for Civil- and Environmental Engineering (EPFL), spring semester 2019, taught by Guillaume Thomas, Schlaepfer Rodolphe
Field-Based Insights into the Implementation of Renewable Energies (2 ECTS)	Doctoral summer school (FH Bern), spring semester 2019, taught by Dujic Drazen, Paolone Mario, Rufer Alfred, various lecturers
Design of experiment (4 ECTS)	Doctoral course for Civil- and Environmental Engineering (EPFL), fall semester 2019/20, taught by Fuerbringer Jean-Marie
Research data management: introduction	EPFL cross-disciplinary training (EPFL), spring semester 2019, taught by EPFL Library research data team
LabVIEW, Core I (EN)	EPFL cross-disciplinary training (EPFL), fall semester 2019/20, taught by Vincent Berseth
Italien A1	Language course (EPFL), fall semester 2019/20, taught by Arianna Mamoli

Teaching

Ouvrages hydrauliques et aménagements hydroélectriques [Hydraulic structures and hydro-electrical facilities]	Teaching assistant for an EPFL Master course for students of civil and environmental engineering in the winter semesters (wss) ws19-20, ws20-21, ws21-22
Ouvrages et aménagements hydraulique [Hydraulic structures and facilities]	Teaching assistant for an EPFL Bachelor course for students of civil and environmental engineering in the summer semesters (sss) ss20, ss21, ss22

Supervision

Study Project Jamet Gregoire Aurelien Marie	Analysis of fluctuating dynamic pressures for scour potential assessment
Study Project Romain Nathan Hippolyte Merlin Van Mol	Pre-study for: Plunge pool rehabilitation with prismatic concrete elements – case study and physical model of Ilarion dam in Greece
Master Thesis Romain Nathan Hippolyte Merlin Van Mol	Plunge pool rehabilitation with prismatic concrete elements – case study and physical model of Ilarion dam in Greece
Master Thesis Robin Schroff	Eco-morphological evaluation of a residual-flow reach restoration measure - Enhancing habitat assessment with a new substrate degradation indicator and digital surveying
Master Thesis Fanny Alexia Gretillat	Inondations du 21 juin 2019 au Val-de-Ruz - Évaluation de la contribution des phénomènes de ruissellement et de remontée de nappe dans l'évènement survenu à Villiers et Dombresson [Flooding of June 21, 2019 in Val-de-Ruz - Evaluation of the contribution of runoff and rising water table phenomena in the event that occurred in Villiers and Dombresson]
Master Thesis Lionel Julien Pattaroni	Influence of bank roughness and bed structure on riverbed morphology

Conferences

Swiss Competence Center for Energy Research - Supply of Energy (SCCER-SoE) Annual Conference 2019	The SCCER-SoE aims to conduct innovative and sustainable research in geo-energy and hydropower. Contribution by a poster: *Integrated sediment management of alpine rivers*. Lausanne, 2019
HYDROPOWER EUROPE Alpine Workshop	HYDROPOWER EUROPE is an EU-funded project that aims to create a forum gathering all the hydropower stakeholders throughout Europe. Lausanne, 2019.
21. Gewässermorphologisches Kolloquium	Hydromorphology in the context of water development objectives - basics, current developments, and challenges. Koblenz, 2019.
4. Informations- und Erfahrungsaustausch Sanierung Geschiebehaushalt der Wasser-Agenda 21	Exchange of experience among experts in Switzerland who are engaged in bedload regime restoration. *Online*, 2020.
River Flow 2020	Organised by the International Association for Hydro-Environment Engineering and Research (IAHR), the conference series River Flow is a scientific conference about the experimental, theoretical, and computational findings on fundamental river flow and transport processes, river morphology and morphodynamics. Contribution by a conference paper: *The sediment challenge of Swiss river corridors interrupted by man-made reservoirs*. *online*, 2020

Colloque 2020 Transport sédimentaire : rivières et barrages réservoirs (TSMR) du Comité Français des Barrages et Réservoirs (CFBR)	A platform for the exchange between science and practice in the topics of river morphology and hydropower. Contribution by a presentation: *Augmentation des sédiments en aval des barrages [Sediment augmentation downstream of dams]*. *online*, 2020
Wasserbau-Symposium 2021	Organised by ETH Zurich, this conference was open to scientists and practitioners under the topic: Hydraulic engineering in times of energy transition, water protection and climate change. Contribution by a conference paper: *Untersuchung der ökomorphologischen Wirksamkeit von Sedimentzugaben unterhalb von Talsperren [Investigation of the eco-morphological effectiveness of sediment augmentation downstream of dams.]*. Zurich, 2021
Forum des Transitions Urbaines	A platform for the exchange between science and practice for landscape planning and urban management with the topic: Reinventing urban rivers. Neuchâtel, 2021
Internationales Symposium für die Sanierung des Geschiebehaushalts 2021	International scientific conference with experts in the field of bedload management. Contribution by a workshop presentation: *Laboratory Experiments on Sediment Augmentation*. Interlaken, 2021
2. Forum Gewässerrevitalisierung der Wasser-Agenda 21	Exchange of experience among experts in Switzerland, who are engaged in river revitalisation projects. Bern, 2020.
Colloque 2021 Transport sédimentaire : rivières et barrages réservoirs (TSMR) du Comité Français des Barrages et Réservoirs (CFBR)	A platform of exchange between science and practice in river morphology and hydropower. Contribution by a presentation: *Augmentation des sédiments en aval des barrages [Sediment augmentation downstream of dams]*. Paris, 2020
Tagung 2022 Kommission Hochwasserschutz, Wasserbau und Gewässerpflege (KOHS)	Expert and stakeholder meeting about the project: Third correction of the Rhone. Visp, 2022
39th IAHR World Congress	International Congress of the IAHR with the topic: From snow to sea. Contribution by a conference paper and poster: *GALET: A deep learning image segmentation model for drone-based grain size analysis of gravel bars*. Granada, 2022
4th International Conference I.S.Rivers	An international scientific conference focusing on research and actions in the service of rivers and large rivers, whether natural or highly anthropised. Contribution by a workshop presentation: *Réinjection sédimentaire en Suisse- Exemple de la Petite Sarine [Sediment augmentation in Switzerland - Example of the Petite Sarine]*. Lyon, 2022
River Flow 2022	Contribution by a conference paper: *Continuous monitoring of morphological changes from sediment augmentation by field measurements and flume experiments*. *online*, 2022
3. Forum Gewässerrevitalisierung der Wasser-Agenda 21	Luzern, 2022.
5. Informations- und Erfahrungsaustausch Sanierung Geschiebehaushalt	Bern, 2022.

Publications

Title	Author	Type	Publisher	State	Contribution of the doctoral candidat according to the Contributor Roles Taxonomy (Credit)												
					Conceptualization	Data curation	Formal Analysis	Funding acquisition	Investigation	Methodology	Project administration	Resources	Software	Supervision	Validation	Visualization	Writing – original draft	Writing – review & editing
Sediment augmentation for river rehabilitation and management - a review	**Mörtl, C.** De Cesare, G.	peer-reviewed journal	Land	published	X	X			X						X	X	X	X
Influence of channel geomorphic units on the evolution of river morphology during low magnitude bed forming floods coupled with sediment augmentation	**Mörtl, C.** Schroff, R. Stähly, S. De Cesare, G.	peer-reviewed journal	Earth Surface Processes and Landforms	submitted	X	X	X		X	X		X			X	X	X	X
The sediment challenge of Swiss river corridors interrupted by man-made reservoirs	**Mörtl, C.** Vorlet, S.L. Manso, P. De Cesare, G.	conference proceedings	Riverflow 2020	published	X	X	X		X	X					X	X	X	X
GALET: A deep learning image segmentation model for drone-based grain size analysis of gravel bars	**Mörtl, C.** Baratier, A. Berhet, J. Duvillard, P. De Cesare, G.	conference proceedings	Proceedings of the 39th IAHR World Congress	published	X	X	X		X			X			X	X	X	X
Continuous monitoring of morphological changes from sediment augmentation by field measurements and flume experiments	**Mörtl, C.** De Cesare, G.	conference proceedings	Riverflow 2022	accepted	X	X	X		X	X		X	X		X	X	X	X
Sedimentzugaben in Fliessgewässern. Überblick über Methoden und Fallbeispiele [Sediment augmentation in flowing waters. Overview of methods and case studies]	**Mörtl, C.** De Cesare, G.	technical journal	Ingenieurbiologie	accepted	X	X			X			X			X	X	X	X

Contribution of the doctoral candidat according to the Contributor Roles Taxonomy (Credit)

Title	Author	Type	Publisher	State	Conceptualization	Data curation	Formal Analysis	Funding acquisition	Investigation	Methodology	Project administration	Resources	Software	Supervision	Validation	Visualization	Writing – original draft	Writing – review & editing
Sediment continuity and augmentation measures	**Mörtl, C.** Schroff, R. De Cesare, G.	technical journal	FactSheet Collection of the project Riverscape – sediment dynamics and connectivity	accepted	X	X	X		X	X		X	X		X	X	X	X
Untersuchung der ökomorphologischen Wirksamkeit von Sedimentzugaben unterhalb von Talsperren [Investigation of the ecomorphological effectiveness of sediment augmentation downstream of dams]	**Mörtl, C.** De Cesare, G.	conference proceedings	VAW-Mitteilung 262 - Tagungsband Wasserbau-Symposium 2021	published	X				X	X					X	X	X	X
Wirkungskontrolle einer Sedimentzugabe: Habitatvielfalt und Kolmation [Eco-morphological evaluation of a sediment augmentation measure]	Schroff, R. **Mörtl, C.** De Cesare, G.	technical journal	WasserWirtschaft	published	X				X		X	X		X				X
Impacts et enjeux de charriage d'une crue artificielle – Exemple de la Petite Sarine 2020 [Effects and bedload related challenges of an artificial flood - Example of the Petite Sarine 2020]	Schroff, R. **Mörtl, C.** Vonlanthen, P. De Cesare, G.	technical journal	Wasser Energie Luft - Eau Energie Air	published								X						X
Plunge pool scour and bank erosion: Assessment of protection measures for Ilarion dam by physical and numerical modelling	Van Mol, R. **Mörtl, C.** Amini, A. Siachou, S. Schleiss, A. J. De Cesare, G.	conference proceedings	HYDRO 2022	published								X		X				X